



**WYDZIAŁ BIOLOGII
i OCHRONY ŚRODOWISKA**
Uniwersytet Łódzki

Stacjonarne Studia Doktoranckie

Genetyki Molekularnej, Cytogenetyki i Biofizyki Medycznej

Michał Juszczak

**Ocena właściwości biologicznych
kompleksów rutenu w badaniach *in vitro***

Assessment of biological properties of ruthenium
complexes in *in vitro* studies

Praca doktorska

wykonana w Katedrze Genetyki Molekularnej

Instytutu Biochemii UŁ

pod kierunkiem

prof. dr hab. Katarzyny Woźniak

Łódź, 2023

*Pragnę podziękować Pani Profesor Katarzynie Woźniak
za wszelką pomoc, opiekę merytoryczną, cierpliwość, a przede wszystkim za ogromne
zrozumienie w obszarze naukowym oraz poza nim.*

*Dziękuję zespołowi Pani Profesor Bogny Rudolf z Katedry Chemii Organicznej UŁ za
udostępnienie nowych związków, przygotowanie odpowiednich analiz, a także wskazówki
dotyczące pracy z kompleksami rutenu.*

*Składam też serdeczne podziękowania pracownikom, koleżankom i kolegom z Uczelni,
a w szczególności Magdalenie Klusce, Paulinie Tokarz oraz Aleksandrze Szustce
za pomocną dłoń, życzliwość i wspaniałą koleżeńską atmosferę.*

*Chciałbym także serdecznie podziękować Aleksandrze, za ogromną pomoc i wsparcie
w trudnych momentach.*

Pracę dedykuję moim Rodzicom.

SPIS TREŚCI

Źródła finansowania	3
Dorobek naukowy.....	4
Wstęp.....	8
Cel pracy	10
Materiały i metody	10
Opis wyników.....	12
Podsumowanie wyników.....	22
Wnioski	25
Literatura uzupełniająca	26
Streszczenie	30
Summary.....	32
Publikacje będące podstawą rozprawy doktorskiej	34
Oświadczenia współautorów.....	133

Źródła finansowania

Badania przeprowadzone w ramach niniejszej rozprawy doktorskiej zostały sfinansowane z następujących źródeł:

- Dotacja celowa na finansowanie działalności polegającej na prowadzeniu badań naukowych lub prac rozwojowych oraz zadań z nimi związanych, służących rozwojowi młodych naukowców oraz uczestników studiów doktoranckich przyznana przez Dziekana Wydziału BiOŚ UŁ,
- Dotacja statutowa i subwencja Katedry Genetyki Molekularnej UŁ.



- Pracę zrealizowano we współpracy z zespołem Profesor Bogny Rudolf z Katedry Chemii Organicznej oraz z Profesorem Marcinem Palusiakiem z Katedry Chemii Fizycznej Wydziału Chemii UŁ.



- Pracę zrealizowano również we współpracy z Profesorem Arkadiuszem Chworosiem z Centrum Badań Molekularnych i Makromolekularnych Polskiej Akademii Nauk w Łodzi.



Dorobek naukowy

Publikacje wchodzące w skład rozprawy doktorskiej

W skład rozprawy doktorskiej wchodzi jedna publikacja przeglądowa oraz cztery prace doświadczalne:

1. **Juszczak M**, Kluska M, Wysokiński D, Woźniak K. Właściwości przeciwnowotworowe związków rutenu – NAMI-A i KP1019. *Postępy Higieny i Medycyny Doświadczalnej*, 2020; 74: 12-19. IF: **0,878**; IF 5-letni: **1,049**; **40** pkt. MEiN
2. **Juszczak M**, Kluska M, Wysokiński D, Woźniak K. DNA damage and antioxidant properties of CORM-2 in normal and cancer cells. *Scientific Reports*, 2020 Jul 22;10(1):12200. IF: **4,379**; IF 5-letni: **5,133**; **140** pkt. MEiN
3. **Juszczak M**, Kluska M, Kosińska A, Palusiak M, Rybarczyk-Pirek AJ, Wzgarda-Raj K, Rudolf B, Woźniak K. Cytotoxicity of piano-stool ruthenium cyclopentadienyl complexes bearing different imidato ligands. *Applied Organometallic Chemistry*, 2022, 36(4), e6595. IF: **4,105**; IF 5-letni: **3,515**; **100** pkt. MEiN
4. **Juszczak M**, Kluska M, Kosińska A, Rudolf B, Woźniak K. Antioxidant Activity of Ruthenium Cyclopentadienyl Complexes Bearing Succinimidato and Phthalimidato Ligands. *Molecules*, 2022; 27(9):2803. IF: **4,927**; IF 5-letni: **5,110**; **140** pkt. MEiN
5. **Juszczak M**, Das S, Kosińska A, Rybarczyk-Pirek AJ, Wzgarda-Raj K, Tokarz P, Vasudevan S, Chworos A, Woźniak K, Rudolf B. Piano-stool ruthenium(II) complexes with maleimide and phosphine or phosphite ligands: synthesis and activity against normal and cancer cells. *Dalton Transactions*. 2023; 10.1039/d2dt04083b. IF: **4,569**; IF 5-letni: **3,904**; **140** pkt. MEiN

Suma IF: 18,858; IF 5-letni: 18,711; 560 pkt. MEiN

Pozostały dorobek naukowy

Publikacje:

1. **Juszczak M**, Kluska M, Skalski B, Żuchowski J, Stochmal A, Olas B, Woźniak K. Multidirectional effects of saponin fraction isolated from the leaves of sea buckthorn *Elaeagnus rhamnoides* (L.) A. Nelson. *Biomedicine and Pharmacotherapy*, 2021, 111395. IF: **6,027**, IF 5-letni: **5,979**, **100** pkt. MEiN
2. Kluska M, **Juszczak M**, Wysokiński D, Żuchowski J, Stochmal A, Woźniak K. Kaempferol derivatives isolated from *Lens culinaris* Medik. reduce DNA damage induced by etoposide in peripheral blood mononuclear cells. *Toxicology Research*, 2019 Sep 10;8(6):896-907. IF: **2,283**, IF-5-letni: **3,217**, **40** pkt. MEiN
3. Kluska M, **Juszczak M**, Wysokiński D, Woźniak K. Właściwości przeciwnowotworowe kemferolu. *Postępy Biologii Komórki*, 2018; 45(4). IF: **0,163**, IF 5-letni: **0,068**, **20** pkt. MEiN
4. Kluska M, **Juszczak M**, Żuchowski J, Stochmal A, Woźniak K. Kaempferol and Its Glycoside Derivatives as Modulators of Etoposide Activity in HL-60 Cells. *International Journal of Molecular Sciences*, 2021; 22(7):3520. IF: **5,924**, IF 5-letni: **6,132**, **140** pkt. MEiN
5. Kluska M, **Juszczak M**, Żuchowski J, Stochmal A, Woźniak K. Effect of Kaempferol and Its Glycoside Derivatives on Antioxidant Status of HL-60 Cells Treated with Etoposide. *Molecules*, 2022 Jan 6;27(2):333. IF: 4,927, IF 5-letni: 4,558, 140 pkt. MEiN
6. Żuchowski J, Skalski B, **Juszczak M**, Woźniak K, Stochmal A, Olas B. LC/MS Analysis of Saponin Fraction from the Leaves of *Elaeagnus rhamnoides* (L.) A. Nelson and Its Biological Properties in Different *In Vitro* Models. *Molecules*, 2020 Jun 30;25(13):3004. IF: **3,267**, IF 5-letni: **2,791**, **100** pkt. MEiN
7. Wysokiński D, Lewandowska P, Zątak D, **Juszczak M**, Kluska M, Lizińska D, Rudolf B, Woźniak K. Photoactive CO-releasing complexes containing iron - genotoxicity and ability in *HO-1* gene induction in HL-60 cells. *Toxicology Research*, 2019 May 22;8(4):544-551. IF: **2,283**, IF 5-letni: **3,217**, **40** pkt. MEiN

8. Kowalczyk M, Rolnik A, Adach W, Kluska M, **Juszczak M**, Grabarczyk Ł, Wozniak K, Olas B, Stochmal A, Multifunctional compounds in the extract from mature seeds of *Vicia faba* var. minor: Phytochemical profiling, antioxidant activity and cellular safety in human selected blood cells in *in vitro* trials. *Biomedicine and Pharmacotherapy*, Volume 139, 2021, 111718, ISSN 0753-3322. IF: **6,027**, IF 5-letni: **5,979**, **100** pkt. MEiN

Suma IF: 30,853; IF 5-letni: 32,493; 680 pkt. MEiN

Komunikaty zjazdowe:

1. **Juszczak M**, Kluska M, Kosińska A. „Antioxidant properties of novel metallocarbonyl ruthenium complex bearing succinimidato ligand”. VI Ogólnopolska Konferencja Genetyczna Genomica. 20-22 maja 2022, Kraków.
2. **Juszczak M**, Kluska M, Kosińska A. „Ocena właściwości cyto- oraz genotoksycznych nowych kompleksów rutenowych”. VI Ogólnopolska Konferencja Doktorantów Nauk o Życiu BIOOPEN. 15-16 kwietnia 2021, Łódź.
3. **Juszczak M**, Kluska M. „Evaluation of CORM-2 antioxidant properties in human peripheral blood cells (PBMCs) and HL-60 cells”. National Scientific Conference „Knowledge – Key to Success” – 4th edition. 18 stycznia 2020, Toruń.
4. **Juszczak M**, Kluska M, Zobel Z, Wysokiński D. „Ocena uszkodzeń oraz kinetyki naprawy DNA w jednojądrzastych komórkach krwi oraz komórkach HL-60 po inkubacji z CORM-2”. XI Interdyscyplinarna Konferencja Naukowa Tygiel 2019. 23-24 marca 2019, Lublin. **Nagroda za najlepszy poster**
5. Kluska M, **Juszczak M**, Żuchowski J, Woźniak K. „Wpływ kemferolu i jego glikozydowych pochodnych na ekspresję genów *NRF-2*, *NQO-1*, *HO-1*, *SOD-1* i *SOD-2*”. VI Ogólnopolska Konferencja Doktorantów Nauk o Życiu BIOOPEN. 15-16 kwietnia 2021, Łódź.
6. Kluska M, **Juszczak M**, Żuchowski J. „Effect of kaempferol and its glycoside derivatives isolated from lentils (*Lens culinaris* Medik.) on apoptosis induced by etoposide in HL-60 cells”. National Scientific Conference „Knowledge – Key to Success” – 4th edition. 18 stycznia 2020, Toruń.

7. Kluska M, **Juszczak M**, Krzyżanowska-Kowalczyk J, Woźniak K. „Wpływ związków polifenolowych wyizolowanych z soczewicy *Lens culinaris* Medik. na przeciwnowotworowe działanie etopozydu”. XI Interdyscyplinarna Konferencja Naukowa Tygiel 2019. 23-24 marca 2019, Lublin.
8. Rudolf B, Kosińska A, **Juszczak M**, Kluska M, Palusiak M, Rybarczyk-Pirek AJ, Wzgarda-Raj K, Woźniak K. „Cytotoksyczność i genotoksyczność metalokarbonylowych kompleksów rutenowych typu $CpRu(CO)_2\eta^1-N\text{-imidato}$ ”. 63 Zjazd Naukowy Polskiego Towarzystwa Chemicznego. 13-16 września 2021, Łódź.
9. Kosińska A, Rudolf B, **Juszczak M**, Kluska M, Woźniak K. „Biological properties of ruthenium cyclopentadienyl complexes bearing different imidato ligands”. International Symposium on Thermodynamics of Metal Complexes. 16-18 czerwca 2021, Białystok.
10. Zątak D, Wysokiński D, **Juszczak M**, Lizińska D, Kluska M. „Wpływ nowych kompleksów metalokarbonylowych na ekspresję genu *HMOX1*” V Ogólnopolska Konferencja Genetyczna Genomica. 5-7 kwietnia 2019, Kraków.
11. Rudolf B, Kosińska A, Woźniak K, **Juszczak M**, Kluska M. „Pólsandwiczowe kompleksy rutenowe, synteza oraz aktywność biologiczna”. Związki Biologicznie Czynne – Aktywność, Struktura, Synteza. 24-25 czerwca 2022, Białystok.

Skrócony opis prowadzonych prac wraz z omówieniem wyników

Wstęp

Ruten, odkryty w 1844 r. przez rosyjskiego chemika Karla Klause, zawdzięcza swą nazwę Ruthenii, historycznej nazwie Rusi [1]. Jest to rzadki metal przejściowy występujący w ilości zaledwie 0,001 cząstek na milion w skorupie ziemskiej [2]. W układzie okresowym znajduje się w grupie 8., wspólnie z żelazem, osmem oraz hasem. Ruten obok rodu, palladu, osmu, irydu oraz platyny należy do platynowców. Metale te cechują się wysokimi temperaturami topienia, wysoką odpornością cieplną, wysoką odpornością na korozję, a także unikalnymi właściwościami katalitycznymi [3]. Ze względu na te właściwości ruten stosowany jest w przemyśle elektronicznym do produkcji styków elektrycznych oraz rezystorów chipowych. Ponadto, zawierające ruten katalizatory Grubbsa są stosowane w przemyśle chemicznym oraz elektrochemicznym [4]. Kolejnym potencjalnym zastosowaniem platynowców było użycie ich jako związków aktywnych biologicznie, a w szczególności wykazujących potencjał przeciwnowotworowy. Szczególną uwagę w początkowych etapach tych badań zyskała platyna.

Odkrycie przez Rosenberga w latach 60. XX w. cytostatycznych właściwości cisplatyny wobec bakterii *Escherichia coli*, a następnie mysich komórek białaczkowych L1210 było przełomem w badaniach nad lekami przeciwnowotworowymi [5]. Z perspektywy czasu cisplatyna jako związek przeciwnowotworowy odniosła ogromny sukces. Począwszy od jej wprowadzenia do leczenia w 1978 r. jest używana do chwili obecnej w leczeniu nowotworów jąder, jajników, pęcherza moczowego, głowy i szyi oraz niedrobnokomórkowego raka płuc [6]. Jednakże znaczące działania niepożądane terapii oraz ograniczenia dotyczące rodzajów nowotworów, które można leczyć cisplatyną, skłoniły badaczy do poszukiwań alternatywnych związków aktywnych biologicznie opartych o inne metale, takie jak złoto, srebro, iryd czy też ruten [7].

Ruten wykazuje szereg pożądanych cech w kontekście zastosowania go w syntezie kompleksów o potencjalnych właściwościach przeciwnowotworowych. Dane literaturowe wskazują, że ruten może występować na kilku stopniach utlenienia od 0 do +8 [8]. Jednakże w warunkach fizjologicznych występuje głównie na dwóch stopniach utlenienia jako Ru(II) oraz Ru(III), z których to Ru(II) jest uznawany za znacznie bardziej aktywny biologicznie [9].

Różnice w aktywności biologicznej w zależności od stopnia utlenienia, na którym znajduje się ruten, otwierają drogę do aktywacji kompleksów poprzez redukcję. Ubogie w tlen środowisko komórek nowotworowych, predysponuje kompleksy do zmiany stopnia utlenienia z +3 na +2 [10]. Możliwe jest zatem wykorzystanie kompleksów zawierających Ru(III), który po wnikięciu do wnętrza komórki nowotworowej, zostaje zredukowany do Ru(II) [11]. Ze względu na strukturalne podobieństwo pomiędzy żelazem a rutenem, możliwe jest wiązanie się rutenu z białkami wiążącymi żelazo, w szczególności transferyną [12]. Ponadto, ze względu na większe zapotrzebowanie na żelazo w przypadku komórek szybko dzielących się, w tym także nowotworowych, dochodzi do wzrostu liczby receptorów transferynowych na powierzchni tych komórek [13]. Stwarza to możliwość transportu kompleksów rutenowych do wnętrza komórek nowotworowych przez receptory dla żelaza. Badania wykazały, że w komórkach nowotworowych rutenu może być nawet kilkanaście razy więcej niż w przypadku komórek prawidłowych [14]. Dodatkowym aspektem jest czas wymiany ligandów, w przypadku kompleksów Ru(II) zazwyczaj wyrażony w godzinach, co odpowiada długości cyklu komórkowego [15].

W niniejszej pracy doktorskiej dokonano oceny właściwości biologicznych w warunkach *in vitro* 10 kompleksów zawierających ruten. Kompleksy rutenu były zróżnicowane pod względem struktury chemicznej i obejmowały: związek uwalniający tlenek węgla CORM-2, należący do klasy związków CORMs (ang. *carbon monoxide-releasing molecules*), a także nowo zsyntetyzowane kompleksy rutenu zawierające różne ligandy, takie jak maleimid, sukcyimid, ftalimid czy też ligandy fosforoorganiczne – fosfinowe i fosforynowe.

Cel pracy

Celem badań zrealizowanych w niniejszej rozprawie doktorskiej była ocena właściwości biologicznych kompleksów rutenu w warunkach *in vitro*. Badania prowadzono we współpracy z Katedrą Chemii Organicznej UŁ, Katedrą Chemii Fizycznej UŁ oraz Centrum Badań Molekularnych i Makromolekularnych Polskiej Akademii Nauk w Łodzi.

Wykonano badania kompleksów rutenu w warunkach *in vitro*, które miały na celu:

- określenie właściwości cytotoksycznych oraz genotoksycznych,
- określenie możliwości indukcji apoptozy,
- analizę przebiegu cyklu komórkowego,
- określenie potencjału pro- i antyoksydacyjnego,
- określenie zdolności do bezpośredniej interakcji z DNA.

Materiały i metody

Badania w warunkach *in vitro* przeprowadzono na:

- jednojądrzastych komórkach krwi obwodowej (PBMC) izolowanych z kożuszków leukocyтарно-пłytkowych uzyskanych od zdrowych dawców w Centrum Krwiodawstwa i Krwiolecznictwa w Łodzi. Badania te zostały zatwierdzone przez Komisję ds. Etyki Badań Naukowych UŁ (17/KBBN-UŁ/III/2019)
- komórkach ludzkiej ostrej białaczki promielocytowej HL-60 (ATCC® CCL-240™)
- komórkach ludzkiej ostrej białaczki promielocytowej HL-60 (ATCC® CCL-240™) opornych na doksorubicynę (HL-60/DR) (linia otrzymana samodzielnie poprzez długotrwałą ekspozycję na wzrastające stężenia doksorubicyny).

Doświadczenia przeprowadzono z 10 kompleksami rutenu, z których 9 zostało zsyntetyzowanych w Katedrze Chemii Organicznej UŁ, a jeden kompleks został zakupiony (Sigma-Aldrich). Ryciny ze wzorami chemicznymi kompleksów rutenu znajdują się w rozdziale „Opis wyników” (Ryc. 1-5).

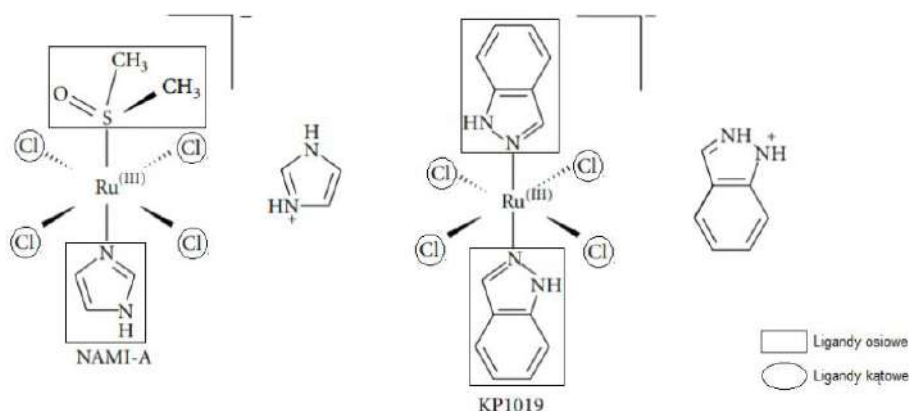
W trakcie analizy właściwości biologicznych kompleksów rutenu badano:

- cytotoksyczność z zastosowaniem testu redukcji resazuryny,
- genotoksyczność z użyciem testu kometowego w wersji alkalicznej,
- zdolność do indukcji apoptozy z użyciem izotiocyanianu fluoresceiny (FITC) sprzężonego z aneksyną V oraz jodku propidyny (PI),
- zdolność do aktywacji kaspaz wykonawczych 3/7 z wykorzystaniem komercyjnego zestawu Caspase-Glo®3/7 Assay kit (Promega, Madison, WI, USA),
- wpływ na przebieg cyklu komórkowego z użyciem PI,
- wpływ na poziom reaktywnych form tlenu (RFT) z użyciem sondy H₂DCF-DA,
- wpływ na ekspresję genu *HMOX1* kodującego oksygenazę hemową 1 (HO-1) z wykorzystaniem PCR w czasie rzeczywistym z użyciem sond TaqMan,
- wpływ na aktywność dysmutazy ponadtlenkowej (SOD) z wykorzystaniem komercyjnego zestawu SOD Assay Kit-WST (Doijindo Molecular Technologies, Kumamoto, Japan),
- zdolność do bezpośredniej interakcji z DNA poprzez test relaksacji plazmidu i dokowanie molekularne.

Opis wyników

Początkowy etap prac nad przygotowaniem rozprawy doktorskiej miał charakter koncepcyjny. Na podstawie dostępnej literatury przygotowany został manuskrypt pt. „Właściwości przeciwnowotworowe związków rutenu – NAMI-A i KP1019” (**publikacja nr 1**), który usystematyzował dostępną wiedzę o związkach rutenowych, a także przybliżył dwa najszersze zbadane pod względem zastosowania terapeutycznego związki rutenowe: NAMI-A oraz KP1019.

NAMI-A ((H₂Im)[*trans*-Ru^{III}Cl₄(DMSO)(Im)]) zawiera w swej strukturze ligandy osiowe: imidazolowy oraz dimetylosulfotlenkowy, ponadto posiada cztery ligandy chlorkowe będące ligandami kątowymi. Z kolei KP1019 ((HInd)[*trans*-Ru^{III}Cl₄(Ind)₂]) posiada dwa ligandy indazolowe będące ligandami osiowymi, a także cztery kątowe ligandy chlorkowe. Wzory strukturalne związków przedstawiono na Ryc. 1.



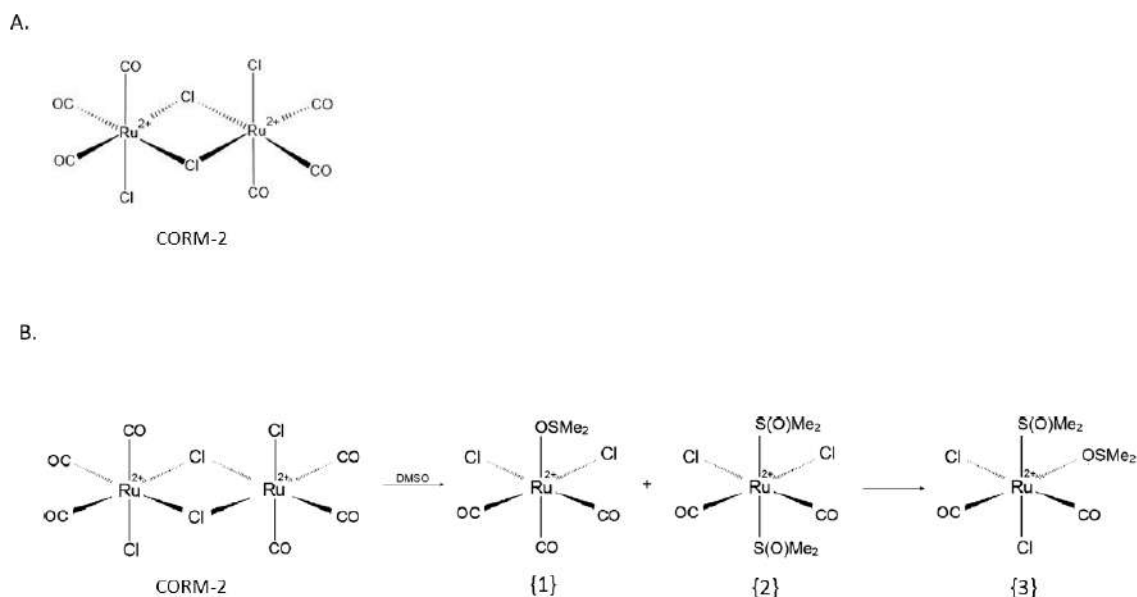
Ryc. 1. Wzory strukturalne NAMI-A oraz KP1019. Na rysunku zaznaczono ligandy obecne w kompleksach, z uwzględnieniem ich podziału na osiowe oraz kątowe.

NAMI-A charakteryzuje się szerokim zakresem właściwości biologicznych. Przeprowadzone badania wykazały zdolność wiązania się NAMI-A do kwasów nukleinowych [16]. Ponadto, wykazano możliwość wiązania się z różnymi białkami, w tym z ferrytyną, co może pozwolić na selektywny transport NAMI-A do wnętrza komórek nowotworowych [17]. Najbardziej obiecującym aspektem działania NAMI-A, są jednak właściwości antymetastatyczne. NAMI-A moduluje proces angiogenezy, najprawdopodobniej poprzez wiązanie tlenu azotu, gazowego transmittera

wykorzystywanego przez komórki nowotworowe w trakcie angiogenezy [18]. Dodatkowo kompleks znacząco obniża ekspresję metaloproteinaz MMP-2 oraz MMP-9, które degradują macierz zewnątrzkomórkową [19]. Ponadto wykazano, że NAMI-A selektywnie wiąże się do włókien kolagenowych, co może utrudniać proces migracji komórek nowotworowych [19].

Kompleks KP1019 oddziałuje na białka cytozolu, przez co prowadzi do stresu oksydacyjnego. Badania wykonane na drożdżach wykazały, że kompleks ten posiada zdolność do indukcji uszkodzeń DNA, co prowadzi do zatrzymania cyklu komórkowego w punkcie kontrolnym związanym z białkiem Rad9 [20]. Związek ten wykazuje także zdolność do tworzenia adduktów z histonem H3 [21]. Dodatkowo intensywne badania transkryptomu drożdży wykazały wpływ KP1019 na procesy takie jak: naprawa uszkodzeń DNA, biogeneza rybosomów, sygnalizacja komórkowa czy też stres osmotyczny [22].

Kolejna praca wchodząca w skład rozprawy doktorskiej (**publikacja nr 2**) dotyczy oceny właściwości biologicznych kompleksu CORM-2 (ang. *tricarbonyldichlororuthenium(II) dimer*) należącego do grupy związków uwalniających tlenek węgla – CORMs (ang. *carbon monoxide-releasing molecules*). Po rozpuszczeniu CORM-2 w roztworze DMSO dochodzi do uwalniania tlenku węgla poprzez wymianę ligandów i przekształceń związku odpowiednio w: *fac*-[RuCl₂(CO)₃(DMSO)] {1} oraz *cis, cis, trans*-[RuCl₂(CO)₂(DMSO)₂] {2}, który z kolei przechodzi w bardziej stabilny *cis-, cis-, cis*-[RuCl₂(CO)₂(DMSO)₂] {3} (odnośniki numerowe – {x} – dotyczą Ryc. 2B). Końcowym produktem reakcji jest CORM-2 w postaci nieaktywnej iCORM-2. Wzór strukturalny CORM-2 przedstawiono na Ryc. 2A.



Ryc. 2. Wzór strukturalny CORM-2 (A), reakcje zachodzące między CORM-2 a DMSO prowadzące do uwolnienia tlenku węgla i rozpadu CORM-2 (B).

Przeprowadzone badania wykazały, że CORM-2 w sposób znaczący wpływa na mechanizmy obrony przed reaktywnymi formami tlenu (RFT), zarówno w warunkach *in vitro*, jak i *in vivo* [23, 24]. Wykazano, że CORM-2 redukuje peroksydację lipidów w osoczu krwi wywołaną przez nadtlenek wodoru [25]. W badaniach przeprowadzonych na myszach CORM-2 redukował stres oksydacyjny indukowany przez doksorubicynę [26]. Prawdopodobnie za antyoksydacyjnymi właściwościami CORM-2 stoi zdolność związku do indukcji oksygenazy hemowej 1 (HO-1), enzymu zaangażowanego w odpowiedź komórki na stres oksydacyjny [27-30].

W pracy doktorskiej wykonywano eksperymenty z CORM-2 oraz iCORM-2. Nieaktywną postać kompleksu uzyskano poprzez rozpuszczenie związku w DMSO oraz całonocną inkubację w temp. 37°C [31]. Doświadczenia przeprowadzono na komórkach jednojądrzastych krwi obwodowej (PBMC) oraz komórkach HL-60. W pierwszym etapie pracy komórki inkubowano z CORM-2 oraz iCORM-2, a następnie dokonano analizy żywotności za pomocą testu redukcji rezasuryny. Zaobserwowano wzrost żywotności po 2 godz. inkubacji z CORM-2 w stężeniu 100 μM dla obu rodzajów komórek. Dłuższa inkubacja komórek (24 godz.) powodowała spadek żywotności, zarówno w przypadku CORM-2, jak i iCORM-2 w stężeniu 100 μM .

Następnie dokonano analizy uszkodzeń DNA oraz kinetyki naprawy DNA z użyciem testu kometowego w wersji alkalicznej. W przypadku komórek PBMC nie zaobserwowano istotnie statystycznego wzrostu uszkodzeń dla CORM-2 oraz iCORM-2 w porównaniu do kontroli. Przeciwna sytuacja miała miejsce w przypadku komórek HL-60, w których zaobserwowano istotnie statystyczny, choć nieznaczny, wzrost uszkodzeń DNA po inkubacji ze związkami w całym zakresie badanych stężeń od 0,01 do 100 μM . Dodatkowo nie odnotowano różnic w poziomie uszkodzeń DNA pomiędzy formą aktywną, a nieaktywną CORM-2.

Analiza kinetyki naprawy DNA wykazała wzrost poziomu uszkodzeń indukowanych przez CORM-2 po 120 min inkubacji naprawczej w komórkach PBMC. W tych komórkach zaobserwowano znaczną różnicę w poziomie uszkodzeń indukowanych przez CORM-2 oraz iCORM-2 po 60 oraz 120 min inkubacji naprawczej. Poziom uszkodzeń DNA dla postaci aktywnej związku zwiększał się w czasie, z kolei w przypadku iCORM uszkodzenia przez cały czas inkubacji naprawczej były na stałym poziomie, zbliżonym do tego obserwowanego w kontroli negatywnej. W komórkach HL-60 nie zaobserwowano wzrostu poziomu uszkodzeń DNA podczas inkubacji naprawczej, zarówno dla CORM-2, jak i iCORM-2.

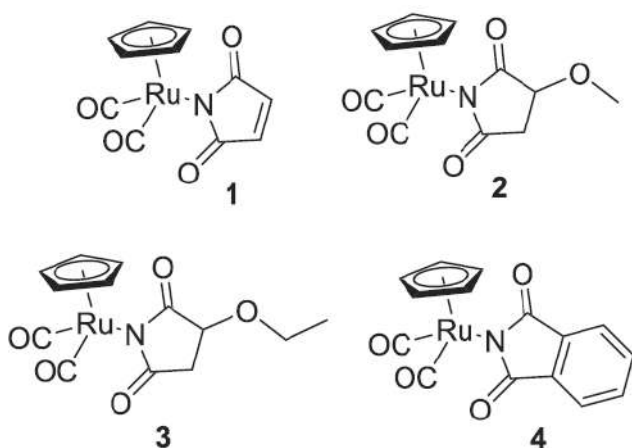
Dokonano także analizy wpływu CORM-2 i iCORM-2 na uszkodzenia oksydacyjne DNA indukowane przez nadtlenek wodoru. W tym celu zastosowano test kometowy w wersji alkalicznej. Wyniki jednoznacznie wykazały, że zarówno CORM-2, jak i iCORM-2 zmniejszają poziom uszkodzeń oksydacyjnych DNA w obu typach komórek. Należy podkreślić, że w przypadku CORM-2 redukcja poziomu uszkodzeń DNA była zdecydowanie większa niż dla iCORM-2 w obu typach komórek.

Kolejna analiza dotyczyła oceny poziomu RFT, mierzonych za pomocą sondy $\text{H}_2\text{DCF-DA}$. W przypadku komórek PBMC zaobserwowano widoczny spadek poziomu RFT indukowanych przez 1 mM nadtlenek wodoru, po pre-inkubacji z CORM-2 oraz iCORM-2. W przypadku 5 mM nadtlenku wodoru zaobserwowano wzrost poziomu RFT dla obu form związku. Bardzo silny efekt antyoksydacyjny CORM-2 zaobserwowano w komórkach HL-60. Pre-inkubacja z CORM-2 znacząco redukowała poziom RFT powstałych w wyniku działania 1 oraz 5 mM nadtlenku wodoru. Pre-inkubacja z iCORM-2 nie wpłynęła w sposób istotny statystycznie na poziom RFT w komórkach HL-60.

Dalsza analiza związana była z określeniem poziomu ekspresji genu *HMOX1* kodującego oksygenazę hemową 1 (HO-1), enzym zaangażowany w odpowiedź

antyoksydacyjną komórek. Względny poziom mRNA określano poprzez zastosowanie reakcji PCR w czasie rzeczywistym przy pomocy sond TaqMan. Wyniki znormalizowano do wartości uzyskanych dla genu referencyjnego *GAPDH*, kodującego dehydrogenazę aldehydu 3-fosfoglicerynowego. Zaobserwowano znaczące zwiększenie poziomu ekspresji genu *HMOX1*, zarówno w PBMC oraz w komórkach HL-60 po inkubacji z CORM-2 w stężeniu 100 μ M. W przypadku PBMC zaobserwowano nieznacznie większy wzrost ekspresji po inkubacji z CORM-2, w porównaniu do iCORM-2. W komórkach HL-60 widoczna jest ponad 50% różnica w indukcji ekspresji pomiędzy CORM-2 a iCORM-2, a nominalnie ekspresja wzrosła niemal 100-krotnie dla CORM-2 i nieco ponad 40-krotnie dla iCORM-2.

Następna publikacja wchodząca w skład niniejszej dysertacji (**publikacja nr 3**) skupiła się na badaniach czterech kompleksów rutenu zsyntetyzowanych przez zespół Profesor Bogny Rudolf z Katedry Chemii Organicznej UŁ. Częścią wspólną wszystkich kompleksów jest obecność rutenowego rdzenia, do którego przyłączone są różne ligandy. Badane kompleksy posiadają następujące ligandy: kompleks 1 (η^5 -cyclopentadienyl)Ru(CO)₂(η^1 -*N*-maleimidato) – ligand maleimidowy; kompleks 2 (η^5 -cyclopentadienyl)Ru(CO)₂-*N*-methoxysuccinimidato oraz kompleks 3 (η^5 -cyclopentadienyl)Ru(CO)₂-*N*-ethoxysuccinimidato – ligand sukcyrimidowy; kompleks 4 (η^5 -cyclopentadienyl)Ru(CO)₂-*N*-phthalimidato – ligand ftalimidowy. Wzory powyższych kompleksów znajdują się na Ryc. 3.



Ryc. 3. Wzory strukturalne kompleksów rutenu 1-4 (publikacja nr 3).

Dane literaturowe dotyczące ligandów, które występują w badanych kompleksach, wskazują na ich zróżnicowane właściwości biologiczne. Maleimid, który w postaci ligandu

obecny jest w kompleksie 1 wykazuje cytotoksyczne działanie względem białaczkowych komórek K562 oraz Jurkat [32]. Z kolei sukcyrimid obecny w postaci ligandu w kompleksach 2 oraz 3 może wykazywać właściwości antyoksydacyjne [33, 34].

W niniejszej pracy badano właściwości biologiczne kompleksów 1-4 względem jednojądrzastych komórek krwi obwodowej (PBMC) oraz komórek HL-60. Ponadto, dokonano analizy związków pełniących rolę ligandów dla poszczególnych kompleksów – maleimidu oraz sukcyrimidu.

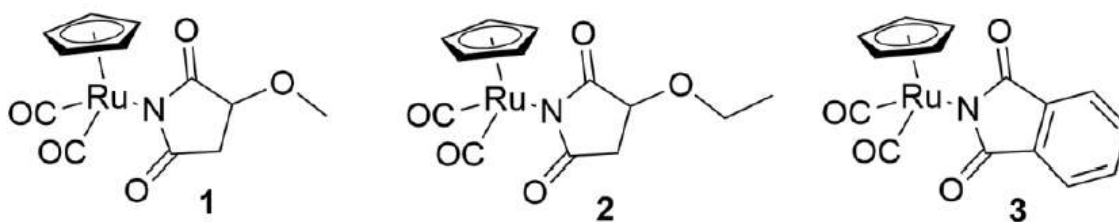
Komórki inkubowano z badanymi kompleksami przez 24 godz., a następnie przeprowadzono analizę żywotności z użyciem testu redukcji resazuryiny. Wyniki wykazały, że najbardziej cytotoksyczny dla obu typów komórek jest kompleks 1. Wartość IC_{50} dla komórek HL-60 była niemal 10-krotnie mniejsza, niż w przypadku PBMC. Kompleksy 2-4 wykazały niewielką cytotoksyczność względem komórek PBMC oraz HL-60. Maleimid był cytotoksyczny na poziomie porównywalnym do kompleksu 1, z kolei sukcyrimid podobnie jak kompleksy 2 oraz 3 nie wpłynął w sposób istotny na żywotność komórek PBMC i HL-60.

Analiza genotoksyczności przeprowadzona za pomocą testu kometowego w wersji alkalicznej wykazała, że związkiem o największym potencjale genotoksycznym jest kompleks 1. Indukował on uszkodzenia DNA od stężenia 25 μ M w przypadku PBMC oraz od stężenia 2,5 μ M w przypadku komórek HL-60. Kompleksy 2-4 nie wykazały właściwości genotoksycznych w komórkach PBMC oraz niewielkie w komórkach HL-60 w stężeniach wyższych niż 50 μ M. Ligand maleimidowy indukował uszkodzenia DNA na zbliżonym poziomie jak kompleks 1, z kolei sukcyrimid nie był genotoksyczny.

Pomiar apoptozy w komórkach HL-60 wykazał jej wyraźną indukcję przez kompleks 1. Istotnie statystyczny wzrost zaobserwowano już w stężeniu 5 μ M, należy podkreślić, że w stężeniach 50 oraz 100 μ M udział komórek apoptotycznych wynosił ponad 90%. Maleimid również wykazał silnie apoptogenne właściwości względem komórek HL-60. Analiza przebiegu cyklu komórkowego wykazała istotnie statystyczne zwiększenie populacji komórek w fazie sub-G1 w przypadku kompleksu 1 w stężeniu 10 μ M, co może świadczyć o wejściu komórek na drogę apoptozy. Inkubacja kompleksów rutenu z genomowym DNA nie wykazała ich zdolności do indukowania pęknięć DNA.

Kolejna publikacja wchodząca w skład rozprawy doktorskiej (**publikacja nr 4**) skupiła się na ocenie właściwości antyoksydacyjnych trzech kompleksów rutenu: kompleksu 1 (η^5 -

cyclopentadienyl)Ru(CO)₂-*N*-methoxysuccinimidato oraz kompleksu 2 (η^5 -cyclopentadienyl)Ru(CO)₂-*N*-ethoxysuccinimidato zawierających ligand sukcyrimidowy oraz kompleksu 3 (η^5 -cyclopentadienyl)Ru(CO)₂-*N*-phthalimidato z ligandem ftalimidowym. Wyniki dotychczas uzyskane wykazały brak właściwości cytotoksycznych tych kompleksów (**publikacja nr 3**), a dostępna literatura wskazuje na możliwy potencjał antyoksydacyjny sukcyrimidu [33, 34]. Z tego powodu zdecydowano o przeprowadzeniu eksperymentów dotyczących właściwości antyoksydacyjnych tych kompleksów. Układ eksperymentalny dla wszystkich oznaczeń obejmował 24 godz. pre-inkubację z kompleksami, a następnie inkubację z nadtlaniem wodoru, pełniącego rolę induktora stresu oksydacyjnego. W pracy przeprowadzono badania na jednojądrzastych komórkach krwi obwodowej (PBMC) oraz na komórkach HL-60. Ponadto, przeprowadzono analizę sukcyrimidu pełniącego funkcję ligandu dla kompleksów 1 oraz 2. Wzory badanych kompleksów w tej publikacji znajdują się na Ryc. 4.



Ryc. 4. Wzory strukturalne kompleksów rutenu 1-3 (publikacja nr 4).

W przypadku oznaczania żywotności komórki PBMC oraz HL-60 pre-inkubowano z kompleksami lub sukcyrimidem w stężeniu 50 μ M przez 24 godz., a następnie inkubowano z nadtlaniem wodoru w stężeniach 0,2, 0,4 oraz 0,6 mM przez 4 godz. Pre-inkubacja ze wszystkimi badanymi kompleksami w sposób istotny statystycznie zwiększała żywotność komórek obu typów. Analogiczna sytuacja miała miejsce w przypadku sukcyrimidu.

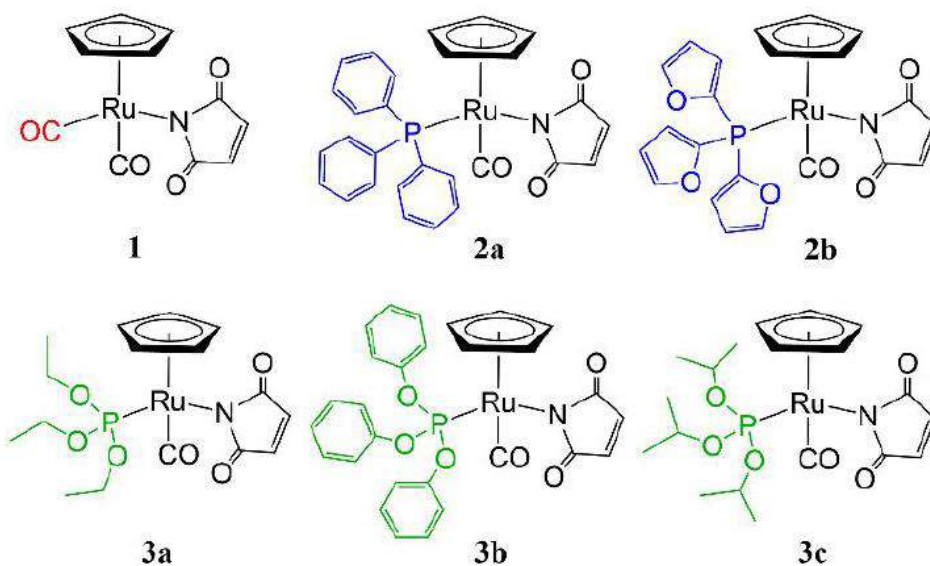
Analiza przebiegu cyklu komórkowego wykazała, że pre-inkubacja z kompleksami 1-3 w sposób istotnie statystyczny zredukowała odsetek komórek występujących w fazie sub-G1. Świadczy to o zmniejszeniu się populacji komórek apoptotycznych. Podobne właściwości wykazał sukcyrimid. Ocena genotoksyczności przeprowadzona w teście kometowym w wersji alkalicznej wykazała, że kompleksy 1-3 znacząco obniżyły oksydacyjne

uszkodzenia DNA w przypadku komórek HL-60. Z kolei w przypadku PBMC, jedynie kompleks 1 obniżył poziom tych uszkodzeń. Sukcynimid w stężeniu 50 μM zmniejszył uszkodzenia DNA jedynie w komórkach HL-60.

W przypadku eksperymentu pozwalającego na pomiar RFT z zastosowaniem sondy $\text{H}_2\text{DCF-DA}$ komórki pre-inkubowano przez 24 godz. z kompleksami 1-3 lub sukcyinidem w stężeniu 50 μM , a następnie inkubowano przez 30 min z nadtlakiem wodoru w stężeniach 1 lub 5 mM. Analiza uzyskanych wyników wykazała, że w przypadku komórek PBMC pre-inkubacja z kompleksami 1 oraz 2 obniżyła poziom RFT, z kolei kompleks 3 oraz sukcyinimid zwiększyły poziom RFT, co jest szczególnie widoczne dla stężenia 5 mM nadtlaku wodoru. Odmienna sytuacja ma miejsce w przypadku komórek HL-60, w których pre-inkubacja z kompleksami 1-3 lub sukcyinidem znacząco obniżyła poziom RFT dla obu stężeń nadtlaku wodoru.

Kolejne oznaczenie dotyczyło pomiaru aktywności dysmutazy nadtlakowej (SOD). Nadtlak wodoru obniża aktywność dysmutazy nadtlakowej [35]. Badania przeprowadzone w ramach pracy doktorskiej wykazały, że kompleksy 1 oraz 2 przywracają aktywność dysmutazy nadtlakowej w przypadku PBMC. Wszystkie badane kompleksy przywróciły aktywność dysmutazy nadtlakowej w komórkach HL-60. Sukcyinimid nie wpłynął na aktywność SOD w przypadku PBMC, natomiast przywrócił aktywność tego enzymu w komórkach HL-60.

Kolejna publikacja składająca się na niniejszą dysertację (**publikacja nr 5**) dotyczyła pięciu nowych kompleksów rutenu: 2a $\text{CpRu}(\text{CO})(\text{PPh}_3)(\eta^1\text{-N-maleimidato})$, 2b $\text{CpRu}(\text{CO})(\text{P}(\text{Fu})_3)(\eta^1\text{-N-maleimidato})$, 3a $\text{CpRu}(\text{CO})(\text{P}(\text{OEt})_3)(\eta^1\text{-N-maleimidato})$, 3b $\text{CpRu}(\text{CO})(\text{P}(\text{OPh})_3)(\eta^1\text{-N-maleimidato})$ oraz 3c $\text{CpRu}(\text{CO})(\text{P}(\text{OiPr})_3)(\eta^1\text{-N-maleimidato})$, które zawierają rutenowy rdzeń oraz ligand maleimidowy. Dodatkowo dołączone są do nich ligandy fosforoorganiczne: fosfinowy w kompleksach 2a-b oraz fosforynowy w przypadku kompleksów 3a-c. Wzory kompleksów analizowanych w publikacji nr 5 znajdują się na Ryc. 5.



Ryc. 5. Wzory strukturalne kompleksów rutenu 1, 2a-b oraz 3a-c (publikacja nr 5).

Badania przeprowadzone w ramach tej publikacji prowadzono na jednojądrzastych komórkach krwi obwodowej (PBMC), na komórkach HL-60 oraz na komórkach HL-60/DR opornych na doksorubicynę.

Wyniki oznaczenia żywotności wykazały, że kompleksy 1, 2a oraz 3a charakteryzują się ponad 10-krotnie mniejszymi wartościami IC_{50} dla komórek HL-60 w porównaniu do PBMC. Z kolei kompleksy 2b, 3b oraz 3c wykazywały zbliżone wartości IC_{50} dla komórek HL-60 oraz PBMC. W przypadku komórek HL-60/DR efekt cytotoksyczny kompleksów był wyraźnie mniejszy niż w przypadku komórek HL-60. Na podstawie uzyskanych wyników do dalszych badań wybrano kompleksy 1, 2a oraz 3a.

Ocena genotoksyczności wykazała, że kompleksy 1, 2a oraz 3a indukują uszkodzenia DNA w stężeniach od 25 μM w przypadku komórek HL-60. W przypadku komórek PBMC efekt genotoksyczny wykazał jedynie kompleks 1. Żaden z kompleksów nie indukował uszkodzeń DNA w komórkach HL-60/DR.

Kolejny aspekt analizy genotoksyczności kompleksów rutenu dotyczył możliwości bezpośredniego oddziaływania z DNA. W tym celu zastosowano test relaksacji plazmidu. Po 2 godz. inkubacji zaobserwowano formę otwartą kolistą (OC) plazmidu dla kompleksów 2b oraz 3a-c. Z kolei po 24 godz. inkubacji w przypadku wszystkich badanych kompleksów zaobserwowano powstanie formy OC, co świadczy o indukcji jednoniciowych pęknięć DNA.

W przypadku kompleksu 3c stwierdzono także obecność formy liniowej (L) plazmidu po inkubacji 24 godz., co może świadczyć o indukcji dwuniciowych pęknięć DNA.

Wykazano ponadto, że kompleksy 1, 2a oraz 3a w stężeniu 10 μ M indukowały apoptozę w komórkach HL-60. Natomiast w przypadku komórek HL-60/DR żaden z badanych kompleksów rutenu nie wpłynął w sposób istotny na indukcję apoptozy.

Dodatkowo przeprowadzono oznaczenie aktywności kaspaz wykonawczych 3/7 w komórkach HL-60. Wyniki wykazały, że kompleksy rutenu 1, 2a oraz 3a w stężeniu 10 μ M w sposób znaczący zwiększyły aktywność kaspaz 3/7.

Badanie kinetyki zmian poziomu RFT wykazało, że kompleksy 1, 2a oraz 3a nie indukują RFT w czasie 2 godz. inkubacji. Wynik ten wyklucza indukcję RFT jako mechanizm odpowiedzialny za cyto- oraz genotoksyczność badanych kompleksów rutenu.

Przeprowadzono także dokowanie molekularne, które miało na celu sprawdzenie możliwości przyłączania się kompleksów rutenu do DNA. Badania obejmowały dwa fragmenty DNA reprezentujące odpowiednio w pełni komplementarny fragment DNA (1BNA) oraz fragment posiadający niesparowanie (4E1U). Badania wykazały, że kompleksy rutenu 1, 2a oraz 3a wiążą się do fragmentu 1BNA, niemniej powinowactwo do fragmentu 4E1U jest większe. Wynik ten sugeruje większy potencjał kompleksów rutenu do wiązania się z uszkodzonym DNA.

Podsumowanie wyników

Wyniki uzyskane w trakcie realizacji pracy doktorskiej wskazują, że badane kompleksy rutenu mają znaczące działanie biologiczne względem komórek prawidłowych PBMC oraz komórek nowotworowych HL-60 w warunkach *in vitro*.

W przypadku kompleksu CORM-2, zarówno w formie aktywnej jak i nieaktywnej iCORM-2, zaobserwowano, że w wysokich stężeniach zmniejszał żywotność komórek PBMC oraz HL-60 (publikacja nr 2). Ponadto wykazano, że CORM-2 indukuje niewielkie uszkodzenia DNA w komórkach HL-60, jednak są one efektywnie naprawiane. CORM-2 znacząco obniżył poziom RFT indukowanych przez 1 mM nadtlenek wodoru, z kolei iCORM-2 wykazał efekt przeciwny dla obu zastosowanych stężeń nadtlenu wodoru (1 mM i 5 mM). Zarówno CORM-2, jak i iCORM-2, zwiększyły poziom ekspresji genu *HMOX1*, kodującego oksygenazę hemową 1 w komórkach PBMC oraz HL-60, niemniej forma aktywna kompleksu indukowała ekspresję znacznie wyraźniej. Ponadto wykazano, że pre-inkubacja z CORM-2 oraz iCORM-2 zmniejsza uszkodzenia oksydacyjne DNA indukowane przez nadtlenek wodoru. Uzyskane wyniki sugerują, że zarówno CORM-2 jak i iCORM-2 wykazują właściwości biologiczne. Głównym czynnikiem odpowiedzialnym za efekt biologiczny CORM-2 wydaje się być tlenek węgla. Należy jednak mieć na uwadze, że iCORM-2 również wykazuje właściwości biologiczne.

Badania nad kompleksami: $(\eta^5\text{-cyclopentadienyl})\text{Ru}(\text{CO})_2(\eta^1\text{-}N\text{-maleimidato})$ (kompleks 1), $(\eta^5\text{-cyclopentadienyl})\text{Ru}(\text{CO})_2\text{-}N\text{-methoxysuccinimidato}$ (kompleks 2), $(\eta^5\text{-cyclopentadienyl})\text{Ru}(\text{CO})_2\text{-}N\text{-ethoxysuccinimidato}$ (kompleks 3) i $(\eta^5\text{-cyclopentadienyl})\text{Ru}(\text{CO})_2\text{-}N\text{-phthalimidato}$ (kompleks 4) wykazały ich zróżnicowane właściwości biologiczne (publikacja nr 3). Kompleks zawierający ligand maleimidowy $(\eta^5\text{-cyclopentadienyl})\text{Ru}(\text{CO})_2(\eta^1\text{-}N\text{-maleimidato})$ (kompleks 1) wykazał znaczne właściwości cytotoksyczne, genotoksyczne, apoptogenne oraz zwiększył populację komórek w fazie sub-G1. Ponadto, kompleks ten wykazał znacznie mniejszy efekt cyto- oraz genotoksyczny w komórkach PBMC w porównaniu do komórek nowotworowych HL-60. Skłania to do prowadzenia dalszych badań nad tym kompleksem w aspekcie jego potencjalnych właściwości przeciwnowotworowych. Z kolei kompleksy rutenu zawierające ligand sukcyimidowy $(\eta^5\text{-cyclopentadienyl})\text{Ru}(\text{CO})_2\text{-}N\text{-methoxysuccinimidato}$ (kompleks 2) oraz $(\eta^5\text{-cyclopentadienyl})\text{Ru}(\text{CO})_2\text{-}N\text{-ethoxysuccinimidato}$ (kompleks 3), a także $(\eta^5\text{-cyclopentadienyl})\text{Ru}(\text{CO})_2\text{-}N\text{-phthalimidato}$ (kompleks 4), wykazały również właściwości biologiczne.

cyclopentadienyl)Ru(CO)₂-N-phthalimidato (kompleks 4) z ligandem ftalimidowym wykazały jedynie niewielką cytotoksyczność względem komórek nowotworowych. Otrzymane wyniki wskazują na kluczowe znaczenie ligandów obecnych w kompleksach rutenu – maleimidowego i sukcyimidowego dla ich właściwości biologicznych.

Wykazano, że pre-inkubacja z kompleksami rutenu zawierającymi ligand sukcyimidowy: (η^5 -cyclopentadienyl)Ru(CO)₂-N-methoxysuccinimidato (kompleks 1), (η^5 -cyclopentadienyl)Ru(CO)₂-N-ethoxysuccinimidato (kompleks 2) oraz (η^5 -cyclopentadienyl)Ru(CO)₂-N-phthalimidato (kompleks 3) zwiększyła żywotność komórek PBMC oraz HL-60 inkubowanych z nadtlaniem wodoru (publikacja nr 4). Dodatkowo kompleksy te wyraźnie zredukowały populację komórek HL-60 znajdującą się w fazie sub-G1 cyklu komórkowego. Kompleksy rutenu z ligandem sukcyimidowym oraz ftalimidowym istotnie zredukowały poziom uszkodzeń oksydacyjnych DNA oraz zmniejszyły poziom RFT indukowanych przez nadtlenek wodoru. Ponadto badania wykazały, że kompleksy rutenu przywróciły aktywność dysmutazy ponadtlenkowej (SOD). Uzyskane wyniki wskazują, że kompleksy zawierające ligand sukcyimidowy oraz ftalimidowy wykazują właściwości antyoksydacyjne.

Analiza żywotności komórek PBMC, HL-60 oraz HL-60/DR wykazała, że kompleksy zawierające ligand maleimidowy (η^5 -cyclopentadienyl)Ru(CO)₂(η^1 -N-maleimidato) (kompleks 1), CpRu(CO)(PPh₃)(η^1 -N-maleimidato) (kompleks 2a), CpRu(CO)(P(Fu)₃)(η^1 -N-maleimidato) (kompleks 2b), CpRu(CO)(P(OEt)₃)(η^1 -N-maleimidato) (kompleks 3a), CpRu(CO)(P(OPh)₃)(η^1 -N-maleimidato) (kompleks 3b) i CpRu(CO)(P(OiPr)₃)(η^1 -N-maleimidato) (kompleks 3c), wykazują znaczące właściwości cytotoksyczne jedynie względem komórek HL-60 (publikacja nr 5). Dla komórek HL-60/DR efekt cytotoksyczny jest zdecydowanie mniejszy. Wśród badanych kompleksów trzy z nich: (η^5 -cyclopentadienyl)Ru(CO)₂(η^1 -N-maleimidato) (kompleks 1), CpRu(CO)(PPh₃)(η^1 -N-maleimidato) (kompleks 2a) oraz CpRu(CO)(P(OEt)₃)(η^1 -N-maleimidato) (kompleks 3a) wykazały niewielką cytotoksyczność względem komórek prawidłowych. Wszystkie z trzech wyżej wymienionych kompleksów wykazały silne właściwości apoptogenne. Kompleksy te mogą oddziaływać bezpośrednio z DNA, co potwierdziły badania *in silico* oraz test konformacji plazmidu. Przeprowadzone analizy wykluczyły generowanie RFT jako mechanizm odpowiadający za cyto- oraz genotoksyczność kompleksów rutenu. Uzyskane wyniki sugerują, że CpRu(CO)(PPh₃)(η^1 -N-maleimidato) (kompleks 2a)

i $\text{CpRu}(\text{CO})(\text{P}(\text{OEt})_3)(\eta^1\text{-N-maleimidato})$ (kompleks 3a) wykazują znaczący potencjał przeciwnowotworowy, jednocześnie nie wykazując działania cytotoksycznego względem komórek prawidłowych.

Wyniki zaprezentowane w ramach niniejszej rozprawy doktorskiej dotyczą modelu badawczego *in vitro* opartego na komórkach prawidłowych PBMC oraz komórkach nowotworowych HL-60. Stanowią one podstawę do dalszych, bardziej szczegółowych analiz dotyczących biologicznych właściwości kompleksów rutenu. Różnorodność efektów biologicznych wykazywanych przez badane kompleksy rutenu skłania do prowadzenia dalszych badań w dwóch niezależnych kierunkach – analizy aktywności przeciwnowotworowej oraz oceny potencjału antyoksydacyjnego.

Wnioski

Uzyskane w pracy wyniki pozwalają na sformułowanie następujących wniosków:

- Kompleksy rutenu w zależności od ligandów wykazują szereg właściwości biologicznych w komórkach prawidłowych PBMC i nowotworowych HL-60.
- Tlenek węgla uwalniany z kompleksu CORM-2 odpowiada za właściwości antyoksydacyjne tego związku.
- Kompleksy rutenu zawierające ligand maleimidowy wykazują znacznie silniejsze właściwości cyto- oraz genotoksyczne w porównaniu do kompleksów zawierających ligand sukcyimidowy i ftalimidowy.
- Kompleksy rutenu zawierające ligand sukcyimidowy i ftalimidowy wykazują właściwości antyoksydacyjne w komórkach prawidłowych PBMC i nowotworowych HL-60.
- Dwa kompleksy rutenu zawierające ligand maleimidowy oraz ligandy fosforoorganiczne – fosfinowy $\text{CpRu}(\text{CO})(\text{PPh}_3)(\eta^1\text{-N-maleimidato})$ (kompleks 2a) i fosforynowy $\text{CpRu}(\text{CO})(\text{P}(\text{OEt})_3)(\eta^1\text{-N-maleimidato})$ (kompleks 3a) są cyto- i genotoksyczne jedynie dla komórek HL-60.

Literatura uzupełniająca:

1. Sahu A. K. , Dash D. K. , Mishra K., P. Mishra S., Yadav R., Kashyap P. (2018). Properties and Applications of Ruthenium. In M. S. Seehra, & A. D. Bristow (Eds.), Noble and Precious Metals – Properties, Nanoscale Effects and Applications. IntechOpen. <https://doi.org/10.5772/intechopen.76393>
2. Zuba I, Zuba M, Piotrowski M, Pawlukojć A. Ruthenium as an important element in nuclear energy and cancer treatment. *Appl Radiat Isot.* 2020;162:109176. Doi:10.1016/j.apradiso.2020.109176
3. Katsuhiko Nose, Toru H. Okabe, Chapter 2.10 – Platinum Group Metals Production, Editor(s): Seshadri Seetharaman, Treatise on Process Metallurgy, Elsevier, 2014, Pages 1071-1097, ISBN 9780080969886
4. Godlewska-Żyłkiewicz B, Zambrzycka E, Leśniewska B, Wilczewska AZ. Separation of ruthenium from environmental samples on polymeric sorbent based on imprinted Ru(III)-allyl acetoacetate complex. *Talanta.* 2012;89:352-359. Doi:10.1016/j.talanta.2011.12.040
5. Rosenberg B, VanCamp L, Trosko JE, Mansour VH. Platinum compounds: a new class of potent antitumour agents. *Nature.* 1969;222(5191):385-386. Doi:10.1038/222385a0
6. Simpson PV, Desai NM, Casari I, Massi M, Falasca M. Metal-based antitumor compounds: beyond cisplatin. *Future Med Chem.* 2019;11(2):119-135. Doi:10.4155/fmc-2018-0248
7. Gasser G, Ott I, Metzler-Nolte N. Organometallic anticancer compounds. *J Med. Chem.* 2011;54(1):3-25. Doi:10.1021/jm100020w
8. Ferraro MG, Piccolo M, Misso G, Santamaria R, Irace C. Bioactivity and Development of Small Non-Platinum Metal-Based Chemotherapeutics. *Pharmaceutics.* 2022;14(5):954. Published 2022 Apr 28. Doi:10.3390/pharmaceutics14050954
9. Jabłońska-Wawrzycka A, Rogala P, Michałkiewicz S, Hodorowicz M, Barszcz B. Ruthenium complexes in different oxidation states: synthesis, crystal structure, spectra and redox properties. *Dalton Trans.* 2013;42(17):6092-6101. Doi:10.1039/c3dt32214a
10. Schluga P, Hartinger CG, Egger A, et al. Redox behavior of tumor-inhibiting ruthenium(III) complexes and effects of physiological reductants on their binding to GMP. *Dalton Trans.* 2006;(14):1796-1802. Doi:10.1039/b511792e

11. Trédan O, Galmarini CM, Patel K, Tannock IF. Drug resistance and the solid tumor microenvironment. *J Natl Cancer Inst.* 2007;99(19):1441-1454. Doi:10.1093/jnci/djm135
12. Liang JX, Zhong HJ, Yang G, Vellaisamy K, Ma DL, Leung CH. Recent development of transition metal complexes with in vivo antitumor activity. *J Inorg Biochem.* 2017;177:276-286. Doi:10.1016/j.jinorgbio.2017.06.002
13. Lodhi MS, Khan MT, Bukhari SMH, et al. Probing Transferrin Receptor Overexpression in Gastric Cancer Mice Models. *ACS Omega.* 2021;6(44):29893-29904. Published 2021 Oct 27. Doi:10.1021/acsomega.1c04382
14. Lucaciu RL, Hangan AC, Sevastre B, Oprean LS. Metallo-Drugs in Cancer Therapy: Past, Present and Future. *Molecules.* 2022;27(19):6485. Published 2022 Oct 1. Doi:10.3390/molecules27196485
15. Lee SY, Kim CY, Nam TG. Ruthenium Complexes as Anticancer Agents: A Brief History and Perspectives. *Drug Des Devel Ther.* 2020;14:5375-5392. Published 2020 Dec 3. Doi:10.2147/DDDT.S275007
16. Groessl M, Tsybin YO, Hartinger CG, Keppler BK, Dyson PJ. Ruthenium versus platinum: interactions of anticancer metallodrugs with duplex oligonucleotides 27onization27ed by electrospray 27onization mass spectrometry. *J Biol Inorg Chem.* 2010;15(5):677-688. Doi:10.1007/s00775-010-0635-0
17. Ciambellotti S, Pratesi A, Severi M, et al. The NAMI A – human ferritin system: a biophysical characterization. *Dalton Trans.* 2018;47(33):11429-11437. Doi:10.1039/c8dt00860d
18. Castellarin A., Zorzet S., Bergamo A., Sava G.: Pharmacological activities of ruthenium complexes related to their NO scavenging properties. *Int. J. Mol. Sci.*, 2016; 17: E1254
19. Gu L, Li X, Ran Q, Kang C, Lee C, Shen J. Antimetastatic activity of novel ruthenium (III) pyridine complexes. *Cancer Med.* 2016;5(10):2850-2860. Doi:10.1002/cam4.826
20. Bierle LA, Reich KL, Taylor BE, et al. DNA Damage Response Checkpoint Activation Drives KP1019 Dependent Pre-Anaphase Cell Cycle Delay in *S. cerevisiae* [published correction appears in *PLoS One.* 2015;10(10):e0141518]. *PLoS One.* 2015;10(9):e0138085
21. Singh V, Azad GK, Mandal P, Reddy MA, Tomar RS. Anti-cancer drug KP1019 modulates epigenetics and induces DNA damage response in *Saccharomyces cerevisiae*. *FEBS Lett.* 2014;588(6):1044-1052. Doi:10.1016/j.febslet.2014.02.017

22. Golla U, Swagatika S, Chauhan S, Tomar RS. A systematic assessment of chemical, genetic, and epigenetic factors influencing the activity of anticancer drug KP1019 (FFC14A). *Oncotarget*. 2017;8(58):98426-98454. Published 2017 Sep 30. Doi:10.18632/oncotarget.21416
23. Zhang DD, Liang YF, Qi J, et al. Carbon Monoxide Attenuates High Salt-Induced Hypertension While Reducing Pro-inflammatory Cytokines and Oxidative Stress in the Paraventricular Nucleus. *Cardiovasc Toxicol*. 2019;19(5):451-464. Doi:10.1007/s12012-019-09517-w
24. Lee CW, Chi MC, Hsu LF, et al. Carbon monoxide releasing molecule-2 protects against particulate matter-induced lung inflammation by inhibiting TLR2 and 4/ROS/NLRP3 inflammasome activation. *Mol Immunol*. 2019;112:163-174. Doi:10.1016/j.molimm.2019.05.005
25. Adach W, Olas B. The role of CORM-2 as a modulator of oxidative stress and hemostatic parameters of human plasma in vitro. *PloS One*. 2017;12(9):e0184787. Doi:10.1371/journal.pone.0184787
26. Soni H, Pandya G, Patel P, Acharya A, Jain M, Mehta AA. Beneficial effects of carbon monoxide-releasing molecule-2 (CORM-2) on acute doxorubicin cardiotoxicity in mice: role of oxidative stress and apoptosis. *Toxicol Appl Pharmacol*. 2011;253(1):70-80. Doi:10.1016/j.taap.2011.03.013
27. Moon H, Jang JH, Jang TC, Park GH. Carbon Monoxide Ameliorates 6-Hydroxydopamine-Induced Cell Death in C6 Glioma Cells. *Biomol Ther*. 2018;26(2):175-181. Doi:10.4062/biomolther.2018.009
28. Park SJ, Lee SK, Lim CR, et al. Heme oxygenase-1/carbon monoxide axis suppresses transforming growth factor- β 1-induced growth inhibition by increasing ERK1/2-mediated phosphorylation of Smad3 at Thr-179 in human hepatocellular carcinoma cell lines. *Biochem Biophys Res Commun*. 2018;498(3):609-615. Doi:10.1016/j.bbrc.2018.03.030
29. Chien PT, Lin CC, Hsiao LD, Yang CM. Induction of HO-1 by carbon monoxide releasing molecule-2 attenuates thrombin-induced COX-2 expression and hypertrophy in primary human cardiomyocytes. *Toxicol Appl Pharmacol*. 2015;289(2):349-359. Doi:10.1016/j.taap.2015.09.009
30. Yang CM, Lin CC, Lee IT, et al. c-Src-dependent transactivation of EGFR mediates CORM-2-induced HO-1 expression in human tracheal smooth muscle cells. *J Cell Physiol*. 2015;230(10):2351-2361. Doi:10.1002/jcp.24912

31. Babu D, Leclercq G, Motterlini R, Lefebvre RA. Differential Effects of CORM-2 and CORM-401 in Murine Intestinal Epithelial MODE-K Cells under Oxidative Stress. *Front Pharmacol.* 2017;8:31. Published 2017 Feb 8. Doi:10.3389/fphar.2017.00031
32. Machado KE, de Oliveira KN, Andreossi HM, et al. Apoptotic events induced by maleimides on human acute leukemia cell lines. *Chem Res Toxicol.* 2013;26(12):1904-1916. Doi:10.1021/tx400284r
33. Alshehri OM, Mahnashi MH, Sadiq A, et al. Succinimide Derivatives as Antioxidant Anticholinesterases, Anti- α -Amylase, and Anti- α -Glucosidase: In Vitro and In Silico Approaches. *Evid Based Complement Alternat Med.* 2022;2022:6726438. Published 2022 Jul 30. Doi:10.1155/2022/6726438
34. Sadiq A, Mahmood F, Ullah F, et al. Synthesis, anticholinesterase and antioxidant potentials of ketoesters derivatives of succinimides: a possible role in the management of Alzheimer's. *Chem Cent J.* 2015;9:31. Published 2015 May 26. Doi:10.1186/s13065-015-0107-2
35. Gottfredsen RH, Larsen UG, Enghild JJ, Petersen SV. Hydrogen peroxide induce modifications of human extracellular superoxide dismutase that results in enzyme inhibition. *Redox Biol.* 2013;1(1):24-31. Published 2013 Jan 11. Doi:10.1016/j.redox.2012.12.004

Streszczenie

W niniejszej pracy doktorskiej pt. „Ocena właściwości biologicznych kompleksów rutenu w badaniach *in vitro*” dokonano analizy dziesięciu kompleksów rutenu pod kątem ich właściwości biologicznych.

Badania wykonano na jednojądrzastych komórkach krwi obwodowej (PBMC) izolowanych z kożuszków leukocyтарно-пłytkowych, pochodzących od zdrowych dawców, na komórkach ostrej białaczki promielocytowej HL-60 oraz na komórkach HL-60/DR opornych na doksorubicynę.

Realizacja celu badawczego, którym była ocena właściwości biologicznych kompleksów rutenu w warunkach *in vitro*, odbyła się poprzez analizę:

- cytotoksyczności,
- genotoksyczności,
- możliwości indukcji apoptozy,
- przebiegu cyklu komórkowego,
- indukcji reaktywnych form tlenu (RFT),
- wpływu na oksydacyjne uszkodzenia DNA,
- indukcji genu *HMOX1* kodującego oksygenazę hemową 1 (HO-1),
- wpływu na aktywność dysmutazy ponadtlenkowej (SOD),
- wpływu na aktywność kaspaz 3/7,
- bezpośredniej interakcji z DNA.

Uzyskane wyniki pozwoliły na wyodrębnienie kompleksów rutenu cechujących się właściwościami antyoksydacyjnymi – są to kompleksy z ligandem sukcyrimidowym (η^5 -cyclopentadienyl)Ru(CO)₂-*N*-methoxysuccinimidato oraz (η^5 -cyclopentadienyl)Ru(CO)₂-*N*-ethoxysuccinimidato i ligandem ftalimidowym (η^5 -cyclopentadienyl)Ru(CO)₂-*N*-phthalimidato (publikacji nr 4) oraz CORM-2 (publikacja nr 2), a także właściwościami cytotoksycznymi i genotoksycznymi – są to kompleksy z ligandem maleimidowym (publikacje nr 3 i 5). Kompleksy o potencjale antyoksydacyjnym znacząco obniżały poziom uszkodzeń oksydacyjnych DNA oraz poziom RFT. Wśród kompleksów o właściwościach cytotoksycznych największy potencjał wykazywały kompleksy (η^5 -cyclopentadienyl)Ru(CO)₂(η^1 -*N*-maleimidato), CpRu(CO)(PPh₃)(η^1 -*N*-maleimidato) oraz

$\text{CpRu(CO)(P(OEt)}_3)(\eta^1\text{-}N\text{-maleimidato)}$). Kompleksy te znacząco obniżały żywotność komórek nowotworowych HL-60, indukowały w nich uszkodzenia DNA oraz apoptozę. W przypadku komórek opornych na doksorubicynę HL-60/DR kompleksy te nie wykazywały znaczącego efektu cytotoksycznego i genotoksycznego.

Przeprowadzona w niniejszej pracy doktorskiej analiza aktywności biologicznej nowych kompleksów rutenu pozwoliła na wyselekcjonowanie związków cyto- oraz genotoksycznych dla komórek HL-60, a z drugiej strony, także kompleksów o potencjale antyoksydacyjnym. Stwarza to możliwość prowadzenia dalszych badań nad kompleksami rutenu w dwóch niezależnych kierunkach – analizy właściwości przeciwnowotworowych oraz antyoksydacyjnych.

Summary

In the present dissertation "Assessment of biological properties of ruthenium complexes in *in vitro* studies" ten ruthenium complexes were analyzed in terms of their biological properties.

The tests were performed on peripheral blood mononuclear cells (PBMC) isolated from buffy coats from healthy donors, on HL-60 acute promyelocytic leukemia cells, and on HL-60/DR cells resistant to doxorubicin.

The research objective, which was the assessment of the biological properties of ruthenium complexes *in vitro*, was carried out by analyzing:

- cytotoxicity,
- genotoxicity,
- induction of apoptosis,
- cell cycle arrest,
- induction of reactive oxygen species (ROS),
- influence on oxidative DNA damage,
- induction of the *HMOX1* gene encoding heme oxygenase 1 (HO-1),
- influence on the activity of superoxide dismutase (SOD),
- influence on the activity of caspases 3/7,
- direct interaction with DNA,

The obtained results allowed for the selection of ruthenium complexes with antioxidant properties – complexes with succinimide ligand (η^5 -cyclopentadienyl)Ru(CO)₂-*N*-methoxysuccinimidato and (η^5 -cyclopentadienyl)Ru(CO)₂-*N*-ethoxysuccinimidato and phthalimide ligand (η^5 -cyclopentadienyl)Ru(CO)₂-*N*-phthalimidato (publication no. 4) and CORM-2 (publication no. 2), as well as cytotoxic and genotoxic properties – complexes with maleimide ligand (publications no. 3 and 5). Complexes with antioxidant potential significantly reduced the level of oxidative DNA damage and the level of ROS. Among the complexes with cytotoxic properties, the highest potential was shown by complexes (η^5 -cyclopentadienyl)Ru(CO)₂(η^1 -*N*-maleimidato), CpRu(CO)(PPh₃)(η^1 -*N*-maleimidato) and CpRu(CO)(P(OEt)₃)(η^1 -*N*-maleimidato). These complexes significantly reduced the viability

of HL-60 cancer cells, induced DNA damage and apoptosis. In the case of HL-60/DR cells, these complexes did not show significant cytotoxic and genotoxic effects.

The analysis of the biological activity of the new ruthenium complexes carried out in this doctoral thesis allowed for the selection of cytotoxic and genotoxic compounds for HL-60 cells, and on the other hand, also complexes with antioxidant potential. This creates the possibility of conducting future research on ruthenium complexes in two independent directions – anticancer and antioxidant properties.

Publikacje będące podstawą rozprawy doktorskiej

Received: 21.05.2019
Accepted: 12.09.2019
Published: 19.02.2020

Właściwości przeciwnowotworowe związków rutenu – NAMI-A i KP1019

Anti-cancer properties of ruthenium compounds: NAMI-A and KP1019

Michał Juszczak, Magdalena Kluska, Daniel Wysokiński, Katarzyna Woźniak

Katedra Genetyki Molekularnej, Wydział Biologii i Ochrony Środowiska, Uniwersytet Łódzki

Streszczenie

Badania nad nowymi terapiami nowotworów to jedno z najważniejszych wyzwań współczesnej medycyny i biologii. Wiele dekad badań przyniosło wymierne korzyści zarówno w poznaniu mechanizmów molekularnych leżących u podstaw nowotworzenia, jak i w postaci rozwoju metod terapii nowotworów. Mimo to nowotwory nadal do schorzeń o najwyższej śmiertelności, a ich zwalczanie w wielu przypadkach jest nieskuteczne i obciążone wieloma działaniami niepożądanymi. Strategie terapeutyczne, dotyczące zarówno celowanego działania w ogniska komórek nowotworowych, jak i zapobieganie ich przerzutowaniu, skupiają się przede wszystkim na poszukiwaniu nowych związków chemicznych, wśród których istotną rolę zajmują kompleksy zawierające różne metale. Duże nadzieje wiąże się obecnie ze związkami zawierającymi ruten, a w artykule przedstawiono stan wiedzy nad zastosowaniem w terapii antynowotworowej dwóch związków tego typu – NAMI-A i KP1019.

Słowa kluczowe:

kompleksy rutenu • NAMI-A • KP1019 • cytotoksyczność • metastaza • transferyna

Summary

Cancer research is among the key challenges in current medicine and biology. Many decades of investigations have brought measurable benefits in both areas with regard to expanding the knowledge of the molecular mechanism of cancer and developing treatment strategies. Despite that cancers are still among diseases with the highest mortality rate, and cancer treatment is often unsuccessful and connected with severe side effects. The development of therapeutic strategies in both targeting the primary tumor origin and preventing metastasis is largely based on testing newly synthesized chemical agents, including a group of metal-containing complexes. It seems that ruthenium-containing complexes are of high potential in cancer therapy, and our work presents the current data about the application of ruthenium-based complexes – NAMI-A and KP1019 in cancer therapy.

Keywords:

ruthenium complexes • NAMI-A • KP1019 • cytotoxicity • metastasis • transferrin

GICID 01.3001.0013.8549
DOI: 10.5604/01.3001.0013.8549
Word count: 4621
Tables: –
Figures: 3
References: 62

Adres autorki: prof. dr hab. Katarzyna Woźniak, Katedra Genetyki Molekularnej, Wydział Biologii i Ochrony Środowiska, Uniwersytet Łódzki, ul. Pomorska 141/143, 90-236 Łódź; e-mail: katarzyna.wozniak@biol.uni.lodz.pl

Wykaz skrótów: **ATF-3** – aktywator transkrypcji (activating transcription factor 3); **DDR** – odpowiedź na uszkodzenia DNA (DNA damage response); **HIF-1** – czynnik indukowany hipoksją (hypoxia-inducible factor 1); **ILK** – kinaza związana z integrzynami (integrin-linked kinase); **MMP** – metaloproteinaza macierzy zewnątrzkomórkowej (matrix metalloproteinase); **MTT** – test proliferacji komórek (MTT Cell Proliferation Assay); **RFT** – reaktywne formy tlenu (reactive oxygen species); **TGF-β1** – transformujący czynnik wzrostu beta 1 (transforming growth factor β1); **VEGF** – czynnik wzrostu śródbłonnka naczyń (vascular endothelial growth factor).

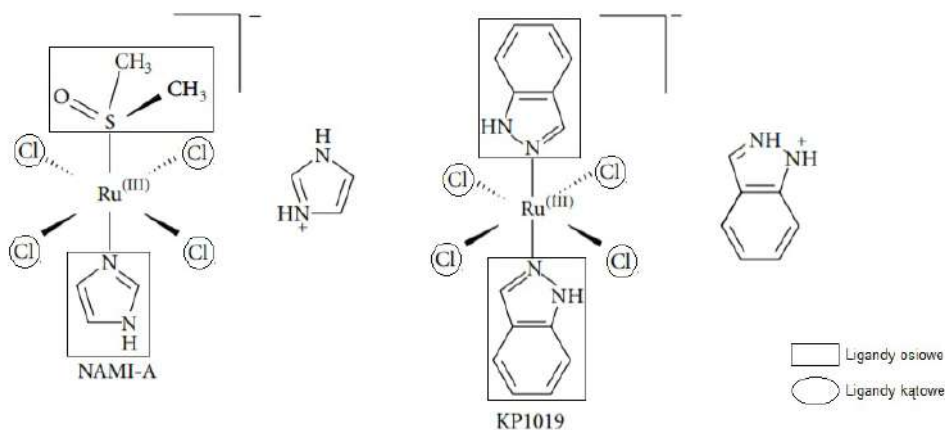
WSTĘP

W ciągu ostatnich kilkudziesięciu lat popularnymi lekami przeciwnowotworowymi były związki platyny. Wśród nich nadal najczęściej jest stosowana cisplatyna wykorzystywana u chorych z nowotworami m.in. jajnika, płuca, głowy i szyi [53]. Niestety, związek ten wykazuje znaczące działania niepożądane obejmujące: nefrotoksyczność, neurotoksyczność, utratę włosów czy też wymioty [21]. Rozpoczęto badania nad nowymi związkami, których stosowanie nie wiązałoby się z tak poważnymi działaniami niepożądanymi. Badania objęły szeroki zakres kompleksów zawierających: żelazo, osm, iryd, rod, złoto, a także ruten [27, 54].

Analizy wykazały, że ruten i jego kompleksy mają właściwości, które wyróżniają go wśród innych metali. Jest to m.in. duża stabilność, która wiąże się z czasem wymiany ligandów, który w związkach rutenu zazwyczaj wyraża się w godzinach, co odpowiada czasowi potrzebnemu do podziałów komórkowych [58]. Ruten może przyjmować stopnie utlenienia od II do IV, których zmiana (poprzez proces utleniania czy redukcji) jest możliwa w warunkach fizjologicznych [13]. Ubogie w tlen środowisko komórki nowotworowej stwarza warunki promujące redukcję Ru(III) do Ru(II), co powoduje wzrost aktywności kompleksu i interakcji z różnymi cząsteczkami w komórce [1]. Ukierunkowuje to działanie związków rutenu na komórki nowotworowe. W przeciwieństwie do cisplatyny, kompleksy

oparte o rdzeń rutenowy nie wykazują dużej cytotoksyczności na komórki prawidłowe. Ponadto badania biochemiczne i histopatologiczne wykazały niewielką neuro- oraz nefrotoksyczność związków rutenu w porównaniu do związków platyny [6]. Inną istotną właściwością rutenu jest jego zdolność do naśladowania żelaza, co przejawia się wiązaniem do transferyny. Komórki nowotworowe, ze względu na zmieniony metabolizm, mają większe zapotrzebowanie na żelazo w porównaniu do komórek prawidłowych [32]. Jest to kolejny mechanizm ukierunkowujący działanie związków rutenu na komórki nowotworowe.

NAMI-A i KP1019 to dwa koordynacyjne związki rutenu (III), które poddano badaniom klinicznym. Badania pierwszej fazy zakończyły się w 2004 r. dla NAMI-A i w 2008 r. dla KP1019 [5, 40]. Ich aktywność opiera się na przyłączeniu sześciu ligandów, które można podzielić na osiowe i kątowe. Dwa ligandy osiowe zawierające atomy siarki bądź azotu są odpowiedzialne za właściwości steryczne. Cztery ligandy kątowe mogą być zastąpione innymi pod wpływem warunków panujących w komórce, np. związanych ze zmianą pH [19]. NAMI-A ((H₂Im)[trans-Ru^{III}Cl₄(DMSO)(Im)]) to kompleks rutenu, zawierający w swojej sferze koordynacyjnej ligandy osiowe – dimetylosulfotlenkowy (DMSO) i imidazolowy oraz kątowe – cztery jony chlorkowe (ryc. 1). Natomiast KP1019 ((HInd)[trans-Ru^{III}Cl₄(Ind)₂]) to związek, w którym ruten tworzy kompleks z czterema jonami chlorkowymi, a także dwoma indazolowymi (ryc. 1).



Ryc. 1. Budowa NAMI-A oraz KP1019

CYTOTOKSYCZNOŚĆ NAMI-A I KP1019

Oprócz terapeutycznego wpływu danego związku, istotnym jego działaniem jest cytotoksyczność względem komórek prawidłowych. Wiąże się to z występowaniem oraz intensywnością działań niepożądanych i dlatego trzeba je uwzględniać jako dodatkowy czynnik w terapeutycznym zastosowaniu danego związku [61]. Oceniając cytotoksyczność względem komórek prawidłowych, wykazano, że NAMI-A wykazuje ją w niewielkim stopniu [4]. Wykazano także, że NAMI-A działa bardzo cytotoksycznie, nawet w niewielkich stężeniach na niektóre komórki białaczkowe, takie jak HL-60 i K562 [50].

Badania wykazały, że zarówno KP1019, jak i sól sodowa tego związku KP1339, mają niewielką, zbliżoną do siebie cytotoksyczność na komórki prawidłowe. Można zatem przypuszczać, że działają według podobnego mechanizmu, a modyfikacja chemiczna KP1019 prowadząca do powstania soli KP1339 o lepszej rozpuszczalności, nie ogranicza potencjału terapeutycznego związku [34]. Porównano także cytotoksyczność KP1019 i KP1339 z cisplatyną i etopozydem. Badania przeprowadzone na liniach komórkowych raka jelita grubego (HT29 i SW480) wykazały znacząco mniejszą cytotoksyczność kompleksów rutenowych [36]. Przeprowadzono ponadto badania, które dowiodły, że KP1339 aktywuje kaspazy-3, -7 i -8 w komórkach nowotworowych trzustki Caspan-1, prowadząc do ich apoptozy [55].

W innych badaniach udowodniono, że jony różnych metali mogą wpływać na cytotoksyczność KP1019. Analiza żywotności komórek HeLa testem MTT wykazała znaczące zwiększenie cytotoksyczności KP1019 w obecności jonów: glinu, kadmu, miedzi, a zwłaszcza cynku [28].

TRANSPORT WE KRWI

Transport związków zawierających ruten bada wielu uczonych m.in. z powodu zdolności jonów Ru(III) do naśladowania Fe(III). Stwarza to możliwości zastosowania w terapii strategii tzw. konia trojańskiego, która w założeniu pozwoliłaby na wprowadzenie do komórki związków zawierających ruten przez fizjologiczną drogę transportu żelaza z wykorzystaniem transferyny [42]. Wykazano, że NAMI-A może się wiązać do transferyny i albuminy, tworząc stabilne addukty w różnych stosunkach molowych [8]. Wykonano badania dowodzące, że addukty, które powstają między albuminą i NAMI-A, są aktywne farmakologicznie. Działanie takie może mieć związek z antymetastatyczną aktywnością, która przejawia się m. in. przez zwiększenie adhezji komórkowej [46].

Przeprowadzono także badania dotyczące oddziaływania KP1019 i transferyny w postaci wolnej od żelaza (apotransferyna). Badania spektroskopowe dostarczyły dowodów na formowanie adduktów apotransferyny i KP1019 [37]. Wykonano także badania krystalograficzne z wykorzystaniem apolaktoferyny, która wykazuje znaczne podobieństwo do transferyny, zarówno strukturalne, jak i funkcjonalne, jednak charakteryzuje się więk-

szą zdolnością do formowania kryształów. Wyniki badań wykazały, że fragment kompleksu zawierający ruten łączy się koordynacyjnie z histydyną w pozycji 253, znajdująca się w miejscu wiążącym żelazo [38]. Ta interakcja tłumaczyłaby zdolność rutenu do naśladowania żelaza.

INTERAKCJE Z KWASAMI NUKLEINOWYMI

Porównano zdolność NAMI-A, KP1019 i cisplatyny do tworzenia adduktów z DNA i wykazano, że potencjał do ich formowania dla obu związków zawierających ruten jest znacząco niższy niż cisplatyny. Preferencyjnym miejscem wiązania związków rutenowych z DNA, podobnie jak w przypadku cisplatyny, jest guanina [30]. Badacze sprawdzili interakcje, które zachodzą między NAMI-A i DNA. Badania miały na celu określenie preferencji do tworzenia wiązań między rutenem znajdującym się w centrum cząsteczki NAMI-A, a poszczególnymi atomami występującymi w zasadach azotowych. Wyniki badań wykazały, że zdolność rutenu do wiązania się z atomami azotu w cząsteczce guaniny jest zależna od stopnia uwodnienia NAMI-A. Zarówno w jednowodnym, jak i dwuwodnym NAMI-A najbardziej preferowanym atomem był azot w pozycji 7, który okazuje się skuteczniejszy od atomów azotu w pozycji 3 oraz 1. Wiązanie między rutenem a N7G według obliczeń jest stabilizowane przez największą liczbę wiązań wodorowych [22]. W przypadku KP1019 interakcje z DNA powodują formowanie wiązań krzyżowych oraz indukcję pęknięć nici. Ponadto wiązanie się do DNA wpływa na konformację podwójnej helisy [12]. Badania wykonane w 2011 r. wykazały, że NAMI-A oddziałuje z RNA drożdży w liczbie 2-5 kompleksów Ru-RNA na rybosom [35]. Uzyskane wyniki wskazywały, że RNA może być potencjalnym celem oddziaływania NAMI-A. W innych badaniach skupiono się na zdolności zarówno NAMI-A, jak i KP1019 do wiązania się z tRNA^{Phe}. Po raz pierwszy zaobserwowano interakcję KP1019 z RNA. Zaproponowano następujące mechanizmy interakcji związków rutenowych z RNA: elektrostatyczne oddziaływanie dla NAMI-A oraz interkalację między zasady w cząsteczce tRNA^{Phe} dla KP1019. Otrzymane wyniki wskazują, że interakcje z tRNA^{Phe} mogą odgrywać potencjalną rolę w działaniu KP1019 i najprawdopodobniej nie mają wpływu na działanie NAMI-A [23].

INTERAKCJE Z BIAŁKAMI

Ze względu na stosunkowo słabe interakcje związków rutenowych z DNA, zajęto się ich oddziaływaniami z białkami. Przeprowadzono m.in. badania dotyczące interakcji NAMI-A z lizozymem jaja kurzego. Badania krystalograficzne wykazały, że kompleks rutenowy utracił wszystkie dołączone ligandy i jako wolny jon wszedł w interakcję z lizozymem przez utworzenie wiązań koordynacyjnych z dwoma odrębnymi kwasami asparginowymi białka w pozycjach 101 i 119 [45].

Białkiem, które badano pod kątem interakcji ze związkami rutenu była także anhydraza węglanowa. W przypadku interakcji z tym białkiem badania wskazały na koordyna-

cyjne wiązanie się wolnego jonu rutenu z grupą imidazolową histydyny 64 [17]. Badacze przeanalizowali ponadto potencjalne interakcje między NAMI-A i ferrytyną, a dokładniej jej podjednostką H. Wyniki umożliwiły identyfikację miejsca wiążącego ruten. Jon rutenu utworzył wiązanie koordynacyjne z histydyną w pozycji 105. Powstały addukt między NAMI-A, a podjednostką H ferrytyny może być potencjalnie wykorzystany jako selektywny nośnik jonów rutenowych do komórek nowotworowych [20].

Następne badania dotyczyły interakcji KP1019 z albuminą ludzkiej surowicy. Analizowana struktura białka wykazała obecność dwóch miejsc, w których był związany ruten. Oba centra metalowe zostały związane z azotem obecnym w grupie imidazolowej histydyny w pozycjach 146 oraz 242 [11]. Zbadano także, czy NAMI-A wchodzi w interakcję z tym białkiem. Wyniki, podobnie jak w przypadku KP1019, wskazały na utworzenie wiązań koordynacyjnych z grupą imidazolową histydyny [60]. Na podstawie tych doświadczeń zaproponowano mechanizm „rutenacji białka” przez NAMI-A, który byłby następujący: kompleks ulega degradacji przez odłączenie się ligandów, a jon rutenu przyłącza się do białka, głównie przez grupę imidazolową histydyny bądź grupę karboksylową kwasu asparaginowego lub glutaminowego [44].

ANTYMETASTATYCZNE WŁAŚCIWOŚCI NAMI-A

Przerzutowanie (inaczej metastaza), będące jednym z aspektów progresji nowotworu, jest procesem złożonym. Przerzuty są zazwyczaj najczęstszą przyczyną zgonów pacjentów z chorobą nowotworową. Późne wykrycie nowotworu i diagnoza w stadiach, w których stwierdza się pojawienie nowych ognisk komórek nowotworowych, oddalonych od pierwotnego miejsca, bardzo zawęża metody, które można wykorzystywać w terapii [2, 39]. Dlatego też poszukiwanie związków, które wykazują dużą skuteczność względem przerzutów nowotworowych, zyskuje coraz większe znaczenie pod kątem strategii leczenia [26].

Jednym z pierwszych etapów przerzutowania jest aktywacja czynnika indukowanego hipoksją HIF-1 α [47]. Komórka, aby uniknąć apoptozy spowodowanej hipoksją, zwiększa ekspresję HIF-1 α , który po wnikięciu do jądra i związaniu z HIF-1 β , może indukować ekspresję m.in. czynnika wzrostu śródbłonnka naczyń (VEGF) odpowiedzialnego za powstawanie nowych naczyń krwionośnych [51]. Aby mógł się dalej rozwijać nowotwór, niezbędna jest degradacja macierzy zewnątrzkomórkowej, która otacza komórki nowotworowe. W jej przebudowie główną rolę odgrywają metaloproteiny macierzy zewnątrzkomórkowej (MMP). Enzymy te degradują macierz zewnątrzkomórkową, a to ogranicza barierę fizyczną do rozwoju nowotworu, a ponadto otwiera drogę do naczyń krwionośnych i limfatycznych, którymi komórki nowotworowe rozprzestrzeniają się w organizmie [24]. Warunkiem koniecznym, który muszą spełnić komórki mające zapoczątkować przerzutowanie jest nabyte zdolności do przeżycia, mimo braku kontaktu z innymi

komórkami i macierzą zewnątrzkomórkową, czyli anoikis. Znaczącą rolę odgrywają tutaj kinazy związane z integrinami (ILK) [16]. Pod wpływem mikrośrodowiska guza dochodzi do zmiany fenotypu komórki nowotworowej na taki, który charakteryzuje się zwiększoną mobilnością (przejście epitelialno-mezenchymalne). Komórka w czasie przejścia traci ścisłe połączenia z innymi komórkami, a jej cytoskielet ulega reorganizacji, co pozwala na uzyskanie fenotypu inwazyjnego [62].

Zestawiono aktywności koordynacyjnych związków rutenowych, w tym NAMI-A i KP1019, pod kątem hamowania rozwoju komórek guza pierwotnego i komórek zdolnych do metastazy. Wyniki wykazały brak selektywnej cytotoksyczności KP1019 na oba typy komórek, a także bardzo wysoką selektywność NAMI-A pod kątem cytotoksycznego działania względem komórek metastatycznych [59]. Duża aktywność antymetastatyczna NAMI-A wskazuje na selektywność działania związku, a także na mechanizm działania odmienny od leków opartych o platynę. Aktywność antymetastatyczna NAMI-A jest niezależna od dawki, częstości stosowania, drogi podawania związku i zaawansowania rozwoju guza [3]. Badania wykonane na linii komórkowej śródbłonnka ECV304 wskazują na potencjał NAMI-A do modulowania procesu angiogenezy. Przypuszcza się, że ważną rolę odgrywa zdolność wiązania przez NAMI-A tlenku azotu (NO), przez co zmniejsza się dostępność tego gazowego transmittera, który jest wykorzystywany przez komórki nowotworowe do modulowania procesu angiogenezy [18].

NAMI-A obniża ekspresję metaloproteinaz MMP-2 oraz MMP-9 [31]. Przeprowadzono ponadto badania nad wpływem NAMI-A na aktywność TGF- β 1, co wiązało się także z oceną redukcji migracji komórek linii HBL-100, MCF-7 i MDA-MB-231. Wyniki wykazały, że w przypadku linii HBL-100, będącej odpowiednikiem komórek prawidłowych, związek nie wpłynął w żaden sposób na ilość białka TGF- β 1, a w obu liniach nowotworowych MCF-7 oraz MDA-MB-231 zaobserwowano znaczące obniżenie jego ilości. Spadek poziomu białka TGF- β 1 obserwowano w stężeniu 1 μ M w komórkach MDA-MB-231 i 10 μ M w komórkach MCF-7. Po zastosowaniu NAMI-A w stężeniu 100 μ M zaobserwowano gwałtowny wzrost ilości TGF- β 1. Zaobserwowano ponadto znaczące obniżenie inwazyjności linii MDA-MB-231 oraz MCF-7 po zastosowaniu stężenia 100 μ M, co świadczy o tym, że prawdopodobnie za antymetastatyczną aktywność NAMI-A odpowiada inne białko [14].

NAMI-A zmniejsza poziom integryny α 5 β 1 na powierzchni komórek HCT-116. Badania wykazały, że najskuteczniejsza inhibicja ekspresji genów obu podjednostek tej integryny występowała po zastosowaniu NAMI-A w stężeniu 1 μ M. Zastosowanie stężenia 100 μ M spowodowało zwiększenie ekspresji genu kodującego podjednostkę α 5, co nie wiąże się ze zwiększeniem aktywności integryny α 5 β 1, gdyż do prawidłowego funkcjonowania potrzebuje ona zarówno podjednostki α 5, jak i β 1 [48].

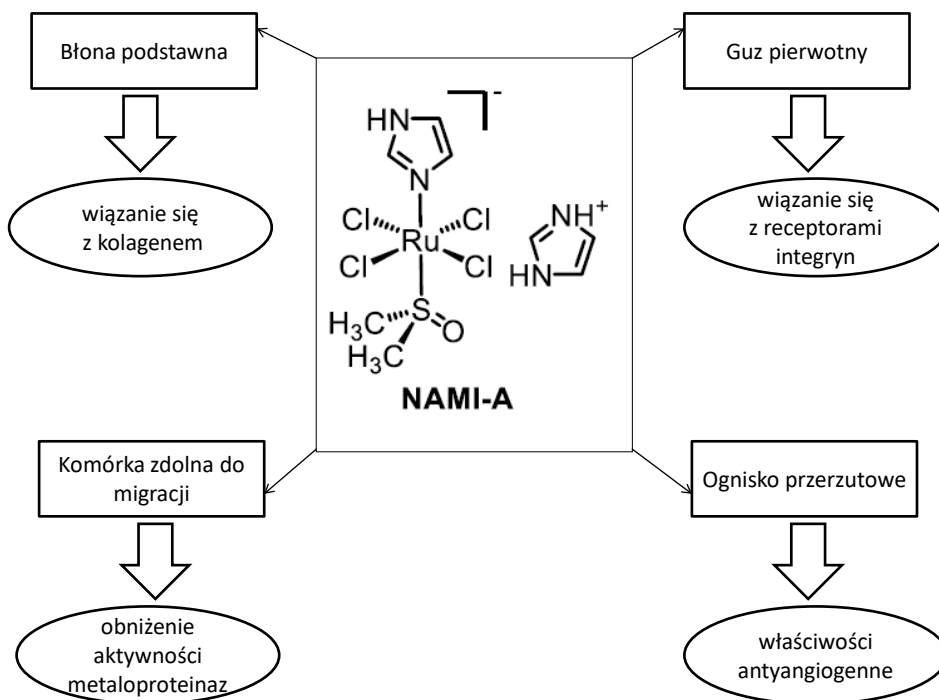
W ostatnich latach przeprowadzono badania mające na celu sprawdzenie, jaki wpływ ma NAMI-A na ekspresję genów zaangażowanych w proces metastazy. Badania przeprowadzono na komórkach raka jelita grubego linii HCT-116. W trzech badanych genach - *ABL-2*, *ATF-3*, *RND-1* zaobserwowano znaczące obniżenie ich ekspresji [9]. Badania wykonane na modelu zwierzęcym wykazały, że NAMI-A selektywnie wiąże się do włókien kolagenowych, a także błony podstawnej znajdującej się w okolicach guza. Może to doprowadzić do interkalacji związku do sieci kolagenowej, przez co komórkom nowotworowym jest trudniej rozpocząć migrację [41].

Interakcje biologiczne odpowiadające za antymetastatyczne właściwości NAMI-A przedstawiono na ryc. 2.

MECHANIZM DZIAŁANIA KP1019

Niedawno przeprowadzone badania wykazały, że mechanizm działania KP1019 oraz NAMI-A jest odmienny, a przyczyny tego upatruje się w różnicach w procesie uwodnienia oraz aktywacji rutenu [43]. Głównym czynnikiem wydaje się jednak drastyczna różnica w wychwycie komórkowym obu związków. Wykazano bardzo znaczące różnice w wychwycie komórkowym, który okazał się minimalny dla NAMI-A w porównaniu do KP1019 [29]. Badania przeprowadzone w 2016 r. na komórkach raka okrężnicy wykazały, że KP1339 może oddziaływać na białka obecne w cytozolu, a to wywołuje stres oksydacyjny i stres retikulum endoplazmatycznego. Możliwe jest wejście komórki na mitochondrialny szlak apopto-

tyczny w wyniku powstałych uszkodzeń [25]. Otrzymane wyniki skłoniły badaczy do sprawdzenia, czy mechanizm działania oparty o zwiększone wytwarzanie reaktywnych form tlenu to główne oddziaływanie KP1019, czy też tylko jeden z możliwych mechanizmów, przez który może działać ten związek. Wykonano wiele eksperymentów na drożdżach jako organizmach modelowych. Wysoka homologia między białkami drożdżowymi i ludzkimi pozwala na odkrycie potencjalnego wpływu KP1019 na komórki człowieka [57]. Ekspozycja komórek drożdży na KP1019 powoduje uszkodzenia DNA, które indukują odpowiedź komórki (DDR). Odpowiedź ta zatrzymuje cykl komórkowy w punkcie kontrolnym związanym z białkiem Rad9. W przypadku mutantów pozbawionych genu *Rad9* obserwowano zdecydowanie większą wrażliwość komórek na KP1019, co świadczy o krytycznej roli DDR w tolerancji na ten związek [10]. Wykazano, że pewne zewnętrzne czynniki mogą modulować cytotoksyczny potencjał KP1019. Obecność jonów metali, takich jak: miedź, mangan, cynk czy glin zwiększają cytotoksyczność związku najprawdopodobniej przez synergistyczne oddziaływanie z KP1019. Wykazano także, że aktywność związku zmniejsza się przez działanie zredukowanego glutationu (GSH), który redukuje wychwyt komórkowy KP1019. Jony Fe^{2+} także zmniejszają aktywność KP1019, jednak wyjaśnienie tego wymaga dalszych badań [5]. Wykazano, że KP1019 tworzy addukty z histonem H3. Ponadto zakrojone na szeroką skalę analizy transkryptomu drożdży po ekspozycji na KP1019 wykazały znaczące zmiany ekspresji genów zaangażowanych w różne procesy komórkowe, takie jak: sygnalizacja komórkowa, naprawa uszkodzeń DNA, bioge-



Ryc. 2. Interakcje biologiczne odpowiadające za antymetastatyczne właściwości NAMI-A (wg [5] zmodyfikowano)

neza rybosomów czy stres osmotyczny, w który zaangażowane jest białko Hog1. Analiza komputerowa wskazała homologiczne geny człowieka, na ekspresję których może wpływać KP1019 [28]. Schemat przedstawiający poznane oraz przewidywane cele molekularne KP1019 przedstawiono na ryc. 3.

BADANIA *IN VIVO* Z WYKORZYSTANIEM NAMI-A I KP1019

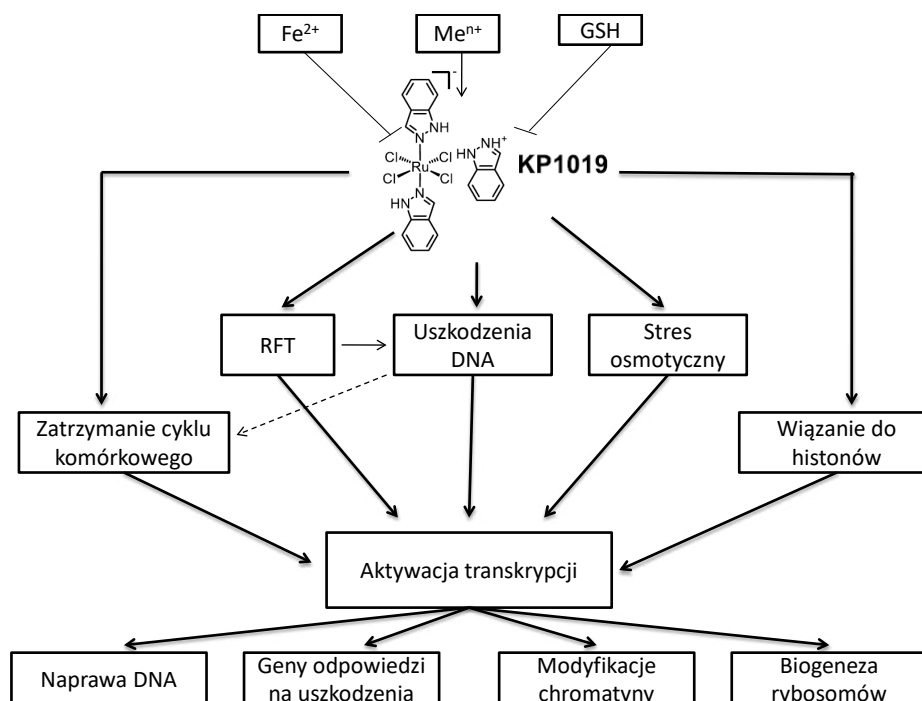
NAMI-A był pierwszym związkiem rutenowym, który został podany pacjentom. Pierwsza faza badań klinicznych rozpoczęła się w 1999 r. i objęła 24 pacjentów z różnymi typami nowotworów, w tym: okrężnicy, jelita grubego i niedrobnokomórkowego raka płuca [5]. Najbardziej obiecujące rezultaty uzyskano u pacjentów z niedrobnokomórkowym rakiem płuca. Rozwój nowotworu u jednego z pacjentów został zatrzymany na 21 tygodni. Korelowało to z wynikami badań prowadzonych na mysich modelach raka płuca, co sugerowało rozpoczęcie dalszych badań klinicznych nad zastosowaniem NAMI-A jako leku przeciwko temu rakowi [52].

Przeprowadzono testy przedkliniczne z KP1019 na szczurach z platynoopornym rakiem jelita grubego, który pod względem histologicznym przypomina ludzki nowotwór jelita grubego. Zaobserwowano znaczącą redukcję masy guza sięgającą 70% [56]. Ponadto wykonano badania na myszach, u których indukowano nowotwór piersi. Testy wykazały dużą skuteczność KP1019 w zwalczaniu guzów pierwotnych [7]. KP1019 był drugim po NAMI-A kompleksem rutenowym, z którym rozpoczęto badania kliniczne. Badania I fazy objęły niewielką 8-osobową grupę

pacjentów z różnymi nowotworami, m.in. wątroby, odbytnicy i endometrium. U 5 pacjentów stwierdzono ustabilizowanie się choroby na co najmniej 8 tygodni [33]. Postanowiono także sprawdzić, czy zwiększenie rozpuszczalności związku zwiększy jego potencjał przeciwnowotworowy, w tym celu zaczęto badania z solą KP1339. Badanie kliniczne KP1339 przeprowadzono u 46 pacjentów z różnymi typami nowotworów, w tym jelita grubego, niedrobnokomórkowego raka płuca oraz nowotworów głowy i szyi. Zatrzymanie rozwoju nowotworu wystąpiło u ponad 25% pacjentów [15, 49].

PODSUMOWANIE

Poszukiwanie nowych, skuteczniejszych metod w terapii nowotworów należy do niezwykle istotnych kierunków badań we współczesnych naukach biomedycznych. Kompleksy metali należą do obiecujących grup wśród współcześnie testowanych pod tym kątem substancji. Cisplatyna jest bardzo skutecznym lekiem w terapii wielu typów nowotworów i stanowi niejako punkt odniesienia dla nowych, potencjalnych leków zawierających metal. Badania nad kompleksami zawierającymi ruten NAMI-A i KP1019 są obiecujące, zwłaszcza pod kątem niewielkiej toksyczności tych związków na komórki prawidłowe, jak również pod kątem ich działania antymetastatycznego. Precyzyjne mechanizmy działania NAMI-A i KP1019 nie są dokładnie poznane i wymagają dalszych badań. Zaznaczyć jednak należy, iż według dostępnych danych, mechanizm działania cisplatyny oraz scharakteryzowanych w artykule kompleksów rutenowych jest różny, ponieważ cisplatyna oddziałuje



Ryc. 3. Poznane oraz potencjalne cele biologiczne KP1019 (wg [5] zmodyfikowano)

przede wszystkim z DNA, natomiast w kompleksach rutenowych mechanizm działania opiera się na oddziaływaniu z białkami, a także wpływa na poziom ekspresji wielu genów. Wnioskować zatem można, że działanie

kompleksów rutenowych opiera się na bardziej złożonych interakcjach ze składnikami komórki i wymaga dalszych badań w celu ich pełniejszego poznania.

PIŚMIENNICTWO

- [1] Abid M., Shamsi F., Azam A.: Ruthenium complexes: An emerging ground to the development of metallopharmaceuticals for cancer therapy. *Mini Rev. Med. Chem.*, 2016; 16: 772–786
- [2] Adeel M.M., Qasim M., Ashfaq U.A., Masoud M.S., Rehman M.U., Qamar M.T., Javed M.R.: Modelling and simulation of mutant alleles of breast cancer metastasis suppressor 1 (BRMS1) gene. *Bioinformatics*, 2014; 10: 454–459
- [3] Alessio E.: Thirty years of the drug candidate NAMI-A and the myths in the field of ruthenium anticancer compounds: A personal perspective. *Eur. J. Inorg. Chem.*, 2017: 1549–1560
- [4] Alessio E., Messori L.: The deceptively similar ruthenium(III) drug candidates KP1019 and NAMI-A have different actions. What did we learn in the past 30 years? *Met. Ions Life Sci.*, 2018; 18: 141–170
- [5] Alessio E., Messori L.: NAMI-A and KP1019/1339, two iconic ruthenium anticancer drug candidates face-to-face: A case story in medicinal inorganic chemistry. *Molecules*, 2019; 24: 1995
- [6] Anchuri S.S., Thota S., Yerra R., Devarakonda K.P., Dhulipala S.: Novel mononuclear ruthenium(II) compounds in cancer therapy. *Asian Pac. J. Cancer Prev.*, 2012; 13: 3293–3298
- [7] Bergamo A., Masi A., Jakupec M.A., Keppler B.K., Sava G.: Inhibitory effects of the ruthenium complex KP1019 in models of mammary cancer cell migration and invasion. *Met. Based Drugs*, 2009; 681270
- [8] Bergamo A., Messori L., Piccioli F., Cocchiello M., Sava G.: Biological role of adduct formation of the ruthenium(III) complex NAMI-A with serum albumin and serum transferrin. *Invest. New Drugs*, 2003; 21: 401–411
- [9] Bergamo A., Pelillo C., Chambery A., Sava G.: Influence of components of tumour microenvironment on the response of HCT-116 colorectal cancer to the ruthenium-based drug NAMI-A. *J. Inorg. Biochem.*, 2017; 168: 90–97
- [10] Bierle L.A., Reich K.L., Taylor B.E., Blatt E.B., Middleton S.M., Burke S.D., Stultz L.K., Hanson P.K., Partridge J.F., Miller M.E.: DNA damage response checkpoint activation drives KP1019 dependent pre-anaphase cell cycle delay in *S. cerevisiae*. *PLoS One*, 2015; 10: e138085
- [11] Bijelic A., Theiner S., Keppler B.K., Rompel A.: X-ray structure analysis of indazolium trans-[tetrachlorobis(1*H*-indazole) ruthenate(III)] (KP1019) bound to human serum albumin reveals two ruthenium binding sites and provides insights into the drug binding mechanism. *J. Med. Chem.*, 2016; 59: 5894–5903
- [12] Brabec V., Kasparkova J.: Ruthenium coordination compounds of biological and biomedical significance. DNA binding agents. *Coord. Chem. Rev.*, 2018; 376: 75–94
- [13] Bratsos I., Jedner S., Gianferrara T., Alessio E.: Ruthenium anticancer compounds: challenges and expectations. *Chimia*, 2007; 61: 692–697
- [14] Brescacin L., Masi A., Sava G., Bergamo A.: Effects of the ruthenium-based drug NAMI-A on the roles played by TGF- β 1 in the metastatic process. *J. Biol. Inorg. Chem.*, 2015; 20: 1163–1173
- [15] Burris H.A., Bakewell S., Bendell J.C., Infante J., Jones S.F., Spigel D.R., Weiss G.J., Ramanathan R.K., Ogden A., Von Hoff D.: Safety and activity of IT-139, a ruthenium-based compound, in patients with advanced solid tumours: a first-in-human, open-label, dose-escalation phase I study with expansion cohort. *ESMO Open*, 2017; 1: e000154
- [16] Cao Z., Livas T., Kyprianou N.: Anoikis and EMT: Lethal “liaisons” during cancer progression. *Crit. Rev. Oncog.*, 2016; 21: 155–168
- [17] Casini A., Temperini C., Gabbiani C., Supuran C.T., Messori L.: The x-ray structure of the adduct between NAMI-A and carbonic anhydrase provides insights into the reactivity of this metallodrug with proteins. *Chem. Med. Chem.*, 2010; 5: 1989–1994
- [18] Castellarin A., Zorzet S., Bergamo A., Sava G.: Pharmacological activities of ruthenium complexes related to their NO scavenging properties. *Int. J. Mol. Sci.*, 2016; 17: E1254
- [19] Caterino M., Herrmann M., Merlino A., Riccardi C., Montesarchio D., Mroginski M.A., Musumeci D., Ruffo F., Paduano L., Hildebrandt P., Kozuch J., Vergara A.: On the pH-modulated Ru-based prodrug activation mechanism. *Inorg. Chem.*, 2019; 58: 1216–1223
- [20] Ciambellotti S., Pratesi A., Severi M., Ferraro G., Alessio E., Merlino A., Messori L.: The NAMI A-human ferritin system: A biophysical characterization. *Dalton Trans.*, 2018; 47: 11429–11437
- [21] Ciarimboli G.: Membrane transporters as mediators of cisplatin side-effects. *Anticancer Res.*, 2014; 34: 547–550
- [22] Das D., Khan M.S., Barik G., Avastare V., Pal S.: Computational approach to unravel the role of hydrogen bonding in the interaction of NAMI-A with DNA nucleobases and nucleotides. *J. Phys. Chem. A.*, 2018; 122: 8397–8411
- [23] Dwyer B.G., Johnson E., Cazares E., McFarlane Holman K.L., Kirk S.R.: Ruthenium anticancer agent KP1019 binds more tightly than NAMI-A to tRNA Phe. *J. Inorg. Biochem.*, 2018; 182: 177–183
- [24] Fink K., Boratynski L.: Rola metaloproteinaz w modyfikacji macierzy zewnątrzkomórkowej w nowotworowym wroście inwazyjnym, w przetrutowaniu i w angiogenezie. *Postępy Hig. Med. Dośw.*, 2012; 66: 609–628
- [25] Flocke L.S., Trondl R., Jakupec M.A., Keppler B.K.: Molecular mode of action of NKP-1339 – a clinically investigated ruthenium-based drug – involves ER- and ROS-related effects in colon carcinoma cell lines. *Invest. New Drugs*, 2016; 34: 261–268
- [26] Gandalovičová A., Rosel D., Fernandes M., Veselý P., Heneberg P., Čermák V., Petruželka L., Kumar S., Sanz-Moreno V., Brábek J.: Migrastatics-anti-metastatic and anti-invasion drugs: promises and challenges. *Trends Cancer*, 2017; 3: 391–406
- [27] Gasser G., Ott I., Metzler-Nolte N.: Organometallic anticancer compounds. *J. Med. Chem.*, 2011; 54: 3–25
- [28] Golla U., Swagatika S., Chauhan S., Tomar R.S.: A systematic assessment of chemical, genetic, and epigenetic factors influencing the activity of anticancer drug KP1019 (FFC14A). *Oncotarget*, 2017; 8: 98426–98454
- [29] Gransbury G.K., Kappen P., Glover C.J., Hughes J.N., Levina A., Lay P.A., Musgrave I.F., Harris H.H.: Comparison of KP1019 and NAMI-A in tumour-mimetic environments. *Metallomics*, 2016; 8: 762–773
- [30] Groessl M., Tsybin Y.O., Hartinger C.G., Keppler B.K., Dyson P.J.: Ruthenium versus platinum: interactions of anticancer metallo-drugs with duplex oligonucleotides characterised by electrospray ionisation mass spectrometry. *J. Biol. Inorg. Chem.*, 2010; 15: 677–688
- [31] Gu L., Li X., Ran Q., Kang C., Lee C., Shen J.: Antimetastatic activity of novel ruthenium (III) pyridine complex. *Cancer Med.*, 2016; 5: 2850–2860
- [32] Guo W., Zheng W., Luo Q., Li X., Zhao Y., Xiong S., Wang F.: Transferrin serves as a mediator to deliver organometallic ruthenium(II) anticancer complexes into cells. *Inorg. Chem.*, 2013; 52: 5328–5338
- [33] Hartinger C.G., Jakupec M.A., Zorbas-Seifried S., Groessl M., Egger A., Berger W., Zorbas H., Dyson P.J., Keppler B.K.: KP1019, a new redox-active anticancer agent-preclinical development and results of a clinical phase I study in tumor patients. *Chem. Biodivers.*, 2008; 5: 2140–2155

- [34] Heffeter P., Böck K., Atil B., Reza Hoda M.A., Körner W., Bartel C., Jungwirth U., Keppler B.K., Micksche M., Berger W., Koellensperger G.: Intracellular protein binding patterns of the anticancer ruthenium drugs KP1019 and KP1339. *J. Biol. Inorg. Chem.*, 2010; 15: 737–748
- [35] Hostetter A.A., Miranda M.L., DeRose V.J., McFarlane Holman K.L.: Ru binding to RNA following treatment with the antimetastatic prodrug NAMI-A in *Saccharomyces cerevisiae* and in vitro. *J. Biol. Inorg. Chem.*, 2011; 16: 1177–1185
- [36] Kapitza S., Pongratz M., Jakupec M.A., Heffeter P., Berger W., Lackinger L., Keppler B.K., Marian B.: Heterocyclic complexes of ruthenium(III) induce apoptosis in colorectal carcinoma cells. *J. Cancer Res. Clin. Oncol.*, 2005; 131: 101–110
- [37] Kratz F., Hartmann M., Keppler B., Messori L.: The binding properties of two antitumor ruthenium(III) complexes to apotransferrin. *J. Biol. Chem.*, 1994; 269: 2581–2588
- [38] Kratz F., Keppler B.K., Messori L., Smith C., Baker E.N.: Protein-binding properties of two antitumor Ru(III) complexes to human apotransferrin and apolactoferrin. *Met. Based Drugs*, 1994; 1: 169–173
- [39] Krøigård A.B., Larsen M.J., Lænkholm A.V., Knoop A.S., Jensen J.D., Bak M., Mollenhauer J., Thomassen M., Kruse T.A.: Identification of metastasis driver genes by massive parallel sequencing of successive steps of breast cancer progression. *PLoS One*, 2018; 13: e0189887
- [40] Lazarević T., Rilak A., Bugarčić Z.D.: Platinum, palladium, gold and ruthenium complexes as anticancer agents: Current clinical uses, cytotoxicity studies and future perspectives. *Eur. J. Med. Chem.*, 2017; 142: 8–31
- [41] Liang J., Levina A., Jia J., Kappen P., Glover C., Johannessen B., Lay P.A.: Reactivity and transformation of antimetastatic and cytotoxic rhodium(III)-dimethyl sulfoxide complexes in biological fluids: An XAS speciation study. *Inorg. Chem.*, 2019; 58: 4880–4893
- [42] Luck A.N., Mason A.B.: Structure and dynamics of drug carriers and their interaction with cellular receptors: Focus on serum transferrin. *Adv. Drug Deliv. Rev.*, 2013; 65: 1012–1019
- [43] Meier-Menches S.M., Gerner C., Berger W., Hartinger C.G., Keppler B.K.: Structure-activity relationships for ruthenium and osmium anticancer agents-towards clinical development. *Chem. Soc. Rev.*, 2018; 47: 909–928
- [44] Merlino A.: Interactions between proteins and Ru compounds of medicinal interest: A structural perspective. *Coordin. Chem. Rev.*, 2016; 326: 111–134
- [45] Messori L., Merlino A.: Ruthenium metalation of proteins: the X-ray structure of the complex formed between NAMI-A and hen egg white lysozyme. *Dalton Trans.*, 2014; 43: 6128–6131
- [46] Novohradský V., Bergamo A., Cocchietto M., Zajac J., Brabec V., Mestroni G., Sava G.: Influence of the binding of reduced NAMI-A to human serum albumin on the pharmacokinetics and biological activity. *Dalton Trans.*, 2015; 44: 1905–1913
- [47] Nowakowska A., Tarasiuk J.: Procesy inwazji i przerzutowania komórek opornych na chemioterapię. *Postępy Hig. Med. Dośw.*, 2017; 71: 380–397
- [48] Pelillo C., Mollica H., Eble J.A., Grosche J., Herzog L., Codan B., Sava G., Bergamo A.J.: Inhibition of adhesion, migration and of $\alpha 5\beta 1$ integrin in the HCT-116 colorectal cancer cells treated with the ruthenium drug NAMI-A. *J. Inorg. Biochem.*, 2016; 160: 225–235
- [49] Peti W., Pieper T., Sommer M., Keppler B.K., Giester G.: Synthesis of tumor-inhibiting complex salts containing the anion tetrachlorobis(indazole)ruthenate(III) and crystal structure of the tetraphenylphosphonium salt. *Eur. J. Inorg. Chem.*, 1999; 1551–1555
- [50] Pillozzi S., Gasparoli L., Stefanini M., Ristori M., D'Amico M., Alessio E., Scaletti F., Becchetti A., Arcangeli A., Messori L.: NAMI-A is highly cytotoxic toward leukaemia cell lines: evidence of inhibition of KCa 3.1 channels. *Dalton Trans.*, 2014; 43: 12150–12155
- [51] Popper H.H.: Progression and metastasis of lung cancer. *Cancer Metastasis Rev.*, 2016; 35: 75–91
- [52] Rademaker-Lakhai J.M., van den Bongard D., Plum D., Beijnen J.H., Schellens J.H.: A Phase I and pharmacological study with imidazolium-trans-DMSO-imidazole tetrachlororuthenate, a novel ruthenium anticancer agent. *Clin. Cancer Res.*, 2004; 10: 3717–3727
- [53] Rancoule C., Guy J.B., Vallard A., Ben Mrad M., Rehaïlia A., Magné N.: 50th anniversary of cisplatin. *Bull. Cancer*, 2017; 104: 167–176
- [54] Romero-Canelón I., Sadler P.J.: Next-generation metal anticancer complexes: multitargeting via redox modulation. *Inorg. Chem.*, 2013; 52: 12276–12291
- [55] Schoenhacker-Alte B., Mohr T., Pirker C., Kryeziu K., Kuhn P.S., Buck A., Hofmann T., Gerner C., Hermann G., Koellensperger G., Keppler B.K., Berger W., Heffeter P.: Sensitivity towards the GRP78 inhibitor KP1339/IT-139 is characterized by apoptosis induction via caspase 8 upon disruption of ER homeostasis. *Cancer Lett.*, 2017; 404: 79–88
- [56] Seelig M.H., Berger M.R., Keppler B.K.: Antineoplastic activity of three ruthenium derivatives against chemically induced colorectal carcinoma in rats. *J. Cancer Res. Clin. Oncol.*, 1992; 118: 195–200
- [57] Singh V., Azad G.K., Mandal P., Reddy M.A., Tomar R.S.: Anticancer drug KP1019 modulates epigenetics and induces DNA damage response in *Saccharomyces cerevisiae*. *FEBS Lett.*, 2014; 588: 1044–1052
- [58] Śliwińska-Hill U., Celmer J.: Związki koordynacyjne rutenu jako leki w nowoczesnej terapii przeciwnowotworowej. *Nowotwory*, 2015; 65: 517–528
- [59] Thota S., Rodrigues D.A., Crans D.C., Barreiro E.J.: Ru(II) compounds: Next-generation anticancer metallotherapeutics? *J. Med. Chem.*, 2018; 61: 5805–5821
- [60] Webb M.L., Walsby C.J.: Albumin binding and ligand-exchange processes of the Ru(III) anticancer agent NAMI-A and its bis-DMSO analogue determined by ENDOR spectroscopy. *Dalton Trans.*, 2015; 44: 17482–17493
- [61] Winkler G.C., Barle E.L., Galati G., Kluwe W.M.: Functional differentiation of cytotoxic cancer drugs and targeted cancer therapeutics. *Regul. Toxicol. Pharmacol.*, 2014; 70: 46–53
- [62] Yeung K.T., Yang J.: Epithelial-mesenchymal transition in tumor metastasis. *Mol. Oncol.*, 2017; 11: 28–39

Autorzy deklarują brak potencjalnych konfliktów interesów.



OPEN

DNA damage and antioxidant properties of CORM-2 in normal and cancer cells

Michał Juszcak, Magdalena Kluska, Daniel Wysokiński & Katarzyna Woźniak✉

In this study, we compared the effect of tricarbonyldichlororuthenium (II) dimer (CORM-2) and its CO-depleted molecule (iCORM-2) on human peripheral blood mononuclear cells (PBMCs) and human promyelocytic leukemia HL-60 cells. We determined cell viability, DNA damage and DNA repair kinetics. We also studied the effect of both compounds on DNA oxidative damage, free radical level and HO-1 gene expression. We showed that at low concentrations both CORM-2 and iCORM-2 stimulate PBMCs viability. After 24-h incubation, CORM-2 and iCORM-2, at the concentration of 100 μM , reduce the viability of both PBMCs and HL-60 cells. We also demonstrated that CORM-2 and iCORM-2, in the 0.01–100 μM concentration range, cause DNA damage such as strand breaks and alkaline labile sites. DNA damage was repaired efficiently only in HL-60 cells. CORM-2 significantly reduces oxidative stress induced by 1 mM H_2O_2 in normal and cancer cells. On the contrary, iCORM-2 in HL-60 cells increases the level of free radicals in the presence of 1 and 5 mM H_2O_2 . We also revealed that both CORM-2 and iCORM-2 induce HO-1 gene expression. However, CORM-2 induces this gene to a greater extent than iCORM-2, especially in HL-60 cells at 100 μM . Finally, we showed that CORM-2 and iCORM-2 reduce H_2O_2 -induced DNA oxidative damage. Furthermore, CORM-2 proved to be a compound with stronger antioxidant properties than iCORM-2. Our results suggest that both active CORM-2 and inactive iCORM-2 exert biological effects such as cyto- and genotoxicity, antioxidant properties and the ability to induce the HO-1 gene. The released CO as well as iCORM-2 can be responsible for these effects.

Carbon monoxide (CO) is a colorless, tasteless and odorless gas produced by the burning of fuels and organic materials. It is reported to be the most frequent cause of fatal poisoning with an incidence rate of 31%. CO is readily absorbed and is unchanged by the lungs. CO demonstrates more than 200-fold stronger affinity for hemoglobin compared to oxygen. Therefore, even a small level of CO may cause poisoning. In contrast to hypoxia-inducing toxic concentrations, a low dose of CO or even nanomolar concentrations exert biological activities. CO is produced in low amounts as a byproduct of normal human metabolism by the enzyme called heme oxygenase (HO-1)¹. CO has the ability to reduce the stimulation of guanylate cyclase to generate cyclic guanosine 3',5'-monophosphate (cGMP). As a signaling molecule, CO modulates several p38 mitogen-activated protein kinase (MAPK)-related signaling pathways via both cGMP-dependent and independent processes, directly activates calcium-dependent potassium channels and induces protein kinase B (Akt) phosphorylation via the phosphatidylinositol 3-kinase/Akt pathway². Moreover, CO inhibits mitochondrial respiration by binding the ferrous heme a_3 in the active site of cyclooxygenase (COX), effectively shutting down oxidative phosphorylation, similar to the effects of cyanide and nitric oxide (NO)³. The cGMP-dependent activity of CO includes inhibition of smooth muscle cell proliferation, platelet aggregation, neurotransmission and vasodilation. The CO-mediated cGMP-independent activity comprises anti-inflammatory, anti-apoptotic and antiproliferative effects². Thus, CO at low concentrations may demonstrate a therapeutic potential.

Carbon Monoxide-Releasing Molecules (CORMs) were introduced as a concept of using a chemically bound form of CO as a pro-drug for physiological CO release⁴. There are three main trigger mechanisms to initiate CO release from the metal coordination sphere: ligand-exchange triggered, enzyme-triggered and photo induced release. CORMs usually contain a transition metal core, such as manganese, ruthenium, or iron, surrounded by some carbonyl groups (CO) as a coordinated ligand⁵.

Faculty of Biology and Environmental Protection, Department of Molecular Genetics, University of Lodz, Pomorska 141/143, 90-236 Lodz, Poland. ✉email: katarzyna.wozniak@biol.uni.lodz.pl

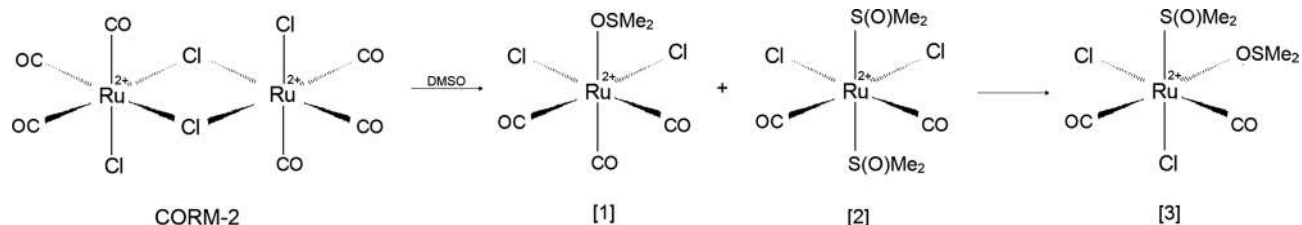


Figure 1. The reaction between CORM-2 and DMSO, whose final product is iCORM-2 marked as [3]. DMSO: $(\text{Me})_2\text{SO}$; [1]: *fac*- $[\text{RuCl}_2(\text{CO})_3(\text{DMSO})]$; [2]: *cis, cis, trans*- $[\text{RuCl}_2(\text{CO})_2(\text{DMSO})_2]$; [3]: *cis, cis, cis*- $[\text{RuCl}_2(\text{CO})_2(\text{DMSO})_2]$ ^{4,11}.

Among several different CORMs synthesized, tricarbonyldichlororuthenium(II) dimer (CORM-2) has been used extensively in *in vitro* and *in vivo* studies^{6–9}. CORM-2 rapidly liberates CO in physiological buffers (half-life of about 1 min at 37 °C and pH 7.4)^{4,10}. CORM-2 is insoluble in water and requires addition of DMSO to induce the liberation of carbon monoxide in a ligand-exchange triggered process leading to *fac*- $[\text{RuCl}_2(\text{CO})_3(\text{DMSO})]$ [1] and *cis, cis, trans*- $[\text{RuCl}_2(\text{CO})_2(\text{DMSO})_2]$ [2] (Fig. 1). Subsequently, *trans*- $[\text{RuCl}_2(\text{CO})_2(\text{DMSO})_2]$ [2] isomer slowly converts to the more stable all *cis* isomer^{3,4}. These final decomposition products are commonly called inactivated CORMs (iCORMs), but may have own biological activity. Further CO-release from the dicarbonyl complex does not occur even upon extended incubation¹¹.

Several reports indicate that CORM-2 significantly influences cellular ROS defense mechanisms under both *in vitro* and *in vivo* conditions^{12,13}. The effect of CORM-2 on tumor cell proliferation, apoptosis and angiogenesis has also been studied^{14–19}. It was shown that CO released by CORM-2 inhibited proliferation and invasion, as well as induced apoptosis in human prostate cancer cell lines – LNCaP and PC-3¹⁹. *In vivo*, CO suppressed tumor growth and induced apoptosis in tumor xenografts in nude mice. Similar results were observed and recorded in the case of non-small-cell lung carcinoma (NSCLC) Calu-3 cells¹⁸. CORM-2 reduced proliferation, migration and invasion of Calu-3 cells. It also increased their apoptosis through downregulation of the Bcl-2/Bax ratio and upregulation of caspase-3 and cytochrome c levels¹⁸. A recent study indicates that among the commercially available CORMs (CORM-1, CORM-2 and CORM-A1) CORM-2 has the largest anti-angiogenic potential for triple-negative breast cancer (TNBC)¹⁴.

CORMs are intensively tested as potential drugs for various diseases, including cancer²⁰. It is assumed that CO carried in the form of CORM-2 will be responsible for potential anti-cancer properties. To verify this hypothesis, we conducted a comparative analysis of CORM-2 and its CO-depleted molecule (iCORM-2) on human peripheral blood mononuclear cells (PBMCs) (normal cells) and human promyelocytic leukemia HL-60 cells. Normally, cytotoxicity analysis is performed in this type of study. We examined the viability of both cell types after 2, 6 and 24 h incubation with CORM-2 and iCORM-2 using the cell viability resazurin assay. Because many anti-cancer drugs are genotoxic, we decided to study the ability of CORM-2 and iCORM-2 to induce DNA damage, as well as the efficiency of their repair by the comet assay. Another mechanism of action of anti-cancer compounds is the ability to induce oxidative stress. In our study, we measured the effect of CORM-2 and iCORM-2 on free radicals *per se*, as well as their effect on H_2O_2 -induced oxidative stress by using a probe H_2DCFDA . CORM-2 showed stronger antioxidant properties than iCORM-2, because CO has reducing power. We then decided to investigate whether the induction of the HO-1 gene may be related with the antioxidant properties of CORM-2 and iCORM-2. Finally, we examined whether CORM-2 can protect DNA against oxidative damage. Our research has shown that not only CO released from CORM-2, but also iCORM-2 show biological activity in normal and cancer cells.

Materials and methods

Chemicals. Tricarbonyldichlororuthenium(II) dimer (CORM-2), low-melting-point (LMP) and normal-melting-point (NMP) agarose, phosphate buffered saline (PBS), 4',6-diamidino-2-phenylindole (DAPI), resazurin sodium salt, dimethyl sulfoxide (DMSO) and hydrogen peroxide (H_2O_2) were purchased from Sigma-Aldrich (St. Louis, MO, USA). All other chemicals were of the highest commercial grade available. A stock solution of CORM-2 (10 mM) was dissolved in 50% DMSO (DMSO mixed with autoclaved water in ratio 1:1). iCORM-2 was obtained from the CORM-2 stock solution after overnight incubation at 37 °C¹⁰. The final concentration of DMSO was not higher than 0.5% in all samples.

Methods

Cells culture. Peripheral blood mononuclear cells (PBMCs) were isolated from a leucocyte-buffy coat collected from the blood of healthy non-smoking donors from the Blood Bank in Lodz, Poland, as described previously²¹. The study protocol was approved by the Committee for Research on Human Subjects of the University of Lodz (17/KBBN-UŁ/III/2019).

The HL-60 (human promyelocytic leukemia) cell line was obtained from the American Type Culture Collection (ATCC) and cultured as described previously^{21,22}.

Cell viability resazurin assay. The cell viability resazurin assay was performed in a manner similar to the method described by O'Brien et al.²³. Resazurin salt powder was dissolved in sterile PBS buffer. Cells were seeded on 96-well plates in count of 15 000 in the case of HL-60 cells and of 50 000 for PBMCs per well. CORM-2 and

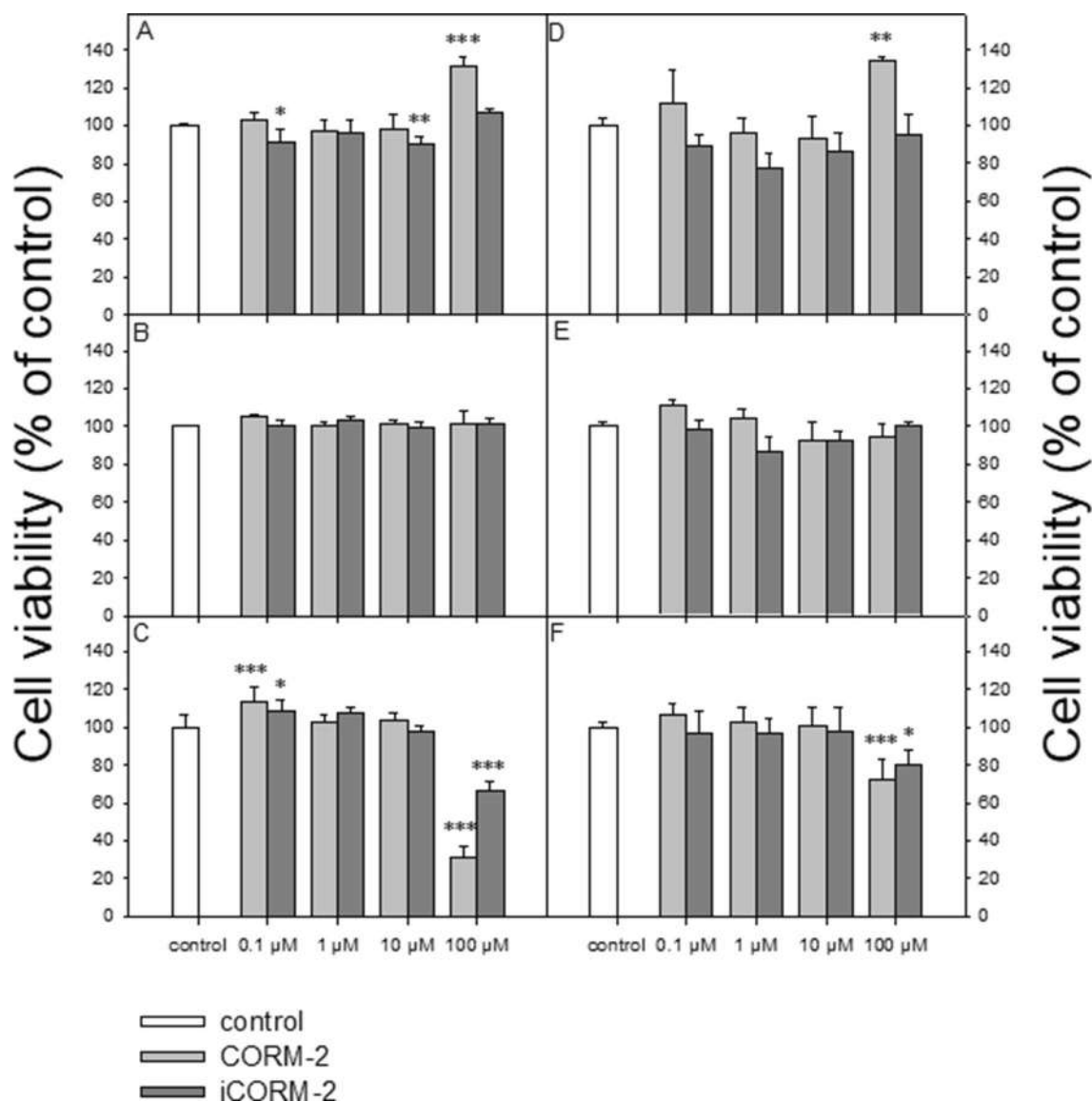


Figure 2. Cell viability, measured as values of relative fluorescence unit (RFU), for PBMCs (A–C) and HL-60 cells (D–F) incubated with CORM-2 or iCORM-2 at 0.1, 1, 10 and 100 μM for: 2 h (A and D), 6 h (B and E) and 24 h (C and F). The figures show mean results from three independent experiments. Error bars denote SD; * $P < 0.05$, ** $P < 0.01$, *** $P < 0.001$.

iCORM-2 were added to the wells to obtain final concentrations of 0.1, 1, 10 and 100 μM, and then incubated for 2, 6 and 24 h at 37 °C in 5% CO₂. Next, 10 μl of resazurin salt was added to each well and the plates again were incubated at 37 °C in 5% CO₂ for 2 h. After that, fluorescence was measured with HT microplate reader Synergy HT (BioTek Instruments, USA) using $\lambda_{ex} = 530/25$ and an $\lambda_{em} = 590/35$ nm. The effects of CORM-2 and iCORM-2 were quantified as the percentage of control fluorescence (Fig. 2).

DNA damage. CORM-2 and iCORM-2 were added to the suspension of the cells to give final concentrations of 0.01, 0.025, 0.05, 0.1, 1, 10, 50 and 100 μM. Both PBMCs and HL-60 cells were incubated for 2 h at 37 °C in 5% CO₂. The experiment included a positive control, i.e. a cells sample incubated with hydrogen peroxide (H₂O₂) at 25 μM for 15 min on ice. The cells after treatment with CORM-2 and iCORM-2 were washed and suspended in the IMDM medium. A freshly prepared suspension of the cells in LMP agarose dissolved in PBS was spread onto microscope slides. The slides were processed as described previously^{21,22}.

DNA repair. PBMCs and HL-60 cells were incubated with CORM-2 and iCORM-2 for 2 h at 37 °C in 5% CO₂ at 100 μM and then were washed and suspended in fresh IMDM medium preheated to 37 °C. DNA repair was assessed by the extent of residual DNA damage detected at each time-point using the comet assay as described previously²².

Effect of CORM-2 on DNA oxidative damage. Based on the results obtained by Babu et al.¹⁰, we investigated CORM-2 as a compound showing potential to reduce DNA oxidative damage. We prepared two experimental schemes of CORM-2 and iCORM-2 incubation with H₂O₂: pre-incubation and pre-incubation + co-incubation. In the first scheme, the cells were initially incubated with 40 μM CORM-2 or iCORM-2 for 1 h at 37 °C in 5% CO₂; then the cells were washed and incubated with 25 or 50 μM H₂O₂ for 15 min on ice. In the second scheme, the cells were initially incubated with 40 μM CORM-2 or iCORM-2 for 1 h at 37 °C in 5% CO₂; then the cells were incubated simultaneously with 40 μM CORM-2 or iCORM-2 and 25 or 50 μM H₂O₂ for 15 min on ice. After incubation in all the schemes, the cells were washed, suspended in LMP agarose and spread onto microscope slide. The slides were processed as described previously^{21,22}.

Comet assay. The comet assay was performed under alkaline conditions according to a procedure described previously^{21,22}.

Evaluation of oxidative stress. In order to measure the production of reactive oxygen species (ROS), the fluorescence of 2',7'-dichlorofluorescein diacetate (H₂DCFDA) was measured. H₂DCFDA is a cell-permeable non-fluorescent probe. 2',7'-dichlorofluorescein diacetate is de-esterified intracellularly and turns into highly fluorescent 2',7'-dichlorofluorescein upon oxidation. The cells (final density 1 × 10⁶ cells/ml) were pre-incubated with 40 μM CORM-2 and 40 μM iCORM-2 for 1 h at 37 °C in Hank's balanced salt solution (HBSS) containing Ca²⁺ and Mg²⁺ (Lonza) in darkness. Next, the cells were washed twice with HBSS containing Ca²⁺ and Mg²⁺ and stained with 20 μM H₂DCFDA (Sigma-Aldrich, St. Louis, MO, USA) for 30 min at 37 °C in darkness. Then, the cells were washed twice with HBSS and incubated with 1 mM and 5 mM H₂O₂ at 37 °C in darkness. The intensity of fluorescence was measured after 15, 30, 45 and 60 min with λ_{ex} = 495 nm and λ_{em} = 530 nm using a microplate reader Synergy HT (BioTek Instruments, USA). The data were analyzed according to the following formula: $(T_x - T_0/T_0) \times 100$, where T_x is the DCF fluorescence measured at the indicated time and T₀ is the DCF fluorescence measured at the beginning of the analysis²⁴.

HO-1 gene expression analysis. CORM-2 and iCORM-2 were added to the suspension of the cells to give final concentrations of 40 and 100 μM. The cells were incubated for 2 h at 37 °C. Total RNA was extracted from each sample after 3 h post-incubation without CORM-2 and iCORM-2. Reverse transcription and real-time PCR reaction were performed as described previously²².

Statistical analysis. The values of the cell viability experiment were presented as mean ± SD from six repeats. The values of the comet assay were expressed as mean + standard error of the mean from three experiments; data from three experiments were pooled, and the statistical parameters were calculated. The statistical analysis was conducted using the Mann–Whitney test (samples with distributions departing from normality) and the Student's t-test (samples with the normal distribution).

HO-1 gene expression was calculated by double delta Ct. Statistics were performed using Student's two-tailed t test. Data were presented as a mean ± SD, relative to control. HO-1 expression was normalized to GAPDH (as a reference gene).

The differences were considered to be statistically significant when the P value was < 0.05.

Results

Cell viability. We used the resazurin reduction assay to determine cell viability after incubation with CORM-2 and iCORM-2. This assay is based on the application of an indicator dye to measure oxidation–reduction reactions, which principally occur in the mitochondria of live cells. The non-fluorescent dark blue dye (resazurin) becomes fluorescently pink at 570 nm and fluorescently red at neutral pH (resorufin), when reduced by metabolically active cells.

We observed an increase in the RFU value after 2 h incubation with CORM-2 at 100 μM in both PBMCs (*P* < 0.001) (Fig. 2A) and HL-60 cells (*P* < 0.01) (Fig. 2D). Under these conditions, we observed a decrease in RFU in PBMCs in the case of iCORM-2 at 0.1 μM (*P* < 0.05) and 10 μM (*P* < 0.01). We did not observe any changes in the RFU values after 6 h incubation of the cells with CORM-2 and iCORM-2 (Fig. 2B,E). After 24 h incubation, we noticed an increase in the RFU values for CORM-2 (*P* < 0.001) and iCORM-2 (*P* < 0.05) at the concentration of 0.1 μM, but only in PBMCs (Fig. 2C). In both cell types, the RFU values decreased after incubation with CORM-2 and iCORM-2 at 100 μM (Fig. 2C,F). Our results indicate that CO released from CORM-2 at a low concentration can increase cell viability. However, both CORM-2 and iCORM-2 were eventually cytotoxic at 100 μM for normal and cancer cells.

DNA damage and repair. Figure 3 shows the level of DNA damage analyzed by the comet assay under alkaline conditions. The comet assay in the alkaline version is a sensitive and simple method of determining the level of DNA damage, including single- and double-strand breaks and alkali-labile sites in living cells²⁵. We observed a significant increase in the level of DNA damage in PBMCs incubated with CORM-2 and iCORM-2 compared to DMSO (Fig. 3A). We also observed a significant increase of DNA damage in the case of HL-60 cells after incubation with CORM-2 and iCORM-2 compared to negative control and DMSO (*P* < 0.001) (Fig. 3B). We did not detect any significant differences in the level of DNA damage between CORM-2 and iCORM-2 in PBMCs and HL-60 cells, except HL-60 cells incubated with 0.1 μM (*P* < 0.001) (Fig. 3B). In this case, we observed a significant decrease of DNA damage in cells incubated with iCORM-2 compared to the level of DNA damage in cells incubated with CORM-2. Figure 4 shows the example images of comets from this experiment.

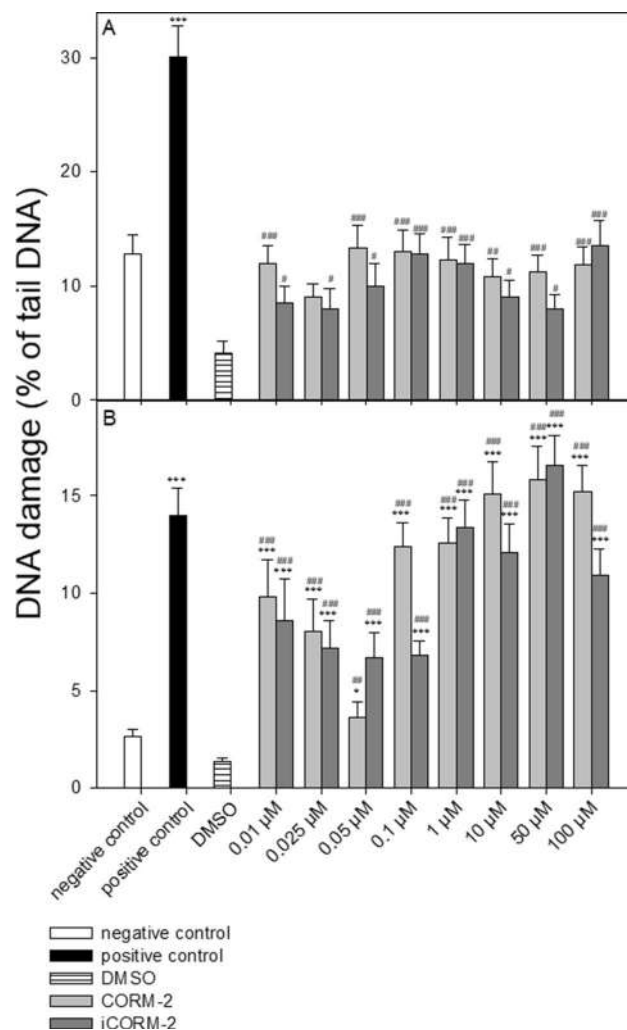


Figure 3. DNA damage, measured as the comet tail DNA (%) of PBMCs (A) and HL-60 cells (B) incubated for 2 h at 37 °C with CORM-2 or iCORM-2 at indicated concentrations, analyzed by the alkaline comet assay. The figures show mean results \pm SEM, $n = 100$; * $P < 0.05$, ** $P < 0.01$, *** $P < 0.001$ compared with negative control and # $P < 0.05$, ## $P < 0.01$, ### $P < 0.001$ compared with DMSO.

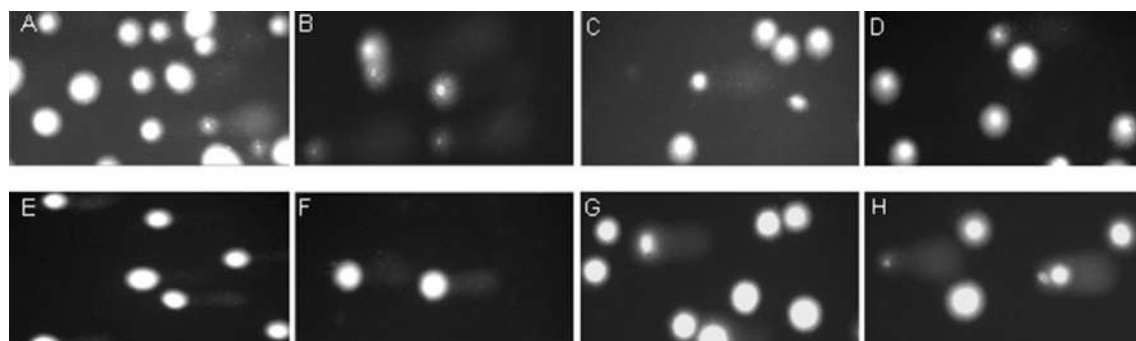


Figure 4. Representative photos of comets obtained in the alkaline version of the comet assay after incubation of PBMCs (C and D) and HL-60 cells (G and H) with CORM-2 and iCORM-2 at 50 μM for 2 h, respectively. (A): PBMCs incubated without CORM-2 or iCORM-2 for 2 h; (E): HL-60 incubated without CORM-2 or iCORM-2 for 2 h; (B): PBMCs incubated with H₂O₂ at 25 μM for 15 min on ice; (F): HL-60 cells incubated with H₂O₂ at 25 μM for 15 min on ice.

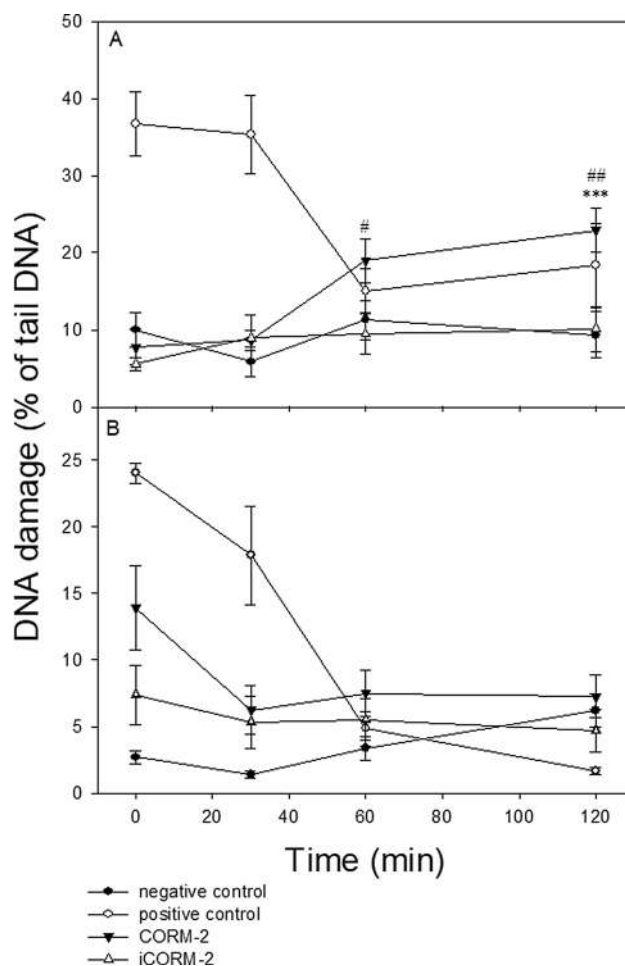


Figure 5. DNA repair of DNA damage induced by CORM-2 and iCORM-2 at 100 for 2 h at 37 °C in PBMCs cells (A) and HL-60 cells (B). Changes in the level of DNA damage were measured in time points: 0 min, 30 min, 60 min and 120 min. The figures show mean results \pm SEM, $n = 100$; *** $P < 0.001$ compared with the extent of DNA damage at time of 120 min in negative control; # $P < 0.05$, ## $P < 0.01$ CORM-2 vs. iCORM-2.

Figure 5 shows DNA damage in PBMCs (A) and HL-60 cells (B) incubated with CORM-2 and iCORM-2 at 100 μ M immediately after 2 h incubation as well as 30, 60 and 120 min later. We observed changes over time in the level of DNA damage after washout of the test compounds. We have determined that the damage was repaired, when the cells which were incubated with CORM-2 or iCORM-2 reached the level of DNA damage in control cells after 120 min repair incubation. We detected that DNA damage induced by CORM-2 in PBMCs was not repaired within 120 min post-incubation (Fig. 5A). We observed a significant difference ($P < 0.001$) in the level of DNA damage between cells incubated with CORM-2 and negative control. We also observed a significant difference in the level of DNA damage between PBMCs incubated with CORM-2 and iCORM-2 after 60 min ($P < 0.05$) and 120 min ($P < 0.01$) (Fig. 5A).

HL-60 cells incubated with CORM-2 and iCORM-2 were able to ensure total repair of DNA damage within the repair incubation time of 120 min (Fig. 5B).

PBMCs and HL-60 cells exposed to 25 μ M H_2O_2 for 15 min on ice (positive control) were able to effectively repair DNA damage within 120 min (Fig. 5A,B). We did not observe any changes in the level of DNA damage during repair incubation of cells exposed to DMSO (data not shown).

Effect of CORM-2 and iCORM-2 on oxidative stress. Figure 6 shows the effect of CORM-2 and iCORM-2 on oxidative stress induced by H_2O_2 in PBMCs and HL-60 cells. In PBMCs, both CORM-2 and iCORM-2 reduced oxidative stress induced by 1 mM H_2O_2 ($P < 0.001$) (Fig. 6A). However, this effect was more pronounced in the case of CORM-2 ($P < 0.001$). After incubation of PBMCs with 5 mM H_2O_2 , we observed an increase in oxidative stress in the cells pre-incubated with CORM-2 ($P < 0.05$) and iCORM-2 ($P < 0.01$) (Fig. 6A).

The effect of CORM-2 on oxidative stress was very strong in HL-60 cells (Fig. 6B). The effect of CORM-2 was significant even in the cells which were not incubated with H_2O_2 . We also observed that CORM-2 reduces oxidative stress in cells incubated with 1 mM H_2O_2 ($P < 0.001$). In the case of HL-60 cells pre-incubated with iCORM-2, we noticed a significant increase in oxidative stress, especially in the cells incubated with 5 mM H_2O_2 ($P < 0.001$).

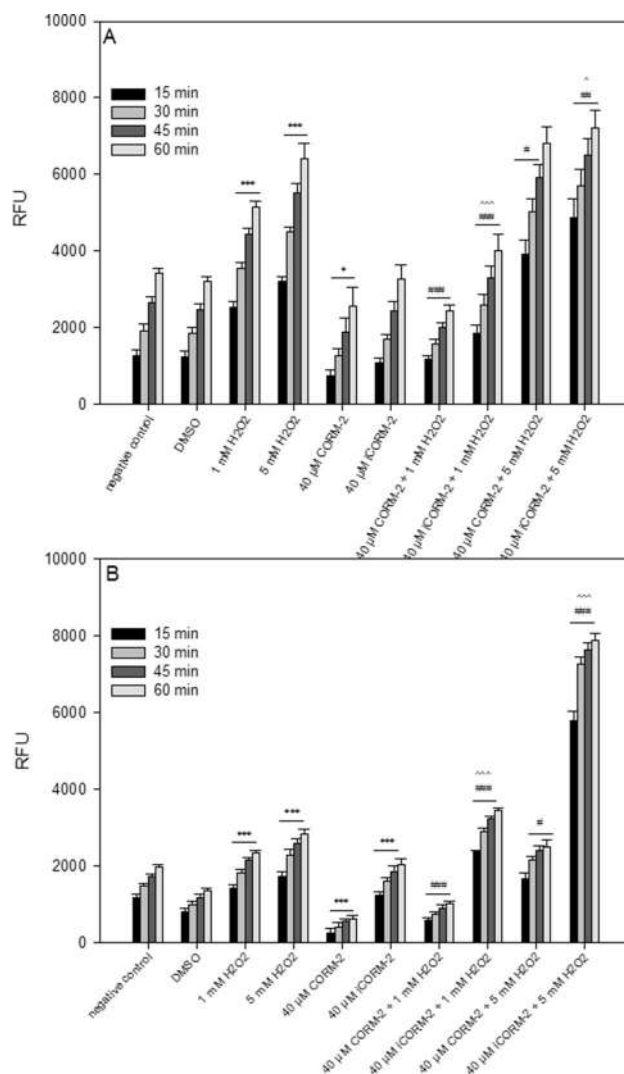


Figure 6. Changes in reactive oxygen species level in PBMCs (A) and HL-60 cells (B) pre-incubated with 40 μM CORM-2 and 40 μM iCORM-2 for 1 h at 37 °C and then incubated with 1 mM or 5 mM H₂O₂ at 37 °C. Changes in RFU were measured after 15 min, 30 min, 45 min and 60 min. Each value represents the mean ± SD, which was calculated from 6 individual experiments; * $P < 0.05$, *** $P < 0.001$ negative control or DMSO vs. H₂O₂ or CORM-2/iCORM-2, respectively; # $P < 0.05$, ## $P < 0.01$, ### $P < 0.001$ H₂O₂ vs. CORM-2/iCORM-2 + H₂O₂; ^ $P < 0.05$, ^^ $P < 0.01$, ^^ $P < 0.001$ CORM-2 + H₂O₂ vs. iCORM-2 + H₂O₂.

Effect of CORM-2 and iCORM-2 on HO-1 gene expression. Figure 7 shows the effects on HO-1 gene expression. Both in PBMCs and HL-60 cells we observed significant HO-1 gene upregulation after incubation with CORM-2 and iCORM-2 ($P < 0.001$). The observed increase was dependent on the concentration of both CORM-2 and iCORM-2. In PBMCs incubated with iCORM-2 at the concentrations of 40 μM and 100 μM, we detected a slightly lower increase of HO-1 gene expression ($P < 0.05$ and $P < 0.001$, respectively) compared to PBMCs incubated with CORM-2 (Fig. 7A).

In HL-60 cells incubated with CORM-2 at 100 μM we noticed a 100-fold increase of HO-1 gene expression (Fig. 7B). Similarly like in PBMCs, we observed a slightly lower increase of HO-1 gene expression after incubation with iCORM-2 at the concentration of 40 μM compared to HL-60 cells incubated with 40 μM CORM-2 ($P < 0.001$). In the case of HL-60 cells incubated with iCORM-2 at the concentration of 100 μM, we detected approximately 50% lower expression of the HO-1 gene compared to the cells incubated with 100 μM CORM-2 ($P < 0.001$).

Effect of CORM-2 and iCORM-2 on DNA oxidative damage. In this experiment we induced DNA oxidative damage in PBMCs and HL-60 cells by using H₂O₂ and we investigated the effect of CORM-2 and iCORM-2 on the level of DNA oxidative damage. We performed these studies in two different experimental systems described in Materials and Methods. The results obtained in the experiment with pre-incubation of the cells with CORM-2 or iCORM-2 clearly showed a significant decrease of DNA oxidative damage induced

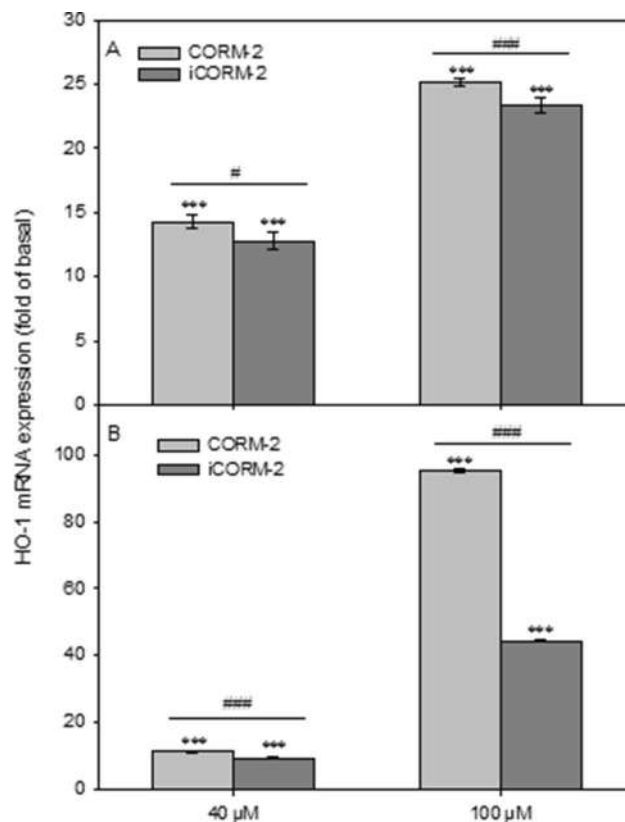


Figure 7. Relative expression of HO-1 gene in PBMCs (A) and HL-60 cells (B) incubated with CORM-2 and iCORM-2, presented as a fold-change in accordance to control (double delta Ct method). Data were normalized to GAPDH gene as a reference. Columns represent mean values \pm SD, which was calculated from 4 individual experiments; *** $P < 0.001$ control vs. CORM-2 or iCORM-2; # $P < 0.05$; ### $P < 0.001$ CORM-2 vs. iCORM-2.

by H_2O_2 ($P < 0.001$) (Fig. 8A,B). This effect was more pronounced in the case of CORM-2 and DNA damage induced by $25 \mu M H_2O_2$. Similarly, in the experiment with pre-incubation and co-incubation with CORM-2 or iCORM-2 we observed a significant decrease of DNA oxidative damage in both PBMCs and HL-60 cells ($P < 0.001$) (Fig. 8C,D).

Discussion

In this study, we examined the effect of CORM-2 and iCORM-2 on human peripheral blood mononuclear cells (PBMCs) and human promyelocytic leukemia HL-60 cells. We determined cell viability, DNA damage and their repair kinetics. We also studied the effect of both compounds on DNA oxidative damage, free radical level and HO-1 gene expression.

Our results indicate that CO released from CORM-2 can increase cell viability (Fig. 2A,C,D). However, we observed a cytotoxic effect of $100 \mu M$ CORM-2 and iCORM-2 after 24 h incubation (Fig. 2C,F). Interestingly, we observed cell stimulation and their increased viability only in PBMCs after 24 h incubation with both CORM-2 and iCORM-2 at $0.1 \mu M$ (Fig. 2C).

The mitochondria are the most recognized cellular targets for carbon monoxide. CO prevents cell death by limiting mitochondrial membrane permeabilization, which inhibits the release of pro-apoptotic factors into the cytosol²⁶. It was found that CORM-2 significantly attenuated 6-hydroxydopamine (6-OHDA)-induced apoptotic cell death in a dose-dependent manner in C6 glioma cells¹⁶. CORM-2 decreased the Bax/Bcl2 ratio and caspase-3 activity, which had been increased by 6-OHDA. Winburn et al. showed that both CORM-2 and iCORM-2 decreased cisplatin-induced caspase-3 activity in MDCK (Madin-Darby canine kidney Cells) and HeK (human embryonic kidney) cells suggesting an anti-apoptotic effect²⁷. On the other hand, it was shown in the same study that both CORM-2 and iCORM-2 induced cellular toxicity by decreased cell viability, abnormal cell cytology, increased apoptosis and necrosis, cell cycle arrest and reduced mitochondrial enzyme activity²⁷.

In our study we showed that both CORM-2 and iCORM-2 induce DNA damage, including DNA single and double strand breaks and alkali labile sites in PBMCs and HL-60 cells (Fig. 3A,B). We did not observe any significant differences between CORM-2 and iCORM-2 in the level of induced DNA damage. HL-60 cells are much more sensitive to both CORM-2 and iCORM-2 compared to normal PBMCs. We observed a significant increase of DNA damage in HL-60 cells after incubation with CORM-2 and iCORM-2 compared to negative control ($P < 0.001$) and DMSO ($P < 0.001$). The difference in the level of DNA damage between PBMCs and HL-60 cells can be associated with the overexpression of transferrin receptors present on the surface of cancer cells. As

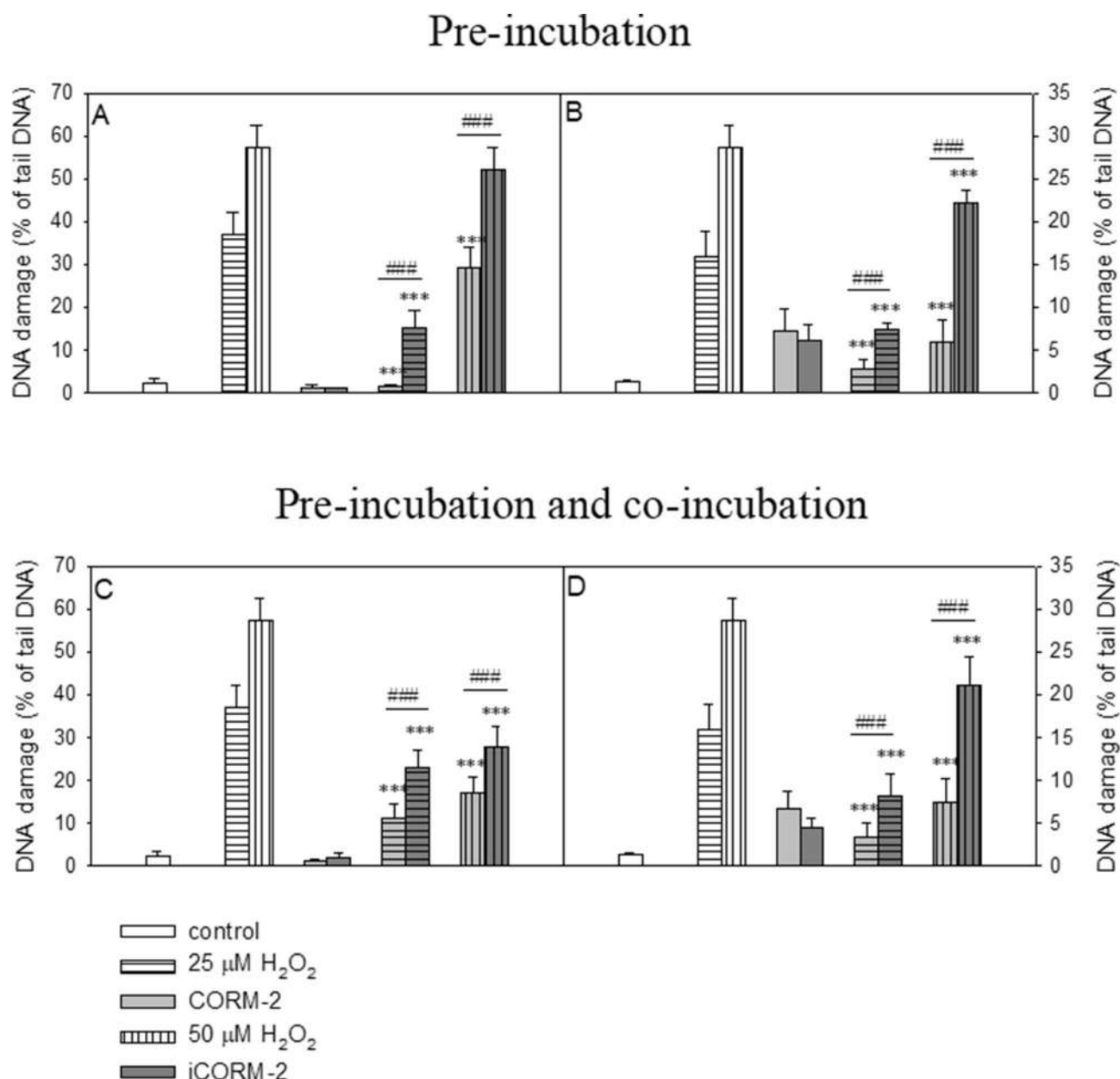


Figure 8. Effects of 40 μM CORM-2 and 40 μM iCORM-2 on H_2O_2 -induced DNA damage in PBMCs (A and C) and HL-60 (B and D). The figures show mean results \pm SEM, $n = 100$; *** $P < 0.001$ compared with H_2O_2 ; ### $P < 0.001$ CORM-2 vs. iCORM2.

previously described, leukemic cells are known to overexpress transferrin receptors²⁸. CORM-2 contains ruthenium, which can mimic iron. It was shown that ruthenium can be up taken into cells by transferrin receptors²⁹.

DNA damage induced by CORM-2 and iCORM-2 in HL-60 cells was effectively repaired within 120 min post-incubation (Fig. 5B). PBMCs did not repair DNA damage induced by CORM-2. On the contrary, we observed an increase of DNA damage in these cells during post-incubation repair (Fig. 5A). DNA damage induced by iCORM-2 in PBMCs was effectively repaired. Possible reasons for this may include differences in the activity of DNA repair systems in normal and cancer cells. The presence of c-MYC oncogene in HL-60 may be responsible for more effective DNA repair compared to PBMCs. It was found that increased expression of c-MYC results in a decrease of BIN1 (Bridging Integrator 1) protein expression. BIN1 binds to PARP1 and inhibits its activity. Decreased expression of BIN1 causes induction of PARP and can stimulate DNA repair³⁰. On the other hand, it was shown that HO-1 induction or exposure to CO induces homologous recombination-mediated DNA repair through ataxia-telangiectasia mutated/ataxia telangiectasia and Rad3-related (ATM/ATR) protein³¹. Effective repair of CORM-2-induced DNA damage may be also associated with high mobility group box 1 protein (HMGB-1). It was found that CORM-2 treatment prevents nuclear-cytoplasmic translocation of this protein in primary mouse renal proximal tubular epithelial cells (RPTECs)³². HMGB1 protein accumulated in cellular nuclei as a result of CORM-2 action might stimulate DNA repair³³.

We suggest that DNA damage induced by CORM-2 and iCORM-2 may result from the presence of ruthenium in these molecules. Many types of interactions of ruthenium-containing compounds with DNA have been described in the literature such as coordinative, intercalative, minor groove binding, sequence specificity of DNA binding, the ability of ruthenium compounds to condense and cleave DNA, binding to A- and Z-DNA, DNA quadruplexes and other unusual DNA structures³⁴. Ruthenium, similarly to other transition metals such as Fe, Cr and Cu, can damage cells by producing free radicals. It was shown that CORM-2 caused DNA damage in bacteria cells³⁵. Bacteria cells treated with CORM-2 contained higher levels of free iron arising from the destruction of iron-sulfur proteins. Moreover, Tavares et al. showed that CORM-2 generated hydroxyl radicals in a cell-free solution, a process that was abolished by scavenging CO³⁵. It was demonstrated that the radical formation from CORM-2 is closely associated with the presence of CO ligands as no radical species were observed in the inactive compound devoid of CO, iCORM-2³⁵. Our study of the cell system revealed that CORM-2 at 40 μM does not induce free radicals (Fig. 6A,B). On the contrary, this compound reduces free radicals even in cells not exposed to oxidative stress. We observed free radical generation in HL-60 cells pre-incubated with 40 μM iCORM-2 (Fig. 6B). In the presence of 5 mM H₂O₂, especially in HL-60 cells pre-incubated with 40 μM iCORM-2, we demonstrated a significant increase in the level of free radicals compared to cells pre-incubated with 40 μM CORM-2 ($P < 0.001$) (Fig. 6B). Our results clearly indicate that the ability of CORM-2 to reduce oxidative stress depends on CO.

The antioxidant properties of CORM-2 are very well documented. Studies of serum plasma showed that CORM-2 reduces lipid peroxidation induced by H₂O₂ and also by H₂O₂/Fe⁶. Moreover, in human umbilical vein endothelial cells, CORM-2 administration diminishes oxidative stress induced by hypoglycemia³⁶. In vivo, in hypothalamic paraventricular nucleus of Male Dahl Salt-Sensitive rats, inflammation and oxidative stress were induced through high-salt-induced hypertension. As it was shown, a microinjection of CORM-2 decreased the level of ROS, while the levels of CU/Zn-SOD and HO-1 were elevated¹³. CORM-2 also reduces the ROS-dependent doxorubicin cardiotoxicity in mice. In this study, mice were treated with doxorubicin and cardiotoxicity was evaluated by markers such as creatine kinase, lactate dehydrogenase, malondialdehyde and total antioxidant status in serum. Co-treatment of CORM-2 led to a significant reduction of those markers, while the level of HO-1 was markedly elevated⁸. Another study showed that a very low concentration of CORM-2 (50 nM) significantly reduced trimethyltin-induced superoxide production in SH-SY5Y neuroblastoma cells³⁷. Moreover, pretreatment with CORM-2 significantly inhibited airborne particulate matter-induced mitochondria-derived ROS production in human pulmonary alveolar epithelial cells (HPAEPiCs)¹². An experiment carried out on the human gastric cancer AGS cell line confirmed the antioxidant properties of CORM-2 involving significant inhibition of IL-1 β -induced ROS production¹⁵. Pretreatment with CORM-2 inhibited angiotensin-II-induced ROS generation in human aortic smooth muscle cells (HASMCs). Therefore, CORM-2 can play the role of a protective antioxidant in heart and blood vessels⁹. An in vivo study performed on rats exhibited a decrease in oxidative damage of DNA after exposure to CORM-2. The concentration of 8-OHG measured in gastric mucosa cells after exposure to ischemia/reperfusion was significantly lower for CORM-2 compared to the vehicle (DMSO and saline in ratio 1:10)⁷.

The cytoprotective properties of CORM-2 observed by us and by other researchers may result from the ability of this compound to induce HO-1^{7,16,17,38,39}. It was shown that CORM-2-induced HO-1 expression was mediated through a Pyk2/PDGFR/PI3K/Akt/FoxO1/Sp1-dependent manner and exerted a cytoprotective effect in human cardiomyocytes³⁸. Moreover, it was observed that CORM-2 activates the c-SRC/EGFR/PI3K/Akt/JNK1/2 and p38 MAPK pathways, which cause Nrf2 activation and HO-1 expression in human tracheal smooth muscle cells (HTSMCs)³⁹. In human hepatocellular carcinoma cell lines (HCC), the HO-1/CO axis conferred resistance to the TGF- β growth inhibitory signal by increasing Smad3 phosphorylation at Thr-179 via the ERK1/2 pathway¹⁷. HO-1 is considered to be a potential target in cancer therapy, including leukemia⁴⁰. Our results indicate that both CORM-2 and iCORM-2 induce expression of HO-1 in PBMCs and HL-60 cells (Fig. 7A,B). However, after incubation of HL-60 cells with 100 μM CORM-2, we observed a twofold increase in HO-1 expression compared to HL-60 cells incubated with iCORM-2 (Fig. 7B). This result confirms previous conclusions, mentioned above, that CO released from CORM-2 increases HO-1 expression. The increase in HO-1 expression in PBMCs and HL-60 cells observed after incubation with iCORM-2 is probably due to the presence of ruthenium. Therefore, it should be assumed that an increase in HO-1 expression noticeable after incubation of the cells with CORM-2 is due to both the release of CO and the presence of iCORM-2.

The results of our studies regarding the reduction of the level of free radicals and induction of the HO-1 gene by CORM-2 and iCORM-2 prompted us to investigate whether these compounds can protect DNA against oxidative damage. Using the comet assay we measured the level of DNA oxidative damage in PBMCs and HL-60 cells pre-incubated only as well as pre- and co-incubated with CORM-2 and iCORM-2 at the concentration of 40 μM (Fig. 8). We observed a significant reduction in DNA oxidative damage in the two experimental systems for both CORM-2 and iCORM-2. However, the protective effect was significantly greater in the case of CORM-2. The results recorded confirm our assumptions that the ability of CORM-2 to reduce DNA oxidative damage is caused by both the released CO and also by the metal core of CORM-2. Some ruthenium complexes have been shown to have antioxidant properties^{41–43}. Two main oxidation states, i.e. Ru(II) and Ru(III), are accessible for ruthenium species in physiological solution. In both oxidation states the Ru ion is a six-coordinate complex with octahedral geometry and has good affinity to nitrogen and sulfur ligands⁴⁴. CORM-2 after releasing CO can form Ru(CO)₂ adducts, preferentially with histidine residues, as demonstrated with synthetic peptides using mass-spectrometry analysis⁴⁵. Moreover, it was shown that functional consequences of these adducts can be diverse. While KCa1.1 channels were activated, channels Kv11.1, Kv10.1, and Kv1.5 were inhibited by CORM-2 in a CO-independent manner. Thus, CORM-2 seems can serious side effects as a drug.

Our results indicate that not only CORM-2 but also iCORM-2 has a biological effect on normal and cancer cells. Depending on the incubation time and concentration, they can be cytotoxic or stimulate cell viability.

CORM-2 and iCORM-2 induce DNA damage that is effectively repaired in cancer cells. We also showed that CORM-2 effectively reduces oxidative stress while iCORM-2 increases this stress. In addition, CORM-2 induces HO-1 expression to a much greater extent than iCORM-2. We observed about a 100-fold increase in the expression of this gene in HL-60 cells after incubation with 100 μ M CORM-2. Interestingly, both compounds have a protective effect on oxidative DNA damage. This may indicate that not only the released CO but also iCORM-2, to which new ligands attach, have antioxidant properties.

The results presented by us indicate that the border between the cytoprotective and cytotoxic properties of CORM-2 is extremely narrow. Further studies on CORMs containing ruthenium are needed in order to determine their usefulness as therapeutic CO transporters in humans.

Received: 13 February 2020; Accepted: 30 June 2020

Published online: 22 July 2020

References

- Ng, P. C. Y., Long, B. & Koefman, A. Clinical chameleons: an emergency medicine focused review of carbon monoxide poisoning. *Int. Emerg. Med.* **13**(2), 223–229. <https://doi.org/10.1007/s11739-018-1798-x> (2018).
- Levy, R. J. Carbon monoxide and anesthesia-induced neurotoxicity. *Neurotoxicol. Teratol.* **60**, 50–58. <https://doi.org/10.1016/j.nt.2016.09.002> (2017).
- Rose, J. J. *et al.* Carbon monoxide poisoning: pathogenesis, management, and future directions of therapy. *Am. J. Respir. Crit. Care Med.* **195**(5), 596–606. <https://doi.org/10.1164/rccm.201606-1275CI> (2017).
- Motterlini, R. *et al.* Carbon-monoxide-releasing molecules: characterization of biochemical and vascular activity. *Circ. Res.* **90**, e17–e24. <https://doi.org/10.1161/hh0202.104530> (2002).
- Schatzschneider, U. Novel lead structures and activation mechanisms for CO-releasing molecules (CORMs). *Br. J. Pharmacol.* **172**(6), 1638–1650. <https://doi.org/10.1111/bph.12688> (2015).
- Adach, W. & Olas, B. The role of CORM-2 as a modulator of oxidative stress and hemostatic parameters of human plasma in vitro. *PLoS ONE* **12**(9), e0184787. <https://doi.org/10.1371/journal.pone.0184787> (2017).
- Magierowska, K. *et al.* Oxidative gastric mucosal damage induced by ischemia/reperfusion and the mechanisms of its prevention by carbon monoxide-releasing tricarbonyldichlororuthenium (II) dimer. *Free Radic. Biol. Med.* **145**, 198–208. <https://doi.org/10.1016/j.freeradbiomed.2019.09.032> (2019).
- Soni, H. *et al.* Beneficial effects of carbon monoxide-releasing molecule-2 (CORM-2) on acute doxorubicin cardiotoxicity in mice: role of oxidative stress and apoptosis. *Toxicol. Appl. Pharmacol.* **253**, 70–80. <https://doi.org/10.1016/j.taap.2011.03.013> (2011).
- Tsai, M. H. *et al.* CO-releasing molecules CORM2 attenuates angiotensin II-induced human aortic smooth muscle cell migration through inhibition of ROS/IL-6 generation and matrix metalloproteinases-9 expression. *Redox. Biol.* **12**, 377–388. <https://doi.org/10.1016/j.redox.2017.02.019> (2017).
- Babu, D. *et al.* Differential effects of CORM-2 and CORM-401 in murine intestinal epithelial MODE-K cells under oxidative stress. *Front. Pharmacol.* **8**, 31. <https://doi.org/10.3389/fphar.2017.00031> (2017).
- Simpson, P. V. & Schatzschneider, U. Small signaling molecules and CO-releasing molecules (CORMs) for the modulation of the cellular redox metabolism. Chapter 13. In *Redox-Active Therapeutics, Oxidative Stress in Applied Basic Research and Clinical Practice* (eds Batinić-Haberle, I. *et al.*) (Springer, Cham, 2016). https://doi.org/10.1007/978-3-319-30705-3_13.
- Lee, C.-W. *et al.* Carbon monoxide releasing molecule-2 protects against particulate matter-induced lung inflammation by inhibiting TLR2 and 4/ROS/NLRP3 inflammasome activation. *Mol. Immunol.* **112**, 163–174. <https://doi.org/10.1016/j.molimm.2019.05.005> (2019).
- Zhang, D. D. *et al.* Carbon monoxide attenuates high salt-induced hypertension while reducing pro-inflammatory cytokines and oxidative stress in the paraventricular nucleus. *Cardiovasc. Toxicol.* **19**(5), 451–464. <https://doi.org/10.1007/s12012-019-09517-w> (2019).
- Kourti, M. *et al.* Repurposing old carbon monoxide-releasing molecules towards the anti-angiogenic therapy of triple-negative breast cancer. *Oncotarget* **10**(10), 1132–1148. <https://doi.org/10.18632/oncotarget.26638> (2019).
- Lian, S. *et al.* Carbon monoxide releasing molecule-2 ameliorates IL-1 β -induced IL-8 in human gastric cancer cells. *Toxicology* **361–362**, 24–38. <https://doi.org/10.1016/j.tox.2016.07.003> (2016).
- Moon, H., Jang, J. H., Jang, T. C. & Park, G. H. Carbon monoxide ameliorates 6-hydroxydopamine-induced cell death in C6 glioma cells. *Biomol. Ther. (Seoul)* **26**(2), 175–181. <https://doi.org/10.4062/biomolther.2018.009> (2018).
- Park, S. J. *et al.* Heme oxygenase-1/carbon monoxide axis suppresses transforming growth factor- β 1-induced growth inhibition by increasing ERK1/2-mediated phosphorylation of Smad3 at Thr-179 in human hepatocellular carcinoma cell lines. *Biochem. Biophys. Res. Commun.* **498**(3), 609–615. <https://doi.org/10.1016/j.bbrc.2018.03.030> (2018).
- Shao, L. *et al.* Carbon monoxide releasing molecule-2 suppresses proliferation, migration, invasion, and promotes apoptosis in non-small cell lung cancer Calu-3 cells. *Eur. Rev. Med. Pharmacol.* **22**(7), 1948–1957. https://doi.org/10.26355/eurrev_201804_14720 (2018).
- Yan, Y. *et al.* CO suppresses prostate cancer cell growth by directly targeting LKB1/AMPK/mTOR pathway in vitro and in vivo. *Urol. Oncol.* **36**(6), 312.e1–312.e8. <https://doi.org/10.1016/j.urolonc.2018.02.013> (2018).
- Kourti, M., Jiang, W. G. & Cai, J. Aspects of carbon monoxide in form of CO-releasing molecules used in cancer treatment: more light on the way. *Oxid. Med. Cell Longev.* **2017**, 9326454. <https://doi.org/10.1155/2017/9326454> (2017).
- Kluska, M. *et al.* Kaempferol derivatives isolated from *Lens culinaris* Medik. reduce DNA damage induced by etoposide in peripheral blood mononuclear cells. *Toxicol. Res. (Camb.)* **8**, 896–907. <https://doi.org/10.1039/c9tx00176j> (2019).
- Wysokiński, D. *et al.* Photoactive CO-releasing complexes containing iron: genotoxicity and ability in HO-1 gene induction in HL-60 cells. *Toxicol. Res. (Camb.)* **8**, 544–551. <https://doi.org/10.1039/c9tx00070d> (2019).
- O'Brien, J. *et al.* Investigation of the Alamar Blue (resazurin) fluorescent dye for the assessment of mammalian cell cytotoxicity. *Eur. J. Biochem.* **267**, 5421–5426. <https://doi.org/10.1046/j.1432-1327.2000.01606.x> (2000).
- Corasaniti, M. T. *et al.* Cell signaling pathways in the mechanisms of neuroprotection afforded by bergamot essential oil against NMDA-induced cell death in vitro. *Br. J. Pharmacol.* **151**(4), 518–529. <https://doi.org/10.1038/sj.bjp.0707237> (2007).
- Singh, N. P. *et al.* A simple technique for quantitation of low levels of DNA damage in individual cells. *Exp. Cell. Res.* **175**(1), 184–192. [https://doi.org/10.1016/0014-4827\(88\)90265-0](https://doi.org/10.1016/0014-4827(88)90265-0) (1988).
- Oliveira, S., Queiroga, C. S. & Vieira, H. L. Mitochondria and carbon monoxide: cytoprotection and control of cell metabolism—a role for Ca(2+)? *J. Physiol.* **594**(15), 4131–4138. <https://doi.org/10.1113/JP270955> (2016).
- Winburn, I. C. *et al.* Cell damage following carbon monoxide releasing molecule exposure: implications for therapeutic applications. *Basic Clin. Pharmacol. Toxicol.* **111**, 31–41. <https://doi.org/10.1111/j.1742-7843.2012.00856.x> (2012).
- Dai, Y. *et al.* Antiproliferative and apoptosis triggering potential of paclitaxel-based targeted-lipid nanoparticles with enhanced cellular internalization by transferrin receptors—a study in leukemia cells. *Nanoscale Res. Lett.* **13**, 271. <https://doi.org/10.1186/s11671-018-2688-x> (2018).

29. Naves, M. A. *et al.* Transport of the ruthenium complex Ru(GA)(dppe)(2)]PF(6) into triple-negative breast cancer cells is facilitated by transferrin receptors. *Mol. Pharm.* **16**(3), 1167–1183. <https://doi.org/10.1021/acs.molpharmaceut.8b01154> (2019).
30. Sakthivel, K. M. & Hariharan, S. Regulatory players of DNA damage repair mechanisms: role in cancer chemoresistance. *Biomed. Pharmacother.* **93**, 1238–1245. <https://doi.org/10.1016/j.biopha.2017.07.035> (2017).
31. Otterbein, L. E. *et al.* Heme-oxygenase-1 and carbon monoxide modulate DNA repair through ataxia-telangiectasia mutated (ATM) protein. *PNAS* **108**, 14491–14496. <https://doi.org/10.1073/pnas.1102295108> (2011).
32. Jia, Y. *et al.* Carbon monoxide inhibits the nuclear-cytoplasmic translocation of HMGB1 in an in vitro oxidative stress injury model of mouse renal tubular epithelial cells. *J. Huazhong Univ. Sci. Technol. Med. Sci.* **36**(6), 791–795. <https://doi.org/10.1007/s11596-016-1663-y> (2016).
33. Mandke, P. & Vasquez, K. M. Interactions of high mobility group box protein 1 (HMGB1) with nucleic acids: implications in DNA repair and immune responses. *DNA Repair* **83**, 102701. <https://doi.org/10.1016/j.dnarep.2019.102701> (2019).
34. Brabec, V. & Kasparkova, J. Ruthenium coordination compounds of biological and biomedical significance. DNA binding agents. *Coord. Chem. Rev.* **376**, 75–94. <https://doi.org/10.1016/j.ccr.2018.07.012> (2018).
35. Tavares, A. F. N. *et al.* Reactive oxygen species mediate bactericidal killing elicited by carbon monoxide-releasing molecules. *J. Biol. Chem.* **286**(30), 26708–26717. <https://doi.org/10.1074/jbc.M111.255752> (2011).
36. Nizamutdinova, I. T. *et al.* Carbon monoxide (from CORM-2) inhibits high glucose-induced ICAM-1 expression via AMP-activated protein kinase and PPAR-gamma activations in endothelial cells. *Atherosclerosis* **207**(2), 405–411. <https://doi.org/10.1016/j.atherosclerosis.2009.05.008> (2009).
37. Catino, S. *et al.* Ferulic acid regulates the Nrf2/heme oxygenase-1 system and counteracts trimethyltin-induced neuronal damage in the human neuroblastoma cell line SH-SY5Y. *Front. Pharmacol.* **6**, 305. <https://doi.org/10.3389/fphar.2015.00305> (2016).
38. Chien, P. T., Lin, C. C., Hsiao, L. D. & Yang, C. M. Induction of HO-1 by carbon monoxide releasing molecule-2 attenuates thrombin-induced COX-2 expression and hypertrophy in primary human cardiomyocytes. *Toxicol. Appl. Pharmacol.* **289**(2), 349–359. <https://doi.org/10.1016/j.taap.2015.09.009> (2015).
39. Yang, C. M. *et al.* c-Src-dependent transactivation of EGFR mediates CORM-2-induced HO-1 expression in human tracheal smooth muscle cells. *J. Cell. Physiol.* **230**(10), 2351–2361. <https://doi.org/10.1002/jcp.24912> (2015).
40. Salerno, L. *et al.* Heme oxygenase-1: A new druggable target in the management of chronic and acute myeloid leukemia. *Eur. J. Med. Chem.* **142**, 163–178. <https://doi.org/10.1016/j.ejmech.2017.07.031> (2017).
41. Mohankumar, A. *et al.* Organoruthenium(II) complexes attenuate stress in *Caenorhabditis elegans* through regulating antioxidant machinery. *Eur. J. Med. Chem.* **168**, 123–133. <https://doi.org/10.1016/j.ejmech.2019.02.029> (2019).
42. Mohanraj, M., Ayyannan, G., Raja, G. & Jayabalakrishnan, C. Synthesis, spectral characterization, DNA interaction, radical scavenging and cytotoxicity studies of ruthenium(II) hydrazine complexes. *J. Photochem. Photobiol. B* **158**, 164–173. <https://doi.org/10.1016/j.jphotobiol.2016.03.005> (2016).
43. Paula, M. M. *et al.* Antioxidant activity of new ruthenium compounds. *Redox Report: Commun. Free Radical. Res.* **10**(3), 139–143. <https://doi.org/10.1179/135100005X38897> (2005).
44. Lazarević, T., Rilak, A. & Bugar, Z. D. Platinum, palladium, gold and ruthenium complexes as anticancer agents: current clinical uses, cytotoxicity studies and future perspectives. *Eur. J. Med. Chem.* **142**, 8–31. <https://doi.org/10.1016/j.ejmech.2017.04.007> (2017).
45. Gessner, G. *et al.* CO-independent modification of K⁺ channels by tricarbonyldichlororuthenium(II) dimer (CORM-2). *Eur. J. Pharmacol.* **815**, 33–41. <https://doi.org/10.1016/j.ejphar.2017.10.006> (2017).

Author contributions

M.J., D.W. and K.W. wrote the main manuscript. M.J. and M.K. made all the experiments. M.J. and K.W. prepared all figures. All authors reviewed the manuscript.

Competing interests

The authors declare no competing interests.

Additional information

Correspondence and requests for materials should be addressed to K.W.

Reprints and permissions information is available at www.nature.com/reprints.

Publisher's note Springer Nature remains neutral with regard to jurisdictional claims in published maps and institutional affiliations.











Open Access This article is licensed under a Creative Commons Attribution 4.0 International License, which permits use, sharing, adaptation, distribution and reproduction in any medium or format, as long as you give appropriate credit to the original author(s) and the source, provide a link to the Creative Commons license, and indicate if changes were made. The images or other third party material in this article are included in the article's Creative Commons license, unless indicated otherwise in a credit line to the material. If material is not included in the article's Creative Commons license and your intended use is not permitted by statutory regulation or exceeds the permitted use, you will need to obtain permission directly from the copyright holder. To view a copy of this license, visit <http://creativecommons.org/licenses/by/4.0/>.

© The Author(s) 2020

FULL PAPER

Cytotoxicity of piano-stool ruthenium cyclopentadienyl complexes bearing different imidato ligands

Michał Juszcak¹  | Magdalena Kluska¹  | Aneta Kosińska²  |
 Marcin Palusiak³  | Agnieszka J. Rybarczyk-Pirek³  | Kinga Wzgarda-Raj³  |
 Bogna Rudolf²  | Katarzyna Woźniak¹ 

¹Faculty of Biology and Environmental Protection, Department of Molecular Genetics, University of Lodz, Lodz, Poland

²Faculty of Chemistry, Department of Organic Chemistry, University of Lodz, Lodz, Poland

³Faculty of Chemistry, Department of Physical Chemistry, University of Lodz, Lodz, Poland

Correspondence

Katarzyna Woźniak, Faculty of Biology and Environmental Protection, Department of Molecular Genetics, University of Lodz, Pomorska 141/143, Lodz 90-236, Poland.
 Email: katarzyna.wozniak@biol.uni.lodz.pl

Bogna Rudolf, Faculty of Chemistry, Department of Organic Chemistry, University of Lodz, Lodz 91-403, Poland.
 Email: bogna.rudolf@chemia.uni.lodz.pl

Abstract

In these studies, we investigated a cytotoxic and genotoxic potential of four ruthenium cyclopentadienyl complexes bearing different imidato ligands: (η^5 -cyclopentadienyl)Ru (CO)₂(η^1 -*N*-maleimidato) (**1**), (η^5 -cyclopentadienyl)Ru (CO)₂-*N*-methoxysuccinimidato (**2**), (η^5 -cyclopentadienyl)Ru (CO)₂-*N*-ethoxysuccinimidato (**3**), and (η^5 -cyclopentadienyl)Ru (CO)₂-*N*-phthalimidato (**4**). We used two types of cells—normal peripheral blood mononuclear cells (PBMCs) and leukemic HL-60 cells. We observed that complex **1** was highly cytotoxic and genotoxic, both for normal and cancer cells at concentrations from 0.5 to 250 μ M. Interestingly, complex **1** was 10 times more cytotoxic to HL-60 cells compared with PBMCs. Complexes **2–4** were cytotoxic only for HL-60 cells at the highest used concentrations. Furthermore, we observed an increase in the viability of PBMCs after incubation with succinimide complexes **2** and **3**. We also showed that complex **1** arrested cell cycle in the sub-G1 phase and induced apoptosis. We found that different properties of studied ruthenium complexes depend significantly on the type of imide ligand bind to the ruthenium atom. The density functional theory (DFT) calculation of maleimide and succinimide revealed some significant differences of these compounds that would be related to biological activity. Our results indicate that ruthenium complex **1** should be further investigated in detail for its anti-cancer properties.

KEYWORDS

apoptosis, DNA damage, HL-60 cells, maleimide, succinimide, ruthenium metallocarbonyl complexes, peripheral blood mononuclear cells

1 | INTRODUCTION

Therapeutic strategies, both for targeting tumor cells and preventing their metastasis, largely focus on the search for new chemical compounds. Among them, complexes of various metals occupy an important place. Many studies are directed to compounds of ruthenium as an

alternative to conventional platinum drugs.^[1–5] Compared with platinum compounds, ruthenium complexes exhibit certain different physical, chemical, and biological properties. The first difference is the geometry of compounds octahedral for ruthenium complexes and flat square for platinum ions. Another difference is the ease of electron transfer in the Ru(III)/Ru(II) pair. The

reduction of Pt(IV) to Pt(II) causes both a change in the coordination number and the length of bonds between the molecule atoms. Ruthenium complexes show a different side effect profile and significantly lower toxicity to normal cells than platinum complexes. They preferentially accumulate in the tumor mass by transport via transferrin. Moreover, they are reduced to the active form of Ru(II) in the tumor environment. Another difference is the effectiveness of ruthenium compounds against metastatic cells. The activity of ruthenium complexes against hypoxic cancer cells resistant to classical chemotherapy should also be emphasized.^[5]

The piano stool ruthenium complexes consist of the aromatic ring that stabilizes the Ru(II) oxidation state and three other coordinated ligands. Two types of piano stool ruthenium complexes were identified: Ru(η^5 -arene) and Ru(η^5 -cyclopentadienyl). The first type is widely studied for its anticancer properties. For example, the RAPTA-family compounds were evaluated in typical cell-proliferation studies and also in several preclinical models. These compounds exhibit unique anti-metastatic and anti-angiogenic properties. Promising results have been obtained from studies of RAPTA-C, prototypical RAPTA compound. This compound is rapidly cleared from the organs and bloodstream and has low overall toxicity. Moreover, RAPTA-C administered during tumor normalization is more effective than doxorubicin in inhibiting tumor growth, even at lower doses. The development of anticancer RAPTA-C therapy is currently in an advanced preclinical stage.^[6–9] Other new compounds of the RAPTA family, like containing fluorinated arene ligands and curcuminoid ligands, are also being intensively studied in preclinical models.^[7]

The structure–activity relationship of another series of Ru(η^6 -arene) complexes bearing the pyridine-imidazole ligands was studied by G. Espino et al. The activity toward different cancer cell lines such as A2780, A2780cis, and MCF-7 cells and MRC-5 fibroblasts was evaluated. It was found that the arene ring affects strongly the cytotoxic activity and the *p*-cymene derivative was the most active compared with the other studied compounds. These results are in line with the findings that the *p*-cymene complex strongly destabilized the DNA double helix.^[10]

The piano-stool-structured complexes based on the RuCp scaffold are stable and hydrophobic, so they can easily pass the cell membranes. Most RuCp compounds are highly cytotoxic to the human cancer cells tested, with IC₅₀ values in the micromolar and nanomolar range. Most of them are also much more cytotoxic than cisplatin. RuCp compounds act on cisplatin-resistant cell line A2780CisR and on very aggressive cell lines, such as MDA-MB-231, PC-3, and HT-29. In addition, several

RuCp complexes are active against more than one cancer cell line, indicating that these compounds may have some potential as broad-spectrum antitumor agents.^[10–12]

Cyclic imides are known for their biological activity. Their ring structure includes the imide group —CO—N(R)—CO—; thus, they are hydrophobic and neutral and can cross biological membranes in vivo. Therefore, they are of interest for potential use as an antibacterial, antifungal, and analgesic agents.^[13] The cyclic imides received considerable attention also due to their antitumor activity, especially the naphthalimide derivatives, such as mitonafide and amonafide. Previously, the cytotoxic effect of several naphthalimide derivatives on B16-F10 melanoma cells was demonstrated.^[14] The maleimide-based inhibitor of GSK-3 β , 9-ING-41, significantly leads to cell cycle arrest, autophagy, and apoptosis in cancer cells, like bladder cancer cells.^[15] Moreover, 9-ING-41 has the potential for enhancing the antitumor effects of chemotherapeutic drugs. Recently, it was shown that 9-ING-41 impaired the ATR/Chk1 DNA damage response (DDR) signaling pathway induced by gemcitabine in pancreatic cancer cells. Both pharmacologic inhibitions by 9-ING-41 or genetic depletion of GSK-3 β by siRNA led to the degradation of TopBP1, a key molecule that is required for optimal ATR phosphorylation of Chk1, leading to S-phase arrest and DNA repair.^[16]

Herein, we investigated four ruthenium piano stool cyclopentadienyl complexes bearing different imidato ligands: (η^5 -cyclopentadienyl)Ru(CO)₂(η^1 -*N*-maleimidato) (**1**), (η^5 -cyclopentadienyl)Ru(CO)₂-*N*-methoxysuccinimidato (**2**), (η^5 -cyclopentadienyl)Ru(CO)₂-*N*-ethoxysuccinimidato (**3**), and (η^5 -cyclopentadienyl)Ru(CO)₂-*N*-phthalimidato (**4**) (Figure 1).

We analyzed the cytotoxic and genotoxic potential of these complexes in peripheral blood mononuclear cells

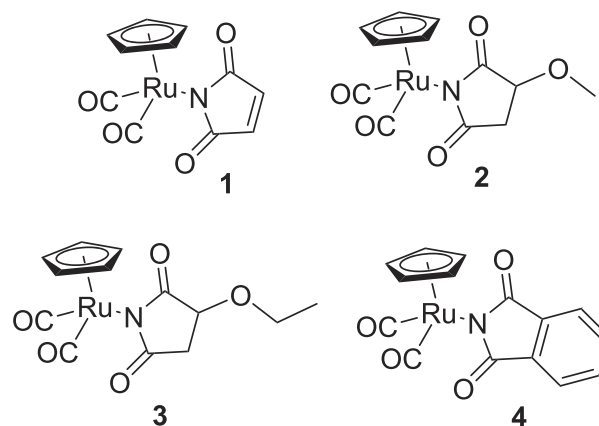


FIGURE 1 The structures of the ruthenium complexes 1–4

(PBMCS) as normal cells and leukemic HL-60 cells. We showed that ruthenium complex **1** was highly cytotoxic and genotoxic. Therefore, we examined the ability of this complex to induce apoptosis in HL-60 cells.

To check the impact of the imidato ligands on the biological activity of studied complexes, we performed all mentioned experiments with free maleimide and succinimide. In the cell viability experiment, we also studied *N*-alkyl and *N*-aryl maleimide and succinimide derivatives.

2 | MATERIALS AND METHODS

Bis(cyclopentadienylrutheniumdicarbonyl) dimer, maleimide, succinimide, phthalimide, *N*-methylsuccinimide, *N*-methylmaleimide, *N*-benzylmaleimide, *N*-phenylmaleimide, CDCl₃, low-melting point (LMP) and normal-melting point (NMP) agarose, phosphate-buffered saline (PBS), 4',6-diamidino-2-phenylindole (DAPI), resazurin sodium salt, dimethyl sulfoxide (DMSO), and hydrogen peroxide (H₂O₂) were purchased from Sigma-Aldrich. Methanol, ethanol, and toluene were purchased from POCH (Polish Chemical Reagents) and used without further purification. All other chemicals were of the highest commercial grade available.

Complex **1** (η^5 -cyclopentadienyl)Ru (CO)₂(η^1 -*N*-maleimidato) was synthesized according to the published procedure.^[17] Alkoxysuccinimide complexes **2** (η^5 -cyclopentadienyl)Ru (CO)₂-*N*-methoxysuccinimidato and **3** (η^5 -cyclopentadienyl)Ru (CO)₂-*N*-ethoxysuccinimidato were synthesized as previously described.^[18,19] Chromatographic purifications were performed on silica gel Merck 60 (230–400 mesh). Infrared (IR) spectra were recorded in KBr on an Fourier Transform InfraRed (FT-IR) NEXUS (Thermo Nicolet) spectrometer. ¹H NMR and ¹³C NMR spectra were recorded on Bruker Avance III (600 MHz) spectrometer. NMR measurements were made in CDCl₃ solution. The chemical shifts were expressed in part per million (ppm). Coupling constants were expressed in Hertz (Hz). Electrospray ionization mass spectrometry (ESI-MS) spectra were recorded in positive mode on the Varian 500-MS LC ion trap spectrometer. Photochemical reactions were carried out using UV lamp TQ 150 Z3.

All quantum chemical calculations were done with a Gaussian set of codes^[20] using ω -B97XD functional^[21] in conjunction with the aug-cc-pVTZ^[22,23] basis set. A full optimization procedure was performed.

All methods were performed in accordance with the relevant guidelines and regulations.

2.1 | Synthesis of ruthenium complex 4

Complex **4** was obtained by a photochemical reaction of CpRu (CO)₂I with phthalimide in the presence of diisopropylamine. A mixture of CpRu (CO)₂I (0.2 g, 0.57 mmol), phthalimide (0.168 g, 1.14 mmol), and diisopropylamine (1.4 ml) in toluene (25 ml) was irradiated with ultraviolet light (UV lamp, $\lambda \approx 350$ nm) for 3 h. Orange dark color turned orange-yellow upon illumination. The formed solid was filtered off, and the filtrate was concentrated in vacuo. The residue was dissolved in chloroform, washed three times with 2.5% aqueous NaOH solution, and dried with MgSO₄. The product was purified by flash chromatography (eluted with chloroform/methanol, 50:1) and crystallized from chloroform/heptane. Yield 98.8 mg (47%). ¹H NMR (600 MHz, CDCl₃): δ 7.64 (dd, *J* = 5.3, 3.0 Hz, 2H, Ar), 7.51 (dd, *J* = 5.4, 3.0 Hz, 2H, Ar), 5.50 (s, 5H, Cp) ppm. ¹³C NMR (151 MHz, CDCl₃): δ 196.80 (s, 2 \times C \equiv O), 179.87 (s, 2 \times C=O), 136.60 (s, Ar), 131.82 (s, Ar), 121.19 (s, Ar), 86.97 (s, Cp). IR (KBr, cm⁻¹) 2037, 1982 (C \equiv O), 1658 (C=O imide). ESI-MS: *m/z* calcd. for C₁₅H₉NO₄Ru (M + H)⁺: 370.07; found: 370.04.

2.2 | X-ray structure determination

X-ray diffraction data for **4** were measured on a four-circle Oxford Diffraction Supernova Dual diffractometer using a two-dimensional area CCD detector and a low-temperature device Oxford Cryosystem cooler. Integration of the intensities, corrections for Lorentz effects, polarization effects, and analytical absorption were performed with CrysAlis PRO.^[24] The crystal structure was solved by direct methods and refined on *F*² using a full-matrix least-squares procedure (SHELXL-2014).^[25] The positions of the hydrogen were introduced in the calculated positions with an idealized geometry and constrained using a rigid body model with isotropic displacement parameters equal to 1.2 of equivalent displacement parameters of their parent atoms. The molecular geometry was calculated by Platon^[26] and WinGX programs.^[27] The relevant crystallographic data are given in Table S1. Atomic coordinates, displacement parameters, and structure factors of the analyzed crystal structures are deposited with Cambridge Crystallographic Data Centre CCDC (reference number: 2055461). The data can be obtained free of charge from The Cambridge Crystallographic Data Centre (<http://www.ccdc.cam.ac.uk/conts/retrieving.html>).

2.3 | Cell culture

PBMCs were isolated from a leucocyte-buffy coat collected from the blood of healthy, nonsmoking donors from the Blood Bank in Lodz, Poland, as described previously.^[23] The study protocol was approved by the Committee for Research on Human Subjects of the University of Lodz (17/KBBN-UŁ/III/2019).

The HL-60 (human promyelocytic leukemia) cell line was obtained from the American Type Culture Collection (ATCC) and cultured in Iscove's Modified Dulbecco's Medium (IMDM) with 15% inactivated fetal bovine serum (FBS), 2-mM L-glutamine, and 25-mM HEPES and a penicillin/streptomycin solution (100 U ml⁻¹ and 100 µg ml⁻¹, respectively) as described previously.^[28]

2.4 | Cell viability resazurin assay

The cell viability resazurin assay was performed similarly to the method described by O'Brien et al.^[29] Resazurin salt powder was dissolved in sterile PBS buffer. Cells were seeded on 96-well plates in count of 15,000 in the case of HL-60 cells and 50,000 for PBMCs per well. Ruthenium complexes, ruthenium chloride, succinimides, and maleimides were added to the wells to obtain final concentrations from the range 0.5–250 µM and then incubated for 24 h at 37°C in 5% CO₂. Next, 10 µl of resazurin salt was added to each well, and the plates again were incubated at 37°C in 5% CO₂ for 2 h. After that, fluorescence was measured with HT microplate reader Synergy HT (Bio Tek Instruments, USA) using $\lambda_{\text{ex}} = 530/25$ and $\lambda_{\text{em}} = 590/35$ nm. The effects of ruthenium complexes, ruthenium chloride, and imides were quantified as the percentage of control fluorescence.

IC₅₀ (half maximal inhibitory concentration) values were calculated according to the rules provided on the website (<https://www.aatbio.com/tools/ic50-calculator>).

2.5 | DNA damage by the comet assay

Ruthenium complexes, succinimide, maleimide, and ruthenium chloride were added to the suspension of the cells to give final concentrations from the range 2.5–250 µM. Both PBMCs and HL-60 cells were incubated for 2 h at 37°C in 5% CO₂. The experiment included a positive control, that is, a cell sample incubated with hydrogen peroxide (H₂O₂) at 25 µM for 15 min on ice.

The comet assay was performed under alkaline conditions according to a procedure described by Singh et al.^[30] in accordance with the guidelines provided by Azqueta and Collins.^[31] After incubation, a freshly

prepared suspension of the cells in 0.75% LMP agarose was spread onto microscope slides that were precoated with 0.5% NMP agarose. Then, the cells were lysed for 1 h at 4°C in a buffer containing 2.5-M NaCl, 0.1-M EDTA, 10-mM Tris, 1% Triton X-100, pH 10. After cells lysis, the slides were placed in an electrophoresis unit. DNA was allowed to unwind for 20 min in the solution containing 300-mM NaOH and 1-mM EDTA, pH > 13. Electrophoretic separation was performed in the solution containing 30-mM NaOH and 1-mM EDTA, pH > 13 at an ambient temperature of 4°C for 20 min at an electric field strength of 0.73 V cm⁻¹ (28 mA). Then, the slides were washed in water, drained, stained with 2 µg ml⁻¹ of DAPI, and covered with coverslips. To prevent additional DNA damage, all experiments were conducted under limited light or in the dark. The comets were analyzed as described previously.^[23]

2.6 | Apoptosis

Apoptosis was measured using the FITC Annexin V Apoptosis Detection Kit II (BD Biosciences, San Jose, USA) according to the manufacturer's procedure and as we previously conducted this experiment.^[32] The HL-60 cells were seeded in 6-well plates at the concentration of 2×10^5 cells ml⁻¹. Then, the cells were incubated with complex **1**, ruthenium chloride, succinimide, and maleimide for 24 h at 37°C. The cells incubated with 20-µM camptothecin (CAM) for 24 h at 37°C were a positive control. After incubation, the cells were collected and washed twice with ice-cold PBS. The cells were resuspended in 1 × binding buffer (100 µl) and incubated with FITC Annexin V (5 µl) and propidium iodide (PI) (5 µl) for 15 min at room temperature in the dark. Then, 400 µl of binding buffer was added to each tube, and the samples were measured within 1 h using the LSR II flow cytometer (Becton Dickinson, San Jose, CA, USA) equipped with 488-nm laser excitation and BD FACSDiva software v4.1.2. The percentage of apoptotic cells was expressed as a population of FITC Annexin V-positive cells. The experiments were performed in triplicate. Every analysis was performed on at least 10,000 events.

2.7 | Cell cycle

HL-60 cells were seeded in 6-well plates at density of 0.5×10^6 cells ml⁻¹. Cells were incubated with tested compounds for 24 h at 37°C. As positive control served 100 ng ml⁻¹ of nocodazol (NOC), then the cells were collected and washed twice with PBS. Next, the cells were

pelleted resuspended in PBS and put on ice for 15 min. Then, one volume of -20°C absolute ethanol was added, and the samples were stored at 4°C . Before the analysis, samples were resuspended in $300\ \mu\text{l}$ of staining solution containing $40\ \mu\text{g ml}^{-1}$ of PI and $200\ \mu\text{g ml}^{-1}$ of RNase A. Samples were incubated for 30 min at 37°C in the dark until analysis. DNA content was analyzed using LSRII flow cytometer (Becton Dickinson, San Jose, CA, USA).

2.8 | Genomic DNA isolation

Genomic DNA was isolated using a commercially available kit (Extractme Genomic DNA Kit, Blirt, Gdańsk, Poland) following the manufacturer's protocol. DNA was isolated from HL-60 cells in number 12×10^6 cells. The concentration and purity of DNA were measured by BioTek Synergy HT Microplate Reader (BioTek Instruments, Winooski, VT, USA). Finally, we obtained $450\ \mu\text{l}$ of genomic DNA at the concentration of $160\ \text{ng}\ \mu\text{l}^{-1}$ and purity 1.9.

2.9 | Incubation of genomic DNA with complexes and ligands

Genomic DNA in the amount of 600 ng was incubated for 2 h at 37°C with ruthenium complexes **1–4**, maleimide, succinimide, and ruthenium chloride at concentrations mostly correspond to use in the comet assay ($5\text{--}250\ \mu\text{M}$) in a final volume of $25\ \mu\text{l}$. Genomic DNA was analyzed by using 0.5% agarose gel electrophoresis in $1 \times$ TAE buffer; $10\ \mu\text{l}$ of DNA sample after incubation with tested compounds was mixed with $2\ \mu\text{l}$ of DNA Gel Loading Dye ($6\times$) (Thermo Fisher Scientific, Waltham, MA, USA). To each well was added DNA in the amount of 200 ng. Electrophoresis was run for 90 min at 90 V in $1 \times$ TAE buffer. During each electrophoresis, we also separated $3\ \mu\text{l}$ of 1 kb DNA ladder (Quick-Load Purple 1 kb DNA ladder, New England Biolabs, Ipswich, MA, USA) (data not shown).

2.10 | Statistical analysis

Cell viability experiment values are presented as the mean \pm SD of six replicates. Values in the comet test are

expressed as mean + standard error of the mean of three experiments; data from three experiments were collected, and statistical parameters were calculated. Statistical analysis was performed using the Mann–Whitney test (samples with distributions departing from normality) and the Student *t* test (normal distribution of the sample). Differences were considered statistically significant when the *p* value was <0.05 .

3 | RESULTS AND DISCUSSION

3.1 | Synthesis of complexes **1–4**

Complexes **1** and **4** CpRu (CO) $_2$ (η^1 -maleimidato) and CpRu (CO) $_2$ (η^1 -*N*-phthalimidato)) were obtained in a photochemical process. Solution of CpRu (CO) $_2$ I and maleimide or phthalimide respectively was irradiated by UV light in the presence of diisopropylamine. Synthesis of complex **1** was already reported,^[17] while complex **4** is a newly synthesized ruthenium metallocarbonyl compound (Scheme 1).

The crude product was purified by flash chromatography on silica gel. The molecular structure of **4** was established by ^1H , ^{13}C NMR, IR, mass spectrometry, and single-crystal diffraction (Figure 2). Complexes **2** CpRu (CO) $_2$ (η^1 -3-methoxysuccinimidato) and **3** CpRu (CO) $_2$ (η^1 -3-ethoxysuccinimidato) were synthesized in Oxa-Michael reaction of complex **1** with methanol or ethanol respectively in the presence of K_2CO_3 according to the previously published method.^[18,19]

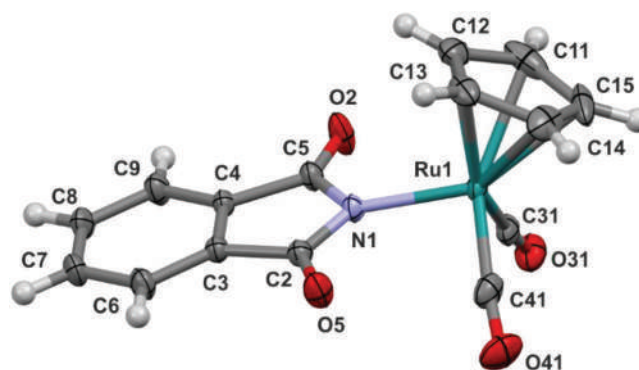
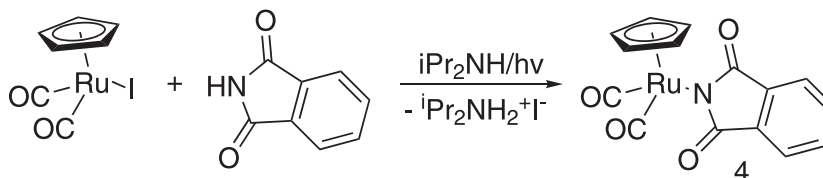


FIGURE 2 Molecular structure of **4** with atom labeling scheme. Displacement ellipsoid are drawn in 40% probability level



SCHEME 1 Synthesis of metallocarbonyl complex **4**

3.2 | Crystal structure description

The molecular and crystal structure of **4** was determined by the X-ray diffraction method. Crystals suitable for measurements were obtained from chloroform/heptane. Crystal data, selected bond lengths and angles are given in Tables S1 and S2. Compound **4** crystallizes in the centrosymmetric monoclinic space group $P2_1/n$ with one molecule in the asymmetric unit. Molecular diagrams with atom labeling schemes are presented in Figure 2. Ruthenium Ru1 atom is bonded to the cyclopentadienyl ring (C11–C12–C13–C14–C15), two carbonyl ligands (C31–O31 and C41–O41) and the heterocyclic nitrogen atom N1 of the phthalimidato ligand. Bond lengths of ruthenium atom to carbonyl ligands and to center of gravity of cyclopentadienyl ring (Cp1) are of similar range and equal approximately 1.88 Å, while Ru–N1 bond is evidently longer (compare data presented in Table S2). Two carbonyl and phthalimidato ligands are positioned almost perpendicularly in respect to one another with angles about 91° with cyclopentadienyl ring on the opposite side of ruthenium atom thus forming conformation of “piano chair” as presented in Figure 2.

A possible rotation of phthalimidato ligand around metal–ligand Ru1–N1 bond influences the final molecular conformation. In the crystal structure, the ideal C_s molecular symmetry (with mirror plane passing through positions of Ru1, N1 atoms, midpoints of C3–C4 and C7–C8 bonds, and Cg1 centroid) is not retained as seen from the comparison of torsion angles along Ru1–N1 bond (for ligand O31–C31: $\angle C31\text{--}Ru1\text{--}N1\text{--}C2 = -57.08$ [14] and $\angle C31\text{--}Ru1\text{--}N1\text{--}C5 = 124.85$ [15]; for ligand O41–C41: $\angle C41\text{--}Ru1\text{--}N1\text{--}C2 = -149.08$ [14] and $\angle C41\text{--}Ru1\text{--}N1\text{--}C5 = 32.85$ [15]). As seen the absolute values of the angles in case of both ligands are completely different. In addition, dihedral angles between phthalimidato ligand best plane (N1, C2, C3, C4, C5, C6, C7, C8, C9, O2, O5, H6, H7, H8, and H9 atoms—PLN1) and carbonyl ligands planes (C31, O31, and Ru1 atoms—PLN2 and C41, O41, and Ru1 atoms—PLN3) have been calculated, and their values are evidently varying: $\angle PLN1, PLN2 = 60.49(4)^\circ$ and $\angle PLN1, PLN3 = 34.80(4)^\circ$.

The reason of such a situation and breaking C_s symmetry results from different schemes of intermolecular interactions of carbonyl groups. In particular, the two neighboring carbonyl O41 and O5 atoms are acceptors of very short C–H···O hydrogen bonds (see Figure S2 and Table S3). Moreover, O41 atom also takes part in CO···OC intermolecular contact of distance shorter than the sum of van der Waals radii: 2.945(1) Å. In contrast, such close interatomic distances are not observed for other carbonyl O31 and O2 atoms, even though there are also observed many intermolecular H···O contacts. It is worth

mentioning that CO bond distances within hydrogen bonds acceptors are a little longer when compared with the other two groups.

Analyses of Cambridge Structural Database (CSD)^[33] indicated 23 crystal structures of metal complexes of a similar coordinative sphere as **4** including cyclopentadienyl ring, carbonyl ligands and azaheterocyclic compounds substituted with carbonyl groups. Among them is reported a crystal structure of CpFe(CO)₂(η^1 -phthalimidato),^[34] a complex compound, which is isostructural with **4** (the same crystal system space group and molecular arrangement in the unit cell).

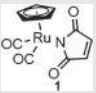
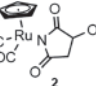
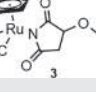
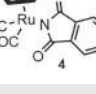
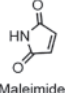
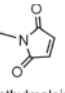
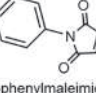
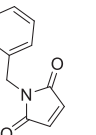
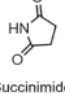
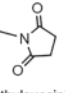
3.3 | Cell viability

We showed that complex **1** was the most cytotoxic for PBMCs and HL-60 cells among studied ruthenium complexes (Table S4).

At low concentrations, we observed an increase of viability, both PBMCs and HL-60 cells, after incubation with complex **1**. But, with increasing concentrations, a decrease in cell viability was observed. At the highest concentration of **1**, the viability of PBMCs was approximately 18% ($p < 0.001$). In contrast to complex **1**, an increase in the viability of PBMCs was observed after incubation with other complexes at all used concentrations in the range from 0.5 to 250 μ M, with the exception of complex **4**, which decreased the PBMCs viability after incubation at the concentration of 250 μ M (Table S4). Ruthenium chloride was used as a control compound, serving as an indicator of the influence of ruthenium itself on cell viability. We observed a slight decrease in PBMCs viability, proportional to the used concentration of ruthenium chloride. At the highest used concentration of 250 μ M, ruthenium chloride decreased the viability of PBMCs to about 90% ($p < 0.001$).

In the case of complex **1**, a sharp decrease in HL-60 cells viability was observed at the concentration of 5 μ M at which the viability was about 55% ($p < 0.001$) compared with about 106% at 2.5 μ M ($p < 0.001$) (Table S4). At the three highest concentrations of **1**, the viability of HL-60 cells was less than 5% ($p < 0.001$). Complex **2** showed cytotoxic properties only at the concentration of 250 μ M, at which the viability was about 56% ($p < 0.001$). Complex **3** was cytotoxic at the concentrations of 100 and 250 μ M, at which the viability was about 57% and 19%, respectively ($p < 0.001$). The effect of **4** was similar to the cytotoxic effect of **3**, a statistically significant decrease in viability was observed at the two highest concentrations, to about 88% and 36%, respectively ($p < 0.001$). Ruthenium chloride at lower concentrations

TABLE 1 IC₅₀ values for ruthenium complexes, maleimides, and succinimides measured after 24-h incubation of PBMCs and HL-60 cells

	PBMCs (μM)	HL-60 cells (μM)
RuCl ₃	>250	>250
	52.95	5.62
	>250	>250
	>250	112.75
	>250	176.65
 Maleimide	14.59	9.67
 N-methylmaleimide	7.37	6.17
 N-phenylmaleimide	10.94	13.39
 N-Benzylmaleimide	5.50	8.12
 Succinimide	>250	>250
 N-methylsuccinimide	>250	>250

Abbreviation: PBMC, peripheral blood mononuclear cell.

had no cytotoxic effects on HL-60 cells, but we noticed a decrease in cell viability from the concentration of 10 μM. At the concentration of 250 μM, we detected the viability at the level of 63% ($p < 0.001$) (Table S4). All ruthenium complexes were more cytotoxic for HL-60 cells compared to PBMCs, as indicated by the IC₅₀ values (Table 1).

Previously, we studied two light-triggered iron CO-releasing molecules, that is, CpFe (CO)₂(η¹-N-maleimidato) **5** and CpFe (CO)₂(η¹-N-succinimidato) **6** (Figure S6).^[35] We demonstrated that succinimide complex **6** was not toxic to HL-60 cells even at high concentrations, in the contrary, maleimide complex **5** showed important toxicity. Interestingly, the same effect was

observed in the case of irradiated and nonirradiated complexes **5** and **6**. Some of us have already reported that the irradiation of iron metalloborane complexes led to degradation of complex and released of CO and free imide.^[19,36]

We also determined the effect of free imides—maleimide, succinimide, and their *N*-substituted derivatives (Figure S7) on the viability of PBMCs and HL-60 cells.

Succinimide and *N*-methylsuccinimide was not cytotoxic for normal and cancer cells in the tested concentration range from 0.5 to 250 μM . In the case of maleimides, we observed a significant decrease in the viability of both types of cells. The *N*-benzylmaleimide turned out to be the most cytotoxic for PBMCs ($\text{IC}_{50} = 5.50 \mu\text{M}$), and for HL-60 cells, the most cytotoxic was *N*-methylmaleimide ($\text{IC}_{50} = 6.17 \mu\text{M}$). Ruthenium complex **1** was the most cytotoxic of all tested compounds— $\text{IC}_{50} = 5.62 \mu\text{M}$ for HL-60 cells (Table 1).

Based on our results, it can be concluded that the high cytotoxicity of complex **1** is tied with the maleimide ligand. This is in line with the literature data on this molecule. For example, it was shown that maleimides presented a good cytotoxic effect on human acute leukemia cells—K562 and Jurkat.^[37] The results of cell cycle analysis, fluorescence microscopy, and Annexin V-FITC assay confirmed that the cells were undergoing apoptosis after incubation with these compounds. The apoptosis induced by maleimides involved the intrinsic pathway, which was evidenced by the increased level of expression of proapoptotic proteins Bax and AIF and the decreased level of expression of anti-apoptotic protein Bcl-2, and the extrinsic pathway only for Jurkat cells, evidenced by the increased level of expression of Fas. Some of these maleimides also caused a decrease in the level of expression of anti-apoptotic protein survivin.^[37] Moreover, the cytotoxic effect of 9-ING-41, a maleimide-based ATP-competitive small molecule glycogen synthase kinase-3 β (GSK-3 β) inhibitor, is well known.^[15,16] Treatment with 9-ING-41 has shown antitumor effects in different human cancers, like neuroblastoma, B-cell lymphoma, glioblastoma, ovarian, pancreatic, renal, and breast cancer. Recently, 9-ING-41 has entered the clinical trials in patients with different advanced cancer.^[15]

Our studies showed that ruthenium complex **1** was more cytotoxic to HL-60 cells compared with normal PBMCs ($\text{IC}_{50} = 5.62 \mu\text{M}$ vs. $\text{IC}_{50} = 52.95 \mu\text{M}$) (Table 1). This large difference in cytotoxicity may be associated with the overexpression of transferrin receptors present on the surface of cancer cells. According to previous reports, leukemic cells are known to overexpress transferrin receptors, and ruthenium can be up taken into cells by transferrin receptors.^[38,39] Another issue we want to

emphasize is the difference in selectivity of complex **1** (9.4) which is greater than that of the maleimide ligand (1.5). The presence of CpRu (CO)₂ moiety made the maleimide ligand less toxic.

Interestingly, after incubation of PBMCs and HL-60 cells at lower concentrations with complexes **2–4**, we observed an increase in cell viability, which indicated the stimulation of cellular metabolism by these complexes. This may be due to the antioxidant properties, which have been confirmed for other ruthenium complexes^[40–42] or is related to the bioactivity of succinimidato ligands.^[43]

3.4 | DNA damage

Complex **1** at the lower concentrations (2.5, 5, and 10 μM) did not show genotoxic properties for PBMCs. As the concentration increased, starting from 25 μM , we observed a statistically significant increase in DNA damage, up to the level of about 53% ($p < 0.001$) for the concentration of 250 μM . In the case of ruthenium complexes **2**, **3**, and **4**, we did not observe any increase in the level of DNA damage in PBMCs in the range of the tested concentrations (Figure 3).

Complex **1** indicated a high ability to induce DNA damage at all used concentrations in HL-60 cells ($p < 0.001$) (Figure 4). At the highest concentration of this complex, we observed DNA damage at the level of 57%. Complex **2** showed no effect on DNA damage in the range of tested concentrations. In the case of complex **3**, the genotoxic properties were observed only at the two highest tested concentrations (100 and 250 μM). The DNA damage was observed at the level of about 7% ($p < 0.001$). Similarly, complex **4** induced light DNA damage only at the three highest concentrations tested ($p < 0.001$) (Figure 4). Ruthenium chloride did not show genotoxic properties for PBMCs (Figure 3) and HL-60 cells (Figure 4) at all tested concentrations. The DMSO, the solvent we use for experiments, did not show genotoxic properties, both for PBMCs and HL-60 (data not shown).

We then examined the level of DNA damage induced by succinimide and maleimide in both PBMCs and HL-60 cells. Succinimide did not cause DNA damage in normal cells (Figure 5) and cancer cells (Figure 6). In the case of maleimide, we observed a significant increase in DNA damage starting from the concentration of 10 μM in both PBMCs and HL-60 cells ($p < 0.001$) (Figures 5 and 6, respectively). After incubation with the highest concentration of maleimide (250 μM), we showed DNA damage at the level of approximately 50% in PBMCs and 60% in HL-60 cells (Figures 5 and 6, respectively). For

FIGURE 3 DNA damage in peripheral blood mononuclear cells (PBMCs) incubated for 2 h at 37°C with ruthenium complexes **1–4** and RuCl₂ analyzed by the alkaline comet assay. The negative control was PBMCs incubated 2 h at 37°C alone. The positive control was PBMCs incubated with H₂O₂ at 25 μM for 15 min on ice. The figure shows mean results ± SEM, *n* = 100; ****p* < 0.001

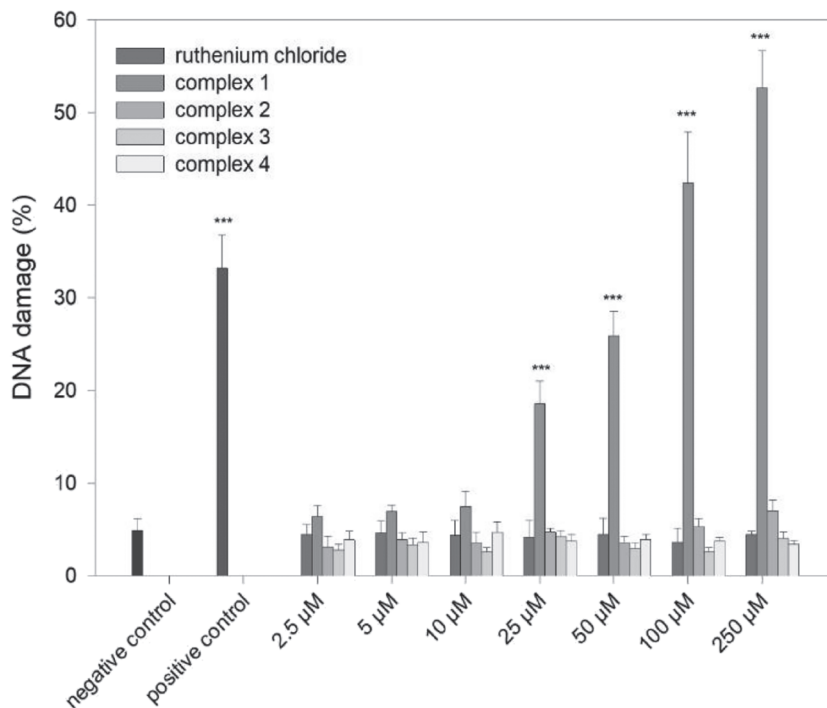
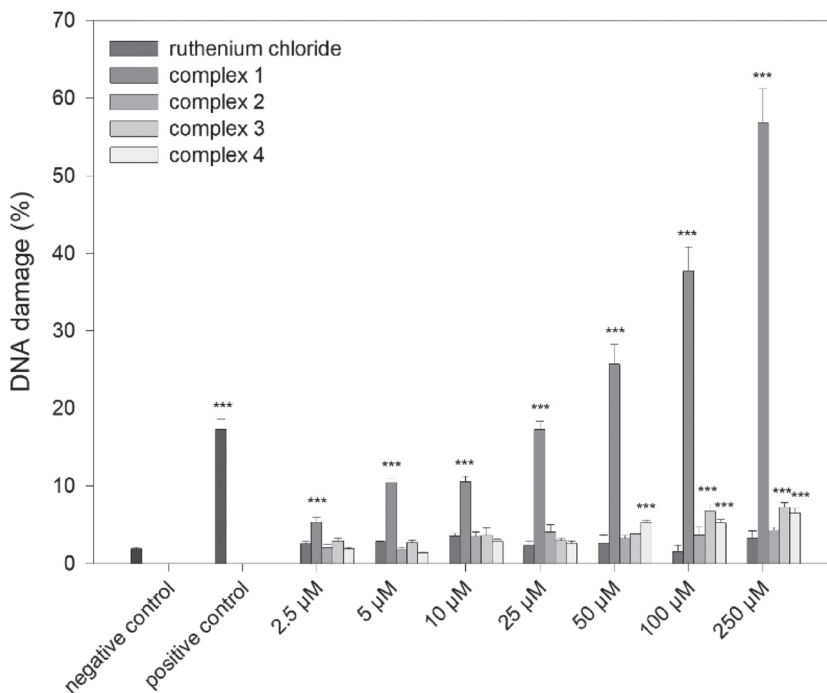


FIGURE 4 DNA damage in HL-60 cells incubated for 2 h at 37°C with ruthenium complexes **1–4** and RuCl₂ analyzed by the alkaline comet assay. The negative control was HL-60 cells incubated for 2 h at 37°C alone. The positive control was HL-60 cells incubated with H₂O₂ at 25 μM for 15 min on ice. The figure shows mean results ± SEM, *n* = 100; ****p* < 0.001



compounds that were tested for DNA damage, cell viability was determined after 2-h incubation using the resazurin reduction method (Table S5).

Figure 7 shows representative photos of the comets obtained after incubation of PBMCs and HL-60 cells with **1** (c), **2** (d), **3** (e), and **4** (f) at the concentration of 50 μM. Picture (c) shows comets with more DNA damage

compared to comets shown in Pictures (d)–(f). Picture (b) shows comets obtained after incubation of the cells with H₂O₂ at 25 μM for 15 min on ice (positive control).

Previously, we also studied the ability to induce DNA damage for iron complexes **5** and **6** (Figure S6). DNA damage induced by succinimide complex **6** was repaired efficiently, while the repair of DNA damage induced by

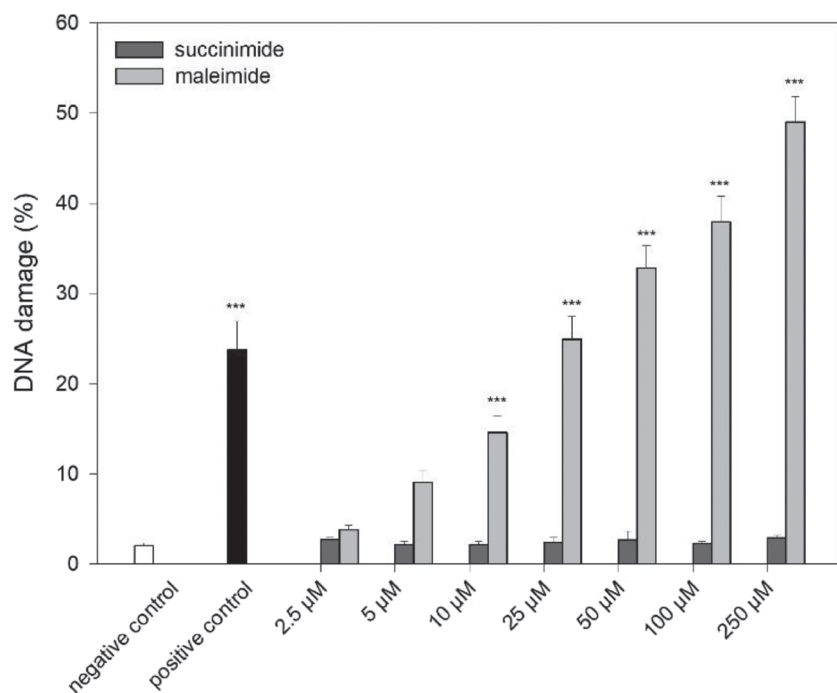


FIGURE 5 DNA damage in peripheral blood mononuclear cells (PBMCs) incubated for 2 h at 37°C with succinimide and maleimide analyzed by the alkaline comet assay. The negative control was PBMCs incubated for 2 h at 37°C alone. The positive control was PBMCs incubated with H₂O₂ at 25 μM for 15 min on ice. The figure shows mean results ± SEM, *n* = 100; ****p* < 0.001

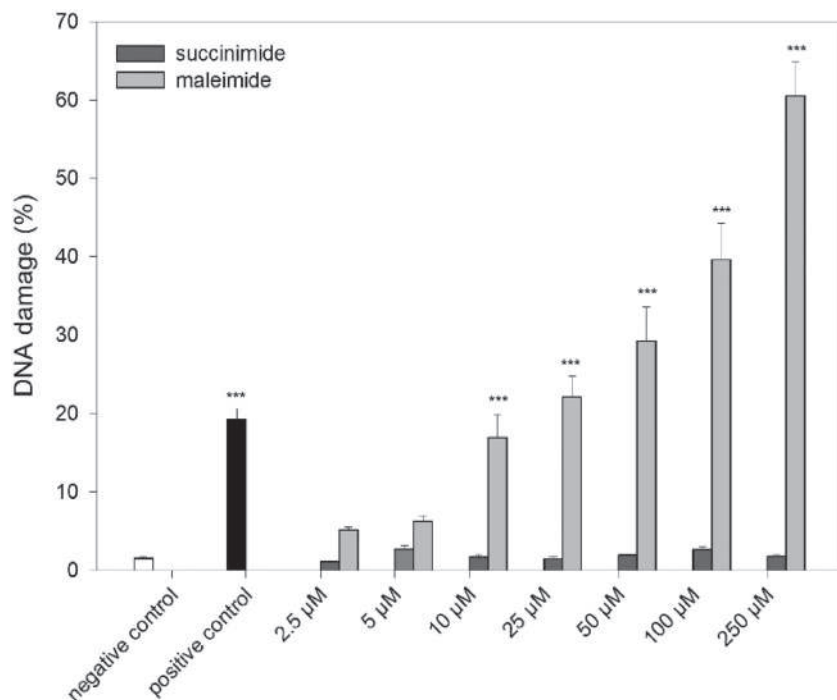
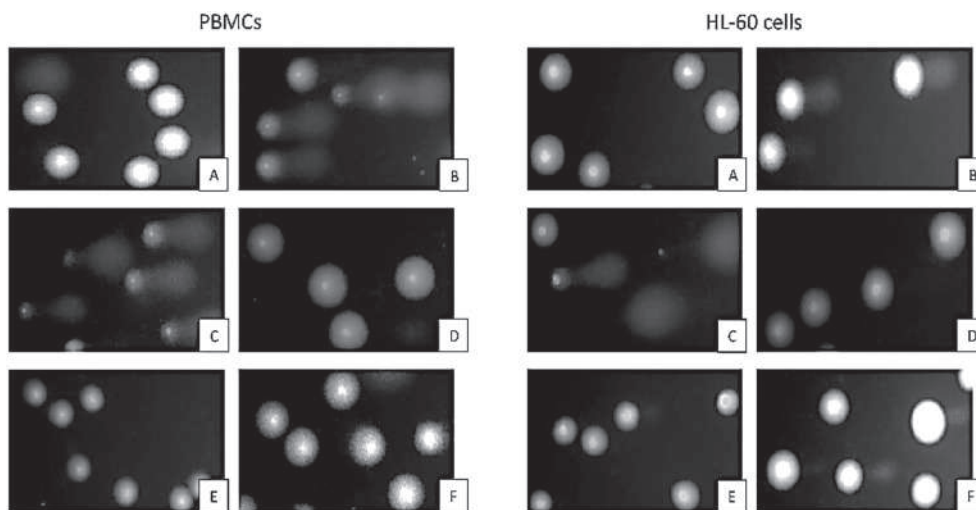


FIGURE 6 DNA damage in HL-60 cells incubated for 2 h at 37°C with succinimide and maleimide analyzed by the alkaline comet assay. The negative control was HL-60 cells incubated for 2 h at 37°C alone. The positive control was HL-60 cells incubated with H₂O₂ at 25 μM for 15 min on ice. The figure shows mean results ± SEM, *n* = 100; ****p* < 0.001

maleimide complex **5** was disturbed.^[35] Similarly, here the complexes containing the succinimide ligand^[2,3] and free succinimide did not damage DNA in either HL-60 cells (Figures 4 and 6) or PBMCs (Figures 3 and 5). Only phthalimide complex **4** damaged DNA at the concentrations of 50, 100, and 250 μM (*p* < 0.001) and succinimide complex **3** at the concentrations of 100 and 250 μM (*p* < 0.001) (Figure 4). Probably some of described

ruthenium complexes entered HL-60 cells and damaged DNA.^[5,44] For research of potential degradation of DNA as a result of the influence of ruthenium complexes **1–4**, maleimide, succinimide, and ruthenium chloride at a high range of concentrations (5–250 μM), we decided to perform electrophoresis of genomic DNA. Before electrophoresis, genomic DNA was incubated for 2 h at 37°C with tested compounds, which corresponds with

FIGURE 7 Representative photos of comets obtained in the alkaline version of the comet assay after incubation of peripheral blood mononuclear cells (PBMCs) and HL-60 cells for 2 h with ruthenium complexes **1–4** (c–f, respectively) at 50 μM . (a) Negative control (untreated PBMCs and HL-60 cells); (b) PBMCs and HL-60 cells incubated with H_2O_2 at 25 μM for 15 min on ice (positive control)



conditions used for the comet assay. Results clearly show homogenous characters of DNA bands, any smears proving degradation of DNA were not observed (Figure S9). Bands of DNA after incubation with complex **1** and ruthenium chloride look very similar, whereas DNA damages measured by the comet assay were extremely different. For example, at the concentration of 100 μM for both compounds, DNA damage was approximately 5% for ruthenium chloride versus approximately 40% for complex **1** (Figure 3). Additionally, each band contains similar amounts of DNA. Finally, results obtained by the comet assay and electrophoresis of genomic DNA show that the mechanism of DNA degradation is probably associated with a cellular response like free radicals generation or apoptosis, not by direct interaction of ruthenium complexes and ligands with DNA.

On the other hand, the participation of the maleimide ligand in the genotoxic effects of complex **1** should not be neglected. We did not find any reference data on DNA damage induced by maleimide and its derivatives. Maleimide was widely studied as the linker that reacts easily with thiol groups present in biomolecules but not for its biological properties.^[45–47] Thus, the mechanism of action of maleimide on DNA is unknown. We can suppose from the presented studies that the double bond of maleimide has an essential impact on its activity because the succinimide—compound of a similar structure but without the $\text{C}=\text{C}$ does not induce DNA damage.

3.5 | Apoptosis and cell cycle

Because we showed a significant cytotoxic and genotoxic effect of complex **1**, we decided to investigate the apoptotic effect of this complex on HL-60 cells. Using the Annexin V-FITC and PI double staining method, we

showed that **1** at the concentrations from 5 to 100 μM induced apoptosis in HL-60 cells (Figure 8). Already from the lowest concentration of 5 μM , we observed a significant statistical increase ($p < 0.001$) in the level of early (Q4) and late (Q2) apoptotic HL-60 cells after incubation with this complex (Figure 8). Late apoptotic cells constituted over 90% of HL-60 cells incubated for 24 h with **1** at the concentration of 100 μM . We also observed that treating cells with 10- μM complex **1** lead to increase in cell level in the sub-G1 phase from 3% to 5.5% ($p < 0.001$) (Table S6). The increase in cell level in the sub-G1 phase can be associated with induction of apoptosis, which corresponds with results obtained by measurement of apoptosis (Figure 8).

We also compared the ability of maleimide and succinimide to induce apoptosis in HL-60 cells. We showed no changes in the distribution of live, necrotic, early and late apoptotic cells between control cells (untreated cells) and cells incubated with succinimide at the concentration range of 5–100 μM (Figure S8b). In the case of maleimide, there were significant changes in the distribution of live, necrotic, and apoptotic cells incubated with this imide at concentrations starting from 10 μM . In the samples incubated with the maleimide at the two highest concentrations, 50 and 100 μM , we observed about 20% of early apoptotic and 80% of late apoptotic HL-60 cells (Figure S8a). We did not demonstrate apoptosis in HL-60 cells after incubation with RuCl_2 at any of the concentrations used (data not shown).

Our results clearly show that the anticancer activity of ruthenium complex **1** is related to the presence of a maleimidato ligand. This is probably due to the carbon-carbon double bond in maleimide, which is mainly responsible for its reactivity. It is well known that maleimide readily undergoes Michael's reaction with

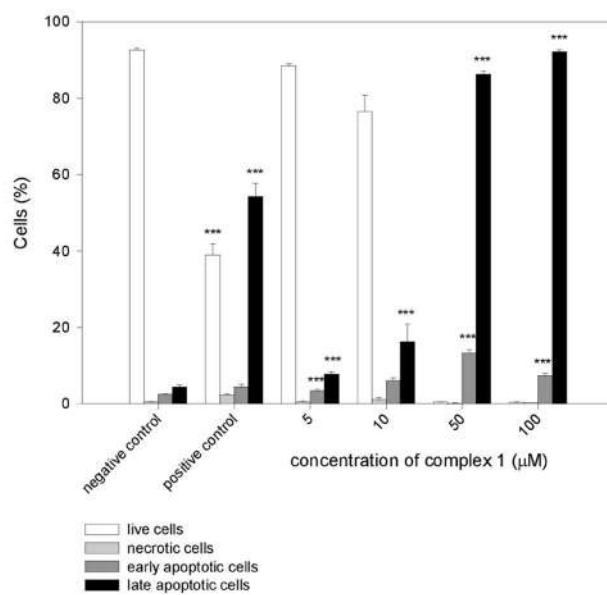
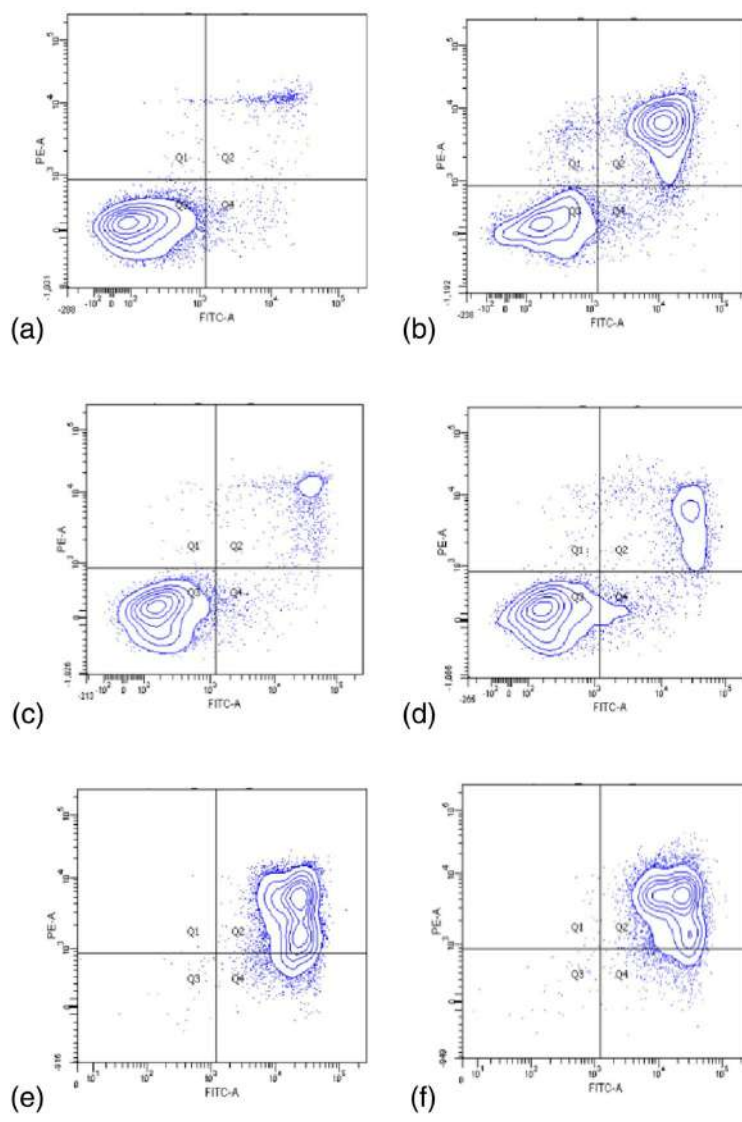


FIGURE 8 Legend on next page.

FIGURE 8 The effect of complex **1** on the apoptosis of HL-60 cells. Representative flow cytometric dot plots showing the percentage of cells in viable (Q3), early apoptotic (Q4), late apoptotic (Q2), and necrotic (Q1) stages for (a) negative control (untreated HL-60 cells), (b) positive control, (c) 5, (d) 10, (e) 50, and (f) 100 μM (top panel). Quantification of apoptotic cells. The cell apoptosis was measured after 24-h incubation with complex **1** (bottom panel). The positive control was cells incubated with 20- μM camptothecin (CAM) for 24 h at 37°C. Data represent means \pm SD of three experiments. *** $p < 0.001$ compared with the negative control

functional groups present in biomolecules (thiol, amino, imidazole groups) and thus are often used in bioconjugation processes.^[45,47,48] Related to the literature, the “maleimide anchor” is frequently introduced to compounds with anticancer activity (like Pt and Ru metal complexes) to develop precursors for binding tumor targeting molecules.^[47,49,50]

The differences in cytotoxicity of maleimide and succinimide derivatives of the same structures were seldom reported in the literature. For example, Sato et al. have tested the analogical maleimide and succinimide derivatives toward HeLa cells using a cell viability assay and found that only the maleimide derivatives were toxic.^[51] In another example, the Pt(IV) complexes were equipped with maleimide or succinimide residue. The idea was to enable simple and fast coupling of thiol-containing targeting molecule (human serum albumin [HSA]) to maleimide Pt complex and to compare the behavior of maleimide and succinimide complexes toward cancer cells. Both Pt complexes displayed anticancer activity. However, the maleimide complex activity was significantly higher than the succinimide one, probably due to the formation of complex HSA bioconjugate.^[47]

We have performed the theoretical calculation of maleimide and succinimide. Very recently, a relation between electronic structure and biological activity was observed for pyrrole-2,5-dione analogs investigated toward their antioxidant properties.^[52] Namely, it has been reported that the lower highest occupied molecular orbital–lowest unoccupied molecular orbital (HOMO–LUMO) energy gap characterizes compounds with higher activity. In the case of maleimide and succinimide, a similar relation may be noticed. See Figure 9 for graphical interpretation. In the case of maleimide, the HOMO–LUMO energy gap is lower by 1.36 eV when comparing with succinimide. This difference is even twice as large as that reported for mentioned pyrrole-2,5-dione analogs. So, the difference in toxicity of maleimide and succinimide may be indicated with the difference in their frontier orbitals energy gap. Note also that in the case of maleimide, its LUMO is a pi-type orbital, similarly, like in the case of pyrrole-2,5-dione analogs and as distinct to succinimide for which LUMO shall be interpreted as a sigma anti bonding one. The HOMO is essentially the same in both. In Figure S10, there is a view on

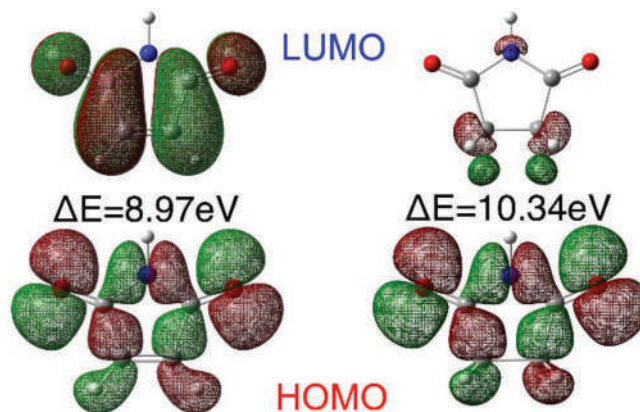


FIGURE 9 Highest occupied molecular orbital (HOMO) and lowest unoccupied molecular orbital (LUMO) isosurfaces calculated for maleimide (left) and succinimide (right) molecules. In all cases, the same value of isosurface was taken. 0.021 a.u

electrostatic potential mapped on electron density iso surface of both maleimide and succinimide. In maleimide, there is a region of partial electron surplus around formally double CC bond. Such region may contribute to various intermolecular interactions, acting as electron-donating center, including stacking interactions and various directional interactions being a Lewis acid (H-bonding, X-bonding, etc.). This is a clearly different situation in the case of succinimide where in this part of the molecule, there is a deficit of electron charge due to presence of (C)H atoms which may form merely weak H-bonds of C–H \cdots A type. In particular, stacking interactions, which have to be excluded in the case of succinimide, may be important in the case of maleimide. For instance, recently it was reported that the presence of this kind interactions (reflected as C \cdots C contacts in crystal packing) is in line with the cytotoxic activity of some flavonoids and chromanones.^[53]

4 | CONCLUSION

Our results showed that complex **1** (η^5 -cyclopentadienyl) Ru (CO) $_2$ (η^1 -*N*-maleimidato) has anticancer potential. It should be emphasized that this complex was about 10 times more cytotoxic to leukemic HL-60 cells compared with normal cells, which indicates its selective

action. Moreover, complex **1** induced DNA damage and apoptosis in HL-60 cells. Ruthenium complexes bearing succinimide ligands showed no cytotoxic and genotoxic properties. In contrast to maleimide complex **1**, an increase in the viability of PBMCs was observed after incubation with succinimide complexes at all used concentrations. Our comparative studies with free maleimides and succinimides and their derivatives showed that the antitumor activity of complex **1** is related to the maleimidato ligand bonded to the ruthenium atom. The density functional theory (DFT) studies of maleimide and succinimide revealed some significant differences, which may be crucial for further biological studies of these groups of compounds. Certainly, our research has a few limitations. It would be interesting to investigate the properties of the ruthenium complexes against other cancer cells. The ruthenium complexes synthesized by us bearing both maleimide and succinimide ligands should be carefully examined in terms of their biological properties and possible use in anticancer therapy.

ACKNOWLEDGMENTS

The authors gratefully acknowledge the University of Lodz, Poland, Faculty of Chemistry and Faculty of Biology and Environmental Protection for financial support. The theoretical computations using the Gaussian 09 set of codes were carried out in the Wrocław Center for Networking and Supercomputing (<http://www.wcss.wroc.pl>). Access to HPC machines and licensed software is gratefully acknowledged.

AUTHOR CONTRIBUTIONS

Michał Juszcak: Investigation. **Magdalena Kluska**: Investigation. **Aneta Kosińska**: Investigation. **Marcin Palusiak**: Investigation. **Agnieszka Rybarczyk-Pirek**: Investigation. **Kinga Wzgarda-Raj**: Investigation. **Bogna Rudolf**: Conceptualization; supervision. **Katarzyna Woźniak**: Conceptualization; supervision.

CONFLICT OF INTEREST


All authors declare that they have no conflict of interest.

DATA AVAILABILITY STATEMENT

Data available in article supplementary material.

ORCID

Michał Juszcak  <https://orcid.org/0000-0003-4055-6102>

Magdalena Kluska  <https://orcid.org/0000-0001-9545-6593>

Aneta Kosińska  <https://orcid.org/0000-0003-3999-6514>

Marcin Palusiak  <https://orcid.org/0000-0002-0032-0878>

Agnieszka J. Rybarczyk-Pirek  <https://orcid.org/0000-0001-7377-7011>

Kinga Wzgarda-Raj  <https://orcid.org/0000-0003-0498-1128>

Bogna Rudolf  <https://orcid.org/0000-0003-0319-0535>

Katarzyna Woźniak  <https://orcid.org/0000-0001-6666-7973>

REFERENCES

- [1] A. Levina, A. Mitra, P. A. Lay, *Metallomics* **2009**, *1*, 458.
- [2] H. Huang, P. Zhang, Y. Chen, K. Qiu, C. Jin, L. Ji, H. Chao, *Dalton Trans.* **2016**, *45*, 13135.
- [3] L. M. Bomfim, F. A. de Araujo, R. B. Dias, C. B. S. Sales, C. A. G. Rocha, R. S. Correa, M. B. P. Soares, A. A. Batista, D. P. Bezerra, *Sci. Rep.* **2019**, *9*, 11483.
- [4] H. Huang, K. Cao, Y. Kong, S. Yuan, H. Liu, Y. Wang, Y. Liu, *Chem. Sci.* **2019**, *10*, 9721.
- [5] K. Lin, Z.-Z. Zhao, H.-B. Bo, X.-J. Hao, J.-Q. Wang, *Front. Pharmacol.* **2018**, *9*, 1323.
- [6] M. Rausch, P. J. Dyson, P. Nowak-Sliwinska, *Adv. Ther.* **2019**, *2*, 1900042.
- [7] B. S. Murray, M. V. Babak, C. G. Hartinger, P. J. Dyson, *Coord. Chem. Rev.* **2016**, *306*, 86.
- [8] S. Thota, D. A. Rodrigues, D. C. Crans, E. J. Barreiro, *J. Med. Chem.* **2018**, *61*, 5805.
- [9] P. Nowak-Sliwinska, J. R. van Beijnum, A. Casini, A. A. Nazarov, G. Wagnières, H. van den Bergh, P. J. Dyson, A. W. Griffioen, *J. Med. Chem.* **2011**, *54*, 3895.
- [10] M. Martínez-Alonso, N. Busto, F. A. Jalón, B. R. Manzano, J. M. Leal, A. M. Rodríguez, B. García, G. Espino, *Inorg. Chem.* **2014**, *53*, 11274.
- [11] T. S. Morais, A. Valente, A. I. Tomaz, F. Marques, M. H. Garcia, *Future Med. Chem.* **2016**, *8*, 527.
- [12] M. Martínez-Alonso, G. Gasser, *Coord. Chem. Rev.* **2021**, *434*, 213736.
- [13] T. N. Bansode, J. V. Shelke, V. G. Dongre, *Eur. J. Med. Chem.* **2009**, *44*, 5094.
- [14] K. E. Machado, K. N. Oliveira, L. Santos-Bubniak, M. A. Licínio, R. J. Nunes, M. C. Santos-Silva, *Bioorg. Med. Chem.* **2011**, *19*, 6285.
- [15] H. Kuroki, T. Anraku, A. Kazama, V. Bilim, M. Tasaki, D. Schmitt, A. P. Mazar, F. J. Giles, A. Ugolkov, Y. Tomita, *Sci. Rep.* **2019**, *9*, 19977.
- [16] L. Ding, V. S. Madamsetty, S. Kiers, O. Alekhina, A. Ugolkov, J. Dube, Y. Zhang, J.-S. Zhang, E. Wang, S. K. Dutta, D. M. Schmitt, F. J. Giles, A. P. Kozikowski, A. P. Mazar, D. Mukhopadhyay, D. D. Billadeau, *Clin. Cancer Res.* **2019**, *25*, 6452.
- [17] B. Rudolf, A. Kubicka, M. Salmain, M. Palusiak, A. J. Rybarczyk-Pirek, S. Wojtulewski, *J. Organomet. Chem.* **2016**, *801*, 101.
- [18] A. Kubicka, E. Fomal, A. B. Olejniczak, A. J. Rybarczyk-Pirek, S. Wojtulewski, B. Rudolf, *Polyhedron* **2016**, *107*, 38.
- [19] A. Kosińska, S. Wojtulewski, M. Palusiak, P. Tokarz, B. Rudolf, *Organometallics* **2021**, *40*, 663.
- [20] M. J. Frisch, G. W. Trucks, H. B. Schlegel, G. E. Scuseria, M. A. Robb, J. R. Cheeseman, G. Scalmani, V. Barone, B. Mennucci, G. A. Petersson, H. Nakatsuji, M. Caricato, X. Li, H. P. Hratchian, A. F. Izmaylov, J. Bloino, G. Zheng, J. L. Sonnenberg, M. Hada, M. Ehara, K. Toyota, R. Fukuda, J.

- Hasegawa, M. Ishida, T. Nakajima, Y. Honda, O. Kitao, H. Nakai, T. Vreven, J. A. Montgomery Jr., J. E. Peralta, F. Ogliaro, M. J. Bearpark, J. Heyd, E. N. Brothers, K. N. Kudin, V. N. Staroverov, R. Kobayashi, J. Normand, K. Raghavachari, A. P. Rendell, J. C. Burant, S. S. Iyengar, J. Tomasi, M. Cossi, N. Rega, N. J. Millam, M. Klene, J. E. Knox, J. B. Cross, V. Bakken, C. Adamo, J. Jaramillo, R. Gomperts, R. E. Stratmann, O. Yazyev, A. J. Austin, R. Cammi, C. Pomelli, J. W. Ochterski, R. L. Martin, K. Morokuma, V. G. Zakrzewski, G. A. Voth, P. Salvador, J. J. Dannenberg, S. Dapprich, A. D. Daniels, Ö. Farkas, J. B. Foresman, J. V. Ortiz, J. Cioslowski, D. J. Fox, GAUSSIAN09, Gaussian Inc., Wallingford, CT, USA, 2009.
- [21] J.-D. Chai, M. Head-Gordon, *Phys. Chem. Chem. Phys.* **2008**, *10*, 6615.
- [22] T. H. Dunning, *J. Chem. Phys.* **1989**, *90*, 1007.
- [23] R. A. Kendall, T. H. Dunning, R. J. Harrison, *J. Chem. Phys.* **1992**, *96*, 6796.
- [24] Rigaku Oxford Diffraction. CrysAlisPRO software system, version 1.171.40.79a; 2020.
- [25] G. M. Sheldrick, *Acta Crystallogr.* **2015**, *C71*, 3.
- [26] A. L. Spek, *Acta Crystallogr. D* **2009**, *65*, 148.
- [27] L. J. Farrugia, *J. Appl. Cryst.* **2012**, *45*, 849.
- [28] M. Juszcak, M. Kluska, D. Wysokiński, K. Woźniak, *Sci. Rep.* **2020**, *10*, 12200.
- [29] J. O'Brien, I. Wilson, T. Orton, F. Pognan, *Eur. J. Biochem.* **2000**, *267*, 5421.
- [30] N. P. Singh, M. T. McCoy, R. R. Tice, E. L. Schneider, *Exp. Cell Res.* **1988**, *175*, 184.
- [31] A. Azqueta, A. R. Collins, *Arch. Toxicol.* **2013**, *87*, 949.
- [32] M. Juszcak, M. Kluska, B. Skalski, J. Żuchowski, A. Stochmal, B. Olas, K. Woźniak, *Biomed. Pharmacother.* **2021**, *137*, 111395.
- [33] C. R. Groom, I. J. Bruno, M. P. Lightfoot, S. C. Ward, *Acta Crystalllogr.* **2016**, *B72*, 171.
- [34] M. Bukowska-Strzyżewska, A. Tosik, D. Wódka, J. Zakrzewski, *Polyhedron* **1994**, *13*, 1689.
- [35] D. Wysokiński, P. Lewandowska, D. Zątak, M. Juszcak, M. Kluska, D. Lizińska, B. Rudolf, K. Woźniak, *Toxicol. Res. (Camb)* **2019**, *8*, 544.
- [36] A. Kubicka, E. Parfieniuk, E. Fornal, M. Palusiak, D. Lizińska, A. Gumieniczek, B. Rudolf, J. Photoch, *Photobiol. A: Chemistry* **2018**, *351*, 115.
- [37] K. E. Machado, K. N. de Oliveira, H. M. S. Andreossi, L. D. S. Bubniak, A. C. R. de Moraes, P. C. Gaspar, E. D. S. Andrade, R. J. Nunes, M. C. Santos-Silva, *Chem. Res. Toxicol.* **2013**, *26*, 1904.
- [38] Y. Dai, J. Huang, B. Xiang, H. Zhu, C. He, *Nanoscale Res. Lett.* **2018**, *13*, 271.
- [39] M. A. Naves, A. E. Graminha, L. C. Vegas, L. Luna-Dulcey, J. Honorato, A. C. S. Menezes, A. A. Batista, M. R. Cominetti, *Mol. Pharm.* **2019**, *16*, 1167.
- [40] M. M. da Silva Paula, C. T. Pich, F. Petronilho, L. B. Drei, M. Rudnicki, M. R. de Oliveira, J. C. F. Moreira, J. A. P. Henriques, C. V. Franco, F. dal Pizzol, *Redox Rep.* **2005**, *10*, 139.
- [41] A. Mohankumar, G. Devagi, G. Shanmugam, S. Nivitha, P. Sundararaj, F. Dallemer, P. Kalaivani, R. Prabhakaran, *Eur. J. Med. Chem.* **2019**, *168*, 123.
- [42] M. Mohanraj, G. Ayyannan, G. Raja, C. Jayabalakrishnan, *J. Photochem. Photobiol. B* **2016**, *158*, 164.
- [43] Z. Zhao, J. Yue, X. Ji, M. Nian, K. Kang, H. Qiao, X. Zheng, *Bioorg. Chem.* **2021**, *108*, 104557.
- [44] V. Brabec, J. Kasparkova, *Coord. Chem. Rev.* **2018**, *376*, 75.
- [45] J. M. J. M. Ravasco, H. Faustino, A. Trindade, P. M. P. Gois, *Chem. A Eur. J.* **2019**, *25*, 43.
- [46] K. Renault, J. W. Freddy, P.-Y. Renard, C. Sabot, *Bioconjug. Chem.* **2018**, *29*, 2497.
- [47] R. Narain, *Chemistry of Bioconjugates: Synthesis, Characterization, and Biomedical Applications*, Wiley **2014**.
- [48] V. Pichler, J. Mayr, P. Heffeter, O. Dömötör, É. A. Enyedy, G. Hermann, D. Groza, G. Köllensperger, M. Galanksi, W. Berger, B. K. Keppler, C. R. Kowol, *Chem. Commun.* **2013**, *49*, 2249.
- [49] M. Hanif, S. Moon, M. P. Sullivan, S. Movassaghi, M. Kubanik, D. C. Goldstone, T. Söhnel, S. M. Jamieson, C. G. Hartinger, *J. Inorg. Biochem.* **2016**, *165*, 100.
- [50] M. Hanif, A. A. Nazarov, A. Legin, M. Groessl, V. B. Arion, M. A. Jakupec, Y. O. Tsybin, P. J. Dyson, B. K. Keppler, C. G. Hartinger, *Chem. Commun.* **2012**, *48*, 1475.
- [51] M. Sato, J. E. Dander, C. Sato, Y.-S. Hung, S.-S. Gao, M.-C. Tang, L. Hang, J. M. Winter, N. K. Garg, K. Watanabe, Y. Tang, *J. Am. Chem. Soc.* **2017**, *139*, 5317.
- [52] G. Mallikarjuna Reddy, A. Camilo, J. Raul Garcia, *Bioorg. Chem.* **2021**, *106*, 104465.
- [53] M. Małecka, J. Kusz, L. Eriksson, A. Adamus-Grabicka, E. Budzisz, *Acta Crystallogr. C Struct. Chem.* **2020**, *76*, 723.

SUPPORTING INFORMATION

Additional supporting information may be found in the online version of the article at the publisher's website.

How to cite this article: M. Juszcak, M. Kluska, A. Kosińska, M. Palusiak, A. J. Rybarczyk-Pirek, K. Wzgarda-Raj, B. Rudolf, K. Woźniak, *Appl Organomet Chem* **2022**, e6595. <https://doi.org/10.1002/aoc.6595>

Cytotoxicity of piano-stool ruthenium cyclopentadienyl complexes bearing different imidato ligands

Michał Juszcak¹, Magdalena Kluska¹, Aneta Kosińska², Marcin Palusiak³, Agnieszka J. Rybarczyk-Pirek³, Kinga Wzgarda-Raj³, Bogna Rudolf^{2*}, Katarzyna Woźniak^{1*}

Supplementary Materials

1.1. Crystallographic and experimental data

Fig. S1. Molecular Hirshfeld surface of **4** mapped with d_{norm} parameter; colored scale from -0.26 (red) to +1.32 (blue) (a); Hirshfeld surface fingerprint plots of selected intermolecular contacts with their percentage (b).

Fig. S2. Intermolecular interactions of **4**: C-H...O hydrogen bond (a); carbonyl...carbonyl interactions (b).

Table S1. Details of the crystal structure determination of **4**.

Table S2. Selected bond lengths [Å] and angles [°].

Table S3. Geometric parameters of selected hydrogen bonds – distances [Å] and angles [°].

1.2. Spectra and spectral data

Fig. S3. 600 MHz ¹H NMR spectrum of **4** in CDCl₃.

Fig. S4. 151 MHz ¹³C NMR spectrum of **4** in CDCl₃.

Fig. S5. IR spectrum of **4** (KBr, cm⁻¹).

1.3. Biological studies

Fig. S6. Structures of iron metallocarbonyl complexes bearing succinimide and maleimide ligands **5** and **6**.

Fig. S7. Structures of maleimides and succinimides.

Fig. S8. The effect of maleimide (**A**), and succinimide (**B**) on the apoptosis of HL-60 cells after 24 h incubation. The positive control were cells incubated with 20 μM camptothecin (CAM) for 24 h at 37°C. Data represent means ± SD of 3 experiments. *** $p < 0.001$ compared with the negative control (untreated HL-60 cells).

Table S4. The viability of PBMCs and HL-60 cells after 24 h incubation with ruthenium complexes.

Table S5. The viability of PBMCs and HL-60 cells after 2 h incubation with ruthenium complexes, maleimide and succinimide.

Table S6. Cell cycle distribution measured by flow cytometry using a staining with propidium iodide (PI) in HL-60 cells incubated for 24 h at 37°C with ruthenium chloride, maleimide and complex 1. The table shows mean results \pm SD; $n = 3$; * $p < 0.05$, ** $p < 0.01$, *** $p < 0.001$.

Figure S9. Electrophoretic separation of genomic DNA incubated for 2 h at 37°C with complex 1 (A), 2 (B), 3 (C), 4 (D), maleimide (E), succinimide (F) and ruthenium chloride (G) at the concentrations of 0, 5, 10, 25, 50, 100, and 250 μ M (1 to 7, respectively).

1.4. Theoretical Calculation

Figure S10. Electrostatic potential mapped on 9×10^{-4} au electron density isosurface of maleimide (a), and succinimide (b) molecule. The same scale of colours was used for both figures, with red corresponding to electron charge surplus (negative ESP) and blue corresponding to electron deficit (positive ESP).

1.5 References

1.1. Crystallographic and experimental data

Hirshfeld surface analysis

Hirshfeld surfaces were generated with the use of CrystalExplorer3.0 program^{1, 2} using the automatic procedures implemented in the program. The obtained molecular surface has been mapped with d_{norm} , a parameter which reflects intermolecular distances. Negative values of d_{norm} indicating contacts shorter than the sum of van der Waals radii are visualized in red, while positive values of contacts longer than the sum of van der Waals radii are colored in blue. The white color denotes intermolecular distances close to van der Waals contacts with d_{norm} equal zero. The Hirshfeld surface fingerprint plots were generated using d_i (distance from the surface to the nearest atom in the molecule itself) and d_e (distance from the surface to the nearest atom in another molecule) as a pair of coordinates, at intervals of 0.01 Å, in two-dimensional histograms.

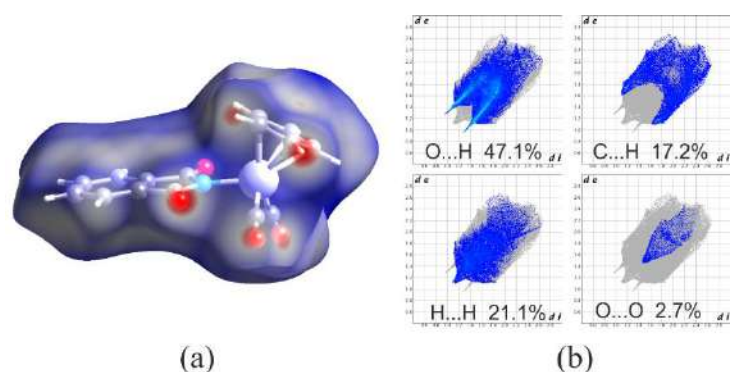


Fig. S1. Molecular Hirshfeld surface of **4** mapped with d_{norm} parameter; colored scale from -0.26 (red) to +1.32 (blue) (a); Hirshfeld surface fingerprint plots of selected intermolecular contacts with their percentage (b).

The summary of intermolecular interactions is described in terms of Hirshfeld surface analysis providing additional insight into the crystal structure. The molecular Hirshfeld surface (HS) of **4** shown in Figure S1a represents the area where molecules come into mutual contacts in solid state. The red circle areas indicate molecular regions of great importance from the point of view of molecular interactions and they occur close to oxygen atoms and CH donors of hydrogen bonds. Among various types of intermolecular contacts the most numerous are O...H ones, which form two sharp, long distinct spikes in the bottom left area in the HS fingerprint (Figure S1b). In turn, C...H contacts are less numerous and their fingerprint motifs are not so elongated while homoatomic H...H and O...O contacts, typically for mono component crystals, form single, symmetric peaks.

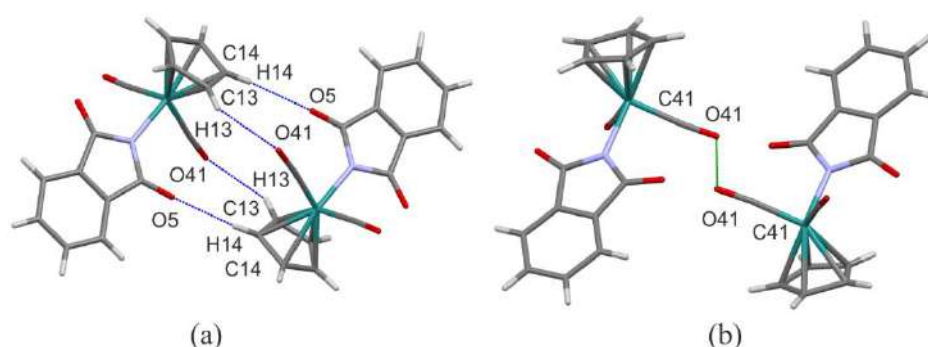


Fig. S2. Intermolecular interactions of **4**: C-H...O hydrogen bond (a); carbonyl...carbonyl interactions (b).

formula	C ₁₅ H ₉ NO ₄ Ru
M [g·mol ⁻¹]	368.3
crystal system, space group	monoclinic, <i>P2₁/n</i>
a [Å]	12.2560(3)
b [Å]	7.9638(2)
c [Å]	15.0812(3)
β [°]	110.669(3)°
V [Å ³], Z	1377.25(6), 4
<i>F</i> (000), μ [mm ⁻¹]	728.0, 1.152
<i>d</i> _x [mg m ⁻³]	1.776
crystal shape and size [mm]	red block, 0.136 x 0.268 x 0.483
λ [Å]	MoKα
T [K]	100
2θ range [°], <i>R</i> _{int}	2.655 - 30.805, 0.0465
data unique / parameters	3816/191
<i>R</i> / <i>wR</i> ² [I > 2σ (I)]	0.0245 / 0.0549
<i>R</i> / <i>wR</i> ² (all data)	0.0290 / 0.0571
Δρ _{min} / Δρ _{max} [e·Å ⁻³]	0.543 / -0.534
Goof on <i>F</i> ²	1.061

Table S1. Details of the crystal structure determination of **4**.

Ru1-N1	2.080(2)
Ru1-C41	1.883(2)
Ru1-C31	1.888(2)
Ru1-Cg1	1.886(3)
Ru1-C11	2.247(2)
Ru1-C12	2.245(2)
Ru1-C13	2.227(2)
Ru1-C14	2.216(2)
Ru1-C15	2.223(2)
O31-C31	1.135(2)
O41-C41	1.141(3)
O2-C2	1.209(2)
O5-C5	1.220(2)
N1-C2	1.389(2)
N1-C5	1.382(2)
C31-Ru1-N1	91.99(6)
C41-Ru1-N1	91.53(7)

C41-Ru1-C31	91.94(9)
C31-Ru1-Cg1	124.76(18)
C41-Ru1-Cg1	125.52(18)
N1-Ru1-Cg1	121.55(19)
O31-C31-Ru1	175.68(16)
O41-C41-Ru1	175.00(18)
C5-N1-C2	110.14(13)
C5-N1-Ru1	126.27(11)
C2-N1-Ru1	123.57(11)
C31-Ru1-N1-C2	57.06(14)
C31-Ru1-N1-C5	-124.86(15)
C41-Ru1-N1-C2	149.06(14)
C41-Ru1-N1-C5	-32.86(13)
Cg1-Ru1-N1-C2	76.63(18)
Cg1-Ru1-N1-C5	101.44(17)

Table S2. Selected bond lengths [\AA] and angles [$^\circ$].

hydrogen bond	D-H	H...A	D...A	\angle D-H...A	symmetry
C13-H13...O41	0.95	2.53	3.320(3)	141	1-x, 1-y, 1-z
C14-H14...O5	0.95	2.38	3.290(3)	160	1-x, 1-y, 1-z

Table S3. Geometric parameters of selected hydrogen bonds – distances [\AA] and angles [$^\circ$].

1.2. Spectra and spectral data

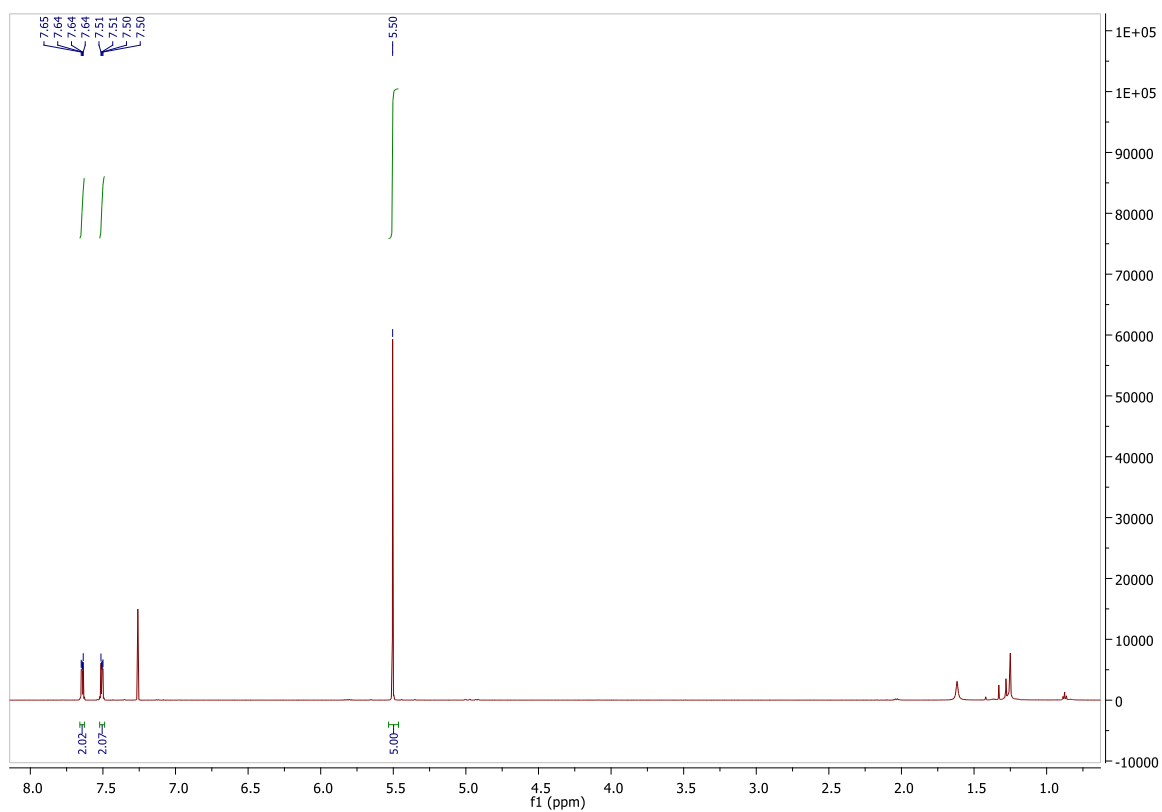


Fig. S3. 600 MHz ^1H NMR spectrum of **4** in CDCl_3 .

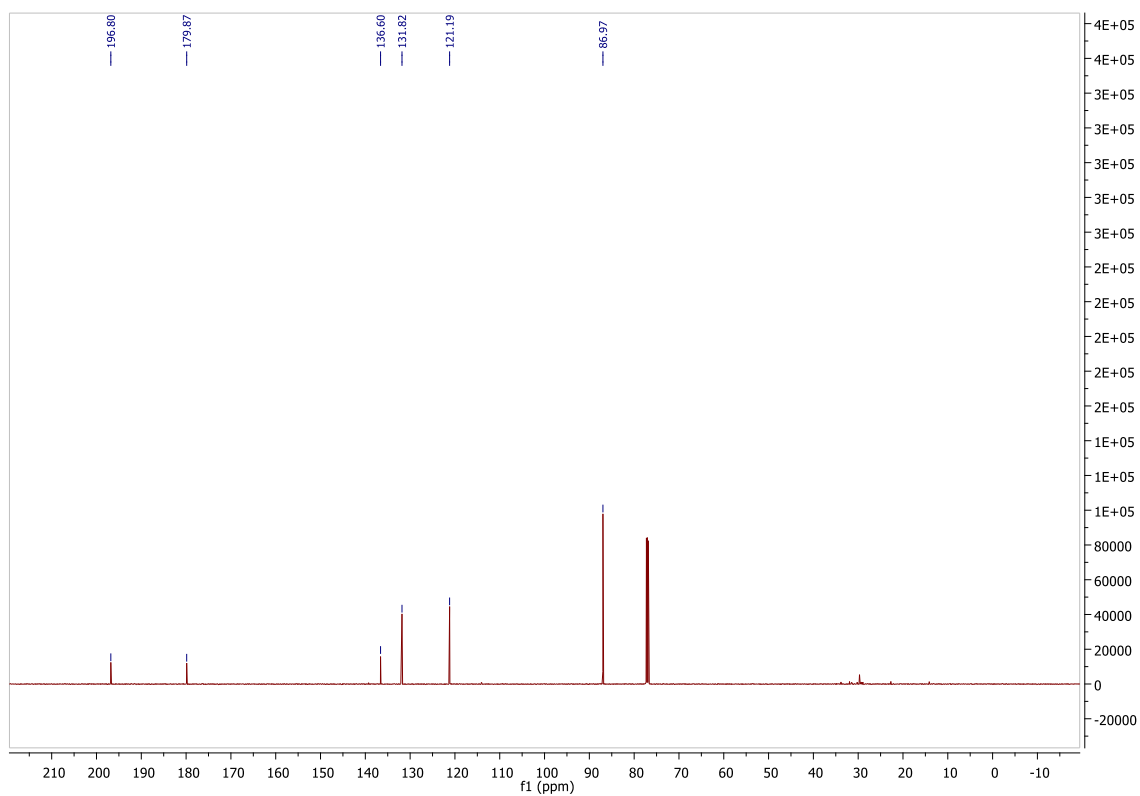


Fig. S4. 151 MHz ^{13}C NMR spectrum of **4** in CDCl_3 .

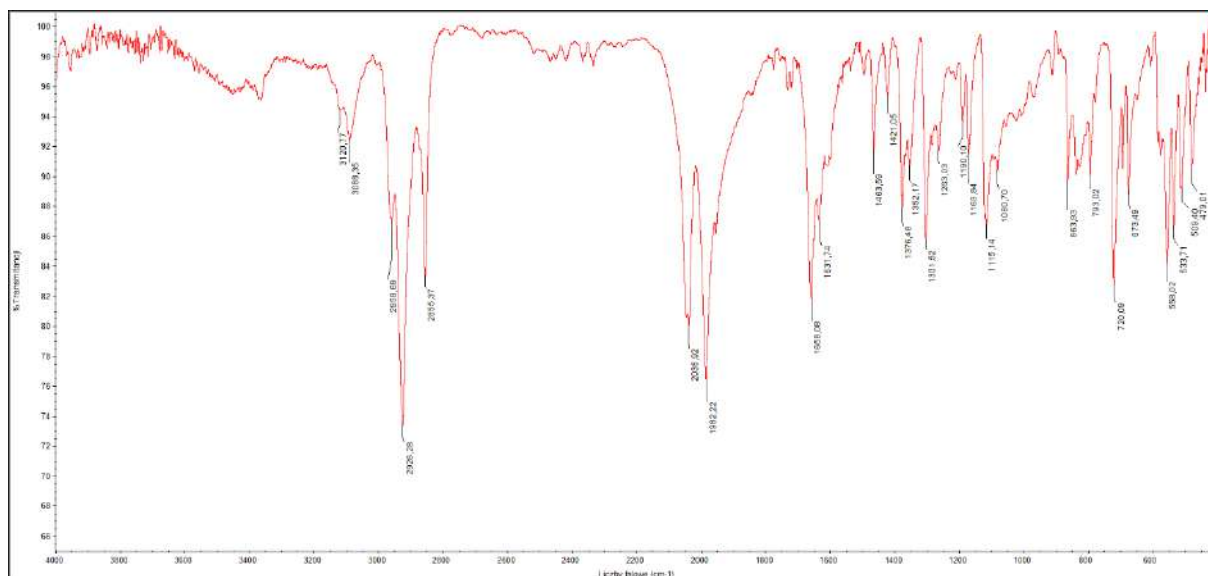


Fig. S5. IR spectrum of **4** (KBr, cm^{-1}).

1.3 Biological studies

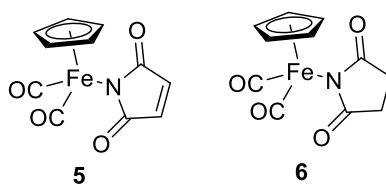


Fig. S6. Structures of iron metallocarbonyl complexes bearing succinimide and maleimide ligands **5** and **6**.

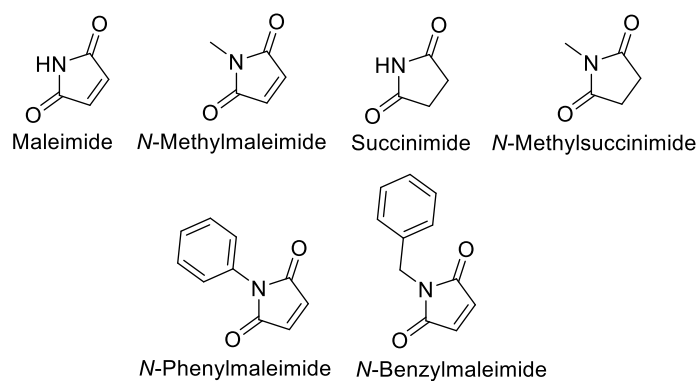


Fig. S7. Structures of maleimides and succinimides.

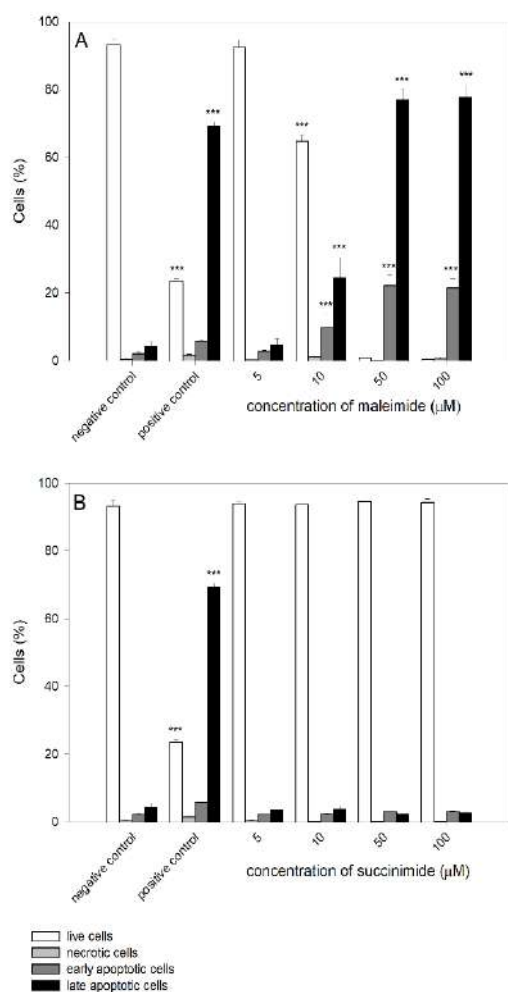


Fig. S8. The effect of maleimide (**A**), and succinimide (**B**) on the apoptosis of HL-60 cells after 24 h incubation. The positive control were cells incubated with 20 μM camptothecin (CAM) for 24 h at 37°C. Data represent means ± SD of 3 experiments. *** $p < 0.001$ compared with the negative control (untreated HL-60 cells).

Concentration (μM)	PBMCs				
	Ruthenium chloride	Complex 1	Complex 2	Complex 3	Complex 4
0.5	98.46 ± 1.45	106.58 ± 2.39 **↑	106.08 ± 2.16 ***↑	107.46 ± 1.65 ***↑	108.97 ± 3.27 ***↑
1	96.24 ± 1.53 *↓	107.61 ± 2.27 *↑	106.36 ± 1.94 ***↑	105.49 ± 2.34 ***↑	107.50 ± 3.07 ***↑
2.5	95.04 ± 2.04 **↓	100.69 ± 3.42	104.63 ± 1.10 ***↑	105.50 ± 4.33 ***↑	107.54 ± 2.07 ***↑
5	93.82 ± 1.30 ***↓	90.86 ± 1.94 ***↓	105.25 ± 1.69 ***↑	107.55 ± 2.13 ***↑	107.39 ± 3.17 ***↑

10	92.67 ± 1.78 ***↓	76.22 ± 2.92 ***↓	104.46 ± 1.07 ***↑	113.00 ± 2.64 ***↑	107.93 ± 4.12 **↑
25	91.84 ± 2.12 ***↓	65.72 ± 1.41 ***↓	105.81 ± 1.70 ***↑	107.90 ± 3.25 ***↑	107.09 ± 4.38 **↑
50	90.92 ± 1.56 ***↓	58.92 ± 1.56 ***↓	106.27 ± 1.74 ***↑	103.66 ± 1.44 *↑	102.54 ± 1.31 *↑
100	90.32 ± 1.67 ***↓	47.08 ± 0.95 ***↓	106.77 ± 2.55 ***↑	104.59 ± 1.54 *↑	101.33 ± 1.88
250	90.41 ± 1.37 ***↓	18.03 ± 1.29 ***↓	106.31 ± 1.39 ***↑	105.00 ± 1.07 *↑	85.39 ± 1.49 ***↓
			HL-60 cells		
0.5	103.18 ± 2.91	120.27 ± 1.99 ***↑	108.49 ± 2.27 ***↑	107.96 ± 3.02 ***↑	114.03 ± 1.99 ***↑
1	103.35 ± 1.72	118.34 ± 1.70 ***↑	108.02 ± 4.01 ***↑	109.15 ± 3.81 ***↑	112.72 ± 0.84 ***↑
2.5	102.45 ± 2.29	105.71 ± 2.26 ***↑	109.14 ± 5.22 ***↑	109.29 ± 4.84 ***↑	112.07 ± 3.54 ***↑
5	98.85 ± 1.31	55.11 ± 2.08 ***↓	107.03 ± 4.66 ***↑	109.58 ± 3.24 ***↑	111.77 ± 4.11 ***↑
10	92.90 ± 1.30 ***↓	29.25 ± 0.54 ***↓	107.77 ± 2.83 ***↑	109.36 ± 7.05 *↑	111.01 ± 3.88 ***↑
25	86.44 ± 1.93 ***↓	18.97 ± 0.52 ***↓	108.15 ± 3.66 ***↑	106.67 ± 4.83 *↑	108.80 ± 5.27 **↑
50	79.13 ± 2.31 ***↓	4.62 ± 0.11 ***↓	112.32 ± 1.36 ***↑	102.22 ± 5.20	103.43 ± 4.57
100	73.73 ± 1.7 ***↓	2.53 ± 0.6 ***↓	97.52 ± 3.47	57.07 ± 1.60 ***↓	88.30 ± 4.36 ***↓
250	62.89 ± 0.94 ***↓	1.60 ± 0.14 ***↓	55.67 ± 4.39 ***↓	18.73 ± 1.00 ***↓	35.87 ± 1.61 ***↓

Table S4. The viability of PBMCs and HL-60 cells after 24 h incubation with ruthenium complexes. The viability for individual samples were calculated relative to control ± SD. Cell viability in the control was taken as 100%. * $p < 0.05$, ** $p < 0.01$, *** $p < 0.001$, ↑ – increase, ↓ – decrease.

Concentration (μM)	PBMCs					Maleimide	Succinimide
	Ruthenium chloride	Complex 1	Complex 2	Complex 3	Complex 4		
0.5	97.5 ± 0.9	102.3 ± 2.2	96.6±1.2**↓	98.6 ± 2.29	98.8 ± 1.98	108.5±1.2***↑	102.1 ± 2.2
1	96.3 ± 3.01	99.4 ± 1.9	95.4±1.7**↓	98.7 ± 1.38	98.2 ± 2.86	111.5±3.8***↑	99.9 ± 1.2
2.5	94.8 ± 2.6*↓	101.5 ± 5.7	95.3±0.7**↓	98.9 ± 1.78	101.7 ± 1.2	105.5 ± 3.5*↑	103.1 ± 4.4
5	95.3 ± 3.4*↓	96.6 ± 1.8*↓	95.8±1.6**↓	99.6 ± 1.68	101.7 ± 2.44	92.4 ± 4.5**↓	99.4 ± 1.7
10	97.0 ± 2.4*↓	92.4±1.7***↓	92.4±1.2***↓	97.3 ± 2.41	100.4 ± 2.06	89.6±3.0***↓	98.7 ± 0.8
25	94.5 ± 3.4*↓	92 ± 1.7***↓	91.7±2.1***↓	95.3±2.5**↓	98.2 ± 2	81.7±3.7***↓	98.5 ± 2.5
50	95.1 ± 2.9*↓	93.6±2.4***↓	91.2±1.2***↓	91.5±2.3***↓	95.3 ± 1.3**↓	60.4±2.1***↓	99.9 ± 4.95

100	91.7±2.0*** ↓	85.8±1.3*** ↓	91.7±0.9*** ↓	90.1±1.5*** ↓	94.9 ± 3.5***↓	39.5±1.4***↓	95.4±1.7**↓
250	75.5±2.2*** ↓	77.9±0.9*** ↓	93.8±1.0*** ↓	84.5±1.7*** ↓	90.6±0.8***↓	8.1 ± 0.9 ***↓	89.5±1.4*** ↓
				HL-60 cells			
0.5	97.9 ± 1.8	98.7 ± 2.2	97.9 ± 2.3	96.9 ± 5.03	99.5 ± 3.08	98.95 ± 2	97.14 ± 3.47
1	96.7±1.2**↓	95.5 ± 2.2* ↓	97.2 ± 2.2	91.7±2.3*** ↓	100.8 ± 4.5	94.8±0.5***↓	99.34 ± 1.37
2.5	95.0±2.1**↓	91.3±1.0*** ↓	97.2 ± 1.3	92.4±2.6*** ↓	98.91 ± 3.1	91.8±1.5***↓	102.51±3.14
5	93.3±1.2*** ↓	87.7±1.6*** ↓	96.5 ± 2.5	89.8±1.2*** ↓	96.59 ± 3.81	53.1±8.3***↓	100.31±1.94
10	93.2±1.9*** ↓	77.9±1.4*** ↓	96.6 ± 3.6	85.4±2.1*** ↓	96.7 ± 1.3**↓	16.2±0.9***↓	98.94 ± 3.92
25	93.0±2.9*** ↓	62.2±1.0*** ↓	97.1 ± 2.2	84.5±2.5*** ↓	95.0 ± 2.5**↓	10.2±0.3***↓	97.34 ± 3.26
50	89.5±3.2*** ↓	10.7±0.2*** ↓	94.8±2.7**↓	78.9±1.2*** ↓	91.7±3.4***↓	6.9±0.18***↓	96.58 ± 4.46
100	77.5±3.1*** ↓	10.4±0.2*** ↓	91.1±3.5*** ↓	76.2±2.6*** ↓	90.56±2.6*** ↓	6.02±0.2***↓	91.5±3.3*** ↓
250	55.3±2.1*** ↓	8.9±0.2***↓	78.9±1.8*** ↓	61.5±0.9*** ↓	73.4±1.4 ***↓	5.97±0.5***↓	78.2±4.6*** ↓

Table S5. The viability of PBMCs and HL-60 cells after 2 h incubation with ruthenium complexes, maleimide and succinimide. The viability for individual samples were calculated relative to control ± SD. Cell viability in the control was taken as 100%. * $p < 0.05$. ** $p < 0.01$. *** $p < 0.001$. ↑ – increase. ↓ – decrease.

Treatment	Sub-G1	G0/G1	S	G2/M
Negative control	2.99 ± 0.12	48.01 ± 1.23	19.35 ± 0.83	28.57 ± 1.4
Positive control (NOC)	26.48 ± 3.01 ***	22.97 ± 1.4 ***	14.60 ± 2.95	35.58 ± 1.8 **
Ruthenium chloride 1 μM	3.34 ± 0.25	50.02 ± 1.44	16.04 ± 0.7	29.75 ± 0.8
Ruthenium chloride 2.5 μM	2.72 ± 0.1	51.92 ± 1.37	15.08 ± 0.25 **	29.87 ± 1.4
Ruthenium chloride 5 μM	3.48 ± 0.35	50.18 ± 1.23	15.29 ± 0.59 **	30.29 ± 1.0
Ruthenium chloride 10 μM	3.13 ± 0.62	53.33 ± 1.05 **	15.66 ± 0.71 **	27.18 ± 1.3
Maleimide 1 μM	3.22 ± 0.22	54.15 ± 2.25 *	12.31 ± 0.46 ***	29.55 ± 1.8
Maleimide 2.5 μM	3.40 ± 0.11	54.01 ± 2.88 *	14.79 ± 2.1 *	27.08 ± 2.5
Maleimide 5 μM	3.56 ± 0.52	48.54 ± 2.56	20.20 ± 0.31	26.97 ± 1.9
Maleimide 10 μM	3.70 ± 0.36	47.83 ± 3.03	21.22 ± 2.85	26.87 ± 0.7
Complex 1 μM	3.37 ± 0.17	54.53 ± 1.8 **	14.55 ± 0.6 **	27.00 ± 2.1
Complex 2.5 μM	4.29 ± 0.6	49.75 ± 1.53	20.29 ± 0.53	25.33 ± 2.5
Complex 5 μM	4.49 ± 0.24	48.24 ± 2.39	21.31 ± 1.31	25.45 ± 1.5
Complex 10 μM	5.45 ± 0.33 ***	40.35 ± 3.15*	19.33 ± 2.09	33.65 ± 2.1 *

Table S6. Cell cycle distribution measured by flow cytometry using a staining with propidium iodide (PI) in HL-60 cells incubated for 24 h at 37°C with ruthenium chloride, maleimide and complex 1. The table shows mean results ± SD; $n = 3$; * $p < 0.05$, ** $p < 0.01$, *** $p < 0.001$.

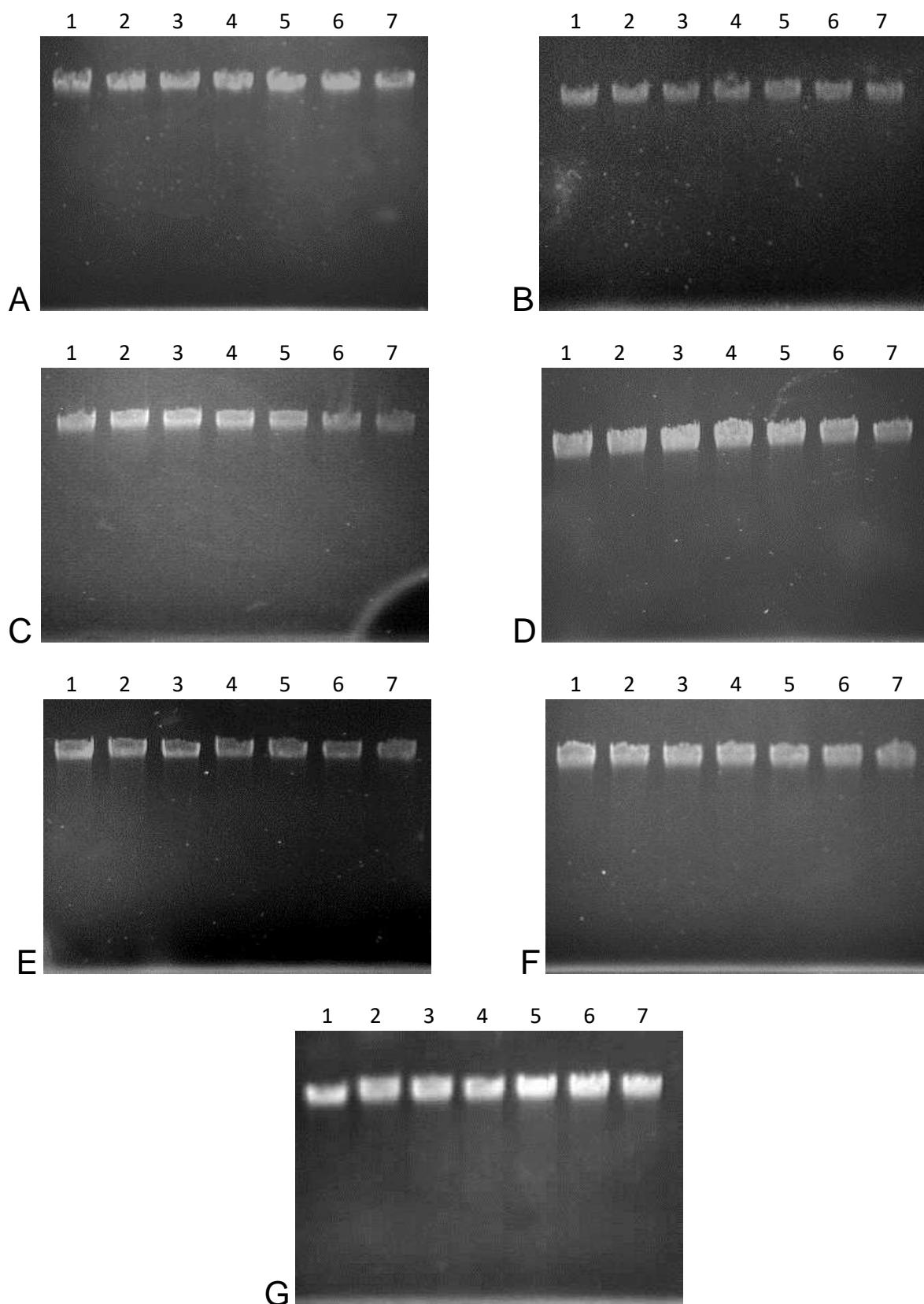


Figure S9. Electrophoretic separation of genomic DNA incubated for 2 h at 37°C with complex 1 (A), 2 (B), 3 (C), 4 (D), maleimide (E), succinimide (F) and ruthenium chloride (G) at the concentrations of 0, 5, 10, 25, 50, 100, and 250 μM (1 to 7, respectively).

1.4. Theoretical calculation

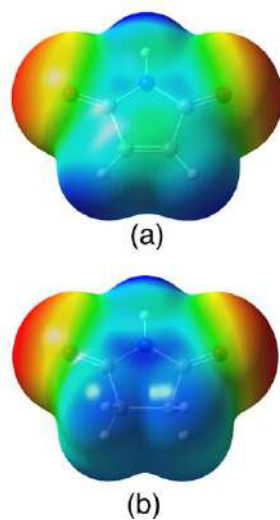



Figure S10. Electrostatic potential mapped on 9×10^{-4} au electron density isosurface of maleimide (a), and succinimide (b) molecule. The same scale of colours was used for both figures, with red corresponding to electron charge surplus (negative ESP) and blue corresponding to electron deficit (positive ESP).

1.5. References

1. McKinnon, J. J.; Fabbiani, F. P. A.; Spackman, M. A., Comparison of Polymorphic Molecular Crystal Structures through Hirshfeld Surface Analysis. *Crystal Growth & Design* **2007**, *7* (4), 755-769.
2. Spackman, M. A.; Jayatilaka, D., Hirshfeld surface analysis. *CrystEngComm* **2009**, *11* (1), 19-32.

Article

Antioxidant Activity of Ruthenium Cyclopentadienyl Complexes Bearing Succinimidato and Phthalimidato Ligands

 Michał Juszcak ¹, Magdalena Kluska ¹, Aneta Kosińska ², Bogna Rudolf ² and Katarzyna Woźniak ^{1,*}

¹ Department of Molecular Genetics, Faculty of Biology and Environmental Protection, University of Lodz, 90-236 Lodz, Poland; michal.juszcak@edu.uni.lodz.pl (M.J.); magdalena.kluska@edu.uni.lodz.pl (M.K.)

² Department of Organic Chemistry, Faculty of Chemistry, University of Lodz, 91-403 Lodz, Poland; aneta.kosinska@chemia.uni.lodz.pl (A.K.); bogna.rudolf@chemia.uni.lodz.pl (B.R.)

* Correspondence: katarzyna.wozniak@biol.uni.lodz.pl

Abstract: In these studies, we investigated the antioxidant activity of three ruthenium cyclopentadienyl complexes bearing different imidato ligands: (η^5 -cyclopentadienyl)Ru(CO)₂-*N*-methoxysuccinimidato (**1**), (η^5 -cyclopentadienyl)Ru(CO)₂-*N*-ethoxysuccinimidato (**2**), and (η^5 -cyclopentadienyl)Ru(CO)₂-*N*-phthalimidato (**3**). We studied the effects of ruthenium complexes **1–3** at a low concentration of 50 μ M on the viability and the cell cycle of peripheral blood mononuclear cells (PBMCs) and HL-60 leukemic cells exposed to oxidative stress induced by hydrogen peroxide (H₂O₂). Moreover, we examined the influence of these complexes on DNA oxidative damage, the level of reactive oxygen species (ROS), and superoxide dismutase (SOD) activity. We have observed that ruthenium complexes **1–3** increase the viability of both normal and cancer cells decreased by H₂O₂ and also alter the HL-60 cell cycle arrested by H₂O₂ in the sub-G1 phase. In addition, we have shown that ruthenium complexes reduce the levels of ROS and oxidative DNA damage in both cell types. They also restore SOD activity reduced by H₂O₂. Our results indicate that ruthenium complexes **1–3** bearing succinimidato and phthalimidato ligands have antioxidant activity without cytotoxic effect at low concentrations. For this reason, the ruthenium complexes studied by us should be considered interesting molecules with clinical potential that require further detailed research.

Keywords: succinimide; phthalimide; ruthenium metallocarbonyl complexes; DNA oxidative damage; ROS; SOD activity; cell cycle; hydrogen peroxide



Citation: Juszcak, M.; Kluska, M.; Kosińska, A.; Rudolf, B.; Woźniak, K. Antioxidant Activity of Ruthenium Cyclopentadienyl Complexes Bearing Succinimidato and Phthalimidato Ligands. *Molecules* **2022**, *27*, 2803. <https://doi.org/10.3390/molecules27092803>

Academic Editor: Artur M. S. Silva

Received: 18 March 2022

Accepted: 24 April 2022

Published: 28 April 2022

Publisher's Note: MDPI stays neutral with regard to jurisdictional claims in published maps and institutional affiliations.



Copyright: © 2022 by the authors. Licensee MDPI, Basel, Switzerland. This article is an open access article distributed under the terms and conditions of the Creative Commons Attribution (CC BY) license (<https://creativecommons.org/licenses/by/4.0/>).

1. Introduction

In recent years, many different ruthenium complexes exhibiting various chemical and biological properties have been synthesized [1]. Complexes with anticancer potential are of particular interest [2–4]. Ruthenium complexes exhibit many features that are desirable among cancer drug candidates. They are less cytotoxic to normal cells compared to cancer cells, in which they can accumulate due to uptake by transferrin receptors. Many of them are active against cells that are metastatic and resistant to conventional chemotherapy. We recently demonstrated that ruthenium complex (η^5 -cyclopentadienyl)Ru(CO)₂(η^1 -*N*-maleimidato) has anticancer potential [4,5]. This complex was about ten times more cytotoxic to leukemic HL-60 cells compared to normal peripheral blood mononuclear cells (PBMCs). Moreover, complex (η^5 -cyclopentadienyl)Ru(CO)₂(η^1 -*N*-maleimidato) induced DNA damage and apoptosis in HL-60 cells.

Many ruthenium complexes show antioxidant activity [6–12]. For example, there are two new ruthenium complexes *cis*-[Ru(NO₂)(bpy)₂(5NIM)]PF₆ and *cis*-[RuCl(bpy)₂(MTZ)]PF₆, where bpy = 2,2'-bipyridine, 5NIM = 5-nitroimidazole, and MTZ = metronidazole have antioxidant properties in vitro. It was shown that these complexes reduced lipid peroxidation and decreased intracellular ROS levels with comparable effectiveness to the standard steroidal drug dexamethasone or α -tocopherol [9]. Similarly, radical scavenging studies

revealed that ruthenium heterocyclic complexes have high activities toward the neutralization of NO and DPPH• (2,2-diphenyl-1-picrylhydrazyl) radicals [11]. Organoruthenium(II) complexes, synthesized and analyzed by Mohankumar et al. [8], effectively scavenged the DPPH• radicals compared to that of standard control ascorbic acid. Moreover, it was shown that some of these complexes also exhibited an excellent *in vivo* antioxidant activity as they were able to increase the survival of worms exposed to lethal oxidative and thermal stresses by reducing the intracellular ROS levels. The gene expression analysis revealed that these ruthenium complexes maintained the intracellular redox status and offered stress protection through the transactivation of antioxidant defense machinery genes *gst-4* and *sod-3*, which are directly regulated by SKN-1 and DAF-16 transcription factors, respectively [8].

Studies have also shown that some ruthenium complexes have a protective effect on the cardiovascular system [13]. For example, it was revealed that a ruthenium *p*-cymene complex with quercetin binds to 3-hydroxy-3-methyl-glutaryl-CoA reductase (HMGR) both *in silico* and *in vitro* and reduces the activity of this endoplasmic, reticulum-bound enzyme that regulates the early stages of cholesterol biosynthesis [14]. It was also observed that this complex had an activity significantly higher than pure quercetin and comparable to those observed for two model drugs, pravastatin and simvastatin. Other ruthenoflavonoid complexes—[Ru(*p*-cym)(chrysin)Cl] and [Ru(*p*-cym)(thiochrysin)Cl]—showed good anti-aggregating activity in washed platelet samples [15]. The complexes were further demonstrated to interfere with several inter-platelet signaling pathways involved in aggregation, such as the integrin α IIb β 3 inside-out and outside-in signaling paths, the phosphoinositide 3-kinase (PI3K) pathway, and the release of granules. Moreover, Ru[Ru(*p*-cym)(thiochrysin)Cl] has been able to inhibit *in vitro* thrombus formation and it was shown to affect haemostasis in mice [15]. It was also found that a mononuclear ruthenium(II) diimine complex along with dietary intervention possesses cardioprotective effects in high-fat high carbohydrate diet-induced prediabetic rats by ameliorating oxidative stress and antioxidant defense enzymes, reducing MAP, restoring the heart to body weight ratio, attenuating derangement in the lipid profile and reducing cardiac inflammatory markers [16].

Recently, we demonstrated that ruthenium complexes (η^5 -cyclopentadienyl)Ru(CO)₂-*N*-methoxysuccinimidato (1), (η^5 -cyclopentadienyl)Ru(CO)₂-*N*-ethoxysuccinimidato (2), and (η^5 -cyclopentadienyl)Ru(CO)₂-*N*-phthalimidato (3) (Figure 1) showed no cytotoxic and genotoxic properties as opposed to the maleimide ligand complex [5]. Moreover, an increase in cell viability was observed after incubation with these complexes. Our comparative studies with free maleimides and succinimides and their derivatives showed that the different biological activity of ruthenium complexes depends mainly on maleimide and succinimide ligands bound to the ruthenium atom [5].

Our previous results prompted us to investigate the antioxidative activity of ruthenium complexes bearing succinimidato and phthalimidato ligands 1–3 (Figure 1) in normal and leukemia cells. Many succinimide derivatives synthesized in recent years show anti-free radical properties and are being investigated for their potential use against neurodegenerative disorders such as Alzheimer's disease, cancer, diabetes mellitus, and worms [17–20]. Here, we incubated human peripheral blood mononuclear cells (PBMCs) and HL-60 leukemic cells with hydrogen peroxide (H₂O₂) to induce oxidative stress. Incubation with H₂O₂ was preceded by pre-incubation of cells with ruthenium complexes 1–3. For comparison, we also pre-incubated the cells with ruthenium chloride (RuCl₃) and succinimide ligand. We investigated the influence of ruthenium complexes 1–3 on viability, cell cycle, and DNA oxidative damage. We also determined their effect on the level of reactive oxygen species (ROS) and superoxide dismutase (SOD) activity.

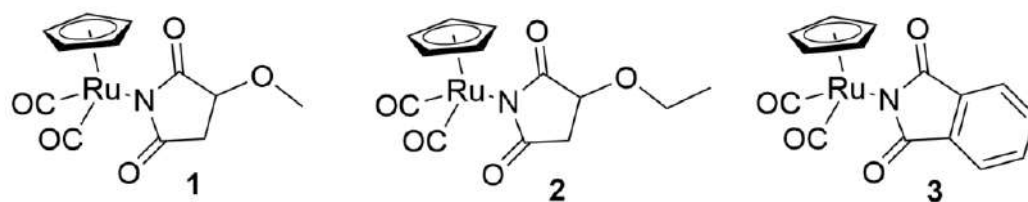


Figure 1. The structures of the ruthenium complexes 1–3.

2. Material and Methods

2.1. Chemicals

Ruthenium complexes 1–3 were synthesized as previously described (1) [21], (2) [22], (3) [5]. IMDM medium and fetal bovine serum (FBS) were obtained from Biowest (Cytogen, Zgierz, Poland). Ruthenium chloride (RuCl_3), 2',7'-dichlorofluorescein (H_2DCFDA), Hank's balanced salt solution (HBSS), dimethyl sulfoxide (DMSO), and hydrogen peroxide (H_2O_2) were purchased from Sigma-Aldrich (St. Louis, MO, USA). Succinimide was purchased from Fluka. All other chemicals were of the highest commercial grade available. A stock solution of complexes and succinimide (10 mM) was dissolved in DMSO.

2.2. Cell Culture

HL-60 (human promyelocytic leukemia) cell line was obtained from the American Type Culture Collection (ATCC) and cultured in Iscove's Modified Dulbecco's Medium (IMDM) with 15% fetal bovine serum, streptomycin/penicillin solution (100 $\mu\text{g}/\text{mL}$ and 100 U/mL). HL-60 cells were cultured in flasks at 37 °C in 5% CO_2 and sub-cultured every 2–3 days to maintain exponential growth.

Peripheral blood mononuclear cells (PBMCs) were isolated from the buffy coats obtained from healthy donors from Central Blood Bank, Lodz. Each donor agreed to donate blood. The first step of isolation of PBMCs was a mix of fresh blood from buffy coats with PBS at ratio 1:1. In the next step, the mixture was centrifuged in a density gradient of Lymphosep (Cytogen, Zgierz, Poland) at 2200 RPM for 20 min with the lowest values of acceleration and deceleration. Then the cells were washed three times by centrifugation with 1% PBS. After isolation cells were suspended in RPMI 1640 medium. The study protocol was approved by the Committee for Research on Human Subjects of the University of Lodz (17/KBBN-UŁ/III/2019).

2.3. Cell Viability

The cell viability resazurin assay was performed similarly to the method described by O'Brien et al. [23]. Resazurin salt powder was dissolved in sterile PBS buffer. PBMCs and HL-60 cells were seeded on 6-well plates at a density of 0.5×10^6 cells/mL. Cells were pre-incubated with ruthenium complexes 1–3, succinimide, and RuCl_3 at a concentration of 50 μM for 24 h at 37 °C in 5% CO_2 . Next, cells were washed with warm PBS. Then, cells were seeded on a 96-well plate in the count of 50,000 for PBMCs and 15,000 for HL-60 cells. Next, cells were incubated with H_2O_2 at concentrations of 0.2, 0.4, and 0.6 mM for 4 h at 37 °C in 5% CO_2 . Next, 10 μL of resazurin salt was added to each well, and the plates again were incubated at 37 °C in 5% CO_2 for 2 h. After that, fluorescence was measured with HT microplate reader Synergy HT (Bio-Tek Instruments, Winooski, VT, USA) using $\lambda_{\text{ex}} = 530/25$ nm and an $\lambda_{\text{em}} = 590/35$ nm. The effects of ruthenium complexes, RuCl_3 , and succinimide on cell viability were quantified as the percentage of control fluorescence.

2.4. Cell Cycle

HL-60 cells were seeded on 6-well plates at a density of 0.5×10^6 cells/mL. The cells incubated with 100 ng/mL nocodazol (NOC) for 24 h at 37 °C were the positive control. The cells were incubated with ruthenium complexes 1–3, succinimide, and RuCl_3 at a concentration of 50 μM for 24 h at 37 °C in 5% CO_2 . Next, cells were washed with warm

PBS. Then, cells were again seeded on 6-well plates. Next, cells were incubated with H₂O₂ at concentrations of 0.1 and 0.2 mM for 24 h at 37 °C in 5% CO₂. Then, cells were collected and washed twice with PBS. After that, cells were resuspended in PBS and put on ice for 15 min. Then, one volume of −20 °C absolute ethanol was added and the samples were stored at 4 °C. Before the analysis, samples were resuspended in 300 µL of staining solution containing 40 µg/mL PI (propidium iodide) 200 µg/mL RNase A. Samples were incubated for 30 min at 37 °C in the dark until analysis. DNA content was analyzed using an LSRII flow cytometer (Becton Dickinson, San Jose, CA, USA).

2.5. Effect of Ruthenium Complexes 1–3 on DNA Oxidative Damage

We pre-incubated cells with complexes 1–3, succinimide, and RuCl₃ at a concentration of 50 µM for 24 h in 37 °C in 5% CO₂, then cells were washed with PBS and incubated with H₂O₂ at 0.025 or 0.05 mM for 15 min on ice. Cell viability after incubation with H₂O₂ was in the range of 95–100% (data not shown). After incubation with H₂O₂ cells were centrifuged, suspended in LMP agarose, and spread onto a microscope slide. The slides were processed as described below in the Section 2.6.

2.6. Comet Assay

The comet assay was performed under alkaline conditions according to the procedure of Tokarz et al. [24]. A freshly prepared cell suspension in 0.75% LMP agarose dissolved in PBS was layered onto microscope slides (Superior, Germany), which were pre-coated with 0.5% NMP agarose. Then, the cells were lysed for 1 h at 4 °C in a buffer containing 2.5 M NaCl, 0.1 M EDTA, 10 mM Tris, 1% Triton X-100, pH = 10. After cell lysis, the slides were placed in an electrophoresis unit. DNA was allowed to unwind for 20 min in the solution containing 300 mM NaOH and 1 mM EDTA, pH > 13.

Electrophoretic separation was performed in the solution containing 30 mM NaOH and 1 mM EDTA, pH > 13 at an ambient temperature of 4 °C (the temperature of the running buffer did not exceed 12 °C) for 20 min at an electric field strength of 0.73 V/cm (28 mA). Then, the slides were washed in water, drained, stained with 2 µg/mL DAPI, and covered with coverslips. To prevent additional DNA damage, the procedure described above was conducted under limited light or in the dark.

2.7. Comet Analysis

The comets were observed at 200× magnification in an Eclipse fluorescence microscope (Nikon, Tokyo, Japan) attached to a COHU 4910 video camera (Cohu, Inc., San Diego, CA, USA) equipped with a UV-1 A filter block and connected to a personal computer-based image analysis system Lucia-Comet v. 6.0 (Laboratory Imaging, Praha, Czech Republic). Fifty images (comets) were randomly selected from each sample and the mean value of DNA in the comet tail was taken as an index of DNA damage (expressed in percent).

2.8. Measurement of Reactive Oxygen Species

To measure reactive oxygen species (ROS), a 2',7'-dichlorofluorescein diacetate (H₂DCFDA) probe was used. H₂DCFDA is a cell membrane-permeable non-fluorescent probe. 2',7'-dichlorofluorescein diacetate is de-esterified intracellularly and turns into highly fluorescent 2',7'-dichlorofluorescein upon oxidation. PBMCs and HL-60 cells were seeded at a density of 2.5 × 10⁶ cells/mL and 0.5 × 10⁶ cells/mL, respectively, and were incubated with ruthenium complexes 1–3, succinimide, and RuCl₃ at a concentration of 50 µM for 24 h at 37 °C in 5% CO₂. Next, the cells were washed twice with HBSS containing Ca²⁺ and Mg²⁺ and stained with 20 µM H₂DCFDA (Sigma-Aldrich, St. Louis, MO, USA) for 30 min at 37 °C in darkness. Then, the cells were washed twice with HBSS and incubated with 1 mM and 5 mM H₂O₂ at 37 °C in darkness. The intensity of fluorescence was measured after 30 min with λ_{ex} = 495 nm and λ_{em} = 530 nm using a microplate reader Synergy HT (Bio-Tek Instruments, Winooski, VT, USA). The data were analyzed according to the

following formula: $(T_x - T_0/T_0) \times 100$, where T_x is the DCF fluorescence measured at the indicated time and T_0 is the DCF fluorescence measured at the beginning of the analysis.

2.9. Measurement of SOD Activity

PBMCs and HL-60 cells were seeded at density 3×10^6 cells/mL and 1×10^6 cells/mL, respectively, in a 75 cm² cell culture flask. The cells were incubated with ruthenium complexes 1–3, succinimide, and RuCl₃ at a concentration of 50 μM for 24 h at 37 °C in 5% CO₂. Next, HL-60 cells were washed with PBS and incubated with 0.1 mM H₂O₂ for 15 min on ice. In the case of PBMCs, we used 0.25 mM H₂O₂ for 15 min at 37 °C. Next, cells were sonicated under the ice in 0.5 mL of PBS for 30 s using the 4710 Series Ultrasonic Homogenizer (Cole-Parmer Instrument Co., Chicago, IL, USA) to obtain cell lysates. SOD activity was measured using the SOD Assay Kit-WST (Dojindo, Kumamoto, Japan) by following the manufacturer's instructions. Cells lysates served as the sample solution. The mixture was placed into each well with 200 μL of WST working solution. Twenty microliters of enzyme working solution were added into each well and mixed thoroughly. The plate was incubated at 37 °C for 20 min. The absorbance was read at 450 nm using a microplate reader Synergy HT (Bio-Tek Instruments, Winooski, VT, USA).

2.10. Statistical Analysis

Data of cell viability, ROS measurement, cell cycle, and SOD activity are presented as the mean values ± standard deviation (SD) of at least three replicates. Values in the comet test are expressed as mean values + standard error of the mean (SEM) of three experiments; data from three experiments were collected and statistical parameters were calculated. Statistical analysis was performed using the Mann–Whitney test (samples with distributions departing from normality) and the Student *t*-test (normal distribution of the sample). Differences were considered statistically significant when the *p*-value was <0.05.

3. Results

3.1. Cell Viability

All experiments were performed with ruthenium complexes 1–3 at a concentration of 50 μM. We chose this concentration based on our previous studies in which we showed an increase in cell viability for both PBMCs and HL-60 after 24 h incubation with ruthenium complexes at 50 μM [5].

After pre-incubation, the cells were incubated with H₂O₂ for 4 h and the viability was determined with a resazurin reduction assay. We observed a significant increase ($p < 0.001$) in the viability of normal and cancer cells pre-incubated with all ruthenium complexes compared to the cells that were not pre-incubated (Figure 2). The cells that were pre-incubated with RuCl₃ under the same conditions showed a further decrease ($p < 0.001$) in viability following incubation with H₂O₂, except for the PBMCs which were incubated with H₂O₂ at 0.4 and 0.6 mM. We also observed a decrease ($p < 0.001$) in the viability of the HL-60 cells that were pre-incubated with succinimide. In the case of the normal cells, we detected the opposite effect of pre-incubation with the ligand—an increase in the viability of PBMCs compared to the cells that were only incubated with H₂O₂ at 0.4 and 0.6 mM ($p < 0.001$).

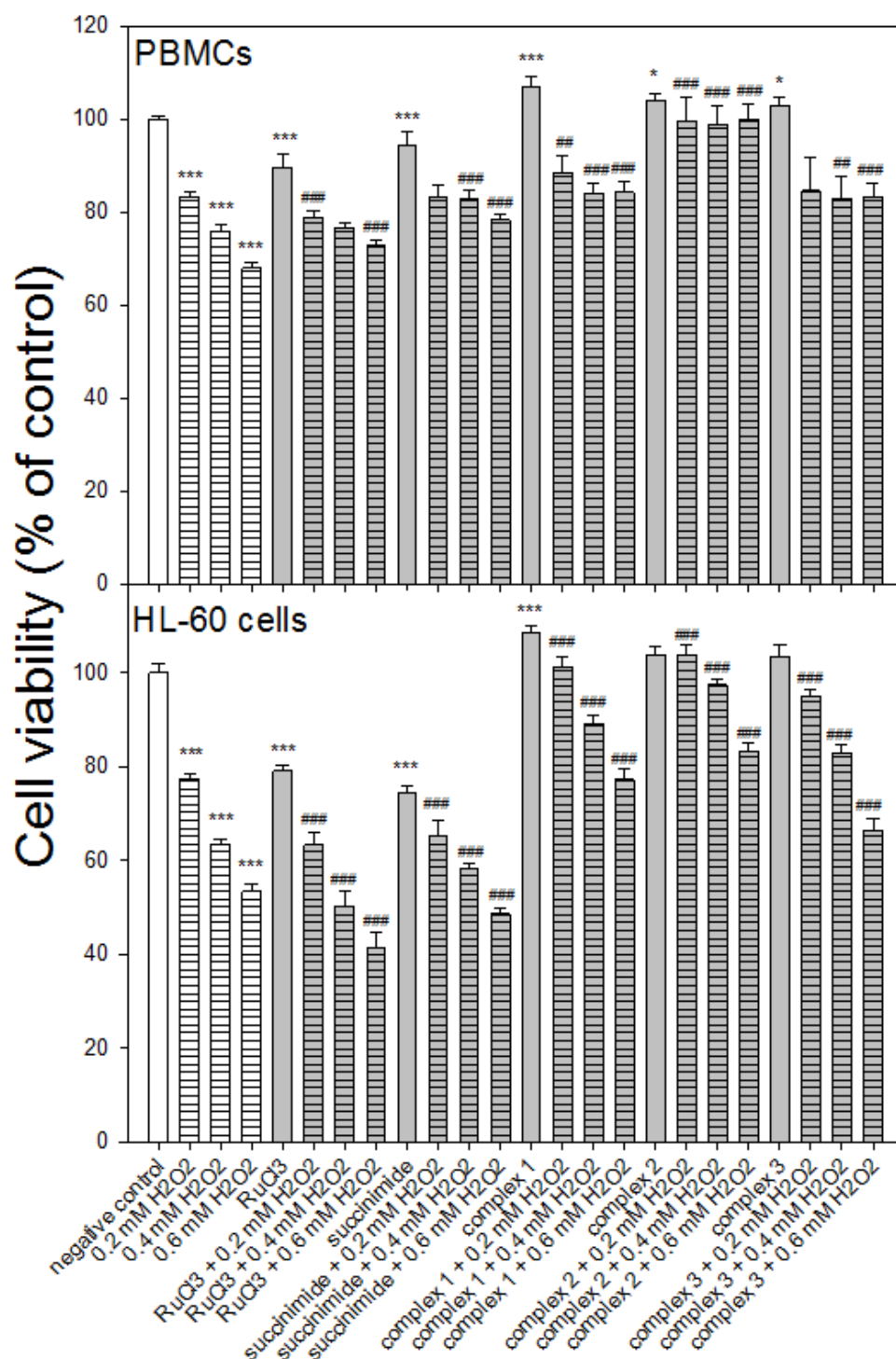


Figure 2. Effect of ruthenium complexes 1–3 at 50 μ M on the viability of PBMCs and HL-60 cells incubated with H₂O₂. The viability for individual samples was calculated relative to negative control (untreated cells) \pm SD. Cell viability in the control was taken as 100%, $n = 6$, * $p < 0.05$, *** $p < 0.001$ vs. negative control, ## $p < 0.01$, ### $p < 0.001$ vs. H₂O₂.

3.2. Cell Cycle

After incubation of HL-60 cells with 0.1 mM H₂O₂, we observed an increase in the number of cells in the sub-G1 ($p < 0.001$), S ($p < 0.001$) and G2/M ($p < 0.01$) phases of the cell cycle and a decrease in the G0/G1 phase ($p < 0.001$) compared to the control cells (Table 1). H₂O₂ at a higher concentration causes a further growth of HL-60 cells in the sub-G1 phase

($p < 0.001$) and a significant decrease in the number of cells in the phases G0/G1 ($p < 0.01$) and G2/M ($p < 0.01$).

We showed a decrease in the number of cells in the sub-G1 phase after pre-incubation with ruthenium complexes 1–3 compared to the cells incubated only with H₂O₂, both at 0.1 and 0.2 mM ($p < 0.001$). A similar decrease in the number of cells was observed in the S phase ($p < 0.001$). In addition, we demonstrated cell arrest in the G2/M phase by pre-incubation of HL-60 cells with complexes 1–3 and incubation with 0.2 mM H₂O₂.

HL-60 cells that were pre-incubated with RuCl₃ or succinimide and then incubated with H₂O₂ showed similar changes in the course of the cell cycle as the cells pre-incubated with ruthenium complexes 1–3 (Table 1).

Table 1. Cell cycle distribution measured by flow cytometry using a staining with propidium iodide in HL-60 cells pre-incubated for 24 h at 37 °C with ruthenium complexes 1–3 at 50 µM and then incubated with H₂O₂ at 0.1 and 0.2 mM for 24 h at 37 °C. The cells incubated with 100 ng/mL nocodazole (NOC) for 24 h at 37 °C were the positive control.

Treatment	DNA Content %			
	Sub-G1	G0/G1	S	G2/M
negative control	1.19 ± 0.14	35.38 ± 1.64	25.66 ± 0.11	37.21 ± 1.72
positive control (NOC 100 ng/mL)	9.93 ± 2.46 ***↑	22.36 ± 6.91 *↓	21.09 ± 3.53	47.8 ± 4.22 *↑
0.1 mM H ₂ O ₂	10.39 ± 0.37 ***↑	11.27 ± 0.88 ***↓	32.73 ± 1.27 ***↑	44.79 ± 0.42 ***↑
0.2 mM H ₂ O ₂	19.83 ± 0.76 ***↑	27.43 ± 0.62 **↓	23.82 ± 2.54	28.84 ± 2.38 **↓
RuCl ₃	2.02 ± 0.43	35.28 ± 2.03	29.87 ± 0.17	32.5 ± 2.42
RuCl ₃ + 0.1 mM H ₂ O ₂	4.73 ± 0.55 ###↓	39.25 ± 0.4 ###↑	26.12 ± 0.35 ###↓	30.02 ± 0.79 ###↓
RuCl ₃ + 0.2 mM H ₂ O ₂	14.01 ± 0.98 ##↓	29.15 ± 1.48	11.6 ± 0.31 ###↓	45.37 ± 1.28 ###↑
succinimide	2.31 ± 0.33	44.42 ± 3.01 *↑	28.48 ± 2.02	24.17 ± 1.63 ***↓
succinimide + 0.1 mM H ₂ O ₂	2.07 ± 0.86 ###↓	41.95 ± 3.29 ###↑	22.63 ± 3.7 ###↓	33.17 ± 1.92 ###↓
succinimide + 0.2 mM H ₂ O ₂	5.12 ± 0.84 ###↓	27.34 ± 2.58	10.76 ± 0.15 ###↓	56.63 ± 1.66 ###↑
complex 1	1.76 ± 0.13	48.81 ± 3.48 **↑	27.59 ± 3.97	21.48 ± 1.00 ***↓
complex 1 + 0.1 mM H ₂ O ₂	2.22 ± 0.36 ###↓	41.71 ± 1.21 ###↑	20.29 ± 2.95 ###↓	35.32 ± 1.31 ###↓
complex 1 + 0.2 mM H ₂ O ₂	5.34 ± 1.42 ###↓	29.82 ± 3.78	9.72 ± 0.29 ###↓	54.96 ± 2.42 ###↑
complex 2	1.69 ± 0.13	49.3 ± 3.58 **↑	26.85 ± 3.54	21.24 ± 0.29 ***↓
complex 2 + 0.1 mM H ₂ O ₂	2.5 ± 0.56 ###↓	40.92 ± 1.8 ###↑	20.59 ± 2.28 ###↓	35.59 ± 0.53 ###↓
complex 2 + 0.2 mM H ₂ O ₂	6.64 ± 1.05 ###↓	27.92 ± 0.87	11.3 ± 0.62 ###↓	54.24 ± 0.92 ###↑
complex 3	1.76 ± 0.17	51.4 ± 0.78 ***↑	25.21 ± 0.66	21.65 ± 0.38 ***↓
complex 3 + 0.1 mM H ₂ O ₂	2.25 ± 0.15 ###↓	43.67 ± 1.54 ###↑	18.11 ± 1.76 ###↓	35.86 ± 1.68 ###↓
complex 3 + 0.2 mM H ₂ O ₂	4.95 ± 1.23 ###↓	29.35 ± 4.14	9.5 ± 1.06 ###↓	56.07 ± 2.53 ###↑

The table shows mean results ± SD, $n = 3$; * $p < 0.05$, ** $p < 0.01$, *** $p < 0.001$ vs. negative control. ## $p < 0.01$, ### $p < 0.001$ vs. 0.1 or 0.2 mM H₂O₂.

3.3. DNA Oxidative Damage

We induced DNA oxidative damage in PBMCs and HL-60 cells using H₂O₂ at two concentrations of 0.025 and 0.05 mM. Then we investigated the influence of pre-incubation with ruthenium complexes 1–3 on oxidative DNA damage (Figure 3). In the PBMCs we observed a statistically significant decrease in oxidative DNA damage for complex 1 ($p < 0.001$) and complex 2 ($p < 0.05$), but only in the case of incubation with H₂O₂ at 0.05 mM (Figure 3). After incubation of the PBMCs with H₂O₂ at a lower concentration of 0.025 mM, we did not observe any of the complexes influencing the level of DNA oxidative damage.

In the case of the pre-incubation of the PBMCs with both RuCl_3 and succinimide, we did not detect changes in the level of DNA oxidative damage induced by H_2O_2 ($p > 0.05$).

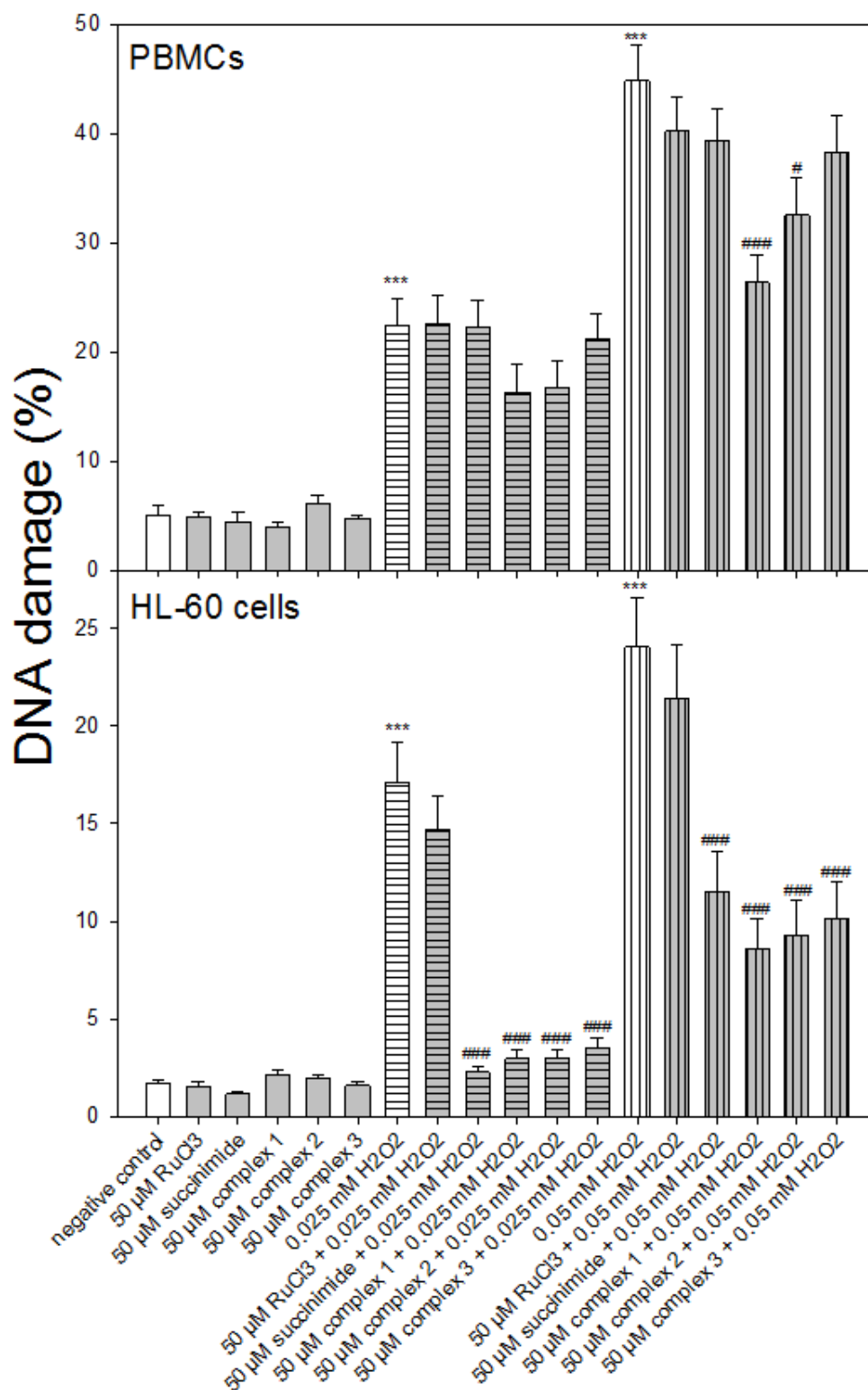


Figure 3. Effect of ruthenium complexes 1–3 at 50 μM on H_2O_2 -induced DNA damage in PBMCs and HL-60. The figures show mean results \pm SEM, $n = 100$; *** $p < 0.001$ vs. negative control; # $p < 0.05$, ### $p < 0.001$ vs. H_2O_2 .

In the experiment with HL-60 cells, we detected a significant decrease in oxidative DNA damage induced by H₂O₂ at 0.025 and 0.05 mM for all ruthenium complexes ($p < 0.001$) (Figure 3). We showed a similar effect—reduction of DNA damage in the cells pre-incubated with succinimide and then incubated with H₂O₂ at both 0.025 and 0.05 mM concentrations. In the HL-60 cells that were pre-incubated with RuCl₃, we did not indicate any change in the oxidative DNA damage level ($p > 0.05$).

3.4. Reactive Oxygen Species Level

We used an H₂DCF-DA probe to determine the effect of ruthenium complexes 1–3 on reactive oxygen species (ROS) induced by H₂O₂ at concentrations of 1 and 5 mM (Figure 4). In the case of PBMCs, we observed a decrease ($p < 0.001$) in the level of ROS for complexes 1 and 2 and 1 mM H₂O₂ (Figure 4). In contrast, complex 3 increased the level of H₂O₂ induced ROS ($p < 0.001$). A similar effect to the one found in complex 3 was observed in the PBMCs pre-incubated with succinimide and then incubated with 5 mM H₂O₂ ($p < 0.001$). Complex 2 has the greatest potential to scavenge ROS in normal cells; it also reduced endogenous ROS levels ($p < 0.001$).

In HL-60 cells, we clearly showed a significant reduction ($p < 0.001$) in ROS levels by all ruthenium complexes (Figure 4). We also observed a similar effect in the HL-60 cells pre-incubated with succinimide and then incubated with H₂O₂ at 1 mM ($p < 0.001$) and 5 mM ($p < 0.01$). All ruthenium complexes and succinimide significantly reduced endogenous ROS levels in contrast to RuCl₃.

3.5. SOD Activity

In this experiment, we investigated the influence of ruthenium complexes on SOD activity under oxidative stress conditions (Figure 5). First, of all, we observed a decrease in SOD activity ($p < 0.001$) after the incubation of PBMCs (Figure 4) and HL-60 cells (Figure 5) with H₂O₂, which corresponds with the results of other research [25,26]. It should be emphasized that in the case of the incubation of HL-60 cells with 0.1 mM H₂O₂, we observed a decrease in SOD activity to 50%, whereas in the case of PBMCs the SOD activity decreased only to a level of about 93% after the use of 0.25 mM H₂O₂. Further increasing the concentration of H₂O₂ to 0.6 mM did not cause any further inhibition of SOD activity in these cells (data not shown).

Our studies clearly showed that all ruthenium complexes increased SOD activity ($p < 0.001$) in HL-60 cells treated with H₂O₂ (Figure 5). We observed a similar effect after the pre-incubation of these cells with succinimide ($p < 0.001$). In the case of HL-60 cells pre-incubated with 50 μM RuCl₃, we did not detect any changes in SOD activity compared to the cells that were not pre-incubated with RuCl₃. In the case of PBMCs, we observed an increase in SOD activity ($p < 0.001$) after pre-incubation with complexes 1 and 2. Complex 3 as well as RuCl₃ and succinimide did not increase SOD activity ($p > 0.05$) (Figure 5).

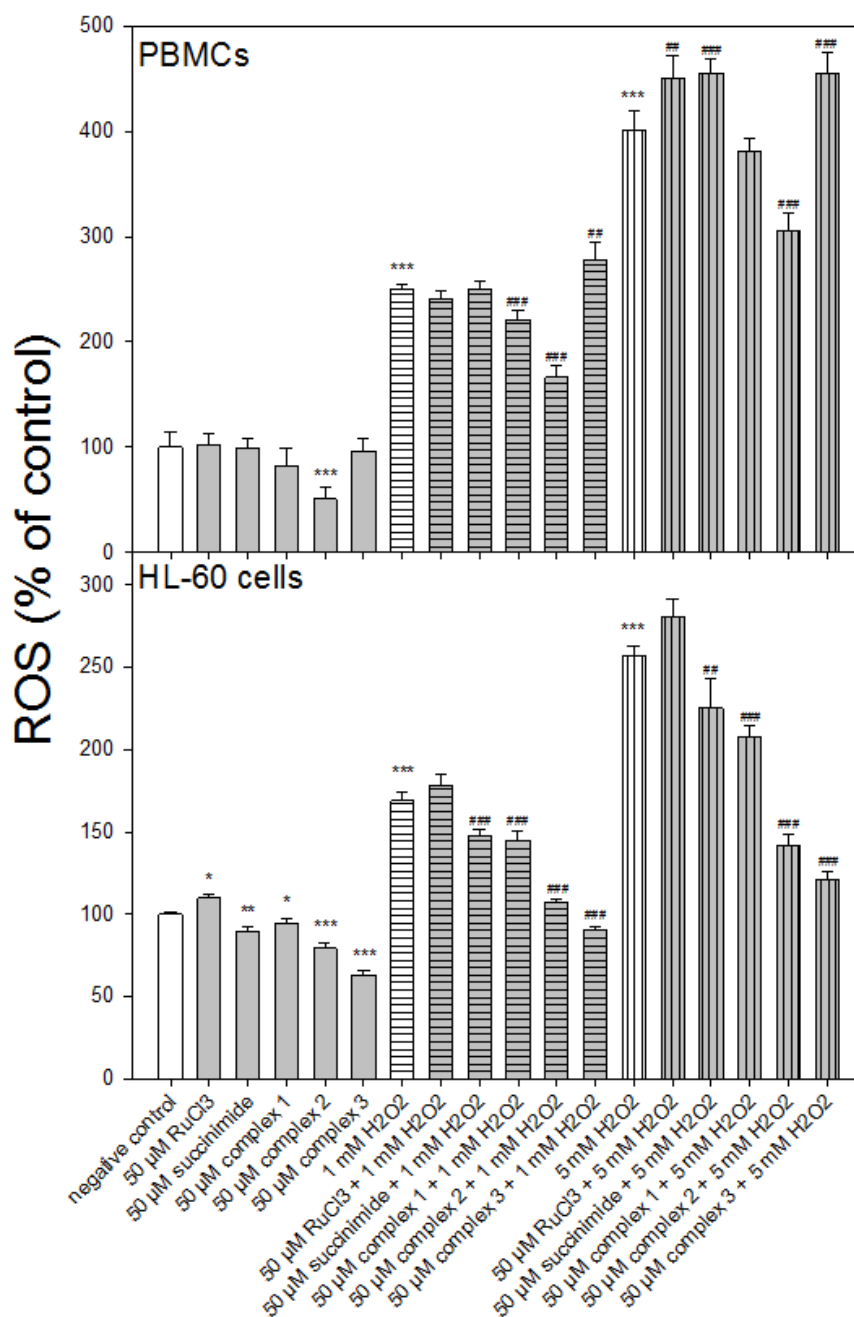


Figure 4. Changes in reactive oxygen species (ROS) level in PBMCs and HL-60 cells pre-incubated with ruthenium complexes 1–3 at 50 μ M for 24 h at 37 $^{\circ}$ C and then incubated with 1 mM or 5 mM H₂O₂ at 37 $^{\circ}$ C. Each value represents the mean \pm SD, $n = 6$; * $p < 0.05$, ** $p < 0.01$, *** $p < 0.001$ vs. negative control; ## $p < 0.01$, ### $p < 0.001$ vs. H₂O₂.

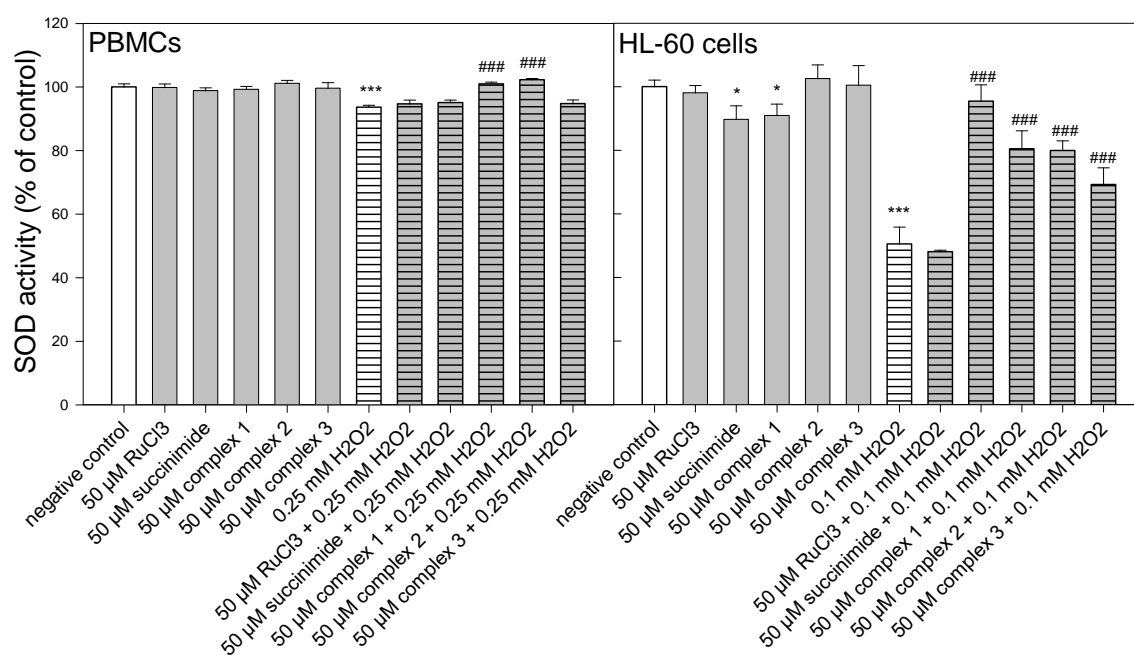


Figure 5. Superoxide dismutase activity in PBMCs and HL-60 cells pre-incubated for 24 h at 37 °C with ruthenium complexes 1–3 at 50 μM and then incubated with H₂O₂ at 0.25 mM in the case of PBMCs and 0.1 mM in the case of HL-60 cells. The figure shows the mean results ± SD, *n* = 3; * *p* < 0.05, and *** *p* < 0.001 vs. negative control; ### *p* < 0.001 vs. H₂O₂. Data were normalized to the negative control, which was assigned as 100% of the SOD activity.

4. Discussion

Here, we investigated the antioxidant activity of three ruthenium complexes with succinimidato and phthalimidato ligands against normal PBMCs and HL-60 leukemic cells. For this purpose, we used 24 h pre-incubation of cells with the complexes and then induced oxidative stress by incubating cells with H₂O₂. A correlation and gene ontology pathway analysis identified a rigid association with genes intertwined in cell cycle progression and proliferation after cell incubation with H₂O₂ [23]. The ten most substantially correlating genes were validated using qPCR, showing complete congruency with the microarray analysis findings. Western blotting confirmed the correlation of cell cycle-related proteins negatively correlating with H₂O₂ IC₂₅. It was also shown that the top genes related to ROS production or antioxidant defense were only in modest correlation [27]. The intracellular concentration of H₂O₂ is regulated tightly, enabling its use as a cellular signaling molecule while minimizing its potential to cause cellular damage [28]. A high concentration of H₂O₂ induces necrosis and a low concentration induces apoptosis. In HL-60 cells H₂O₂-induced apoptosis is regulated by decreased BCL-2 [29]. Moreover, it was shown that H₂O₂ evoked apoptotic events through the increase of Ca²⁺ in HL-60 cells, inducing caspase -9 and -3 activation, induction of the mitochondrial permeability transition pore (mPTP), and activation of proapoptotic proteins [30].

We observed that H₂O₂ at a concentration range between 0.2 and 0.6 mM reduced the viability of normal and cancer cells (Figure 2). In addition, we observed the cell cycle arrest of HL-60 cells in the phase sub-G1 after incubation with H₂O₂ at a concentration of 0.1 and 0.2 mM (Table 1). Our results are in line with the results previously reported on the effects of H₂O₂ on the HL-60 cell cycle [30]. The arrest of cells in the sub-G1 phase may indicate apoptosis under the influence of H₂O₂. This is confirmed by our results on cell viability after incubation with H₂O₂. For both PBMCs and HL-60 cells, we observed a significant reduction in their viability. The pre-incubation of both normal and cancer cells with ruthenium complexes 1–3 increases their viability (Figure 2) and releases cells from the sub-G1 phase (Table 1).

Hydrogen peroxide, by producing hydroxyl radicals (OH^\bullet) through the interaction with metal ions near DNA, induces DNA damage such as modified bases, apurinic/aprimidinic (AP) sites, and single-strand breaks (SSBs). The addition of OH^\bullet at position C8 within the guanine ring generates the oxidative product, 8-oxo-7,8-dihydro-2'-deoxyguanosine (8-oxodG). Similarly, the addition of OH^\bullet at position C8 of deoxyadenosine generates the oxidative product 8-oxo-7,8-dihydro-2'-deoxyadenosine (8-oxodA). These radicals are capable of further reduction or oxidation forming 2,6-diamino-4-hydroxy-5-formamidopyrimidine (FapyGua) or 8-oxo-7,8-dihydroguanine (8-oxoG), in deoxyguanosine or 4,6-diamino-5-formamidopyrimidine (FapyA) or 7,8-dihydro-8-oxoadenine (8-oxoA) in deoxyadenosine. Another prevalent oxidative product is thymine glycol, produced by the insertion of OH^\bullet at position C5 of the thymine rings. Similarly, another oxidation product of cytosine is cytosine glycol, which upon deamination leads to the formation of uracil glycol [31].

Here, we observed a statistically significant decrease in oxidative DNA damage in PBMCs for ruthenium complex **1** ($p < 0.001$) and ruthenium complex **2** ($p < 0.05$) (Figure 3). In the case of HL-60 cells, we noticed a significant decrease in oxidative DNA damage for all ruthenium complexes ($p < 0.001$) (Figure 3). Previously, we detected a protective effect on H_2O_2 -induced oxidative DNA damage by tricarbonyldichlororuthenium (II) dimer (CORM-2) and the CO-depleted molecule (iCORM-2) [32]. This may indicate that not only the released CO but also the iCORM-2, to which new ligands attach, have antioxidant properties. Here, we also observed that ruthenium complexes reduced the level of ROS induced by H_2O_2 in both types of cells (Figure 4). We used the fluorogenic 2',7'-dichlorodihydrofluorescein-diacetate (H_2DCFDA) probe to detect ROS. The acetate groups on H_2DCF allow for diffusion across the plasma membrane, after which both groups are cleaved by intracellular esterases to form H_2DCF . H_2DCF is reactive toward many types of oxidants, including nitrogen dioxide ($\bullet\text{NO}_2$), the carbonate radical anion ($\text{CO}_3^{\bullet-}$), the hydroxyl radical (OH^\bullet), Fe^{2+} , Cu^+ , thiyl radicals (e.g., the glutathione radical; GS^\bullet), and peroxidases (e.g., cytochrome c peroxidase) [33,34]. Importantly, none of the studied ruthenium complexes induced oxidative stress (Figure 4).

Superoxide dismutases (SODs) including MnSOD, Cu/Zn-SOD, and extracellular SOD along with catalase are composed as the first line of defense against ROS. Some studies also showed that oxidative stress downregulated MnSOD in several oxidative stress models induced by H_2O_2 and other oxidants. The oxidative stress-induced downregulation of MnSOD activity causes superoxide radical accumulation and superoxide can be converted to OH^\bullet in the presence of transition metals (e.g., Fenton reaction) [26]. Research carried out by Gottfredsen et al. [31] showed that *hsEC*-SOD is inhibited and fragmented by H_2O_2 . The enzyme was inhibited by H_2O_2 (37 °C, 1 h) in a dose-dependent manner, with an IC_{50} value of 0.8 mM and complete inhibition at ~2 mM. The mechanism of inhibition was similar to that of bovine Cu,Zn-SOD, including the oxidation of proline (Pro 112) and histidine (His 98, His 163) residues proximal to the active site Cu [35,36].

We detected that all ruthenium complexes increased SOD activity ($p < 0.001$) in HL-60 cells treated with H_2O_2 (Figure 5). We observed a similar effect after the pre-incubation of these cells with succinimide ($p < 0.001$). In the case of PBMCs, we observed an increase in SOD activity ($p < 0.001$), decreased by H_2O_2 , after pre-incubation with complexes **1** and **2** (Figure 5). We showed that ruthenium complexes **1** and **2** reversed the H_2O_2 -induced downregulation of SOD to normal levels in PBMCs. We assume that ruthenium complexes are responsible for the restoration of SOD activity in the case of PBMCs and its increase in HL-60 cells due to their ROS scavenging capacity. The numerous studies mentioned in the Introduction have shown that various ruthenium complexes synthesized in recent years have the ability to scavenge ROS and RNS [6–11,16].

Our results show that ruthenium complexes **1–3** bearing succinimidato and phthalimidato ligands at a low concentration of 50 μM protect cells against oxidative stress and do not exhibit cytotoxic activity. Here, we have experimentally confirmed our previous theoretical calculation results on the electronic structure of ruthenium complexes bearing different imidato ligands. We showed that in the case of maleimide, the HOMO-LUMO

(highest occupied molecular orbital and lowest unoccupied molecular orbital) energy gap was lower by 1.36 eV when compared with succinimide [5]. Therefore, we suppose that the antioxidant properties of ruthenium complexes, which we studied here, may be due to the high HOMO-LUMO energy gap. Our current comparative studies of ruthenium complexes bearing succimidato ligands with succinimide, and RuCl₃ indicate that the succinimide ligand, rather than the ruthenium metal center, is responsible for the antioxidant activity of complexes 1–3. We plan to undertake further electrochemical investigations of succinimide and complexes 1–3 to shed some light on this problem. Taking into account the fact that oxidative stress is involved in many human diseases, including cancer, antioxidant treatment involving new molecules that exhibit antioxidant properties in biological systems could be of potential interest from a clinical point of view.

Author Contributions: Conceptualization, M.J., B.R. and K.W.; methodology, M.J., M.K. and A.K.; investigation, M.J., M.K. and A.K.; writing—original draft preparation, M.J. and K.W.; writing—review and editing, B.R. and K.W.; visualization, M.J.; supervision, B.R. and K.W. All authors have read and agreed to the published version of the manuscript.

Funding: This research received no external funding.

Institutional Review Board Statement: The study was approved by the Committee for Research on Human Subjects of the University of Lodz (17/KBBN-UŁ/III/2019).

Informed Consent Statement: Informed consent was obtained from all subjects involved in the study.

Data Availability Statement: Data on reported results are deposited with the authors.

Acknowledgments: The authors gratefully acknowledge the University of Lodz, Poland, the Faculty of Chemistry, and the Faculty of Biology and Environmental Protection for financial support.

Conflicts of Interest: All authors declare that they have no conflicts of interest.

Sample Availability: Samples of the compounds (η^5 -cyclopentadienyl)Ru(CO)₂-*N*-methoxysuccinimidato (1), (η^5 -cyclopentadienyl)Ru(CO)₂-*N*-ethoxysuccinimidato (2), and (η^5 -cyclopentadienyl)Ru(CO)₂-*N*-phthalimidato (3) are available from the authors.

References

1. Singh, A.; Barman, P. Recent Advances in Schiff Base Ruthenium Metal Complexes: Synthesis and Applications. *Top. Curr. Chem.* **2021**, *379*, 29. [[CrossRef](#)] [[PubMed](#)]
2. Kacsir, I.; Sipos, A.; Ujlaki, G.; Buglyó, P.; Somsák, L.; Bai, P.; Bokor, É. Ruthenium Half-Sandwich Type Complexes with Bidentate Monosaccharide Ligands Show Antineoplastic Activity in Ovarian Cancer Cell Models through Reactive Oxygen Species Production. *Int. J. Mol. Sci.* **2021**, *22*, 10454. [[CrossRef](#)]
3. Mahmud, K.M.; Niloy, M.S.; Shakil, M.S.; Islam, M.A. Ruthenium Complexes: An Alternative to Platinum Drugs in Colorectal Cancer Treatment. *Pharmaceutics* **2021**, *13*, 1295. [[CrossRef](#)] [[PubMed](#)]
4. Sun, Q.; Li, Y.; Shi, H.; Wang, Y.; Zhang, J.; Zhang, Q. Ruthenium Complexes as Promising Candidates against Lung Cancer. *Molecules* **2021**, *26*, 4389. [[CrossRef](#)] [[PubMed](#)]
5. Juszczak, M.; Kluska, M.; Kosińska, A.; Palusiak, M.; Rybarczyk-Pirek, A.J.; Wzgarda-Raj, K.; Rudolf, B.; Woźniak, K. Cytotoxicity of piano-stool ruthenium cyclopentadienyl complexes bearing different imidato ligands. *Appl. Organomet. Chem.* **2022**, *36*, e6595. [[CrossRef](#)]
6. Mu, C.; Prosser, K.E.; Harrypersad, S.; MacNeil, G.A.; Panchmatia, R.; Thompson, J.R.; Sinha, S.; Warren, J.J.; Walsby, C.J. Activation by Oxidation: Ferrocene-Functionalized Ru(II)-Arene Complexes with Anticancer, Antibacterial, and Antioxidant Properties. *Inorg. Chem.* **2018**, *57*, 15247–15261. [[CrossRef](#)]
7. Buldurun, K.; Turan, N.; Aras, A.; Mantarçı, A.; Turkan, F.; Bursal, E. Spectroscopic and Structural Characterization, Enzyme Inhibitions, and Antioxidant Effects of New Ru(II) and Ni(II) Complexes of Schiff Base. *Chem. Biodivers.* **2019**, *16*, e1900243. [[CrossRef](#)]
8. Mohankumar, A.; Devagi, G.; Shanmugam, G.; Nivitha, S.; Sundararaj, P.; Dallemer, F.; Kalaivani, P.; Prabhakaran, R. Organoruthenium(II) complexes attenuate stress in *Caenorhabditis elegans* through regulating antioxidant machinery. *Eur. J. Med. Chem.* **2019**, *168*, 123–133. [[CrossRef](#)]
9. Sasahara, G.L.; Gouveia Júnior, F.S.; Rodrigues, R.O.; Zampieri, D.S.; Fonseca, S.; Gonçalves, R.C.R.; Athaydes, B.R.; Kitagawa, R.R.; Santos, F.A.; Sousa, E.H.S.; et al. Nitro-imidazole-based ruthenium complexes with antioxidant and anti-inflammatory activities. *J. Inorg. Biochem.* **2020**, *206*, 111048. [[CrossRef](#)]











10. Nehru, S.; Veeralakshmi, S.; Kalaiselvam, S.; Subin David, S.P.; Sandhya, J.; Arunachalam, S. Protein binding and antioxidant studies of diimine based emissive surfactant-ruthenium(II) complexes. *J. Biomol. Struct. Dyn.* **2021**, *39*, 1535–1546. [[CrossRef](#)]
11. Maikoo, S.; Chakraborty, A.; Vukea, N.; Dingle, L.M.K.; Samson, W.J.; de la Mare, J.A.; Edkins, A.L.; Booyesen, I.N. Ruthenium complexes with mono- or bis-heterocyclic chelates: DNA/BSA binding, antioxidant and anticancer studies. *J. Biomol. Struct. Dyn.* **2021**, *39*, 4077–4088. [[CrossRef](#)] [[PubMed](#)]
12. Elsayed, S.A.; Badr, H.E.; di Biase, A.; El-Hendawy, A.M. Synthesis, characterization of ruthenium(II), nickel(II), palladium(II), and platinum(II) triphenylphosphine-based complexes bearing an ONS-donor chelating agent: Interaction with biomolecules, antioxidant, in vitro cytotoxic, apoptotic activity and cell cycle analysis. *J. Inorg. Biochem.* **2021**, *223*, 111549. [[CrossRef](#)] [[PubMed](#)]
13. Santos, N.E.; Braga, S.S. Redesigning Nature: Ruthenium Flavonoid Complexes with Antitumour, Antimicrobial and Cardioprotective Activities. *Molecules* **2021**, *26*, 4544. [[CrossRef](#)] [[PubMed](#)]
14. Cuccioloni, M.; Bonfili, L.; Mozzicafreddo, M.; Cecarini, V.; Pettinari, R.; Condello, F.; Pettinari, C.; Marchetti, F.; Angeletti, M.; Eleuteri, A.M. A ruthenium derivative of quercetin with enhanced cholesterol-lowering activity. *RSC Adv.* **2016**, *6*, 39636–39641. [[CrossRef](#)]
15. Ravishankar, D.; Salamah, M.; Attina, A.; Pothi, R.; Vallance, T.M.; Javed, M.; Williams, H.F.; Alzahrani, E.M.S.; Kabova, E.; Vaiyapuri, R.; et al. Ruthenium-conjugated chrysin analogues modulate platelet activity, thrombus formation and haemostasis with enhanced efficacy. *Sci. Rep.* **2017**, *7*, 5738. [[CrossRef](#)]
16. Mabuza, L.P.; Gamede, M.W.; Maikoo, S.; Booyesen, I.N.; Ngubane, P.S.; Khathi, A. Cardioprotective effects of a ruthenium (II) Schiff base complex in diet-induced prediabetic rats. *Diabetes Metab. Syndr. Obes.* **2019**, *12*, 217–223. [[CrossRef](#)]
17. Sadiq, A.; Mahmood, F.; Ullah, F.; Ayaz, M.; Ahmad, S.; Haq, F.U.; Khan, G.; Jan, M.S. Synthesis, anticholinesterase and antioxidant potentials of ketoesters derivatives of succinimides: A possible role in the management of Alzheimer's. *Chem. Cent. J.* **2015**, *9*, 31. [[CrossRef](#)] [[PubMed](#)]
18. Hussain, F.; Khan, Z.; Jan, M.S.; Ahmad, S.; Ahmad, A.; Rashid, U.; Ullah, F.; Ayaz, M.; Sadiq, A. Synthesis, in-vitro α -glucosidase inhibition, antioxidant, in-vivo antidiabetic and molecular docking studies of pyrrolidine-2,5-dione and thiazolidine-2,4-dione derivatives. *Bioorg. Chem.* **2019**, *91*, 103128. [[CrossRef](#)]
19. Ahmad, A.; Ullah, F.; Sadiq, A.; Ayaz, M.; Saeed Jan, M.; Shahid, M.; Wadood, A.; Mahmood, F.; Rashid, U.; Ullah, R.; et al. Comparative Cholinesterase, α -Glucosidase Inhibitory, Antioxidant, Molecular Docking, and Kinetic Studies on Potent Succinimide Derivatives. *Drug Des. Dev. Ther.* **2020**, *14*, 2165–2178. [[CrossRef](#)]
20. Waheed, B.; Mukarram Shah, S.M.; Hussain, F.; Khan, M.I.; Zeb, A.; Jan, M.S. Synthesis, Antioxidant, and Antidiabetic Activities of Ketone Derivatives of Succinimide. *Evid. Based Complement. Altern. Med.* **2022**, *2022*, 1445604. [[CrossRef](#)]
21. Kubicka, A.; Fomal, E.; Olejniczak, A.B.; Rybarczyk-Pirek, A.J.; Wojtulewski, S.; Rudolf, B. Oxa-Michael reaction of metallocarbonyl complexes bearing the maleimidato ligand. Reactivity studies with selected hydroxy compounds. *Polyhedron* **2016**, *107*, 38–47. [[CrossRef](#)]
22. Kosińska, A.; Wojtulewski, S.; Palusiak, M.; Tokarz, P.; Rudolf, B. A Useful Synthetic Route to N-Nonsubstituted Succinimides via Light-Induced Degradation of Metallocarbonyl Complexes. *Organometallics* **2021**, *40*, 663–673. [[CrossRef](#)]
23. O'Brien, J.; Wilson, I.; Orton, T.; Pognan, F. Investigation of the Alamar Blue (resazurin) fluorescent dye for the assessment of mammalian cell cytotoxicity. *Eur. J. Biochem.* **2000**, *267*, 5421–5426. [[CrossRef](#)] [[PubMed](#)]
24. Tokarz, P.; Piastowska-Ciesielska, A.W.; Kaarniranta, K.; Blasiak, J. All-Trans Retinoic Acid Modulates DNA Damage Response and the Expression of the VEGF-A and MKI67 Genes in ARPE-19 Cells Subjected to Oxidative Stress. *Int. J. Mol. Sci.* **2016**, *17*, 898. [[CrossRef](#)] [[PubMed](#)]
25. Sampson, J.B.; Beckman, J.S. Hydrogen peroxide damages the zinc-binding site of zinc-deficient Cu,Zn superoxide dismutase. *Arch Biochem. Biophys.* **2001**, *392*, 8–13. [[CrossRef](#)]
26. Emamgholipour, S.; Hossein-Nezhad, A.; Ansari, M. Can Melatonin Act as an Antioxidant in Hydrogen Peroxide-Induced Oxidative Stress Model in Human Peripheral Blood Mononuclear Cells? *Biochem. Res. Int.* **2016**, *2016*, 5857940. [[CrossRef](#)]
27. Bekeschus, S.; Liebelt, G.; Menz, J.; Singer, D.; Wende, K.; Schmidt, A. Cell cycle-related genes associate with sensitivity to hydrogen peroxide-induced toxicity. *Redox Biol.* **2022**, *50*, 102234. [[CrossRef](#)]
28. Heo, S.; Kim, S.; Kang, D. The Role of Hydrogen Peroxide and Peroxiredoxins throughout the Cell Cycle. *Antioxidants* **2020**, *9*, 280. [[CrossRef](#)]
29. Lee, J.E.; Sohn, J.; Lee, J.H.; Lee, K.C.; Son, C.S.; Tockgo, Y.C. Regulation of bcl-2 family in hydrogen peroxide-induced apoptosis in human leukemia HL-60 cells. *Exp. Mol. Med.* **2000**, *32*, 42–46. [[CrossRef](#)]
30. Bejarano, I.; Espino, J.; González-Flores, D.; Casado, J.G.; Redondo, P.C.; Rosado, J.A.; Barriga, C.; Pariente, J.A.; Rodríguez, A.B. Role of Calcium Signals on Hydrogen Peroxide-Induced Apoptosis in Human Myeloid HL-60 Cells. *Int. J. Biomed. Sci. IJBS* **2009**, *5*, 246–256.
31. Barnes, J.L.; Zubair, M.; John, K.; Poirier, M.C.; Martin, F.L. Carcinogens and DNA damage. *Biochem. Soc. Trans.* **2018**, *46*, 1213–1224. [[CrossRef](#)] [[PubMed](#)]
32. Juszcak, M.; Kluska, M.; Wysokiński, D.; Woźniak, K. DNA damage and antioxidant properties of CORM-2 in normal and cancer cells. *Sci. Rep.* **2020**, *10*, 12200. [[CrossRef](#)] [[PubMed](#)]
33. Wrona, M.; Patel, K.; Wardman, P. Reactivity of 2',7'-dichlorodihydrofluorescein and dihydrorhodamine 123 and their oxidized forms toward carbonate, nitrogen dioxide, and hydroxyl radicals. *Free Radic. Biol. Med.* **2005**, *38*, 262–270. [[CrossRef](#)]

34. Reiniers, M.J.; de Haan, L.R.; Reeskamp, L.F.; Broekgaarden, M.; van Golen, R.F.; Heger, M. Analysis and Optimization of Conditions for the Use of 2',7'-Dichlorofluorescein Diacetate in Cultured Hepatocytes. *Antioxidants* **2021**, *10*, 674. [[CrossRef](#)] [[PubMed](#)]
35. Gottfredsen, R.H.; Larsen, U.G.; Enghild, J.J.; Petersen, S.V. Hydrogen peroxide induce modifications of human extracellular superoxide dismutase that results in enzyme inhibition. *Redox Biol.* **2013**, *1*, 24–31. [[CrossRef](#)]
36. Lewandowski, L.; Kepinska, M.; Milnerowicz, H. Inhibition of copper-zinc superoxide dismutase activity by selected environmental xenobiotics. *Environ. Toxicol. Pharmacol.* **2018**, *58*, 105–113. [[CrossRef](#)]



Cite this: DOI: 10.1039/d2dt04083b

Piano-stool ruthenium(II) complexes with maleimide and phosphine or phosphite ligands: synthesis and activity against normal and cancer cells†

Michał Juszczak, ^a Sujoy Das, ^b Aneta Kosińska, ^b
Agnieszka J. Rybarczyk-Pirek, ^c Kinga Wzgarda-Raj, ^c Paulina Tokarz, ^a
Saranya Vasudevan, ^d Arkadiusz Chworos, ^d Katarzyna Woźniak ^{*a} and
Bogna Rudolf ^{*b}

In these studies, we designed and investigated cyto- and genotoxic potential of five ruthenium cyclopentadienyl complexes bearing different phosphine and phosphite ligands. All of the complexes were characterized with spectroscopic analysis (NMR, FT-IR, ESI-MS, UV-vis, fluorescence and XRD (for two compounds)). For biological studies, we used three types of cells – normal peripheral blood mononuclear (PBM) cells, leukemic HL-60 cells and doxorubicin-resistance HL-60 cells (HL-60/DR). We compared the results obtained with those obtained for the complex with maleimide ligand CpRu(CO)₂(η¹-N-maleimidato) **1**, which we had previously reported. We observed that the complexes CpRu(CO)(PPh₃)(η¹-N-maleimidato) **2a** and CpRu(CO)(P(OEt)₃)(η¹-N-maleimidato) **3a** were the most cytotoxic for HL-60 cells and non-cytotoxic for normal PBM cells. However, complex **1** was more cytotoxic for HL-60 cells than complexes **2a** and **3a** (IC₅₀ = 6.39 μM vs. IC₅₀ = 21.48 μM and IC₅₀ = 12.25 μM, respectively). The complex CpRu(CO)(P(OPh)₃)(η¹-N-maleimidato) **3b** is the most cytotoxic for HL-60/DR cells (IC₅₀ = 104.35 μM). We found the genotoxic potential of complexes **2a** and **3a** only in HL-60 cells. These complexes also induced apoptosis in HL-60 cells. Docking studies showed that complexes **2a** and CpRu(CO)(P(Fu)₃)(η¹-N-maleimidato) **2b** have a small ability to degrade DNA, but they may cause a defect in DNA damage repair mechanisms leading to cell death. This hypothesis is corroborated with the results obtained in the plasmid relaxation assay in which ruthenium complexes bearing phosphine and phosphite ligands induce DNA breaks.

Received 21st December 2022,
Accepted 15th February 2023

DOI: 10.1039/d2dt04083b

rsc.li/dalton

Introduction

In 1989, with discovery of NKP-1339 (sodium *trans*-[tetrachlorido-bis(indazole)Ru(III)] and KP1019 (indazolium *trans*-[tetrachlorido-bis(indazole)Ru(III)]), a new class of metal-based anti-cancer drugs were unveiled to the world – ruthenium organic complexes,^{1,2} in

the following years two other compounds were invented with promising anti-metastatic properties; NAMI-A (imidazoliumtrans-[tetrachlorido(dimethyl sulfoxide)(imidazole)Ru(III)] and TLD1443 ([Ru(4,4'-dimethyl-2,2'-bipyridine)2(2-(2',2'':5'',2'''-terthiophene)-imidazo[4,5-f][1,10]phenanthroline)]Cl₂).³⁻⁵ These are the compounds which have proudly completed the Phase-I clinical trial and are knocking on the door for Phase-II.⁶

Drug resistance of cancer cells is one of the major challenges of cancer therapy. Anti-cancer drug resistance can arise from a multitude of mechanisms like impaired drug uptake into the cancer cell, enhanced drug efflux, altered drug target, changed damage recognition/enhanced DNA repair, impaired induction of apoptosis as well as drug sequestration away from its target. Moreover, the entire composition of the tumor microenvironment (TME), containing multiple cell types such as fibroblasts or immune cells, has a strong impact on therapy success and failure.⁶

In recent years, several ruthenium complexes with anti-cancer activity against cisplatin-resistant cells have been

^aUniversity of Lodz, Faculty of Biology and Environmental Protection, Department of Molecular Genetics, Pomorska 141/143, 90-236 Lodz, Poland.

E-mail: katarzyna.wozniak@biol.uni.lodz.pl

^bUniversity of Lodz, Faculty of Chemistry, Department of Organic Chemistry, Tamka 12, 91-403 Lodz, Poland. E-mail: bogna.rudolf@chemia.uni.lodz.pl

^cUniversity of Lodz, Faculty of Chemistry, Department of Physical Chemistry, Pomorska 163/165, 90-236 Lodz, Poland

^dCentre of Molecular and Macromolecular Studies, Polish Academy of Sciences, Sienkiewicza 112, 90-363 Lodz, Poland

† Electronic supplementary information (ESI) available: Comparison table, ¹H NMR, ¹³C NMR, and MS spectra, crystal data, cell viability and apoptosis. CCDC 2209334 2209335. For ESI and crystallographic data in CIF or other electronic format see DOI: <https://doi.org/10.1039/d2dt04083b>



synthesized.^{7–9} Some of them are also being studied to break down doxorubicin resistance.¹⁰ The anti-cancer activity of Doxorubicin (Dox), a member of the anthracycline family, is mainly exerted through the DNA intercalation and topoisomerase-II inhibition in fast-proliferating tumors. However, Dox causes cumulative and dose-dependent cardiotoxicity, which results in increased risks of mortality among cancer patients and thus limiting its wide clinical applications. Several mechanisms has been proposed for doxorubicin-induced cardiotoxicity and oxidative stress, free radical generation and apoptosis are the most widely reported. Apart from this, other mechanisms are also involved in Dox-induced cardiotoxicity such as impaired mitochondrial function, a perturbation in iron regulatory protein, disruption of Ca²⁺ homeostasis, autophagy, the release of nitric oxide and inflammatory mediators and altered gene and protein expression that involved apoptosis. Dox also causes downregulation of DNA methyltransferase 1 (DNMT1) enzyme activity which leads to a reduction in the DNA methylation process. This hypomethylation causes dysregulation in the mitochondrial genes like peroxisome proliferator-activated receptor-gamma coactivator (PGC)-1-alpha (PGC-1 α), nuclear respiratory factor 1 (NRF-1) and mitochondrial transcription factor A (TFAM) unit in the heart. Apart from DNA methylation, Dox treatment also alters the microRNAs levels and histone deacetylase (HDAC) activity.¹¹

Piano-stool ruthenium(II) complexes are becoming notable in last few decades for their structural flexibilities and bioactivities towards metastatic cells.^{12–14} They have been subdivided into types depending upon their structure–activity parameters: Ru(η^6 -arene) and Ru(η^5 -cyclopentadienyl) complexes.^{15,16} Within the first type, half-sandwich ruthenium complexes containing PTA (1,3,5-triaza-7-phosphaadamantane) ligands,^{17–19} and their functionalized derivatives (RAPTA complexes) are being widely acclaimed in anti-cancer experiments and advanced pre-clinical models.^{20,21} While, within the second type, most of the Ru(η^5 -cyclopentadienyl) half-sandwich complexes reported so far are found to be amply cytotoxic towards various human cancer cell lines like A2780CisR, MDA-MB-231, PC-3, and HT-29 *etc.*^{22,23} Their effectivity towards more than one cancer cell lines makes them potential broad-spectrum-anti-tumor agents in recent time.^{24,25}

Some recent works have reported the use of phosphine or phosphite ligands at ruthenium complexes, and most of them concerned Ru(η^6 -*p*-cymene) complexes.^{26–28} In 2011, Hanif *et al.* added phosphite moieties to sugar molecules attached to ruthenium centers in order to improve water solubility of the complexes.²⁹ Recently, Klaimanee *et al.* developed three Ru(II) *p*-cymene complexes with different organophosphorus ligands possessing anti-cancer, antibacterial and anti-fungal activities.³⁰

Most interestingly, Ribeiro *et al.* in 2019, found that the presence of triphenylphosphine significantly increases the antiproliferative potential of [RuCl(PPh₃)(N–N)]Cl complexes, which is apparently due to the capability of triphenylphosphine to intercalate between DNA base pairs. Hence, triphenylphosphine acts as a vehiculizing agent for ruthenium complexes to specific tumor cells.³¹ Li *et al.* also reported the

enhancement of anti-cancer activity with triphenylphosphine ligands in some copper complexes.³² On the other side, Küster's group reported various η^6 -areneruthenium(II) phosphite complexes for the treatment of Alveolar Echinococcosis with cytotoxicity effect on human fibroblasts, Vero cells, and rat hepatoma cells. Authors used triethyl phosphite, triphenyl phosphite and triisopropyl phosphite as ligands and observed that the complexes with triethyl phosphite and triisopropyl phosphite are the most cytotoxic towards cancer cells.³³

Recently, we have found that cyclopentadienyl ruthenium complex bearing maleimidato ligand CpRu(CO)₂(η^1 -N-maleimidato) (**1**) is highly cytotoxic and genotoxic, both for normal and cancer cells at the concentrations from 0.5 to 250 μ M.³⁴

Herein, we introduce five novel ruthenium cyclopentadienyl complexes bearing maleimide and different phosphine/phosphite ligands (**2a**, **2b**, **3a**, **3b** and **3c**) (Fig. 1), derivatized from complex **1** in UV-vis light induced CO ligand exchange process. Triphenylphosphine, tris(2-furyl)phosphine, triethyl phosphite, triphenyl phosphite and triisopropyl phosphite have been chosen for the study.

NMR (¹H, ³¹P, ¹³C), FT-IR, ESI-MS, UV-vis, fluorescence and XRD studies were executed for the characterization and structural analysis of the complexes. The cytotoxic potential of these complexes was analyzed in peripheral blood mononuclear (PBM) cells as normal cells and leukemic HL-60 cells and also doxorubicin-resistant HL-60 cells (HL-60/DR cells). It has been observed that ruthenium complexes **2a** and **3a** are highly cytotoxic for cancer HL-60 cells and non-cytotoxic for normal PBM cells. Therefore, we examined the ability of these complexes to induce DNA damage and apoptosis in cancer cells. We also used the plasmid relaxation assay and docking studies to determine the potential of ruthenium complexes to directly damage DNA.

Results and discussion

Synthesis of complexes **1**, **2a–b** and **3a–c**

Complex **1** CpRu(CO)₂(η^1 -maleimidato) was obtained in previously described photochemical reaction of CpRu(CO)₂I with maleimide in presence of diisopropylamine.¹²

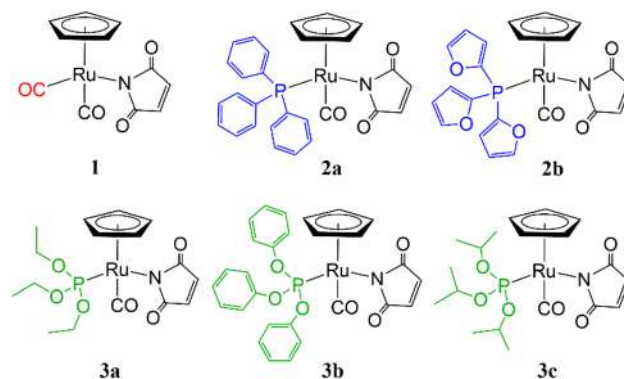
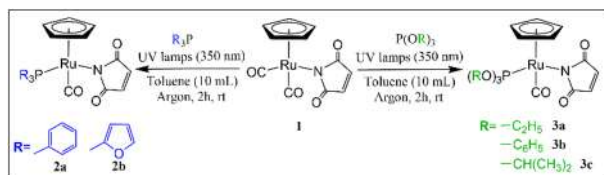


Fig. 1 The structures of the ruthenium complexes **1**, **2a–b** and **3a–c**.



To obtain complexes **2a–b** and **3a–c** we performed the photochemical CO–phosphine/phosphite ligand exchange reaction of **1** (Scheme 1). Similar process was previously described for the iron analog where CpFe(CO)₂(η¹-maleimi-



Scheme 1 Schematic diagram for the synthesis of complexes **2a–b** and **3a–c**.

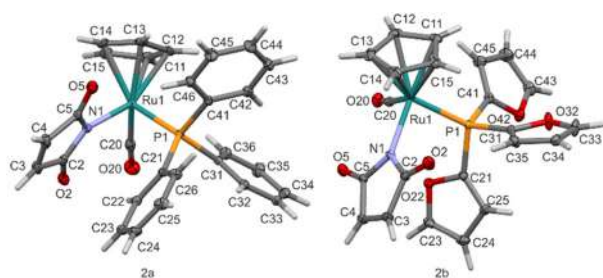


Fig. 2 Molecular structure of **2a** and **2b** with atom labelling scheme. Displacement ellipsoid are drawn with 40% probability level.

Table 1 ³¹P NMR analysis: chemical shifts of the phosphines and phosphites and ruthenium complexes **2a–b** and **3a–c**

Phosphine/ phosphites	³¹ P NMR (ppm)	Ru-complexes	³¹ P NMR (ppm)
P(Ph) ₃	−5.26	2a	56.94
P(Fu) ₃	−77	2b	4.797
P(OEt) ₃	139.1	3a	148.307
P(OPh) ₃	128	3b	140.483
P(OiPr) ₃	139.49	3c	144.502

Table 2 Details of the crystal structure determination of **2a** and **2b** compounds

	2a	2b
Formula/ <i>M</i> [g mol ^{−1}]	C ₂₈ H ₂₂ NO ₃ PRu/552.5	C ₂₂ H ₁₆ NO ₆ PRu/522.4
Crystal system, space group	Orthorhombic, <i>P</i> 2 ₁ 2 ₁ 2 ₁	Triclinic, <i>P</i> $\bar{1}$
<i>a</i> , <i>b</i> , <i>c</i> [Å]	9.5419(1), 14.7114(2), 16.7725(2)	8.1802(1), 8.7067(2), 14.9093(3)
α , β , γ [°]	90, 90, 90	77.209(2), 83.852(2), 76.573(2)
<i>V</i> [Å ³]/ <i>Z</i>	2354.44(5)/4	1005.49(4)/2
<i>F</i> (000)/ μ [mm ^{−1}]	1120.0/1.559	524.0/1.725
Crystal size [mm]/ <i>d</i> _x [mg m ^{−3}]	0.263 × 0.131 × 0.074/1.559	0.107 × 0.077 × 0.063/1.725
λ [Å], <i>T</i> [K]	MoK α /100 K	MoK α /100 K
2 θ range [°]	4.858 to 61.448	4.912 to 61.824
Data collected/unique	36 824/6306 (<i>R</i> _{int} = 0.0392)	22 923/5196 (<i>R</i> _{int} = 0.0369)
<i>R</i> / <i>wR</i> ² [<i>I</i> > 2 σ (<i>I</i>)]	<i>R</i> ₁ = 0.0203/ <i>wR</i> ₂ = 0.0438	<i>R</i> ₁ = 0.0233/ <i>wR</i> ₂ = 0.0519
<i>R</i> / <i>wR</i> ² (all data)	<i>R</i> ₁ = 0.0214/ <i>wR</i> ₂ = 0.0442	<i>R</i> ₁ = 0.0259/ <i>wR</i> ₂ = 0.0530
Goof on <i>F</i> ²	1.015	1.071
$\Delta\rho_{\min}/\Delta\rho_{\max}$ [e Å ^{−3}]	0.37/−0.33	0.44/−0.51
Flack parameter	−0.011(10)	
CCDC number	2209334	2209335

dato) was irradiated with triphenylphosphine by visible light to give CpFe(CO)(PPh)(η¹-maleimidato).³⁵ In present work, ruthenium complex **1** was irradiated by UV-light (360 nm) in the presence of chosen phosphines (triphenylphosphine, tris (2-furyl)phosphine), or phosphites (triethyl phosphite, triphenyl phosphite and triisopropyl phosphite) to give complexes **2a–b** and **3a–c** with good yields (Scheme 1). The crude products were purified by flash chromatography on silica gel. The pure products were characterised by spectroscopic methods (Fig. S2–S26†) and the crystals of **2a** and **2b** were analysed by X-ray (Fig. 2). All of the complexes were stable in the dark at room temperature. Because of some light sensitivity, the purification, characterisation, and crystallisation were performed in the absence of ambient light.

Prominent deshielding of the phosphorus atoms in phosphines and phosphites ligands has been observed upon reaction with complex **1**. The ³¹P NMR analysis revealed that the peaks for the phosphorus atoms in all complexes have been shifted downfield compared to the starting phosphines or phosphites. It is evident that the extent of deshielding is much higher in the case of phosphines (**2a**, **2b**) than that of phosphites (**3a**, **3b**, **3c**) as shown in Table 1.

The absorbance and emission spectra of all complexes were recorded in chloroform. It was observed that complexes **2a–b** and **3a–c** misses characteristic emission peaks; only complex **1** has very weak emission at 358 nm upon excitation at 300 nm (Fig. S27†).

Crystallographic analysis

The results of crystal structure determination are presented in the Table 2. Compound **2a** crystallizes in the non-centrosymmetric orthorhombic *P*2₁2₁2₁ while **2b** in triclinic *P* $\bar{1}$ space groups. Molecular diagrams with atom labelling scheme are presented in Fig. 2. In the both cases ruthenium Ru1 atom is bonded to cyclopentadienyl ring (C11–C12–C13–C14–C15), carbonyl ligand (C20–O20), nitrogen atom N1 of maleimidato ligand and phosphorus P1 of phosphine ligand.

Mean bond length of ruthenium to carbon atoms of cyclopentadienyl rings equals 2.23 Å. In turn, bond lengths of



ruthenium atom to carbonyl ligands and to the center of gravity of cyclopentadienyl ring (Cg1) are of a similar range, approximately 1.87 Å, while Ru–N1 and Ru–P1 bonds are evidently longer respectively about 2.1 Å and 2.3 Å (see Table S1†). Valence angles around Ru1 and between N1 (maleimidato-), P1 (phosphine-) and C1 (carbonyl) atoms are very close to 90°. In turn, angles to the cyclopentadienyl ring (Cg1 in the Table S1†) are of significantly larger values – above 120°. Considering the three-dimensional arrangement of ligands around the metal atom, both compounds can be classified as “piano stool” complexes with cyclopentadienyl ring positioned on the top and other three ligands arranged on the opposite side almost perpendicularly each other (Fig. 2). This molecular conformation is similar to known structures for previously determined ruthenium complexes.³⁴

Assuming cyclopentadienyl as a single ligand, the coordination sphere of Ru1 atom resembles strongly distorted tetrahedron in molecules of the both compounds. The presence of pseudo-tetrahedral arrangement of ligands around metal atom is the source of chirality in the molecule. A formal configuration may be then indicated in the same way as it is used for asymmetric tetrahedral carbon atoms. According the Cahn–Ingold–Prelog rules,³⁶ the ruthenium ligands are listed in the following order: I – phosphine, II – maleimidato, III – carbonyl, IV – cyclopentadienyl. It is especially important for compound **2a** which crystallizes a non-centrosymmetric space group as a conglomerate. It means that an analyzed crystal contains a single enantiomer. Thus, despite the non-stereospecific synthesis which results in both products with *R* and *S* configurations, the sample underwent spontaneous resolution upon crystallization and, as seen in Fig. 2, only *R* ruthenium stereoisomer is observed in the crystal.

The formation of conglomerates with spontaneous resolution is a relatively rare phenomenon which however yields enantiopure crystals. It was first demonstrated by Pasteur with sodium ammonium tartrate.³⁷ Even though it is known that under favorable circumstances pure enantiomers can be obtained from a racemic mixture, factors responsible for spontaneous resolution are poorly understood and predictions are hardly possible.

The process of chiral self-sorting behavior has been recognized not only for organic compounds, but also for metal complexes and metalloorganic species. A spontaneous resolution of various cobalt, ruthenium, tungsten, molybdenum, cobalt, iron or zinc complexes of tetrahedral and octahedral coordination has been reported.^{38–43}

Also seven-coordinate lanthanides complexes of praseodymium, samarium and erbium are chiral and crystallize as conglomerates in non-centrosymmetric *R3* space group.⁴⁴ The phenomenon of conglomerate crystallization was recognized in tetrahedral and octahedral metal–ligand cages.^{45,46} In addition, some approaches to asymmetric catalytic asymmetric synthesis with the use of transition-metal catalyst of ruthenium(II) and palladium, in particular chirality inducer, are known to be employed to achieve homochirality.^{47–49}

As compound **2b** crystallizes centrosymmetric *P1* space group, due to crystallographic inversion symmetry both isomers (*R* and *S*) are present in the unit cell.

For further comparison of the overall molecular geometry between **2a** and **2b** the same isomers (*R*) have been taken to analysis (Table S1†–compare torsion angles). Small differences are observed in values of torsion angles around Ru1–P1 and Ru1–N1 bonds (approximately 20° and 4°) due to twist of phosphine aromatic rings along Ru–P bond. But in general, it does not change significantly the overall molecular conformation as seen in Fig. 3 presenting superposition of molecules along Ru–P1 and Ru–N1 bonds.

Both crystal structures are stabilized by C–H...O interactions of type hydrogen bonds with oxygen of carbonyl groups of furane rings as hydrogen acceptors. Some geometric details of these interactions are presented in the Table S2.† The above interactions can be also described in terms of Hirshfeld surface analysis. Such a molecular surface (HS) represents the area where molecules in the crystal state come into mutual contacts. They are presented in Fig. S1† (right) and mapped with a colour scale of d_{norm} parameter for H...O contacts. As it can be seen red colors resulting from short C–H...O hydrogen bonds occur close to oxygen atoms. In the HS fingerprint plots (Fig. S1b† – left) H...O contacts are presented by two sharp, long distinct spikes in the bottom left area of picture. The greater number of oxygen atoms results in greater percentage of H...O contacts in **2b** compared with **2a**. Also, in this case peaks corresponding to C–H...O hydrogen bonds are elongated (~1.3 Å) as compared to the other structure (>1.35 Å).

Cell viability

Using the method of reducing resazurin to resorufin by metabolically active cells, we examined the viability of cells after 2 and 24 h incubation with ruthenium complexes (Tables S3 and S4,† respectively). Then we determined IC₅₀ doses for all ruthenium complexes against the three tested cell types after incubation for 24 h (Table 3). We have shown that the **3a** complex, with an IC₅₀ of 12.25 μM, is the most cytotoxic for HL-60 cells. This complex was much less cytotoxic to normal cells (IC₅₀ > 250 μM).

The complex **2a** was also selected for further studies because it did not show cytotoxicity for normal PBM cells (IC₅₀ > 250 μM). The IC₅₀ for HL-60 cells for this complex was

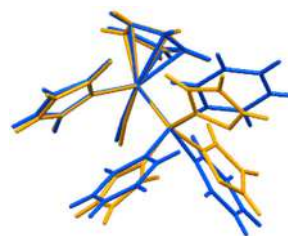


Fig. 3 Comparison of **2a** (dark blue) and **2b** (orange) molecular conformations.



Table 3 IC₅₀ values for ruthenium complexes measured after 24 h incubation of the cells

Ruthenium complexes	HL-60 cells (μM)	HL-60/DR cells (μM)	PBM cells (μM)
1	6.39	240.05	75.29
2a	21.48	>250	>250
2b	35.64	161.37	8.48
3a	12.25	>250	>250
3b	52.47	104.35	7.18
3c	18.88	132.52	11.22

21.48 μM. The remaining **2b**, **3b** and **3c** ruthenium complexes were cytotoxic for both normal and cancer cells.

The HL-60/DR cell line that we obtained, resistant to doxorubicin, was characterized by about 100 times greater resistance to this drug compared to the original cell line (Fig. 4). In the case of HL-60/DR cells, all ruthenium complexes showed significantly lower cytotoxicity compared to HL-60 cells and PBM cells (Table 3). The **3b** complex with an IC₅₀ of 104.35 μM was the most cytotoxic for these cells. Our results indicate that ruthenium complexes do not overcome the doxorubicin resistance in HL-60 cells.

The complex **1** which we studied previously³⁴ was the most cytotoxic ruthenium complex among those currently under investigation for HL-60 cells. The IC₅₀ for this complex was 6.39 μM.

In the case of a short 2 h incubation, an increase in the metabolic activity of cells was observed after incubation with all ruthenium complexes. This is especially noticeable in normal PBM cells (Table S3†). Given the high cytotoxicity to HL-60 cells and the lack of cytotoxicity to normal cells, two new ruthenium complexes **2a** and **3a** were selected for further studies.

DNA damage

Fig. 5a–c show the level of DNA damage analysed by the comet assay under alkaline conditions after incubation with **2a** and

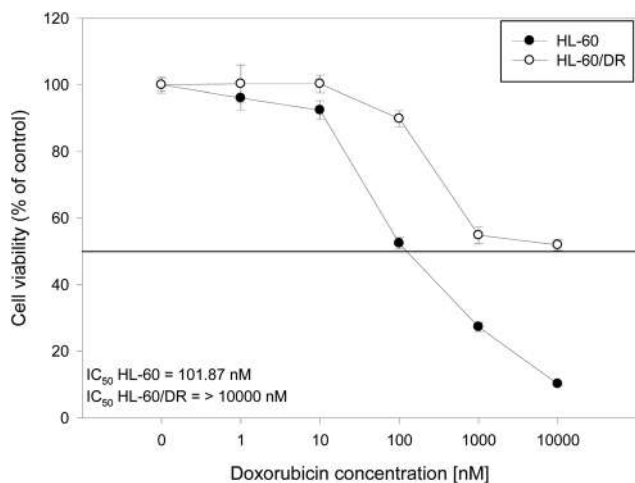


Fig. 4 The comparison of HL-60 cells viability and doxorubicin-resistant HL-60/DR cells after incubation with the drug. The horizontal line represents viability at a level of 50%.

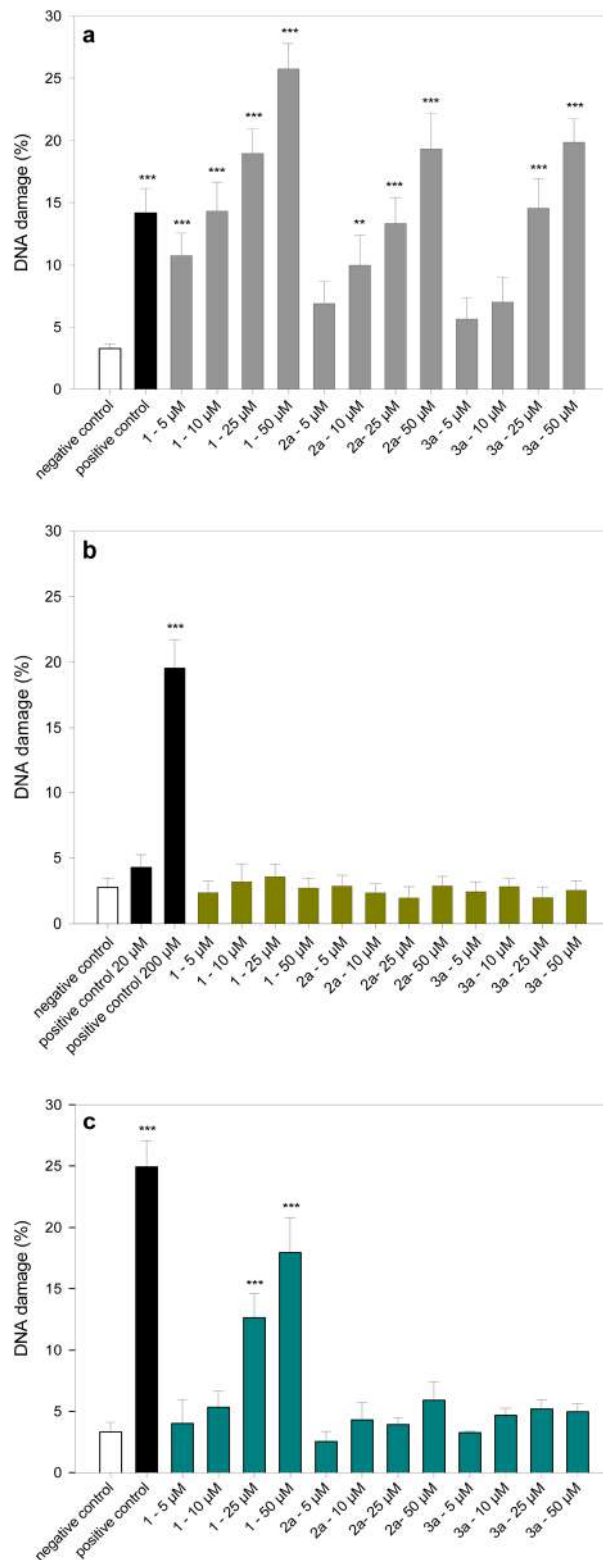


Fig. 5 DNA damage in (a) HL-60 cells (b) HL-60/DR cells and (c) PBM cells incubated for 2 h at 37 °C with ruthenium complexes **1**, **2a** and **3a** analysed by the alkaline comet assay. The negative controls were cells incubated only with the cell culture medium for 2 h at 37 °C. The positive controls were cells incubated with H₂O₂ at 20 μM for 15 min on ice. The figure shows mean results ± SEM, *n* = 100; ** *p* < 0.01; *** *p* < 0.001.



3a complexes. The comet assay in the alkaline version is a sensitive and simple method of determining the level of DNA damage, including single- and double-strand breaks and alkali-labile sites in living cells.⁵⁰ The ruthenium complexes **2a** and **3a** in the concentration range from 5 to 50 μM were selected for the study of DNA damage. At all the concentrations used, the cells after 2 h incubation showed high viability over 90% (Table S3[†]). We observed a significant increase in the level of DNA damage in HL-60 cells incubated with ruthenium complexes **2a** and **3a** (Fig. 5a). The complex **1**, which we studied previously,³⁴ shows the highest genotoxic potential.

It induces DNA damage at all concentrations used, ranging from 5 to 50 μM ($p < 0.001$). At the highest concentration used, the complex **1** causes DNA damage at the level of 25% ($p < 0.001$). Two new ruthenium complexes **2a** and **3a** at this concentration induce DNA damage at the level of 20% ($p < 0.001$). In HL-60/DR cells resistant to doxorubicin, neither complex induces DNA damage (Fig. 5b). We obtained interesting results after incubation of PBM cells with the tested complexes (Fig. 5c). DNA damage was only observed in the case of the complex **1** at the level of 18% at the concentration of 50 μM . This result suggests a selective genotoxic activity of **2a** and **3a** complexes against HL-60 cancer cells. Fig. 6 shows the example images of comet's experiment.

We also investigated the possibility to DNA damage by ruthenium complexes *in vitro*. For this purpose, we used the plasmid relaxation assay. Results obtained from electrophoretic mobility shift analysis (EMSA) showed that pUC19 plasmid which we isolated from the DH5 α *E. coli* cells is presented in supercoiled form (CCC). Overnight treatment at 37 $^{\circ}\text{C}$ with restrictase *Pst*I led to linear form (L) of the plasmid. Incubation of CCC form with complexes **1**, **2a–b**, and **3a–c** at concentration of 50 μM showed a possibility of DNA adducts or breaks, which affected topological changes of the plasmid (Fig. 7). After 2 h of incubation of the plasmid with ruthenium complexes, we see the appearance of the OC form in the case of complexes **2b** and **3a–c** (Fig. 7a). This result demonstrates the possibility of induction of DNA single-strand breaks by these ruthenium complexes *in vitro*. After longer incubation (24 h) the OC form of the plasmid appears in all complexes (Fig. 7b). In the case of the **3c** complex, a linear form (L) of the plasmid is also visible, which proves the possibility of induction of DNA double-strand breaks by this complex.

Apoptosis

To quantify the number of cells in the different stages of apoptosis after incubation with ruthenium complexes, flow cytometry analysis of living cells double labelled with annexin V-FITC (annexin V) and propidium iodide (PI) was performed. In early apoptosis, the membrane phosphatidylserine (PS) translocates from the inner plasma membrane to the external leaflet. Annexin V is a specific fluorescence probe that can be used to detect PS on the plasma membrane surface. PI can pass through the plasma membrane of dead cells to stain the nucleus, which allows the further distinction of early apoptotic and late apoptotic/necrotic cells. The signals can be divided

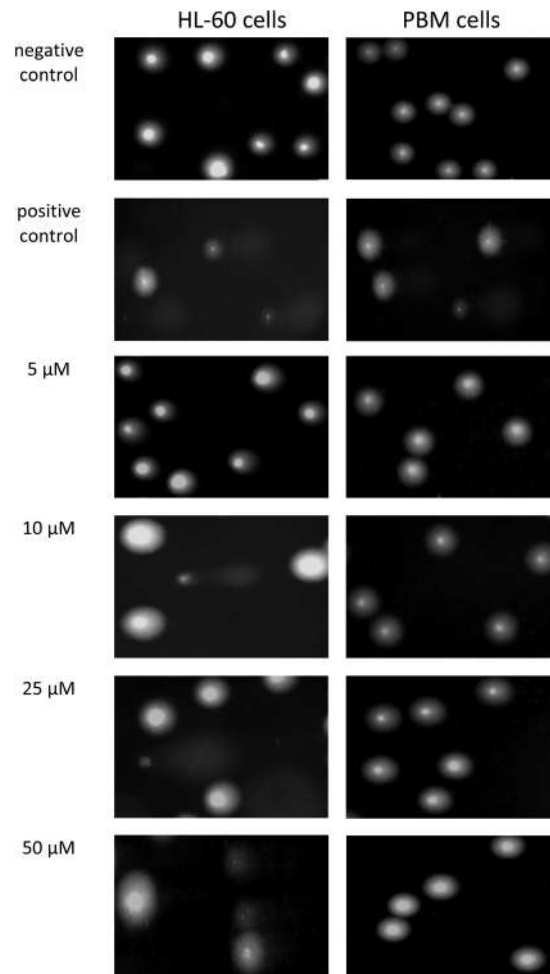


Fig. 6 Representative photos of comet's effect obtained in the alkaline version of the comet assay after incubation of HL-60 cells and PBM cells with complex **2a** at the concentrations of 5, 10, 25 and 50 μM for 2 h at 37 $^{\circ}\text{C}$. The negative controls were cells incubated only with the cell culture medium for 2 h at 37 $^{\circ}\text{C}$. The positive controls were cells incubated with H_2O_2 at 20 μM for 15 min on ice.

into four classes: viable cells, early apoptotic cells, late apoptotic cells and necrotic cells.

We investigated the ability of **2a** and **3a** complexes to induce apoptosis in HL-60 and HL-60/DR cells. In HL-60 cells, both complexes induce apoptosis. The **2a** complex showed a much greater potential for apoptosis. In the case of this complex, after 24 h at concentrations ranging from 10 to 50 μM , almost all cells are apoptotic (Fig. 8 and Fig. S29[†]). In the case of the **3a** complex, apoptotic cells only dominate after incubation at the highest concentration of 50 μM . The ruthenium complex **2a** shows greater potential for apoptosis compared not only to complex **3a** but also to complex **1**. No apoptosis was observed in HL-60/DR cells after incubation with the **1**, **2a** and **3a** complexes (Fig. S30[†]). In these cells, we did not detect apoptosis even after incubation with 20 μM camptothecin for 24 h at 37 $^{\circ}\text{C}$.

Ruthenium has the ability to form complexes at the different oxidative states (from II to IV) which exhibit different



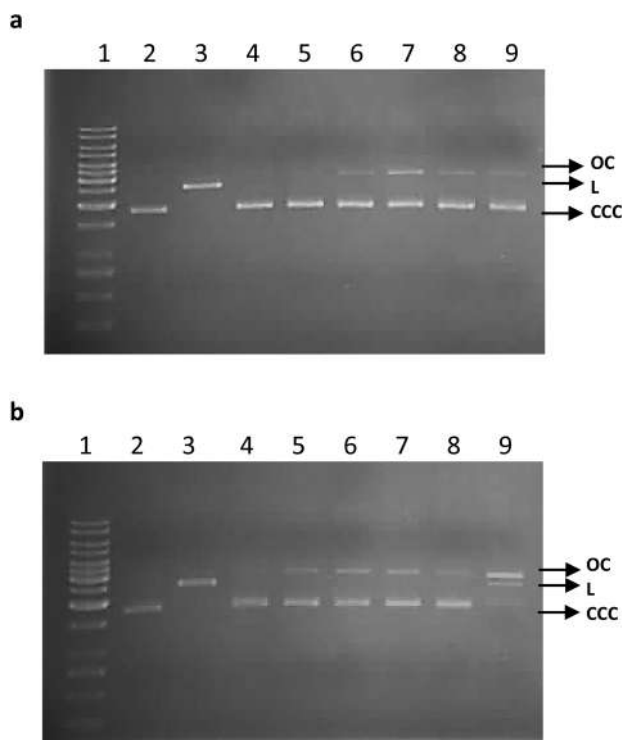


Fig. 7 Plasmid relaxation assay. pUC19 plasmid was incubated for 2 h (a) and 24 h (b) (37 °C) with ruthenium complexes at 50 μ M, and then was resolved on a 1% agarose gel, stained with ethidium bromide and visualized in UV light. Line 1 – DNA ladder; line 2 – pUC19 plasmid (the supercoiled form, CCC); line 3 – pUC19 plasmid incubated with restriction enzyme *Pst*I (the linear form, L); lines 4–9 – pUC19 plasmid incubated with complexes **1**, **2a–b**, and **3a–c**, respectively. OC – the open circular form of pUC19 plasmid.

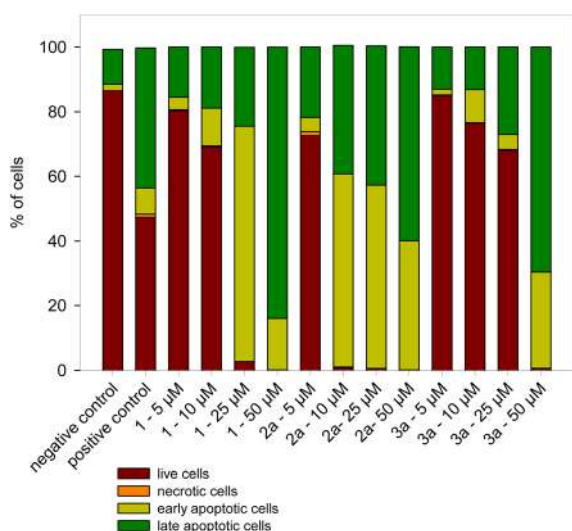


Fig. 8 The effect of ruthenium complexes **1**, **2a** and **3a** on the apoptosis of HL-60 cells. The positive control were cells incubated with 20 μ M camptothecin for 24 h at 37 °C. Data represent means \pm SD of three experiments.

biological activities.⁵¹ Among them, the highest biological activity have complexes on the oxidative state(II), possessing the ability to interact with biomolecules such as DNA or proteins.⁵² The majority of novel synthesized ruthenium compounds, that can exhibit anti-cancer potential are on the oxidative state(II). One of the most common mechanisms of cytotoxicity is the induction of apoptosis. Novel synthesized fluorinated cyclometalated ruthenium(II) complexes led to a significant increase of apoptosis in A549 cells by induction of caspase 3/7 overexpression.⁷ Arene ruthenium(II) complex leads to a significant increase of apoptosis in MCF-7 cells, which is related to high genotoxicity displayed by severe DNA damage.⁵³ Ruthenium(II)/allopurinol complex induced apoptosis in murine breast cancer cells by pro-caspase activation resulting in releasing of caspase 3 and 7 and Becklin-1 cleavage.⁵⁴ Ruthenium(II) complex with lapachol induced reactive oxygen species (ROS)-mediated apoptosis in DU-145 cells.⁵⁵ Moreover, complex increasing expression of cleaved caspases 3 and 9 and induced DNA damage. Ruthenium(II) methylimidazole complexes induce mitochondrial dysfunction in A549 cells, which results overexpression of caspase 9 and finally leads to apoptosis.⁵⁶ These complexes also exhibit the potential to DNA damage. Polypyridyl ruthenium(II) complex disturbs the potential of the mitochondrial membrane in HepG2 cells.⁵⁷ Moreover, the complex causes overproduction of ROS and leads to oxidative DNA damage. Cyclometalated ruthenium(II) β -carboline complex causes caspase 8 and caspase 9 activation which leads to the executioner caspase 3 and induction of apoptosis.⁵⁸ Additionally, these metal complex increases the overproduction of ROS, which generate oxidative DNA damage. Recently, Li *et al.* presented very interesting results regarding the cycloruthenated complex RuZ.⁵⁹ RuZ can self-assemble into nanoaggregates in the cell culture medium, resulting in a high intracellular concentration of RuZ in multi-drug resistance cancer cells. RuZ significantly increased the level of ROS and DNA damage, which caused apoptosis. RuZ inhibited the proliferation of 35 cancer cell lines, of which 7 cell lines were resistant to clinical drugs. Interestingly, the RuZ complex was also active in doxorubicin-resistant MDA-MB-231/Adr mouse tumor xenografts.

We observed that complex **2a** exhibits the highest potential to induce caspase 3/7 activity at 5 and 10 μ M (Fig. 9). This result corresponds with the measurement of apoptosis by flow cytometry, where complex **2a** induced apoptosis in the most effective way (Fig. 8). Moreover, all complexes exhibit the potential to induce caspase 3/7 activity at 10 μ M. Small absolute values of caspase 3/7 activity for 25 and 50 μ M are the result of the high number of late apoptotic cells, which lost metabolic activity due to membrane perforation as determined by annexin V externalization (Fig. 8).

Evaluation of oxidative stress

We used an H₂DCF-DA probe to determine the effect of ruthenium complexes **1**, **2a**, and **3a** on the induction of ROS (Fig. 10). We performed a measurement of ROS generation kinetics, where HL-60 cells were incubated with complexes at



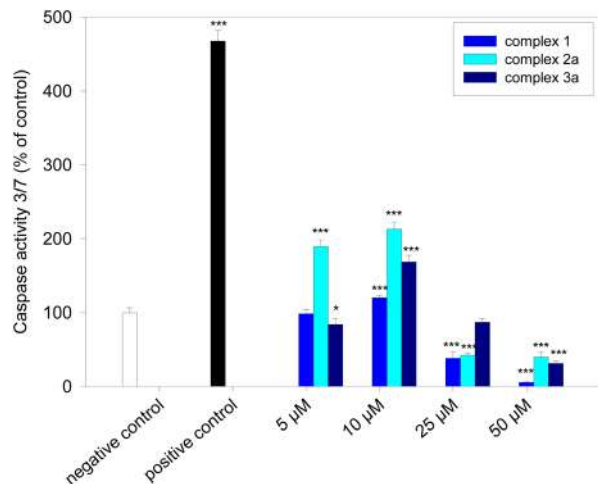


Fig. 9 Effect of ruthenium complexes **1**, **2a** and **3a** on caspase 3/7 activity in HL-60 cells. The cells were incubated with complexes for 24 h at 37 °C. The positive control was sample of cells incubated with 20 μM camptothecin for 24 h at 37 °C. Data represent means \pm SD of four experiments; * $p < 0.05$; *** $p < 0.001$.

the concentrations 5, 10, 25, and 50 μM for 15, 30, 45, 60, 90, and 120 min. Our results clearly showed that any of the tested complexes did not exhibit the potential to induction of ROS within 60 min. Statistically significant increase in ROS level was observed after 90 and 120 min only for complex **3a** at 50 μM (Fig. 10c). Considering the short lifetime of ROS, this increase is more due to the secondary effect of the complex on cell metabolism than the ability of ROS generation by the complex itself. Our results indicate that both DNA damage and apoptosis in HL-60 cells are not caused by ROS formation induced by ruthenium complexes **1**, **2a** and **3a**.

Docking studies

Interaction of newly developed ruthenium(II) complexes with DNA was analysed by computational methods using molecular docking and molecular dynamics, to ascertain whether there is a difference between fully paired DNA, as compared to genomic DNA, and a DNA mismatch, as compared to a damaged DNA fragment. Crystal structures for fully complementary and mismatched DNA were retrieved from the protein data bank, PDB ID: 1BNA (fully complemented) and 4E1U (for a mismatch).^{60,61} The calculated docking energy for selected ruthenium(II) complexes, compounds **1**, **2a** and **2b** with fully complemented DNA (Fig. 11a and S31a, c†) show relatively low binding energy in the range -4.57 to -5.57 (Table 4). However, binding energy for the same complexes with mismatched DNA (Fig. 11b and S31b, d†) are stronger with the lowest difference for the compound **1** ($\Delta\Delta G = 3.98$ kcal mol⁻¹) and much greater for compounds **2a** and **2b** ($\Delta\Delta G = 9.60$ kcal mol⁻¹ and $\Delta\Delta G = 8.04$ kcal mol⁻¹, respectively). Clearly the mismatched DNA (A–A bulge) have higher docking score compared to the fully complementary DNA, which might suggest that the cytotoxic effect of compounds **2a** and **2b** are weakly related to the direct degradation of the

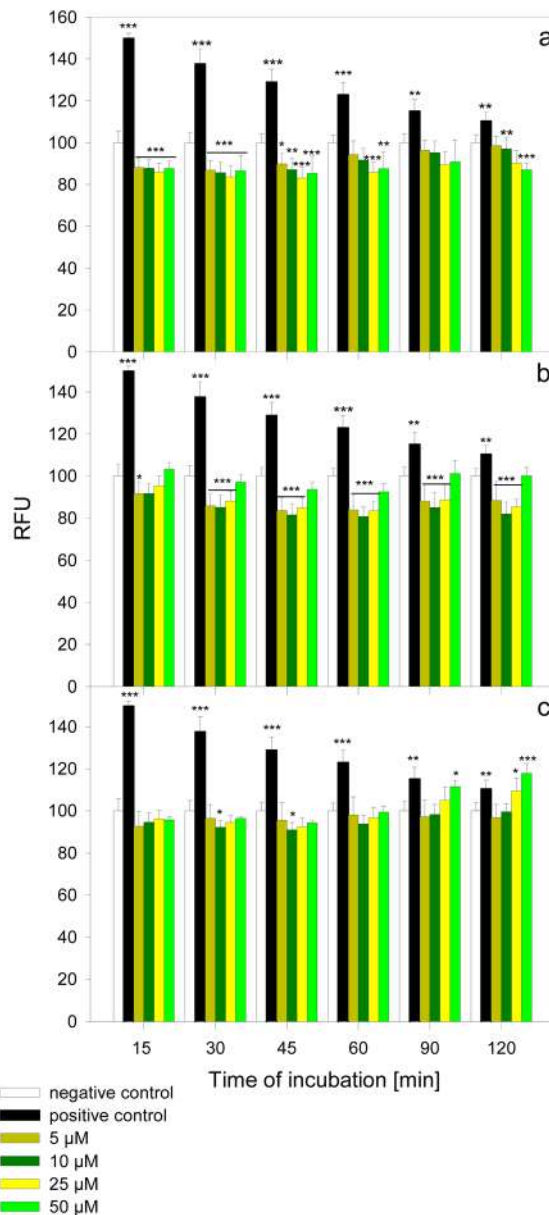


Fig. 10 ROS generation kinetics in HL-60 cells incubated with ruthenium complexes **1** (a), **2a** (b) and **3a** (c) at the concentrations 5, 10, 25, and 50 μM at 37 °C. The positive control were cells incubated with 5 mM H₂O₂ at 37 °C. Data represent means \pm SD of six experiments; * $p < 0.05$; ** $p < 0.01$; *** $p < 0.001$.

genomic DNA but rather are interfering with the cellular repair mechanism and thus causing the damaged DNA accumulation and finally cell death. These results also corroborate with the EMSA analysis (gel study part of this work), where short exposure of plasmid DNA to these compounds does not cause the DNA breakage. This is a new hypothesis and has to be further investigated. These complexes were also analysed using Molecular Dynamics (data not shown), however the data is inconclusive probably due to the some discrepancy in the force field parameters for the ruthenium(II) complexes. To our



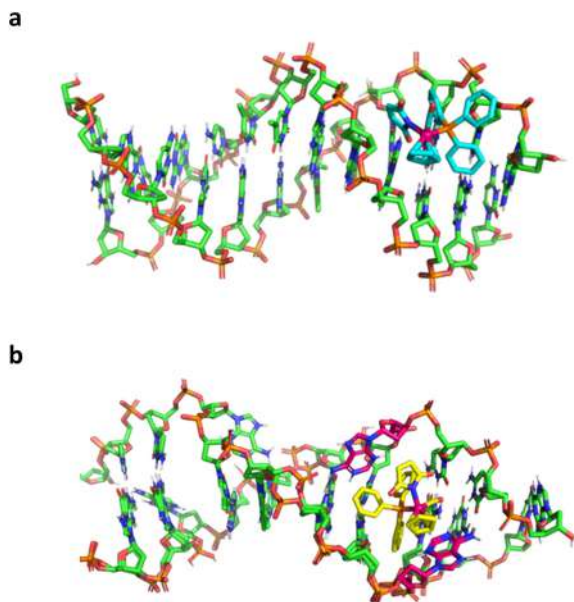


Fig. 11 Ruthenium(II) complex **2a** with fully complemented DNA (a) and mismatched DNA (b).

Table 4 Docking score of DNA and mismatched DNA with ruthenium (II) complexes with maleimide and phosphine or phosphite ligands (**1**, **2a** and **2b**)

Ligand	Fully paired DNA (kcal mol ⁻¹)	Mismatched DNA (kcal mol ⁻¹)
1	-4.57	-8.55
2a	-5.93	-15.53
2b	-5.57	-13.61

knowledge such complexes were never analysed using MD with a DNA fragment.⁶²

Experimental section

Materials and methods

Bis(cyclopentadienylrutheniumdicarbonyl) dimer, maleimide, chloroform-D and all the phosphines and phosphites were purchased from Sigma-Aldrich (Merck). Methanol, and toluene were purchased from POCH (Polish Chemical Reagents) and used as solvents without further purification. All syntheses were carried out under argon. Column chromatographic refinements of the crude products were performed on silica gel 60 (230–400 mesh) purchased from Merck. Infrared (IR) spectra were recorded in KBr on a Fourier Transform InfraRed (FTIR) NEXUS (Thermo Nicolet) spectrometer. Proton, Carbon and Phosphorus NMR spectra were recorded on Bruker Avance III (600 MHz) instrument. NMR data were collected in CDCl₃ solution. The chemical shifts were stated in part per million (ppm). Coupling constants were calculated in Hertz (Hz). Electrospray ionization mass spectrometry (ESI-MS) spectra were recorded on the Varian 500-MS LC ion trap spectrometer.

Absorbance and emission spectra were recorded on PerkinElmer Lambda 45 UV/vis spectrometer and PerkinElmer LS55 Fluorimeter, respectively. Photochemical syntheses were carried out using UV lamp TQ 150 Z3. Relevant guidelines and regulations were followed in all the performed methods. IMDM medium and fetal bovine seRPM (FBS) were obtained from Biowest (Cytogen, Zgierz, Poland). Dimethyl sulfoxide (DMSO), hydrogen peroxide (H₂O₂), low-melting-point (LMP), normal-melting-point (NMP) agarose, phosphate buffered saline (PBS), and 4',6-diamidino-2-phenylindole (DAPI) were purchased from Sigma-Aldrich (USA). All other reagents were obtained at the highest commercially available grades. A stock solution of complexes (10 mM) was dissolved in DMSO. Complex **1** was synthesized following previously published method, by photochemical reaction of CpRu(CO)₂I with maleimide in the presence of diisopropyl amine in toluene.³⁴

Synthesis of **2a–b** and **3a–c**

An argon-saturated solution of **1** (40 mg, 0.12 mmol) and phosphine or phosphite (30 mg, 0.11 mmol) in toluene (10 ml) was illuminated under UV lamp ($\lambda = 350$ nm) for 2 h. The progress of the reaction was continuously monitored with TLC. After completion of the reaction, solvent was evaporated in vacuum.

2a. The crude product was purified by column chromatography using CHCl₃–EtOAc (2 : 3) as eluent to afford a yellow solid. The product was recrystallized from chloroform/heptane.

Yield 32 mg (55%) ¹H NMR (δ , ppm, CDCl₃): 4.974 (5H, s, Cp), 6.219 (2H, s, maleimide), 7.331–7.335 (4H, d, $J = 2.4$ Hz), 7.342–7.349 (8H, d, $J = 4.2$ Hz), 7.366–7.383 (3H, m, $J = 10.2$ Hz). ¹³C NMR (δ , ppm): 205.39, 205.25, 183.93, 136.40, 134.41, 134.09, 133.81, 133.73, 130.20, 130.19, 128.35, 128.28, 85.21 (d). ³¹P NMR (δ , ppm): 56.939. IR (cm⁻¹): 1958 (C≡O); 1644 (C=O, imide); 1334, 694 (P–Ph). ESI-MS: m/z calcd for C₂₈H₂₂RuNO₆P (M + H)⁺, 554.04; found, 554.27.

2b. The crude product was purified by column chromatography using CHCl₃–EtOAc (3 : 2) as eluent to afford a yellow solid. The product was recrystallized from chloroform/heptane.

Yield 15 mg (45%). ¹H NMR (δ , ppm, CDCl₃): 5.20 (5H, s, Cp), 6.435–6.446 (5H, m, maleimide, Fu), 6.797–6.803 (3H, dd, $J = 3.6$ Hz, Fu), 7.635–7.642 (3H, m, $J = 4.2$ Hz, Fu). ¹³C NMR (δ , ppm, CDCl₃): 203.46, 203.31, 183.77, 148.01, 147.98, 147.20, 146.69, 136.65, 122.12, 121.99, 111.37, 111.32, 84.89, 84.87. ³¹P NMR (δ , ppm): 4.797. IR (cm⁻¹): 1965 (C≡O); 1645 (C=O, imide); 1330, 1007, 794 (P–Fu). ESI-MS: m/z calcd for C₂₂H₁₆RuNO₆P (M + H)⁺, 523.98; found, 524.24.

3a. The crude product was purified by column chromatography using CHCl₃–EtOAc (4 : 1) as eluent to afford a yellowish liquid. The product was recrystallized from chloroform/heptane to obtain bright yellow solid. Yield: 21 mg (79%). ¹H NMR (δ , ppm, CDCl₃): 1.209–1.233 (9H, t, $J = 14.4$ Hz, C₂H₅), 3.856–3.912 (6H, m, –CH₂), 5.158–5.160 (5H, d, $J = 1.2$ Hz, Cp), 6.851 (2H, s, maleimide). ¹³C NMR (δ , ppm): 204.00, 203.80, 183.94, 136.91, 84.71, 84.70, 61.32, 61.29, 16.26, 16.22. ³¹P NMR (δ , ppm, CDCl₃): 148.30. IR (cm⁻¹): 1962 (C≡O); 1644



(C=O, imide); 1333, 1023, 939 (P-OEt). ESI-MS: m/z calcd for $C_{16}H_{22}RuNO_6P$ ($M + H$)⁺, 458.03; found, 458.13.

3b. The crude product was purified by column chromatography using $CHCl_3$ -EtOAc (3 : 1) as eluent to afford a yellow solid. The product was recrystallized from chloroform/heptane.

Yield: 25 mg (51%). ¹H NMR (δ , ppm, $CDCl_3$): 4.905 (5H, s, Cp), 6.426 (s, 2H, maleimide), 7.141–7.184 (m, 9H, *o*-,*p*-phenyl), 7.302–7.328 (m, 6H, $J = 15.6$ Hz, *m*-phenyl). ¹³C NMR (δ , ppm): 85.080–85.099 (d), 121.339–121.369 (d), 125.137, 129.796, 136.671, 151.252–151.311 (d), 183.376, 202.128–202.324 (d). ³¹P NMR (δ , ppm): 140.48. IR (cm^{-1}): 1972 (C≡O); 1652 (C=O, imide); 1186, 921, 775 (P-OPh). ESI-MS: m/z calcd for $C_{28}H_{22}RuNO_6P$ ($M + Na$)⁺, 624.01; found, 624.31.

3c. The crude product was purified by column chromatography using $CHCl_3$ -EtOAc (4 : 1) as eluent to afford a yellow solid. The product was recrystallized from chloroform/heptane.

Yield 15 mg (50%). ¹H NMR (δ , ppm, $CDCl_3$): 6.587 (2H, s, maleimide), 5.127–5.129 (5H, d, Cp, $J = 1.2$ Hz), 4.455–4.511 (3H, m, iso-propyl-CH), 1.204–1.226 (18H, t, $J = 13.2$ Hz, iso-propyl-CH₃). ¹³C NMR (δ , ppm): 204.31, 204.11, 184.02, 136.99, 84.98, 84.96, 69.94, 69.90, 24.19, 24.15, 24.10, 24.09. ³¹P NMR (δ , ppm): 144.502. IR (cm^{-1}): 1973 (C≡O); 1651 (C=O, imide); 1008, 974 (P-OⁱPr). ESI-MS: m/z calcd for $C_{19}H_{28}RuNO_6P$ ($M + Na$)⁺, 522.06; found, 522.31.

X-ray structure determination

X-ray diffraction data for **2a** and **2b** compounds were measured on a four-circle Oxford Diffraction Supernova Dual diffractometer using a two-dimensional area CCD detector and a low-temperature device Oxford Cryosystem cooler. Integration of the intensities, corrections for Lorentz effects, polarization effects and analytical absorption were performed with CrysAlis PRO.⁶³ The crystal structures were solved by direct methods and refined on F^2 using a full-matrix least-squares procedure (SHELXL-2014).⁶⁴ The positions of the hydrogen were introduced in the calculated positions with an idealized geometry and constrained using a rigid body model with isotropic displacement parameters equal to 1.2 of equivalent displacement parameters of their parent atoms. The molecular geometry was calculated by Platon⁶⁵ and WinGX programs.⁶⁶ The relevant crystallographic data are given in Table 2. Atomic coordinates, displacement parameters, a structure factors of the analysed crystal structures are deposited with Cambridge Crystallographic Data Centre CCDC <https://www.ccdc.cam.ac.uk/conts/retrieving.html>.

Cell culture

HL-60 (human promyelocytic leukemia) cell line was obtained from the American Type Culture Collection (ATCC) and cultured in Iscove's Modified Dulbecco's Medium (IMDM) medium with 15% fetal bovine serum (FBS), streptomycin/penicillin solution (100 $\mu g\ ml^{-1}$ and 100 U ml^{-1}). HL-60 cells were cultured in flasks at 37 °C in 5% CO₂ and sub-cultured every 2–3 days to maintain exponential growth.

HL-60/DR (doxorubicin-resistant) cell line was derived from HL-60 cell line by long-term exposure to continuous stepwise increments of doxorubicin concentration. Procedure was similar to that previously described.^{67,68} HL-60 cells were incubated with 20 nM doxorubicin for three days, then cells were passage into new flask with 20 nM doxorubicin for another three days. After this time cells were collected and centrifuged in a density gradient of Lymphosep (Cytogen, Zgierz, Poland) at 1700 RPM for 35 min with the lowest values of acceleration and deceleration. The interface layer containing viable cells was transferred into 15 ml tubes. Then cells were washed two times with IMDM medium containing 50 nM doxorubicin and transferred into a new flask. Cells were harvested like normal HL-60 for one week. After that whole procedure was repeated with 50 nM doxorubicin. After this time, we observe a significant increase in the IC₅₀ value (Fig. S28†). To maintain resistance to doxorubicin we added 50 nM doxorubicin every fourth passage.

Peripheral blood mononuclear (PBM) cells were isolated from a leucocyte-buffy coat collected from the blood of healthy, non-smoking donors from the Blood Bank in Lodz, Poland. The study protocol was approved by the Committee for Research on Human Subjects of the University of Lodz (17/KBBN-UŁ/III/2019). The first step of isolation of PBM cells was a mix of a fresh blood from buffy coats with PBS in a ratio of 1 : 1. In the next step, mixture was centrifuged in a density gradient of Lymphosep (Cytogen, Zgierz, Poland) at 2200 RPM for 20 min with the lowest values of acceleration and deceleration. Then the cells were washed three times by centrifugation with 1% PBS. After isolation cells were suspended in RPMI 1640 medium.

Cell viability

The resazurin reduction assay was performed similar to previously described.⁶⁹ Resazurin salt powder was dissolved in sterile PBS. Cells were seeded on the 96-well plates in count of 1×10^3 in the case of HL-60 and HL-60/DR and of 5×10^3 for PBM cells per well. Ruthenium complexes were added to wells to obtain a final concentration of 0.5, 1, 2.5, 5, 10, 25, 50, 100 and 250 μM . In next step plates were incubated at 37 °C in 5% CO₂ for 2 h and 24 h. After the desired time has elapsed 10 μl of resazurin salt was added to each well and plates again were incubated in 37 °C in 5% CO₂ for 2 h. Next fluorescence was measured with microplate reader Synergy HT (Bio-Tek Instruments, USA) using an excitation wavelength of 530/25 and an emission wavelength of 590/35 nm.

Comet assay

Ruthenium complexes **1**, **2a**, and **3a** were added to the suspension of the cells to give final concentrations from the range 5–50 μM . PBM cells, HL-60 and HL-60/DR cells were incubated for 2 h at 37 °C in 5% CO₂. The experiment included a positive control, *i.e.*, a cell sample incubated with hydrogen peroxide (H₂O₂) at 20 μM or 200 μM in the case of HL-60/DR cells for 15 min on ice.



The comet assay was performed under alkaline conditions according to the procedure of Tokarz *et al.*⁷⁰ A freshly prepared cells suspension in 0.75% LMP agarose dissolved in PBS was layered onto microscope slides (Superior, Germany), which were pre-coated with 0.5% NMP agarose. Then, the cells were lysed for 1 h at 4 °C in a buffer containing 2.5 M NaCl, 0.1 M EDTA, 10 mM Tris, 1% Triton X-100, pH = 10. After cells lysis, the slides were placed in an electrophoresis unit. DNA was allowed to unwind for 20 min in the solution containing 300 mM NaOH and 1 mM EDTA, pH > 13.

Electrophoretic separation was performed in the solution containing 30 mM NaOH and 1 mM EDTA, pH > 13 at ambient temperature of 4 °C (the temperature of the running buffer did not exceed 12 °C) for 20 min at an electric field strength of 0.73 V cm⁻¹ (28 mA). Then, the slides were washed in water, drained, stained with 2 µg ml⁻¹ DAPI and covered with cover slips. In order to prevent additional DNA damage, the procedure described above was conducted under limited light or in the dark.

Comet analysis

The comets were observed at 200× magnification in an Eclipse fluorescence microscope (Nikon, Japan) attached to a COHU 4910 video camera (Cohu, Inc., San Diego, CA, USA) equipped with a UV-1 A filter block and connected to a personal computer-based image analysis system Lucia-Comet v. 6.0 (Laboratory Imaging, Praha, Czech Republic). Fifty images (comets) were randomly selected from each sample and the mean value of DNA in comet tail was taken as an index of DNA damage (expressed in percent).

Plasmid relaxation assay

The pUC19 plasmid was isolated from the DH5α *E. coli* cells with AxyPrep Plasmid Miniprep Kit (Axygen) according to the manufacturer's instruction. The isolated plasmid quantity and quality were determined by A260/A280 ratio and gel electrophoresis, respectively. The native form of pUC19 exists mainly in the supercoiled form (CCC) which is characterized by a relatively high electrophoretic mobility. The plasmid was digested with the restrictase *Pst*I (New England Biolabs) to induce linear (L) form. Topological differences between CCC and L forms of the plasmid account for their different electrophoretic mobility. The plasmid at 50 ng µl⁻¹ was incubated for 2 h and 24 h with **1**, **2a**, **2b**, **3a**, **3b**, and **3c** at concentration of 50 µM. Then the samples were subjected to 1% agarose gel electrophoresis with ethidium bromide staining, visualization under UV light (302 nm), scanning by a CCD camera, and analysis with the GeneTools by Syngene (Cambridge, UK) software. During electrophoresis, we also separated 4 µl of 1 kb DNA ladder (GeneRuler 1 kb DNA Ladder, Thermo Scientific, Waltham, MA, USA).

Apoptosis

The FITC Annexin V Apoptosis Detection Kit II (BD Biosciences, PA, USA) was used to evaluation of apoptosis using flow cytometry. HL-60 and HL-60/DR cells were seeded

in each well of a 6-well plate at 2×10^5 cells per ml and incubated for 24 h with ruthenium complexes **1**, **2a** and **3a** at concentrations from the range 5–50 µM. Cells were collected and washed three times with ice-cold PBS. Then cells were suspended in 100 µl of Binding Buffer and transferred to cytometry tubes. FITC annexin V (5 µl) and propidium iodide (5 µl) were added to cytometry tubes, gently vortexed and incubated at room temperature in the dark for 15 min. Then 400 µl of Binding Buffer was added and measured on the LSRII flow cytometer (Becton Dickinson, San Jose, CA, USA). The positive control were cells incubated with 20 µM camptothecin for 24 h at 37 °C.

Caspase 3/7 activity

Caspase 3/7 activity was conducted using the Caspase-Glo@3/7 Assay kit (Promega, Madison, WI, USA) according to the manufacturer's protocol. HL-60 cells were seeded on a 96-well black plate in a count of 10 000 per well. Then cells were incubated with complexes **1**, **2a**, and **3a** for 24 h at 37 °C in 5% CO₂ at the concentrations of 5, 10, 25, and 50 µM. Next 75 µL of Caspase-Glo@3/7 reagent was added to each well and then the plate was gently mixed by orbital shaking. After 30 min of incubation at room temperature, luminescence was measured with a microplate reader Synergy HT (Bio-Tek Instruments, USA). The positive control were cells incubated with 20 µM camptothecin for 24 h at 37 °C.

Evaluation of oxidative stress

In order to measure the production of reactive oxygen species (ROS), the fluorescence of 2',7'-dichlorofluorescein diacetate (H₂DCFDA) was measured. H₂DCFDA is a cell-permeable non-fluorescent probe. 2',7'-Dichlorofluorescein diacetate is de-esterified intracellularly and turns into highly fluorescent 2',7'-dichlorofluorescein upon oxidation. HL-60 cells (final density 0.75×10^6 cells per ml) were stained with 20 µM H₂DCFDA (Sigma-Aldrich, St Louis, MO, USA) for 30 min at 37 °C in darkness. Then, the cells were washed twice with HBSS and incubated with complexes **1**, **2a** and **3a** at 37 °C in darkness at the concentrations of 5, 10, 25 and 50 µM. The intensity of fluorescence was measured after 30, 60, 90 and 120 min with $\lambda_{\text{ex}} = 495$ nm and $\lambda_{\text{em}} = 530$ nm using a microplate reader Synergy HT (BioTek Instruments, USA). The data were analyzed according to the following formula: $(T_X - T_0/T_0) \times 100$, where T_X is the DCF fluorescence measured at the indicated time and T_0 is the DCF fluorescence measured at the beginning of the analysis.

Docking studies

A molecular docking with AutoDock4^{71,72} was used to analyse the interaction (shape and binding energy) of the ruthenium (ii) complexes with maleimide and phosphines ligands (**1**, **2a** and **2b**) with normal and mismatched double stranded DNA fragment. To produce global poses of small molecules, a grid-based docking approach was designed using the Lamarckian genetic algorithm. All the needed parameters for ruthenium metal were added in the Autodock 4.2 parameters file.⁶² The



optimum binding conformation was determined to be the one with the lowest binding energy and the highest number of docking poses and additional MD simulations were conducted on this conformation. The MD simulations of normal and mismatched DNA interacted ruthenium(II) complexes with maleimide and phosphine or phosphite ligands were studied using GROMACS 2021⁷³ for 100 ns.

Statistical analysis

The values of the cell viability experiment were presented as mean \pm SD from six repeats. The values of the comet assay were expressed as mean + standard error of the mean from three experiments; data from three experiments were pooled, and the statistical parameters were calculated. The statistical analysis was conducted using the Mann–Whitney test (samples with distributions departing from normality) and the Student's *t*-test (samples with the normal distribution). The differences were considered to be statistically significant when the *p* value was < 0.05 .

Conclusions

To summarize, our results suggest cyto- and genotoxic potential of ruthenium complexes **2a** and **3a** against HL-60 cancer cells but not against normal PBM cells. The plasmid relaxation assay demonstrated the possibility of induction of DNA single-strand breaks by ruthenium complexes **2a–b** and **3a–c** which increase with the incubation time. These findings corroborate with the docking studies performed for complexes **2a** and **2b**. Based on these results, we conclude that the cytotoxic effects of compounds **2a**, **2b** and/or **3a** are weakly related to the direct degradation of genomic DNA or ROS generation, but may affect the DNA damage repair mechanisms leading to cell death. Our results also indicate that ruthenium complexes **1**, **2a–b** and **3a–c** have small potential to overcome the resistance to doxorubicin in HL-60 cells. In the search for new anticancer drugs, their selective activity towards cancer cells and lack of effect on normal cells are of key importance. For this reason, these ruthenium complexes are expected to open new ways for anticancer research.

Author contributions

Michał Juszcak: Investigation. Sujoy Das: Investigation. Aneta Kosinska: Investigation. Agnieszka Rybarczyk-Pirek: Crystallography, investigation. Kinga Wzgarda-Raj: Crystallography, investigation. Paulina Tokarz: Investigation. Saranya Vasudevan: Docking studies, investigation. Arkadiusz Chworos: Supervision, manuscript writing. Katarzyna Woźniak: Conceptualization, supervision, manuscript writing. Bogna Rudolf: Conceptualization; supervision, manuscript writing.

Conflicts of interest

There are no conflicts to declare.

Acknowledgements

This work was financially supported by the University of Lodz, Poland, Faculty of Chemistry and Faculty of Biology and Environmental Protection. The research described in the article was carried out as part of the Interdisciplinary Research Grant of the University of Lodz (IDUB B2311013000182.07).

References

- R. Trondl, P. Heffeter, C. R. Kowol, M. A. Jakupec, W. Berger and B. K. Keppler, *Chem. Sci.*, 2014, **5**, 2925–2932.
- D. Wernitznig, K. Kiakos, G. Del Favero, N. Harrer, H. Machat, A. Osswald, M. A. Jakupec, A. Wernitznig, W. Sommergruber and B. K. Keppler, *Metallomics*, 2019, **11**, 1044–1048.
- S. Y. Lee, C. Y. Kim and T. G. Nam, *Drug Des., Dev. Ther.*, 2020, **14**, 5375–5392.
- J. P. C. Coverdale, T. Laroija-McCarron and I. Romero-Canelón, *Inorganics*, 2019, **7**(3), 31.
- E. Alessio, *Eur. J. Inorg. Chem.*, 2017, **2017**, 1549–1560.
- A. Valente, A. Podolski-Renić, I. Poetsch, N. Filipović, Ó. López, I. Turel and P. Heffeter, *Drug Resist. Updates*, 2021, **58**, 100778.
- Y. Wen, C. Ouyang, Q. Li, T. W. Rees, K. Qiu, L. Ji and H. Chao, *Dalton Trans.*, 2020, **49**, 7044–7052.
- L. Chen, J. Wang, X. Cai, S. Chen, J. Zhang, B. Li, W. Chen, X. Guo, H. Luo and J. Chen, *Bioorg. Chem.*, 2022, **119**, 105516.
- J. Hildebrandt, N. Häfner, D. Kritsch, H. Görls, M. Dürst, I. B. Runnebaum and W. Weigand, *Int. J. Mol. Sci.*, 2022, **23**(9), 4976.
- B. Ma, L. He, Y. You, J. Mo and T. Chen, *Drug Delivery*, 2018, **25**, 293–306.
- P. S. Rawat, A. Jaiswal, A. Khurana, J. S. Bhatti and U. Navik, *Biomed. Pharmacother.*, 2021, **139**, 111708.
- B. Rudolf, A. Kubicka, M. Salmain, M. Palusiak, A. J. Rybarczyk-Pirek and S. Wojtulewski, *J. Organomet. Chem.*, 2016, **801**, 101–110.
- M. Djukić, M. S. Jeremić, R. Jelić, O. Klisurić, V. Kojić, D. Jakimov, P. Djurdjević and Z. D. Matović, *Inorg. Chim. Acta*, 2018, **483**, 359–370.
- L. Rafols, D. Josa, D. Aguilà, L. A. Barrios, O. Roubeau, J. Cirera, V. Soto-Cerrato, R. Pérez-Tomás, M. Martínez, A. Grabulosa and P. Gamez, *Inorg. Chem.*, 2021, **60**, 7974–7990.
- G. Süss-Fink, *Dalton Trans.*, 2010, **39**, 1673–1688.
- J. Li, M. Tian, Z. Tian, S. Zhang, C. Yan, C. Shao and Z. Liu, *Inorg. Chem.*, 2018, **57**, 1705–1716.



- 17 G. Kovács, A. Rossin, L. Gonsalvi, A. Lledós and M. Peruzzini, *Organometallics*, 2010, **29**, 5121–5131.
- 18 S. Thota, D. A. Rodrigues, D. C. Crans and E. J. Barreiro, *J. Med. Chem.*, 2018, **61**, 5805–5821.
- 19 P. Nowak-Sliwinska, J. R. van Beijnum, A. Casini, A. A. Nazarov, G. Wagnières, H. van den Bergh, P. J. Dyson and A. W. Griffioen, *J. Med. Chem.*, 2011, **54**, 3895–3902.
- 20 B. S. Murray, M. V. Babak, C. G. Hartinger and P. J. Dyson, *Coord. Chem. Rev.*, 2016, **306**, 86–114.
- 21 N. Pagliaricci, R. Pettinari, F. Marchetti, C. Pettinari, L. Cappellacci, A. Tombesi, M. Cuccioloni, M. Hadiji and P. J. Dyson, *Dalton Trans.*, 2022, **51**, 13311–13321.
- 22 M. Martínez-Alonso, N. Busto, F. A. Jalón, B. R. Manzano, J. M. Leal, A. M. Rodríguez, B. García and G. Espino, *Inorg. Chem.*, 2014, **53**, 11274–11288.
- 23 M. Martínez-Alonso and G. Gasser, *Coord. Chem. Rev.*, 2021, **434**, 213736.
- 24 P. R. Florindo, D. M. Pereira, P. M. Borralho, C. M. P. Rodrigues, M. F. M. Piedade and A. C. Fernandes, *J. Med. Chem.*, 2015, **58**, 4339–4347.
- 25 A. I. Tomaz, T. Jakusch, T. S. Morais, F. Marques, R. F. M. de Almeida, F. Mendes, É. A. Enyedy, I. Santos, J. C. Pessoa, T. Kiss and M. H. Garcia, *J. Inorg. Biochem.*, 2012, **117**, 261–269.
- 26 G. Albertin, S. Antoniutti, M. Bortoluzzi and G. Zanardo, *J. Organomet. Chem.*, 2005, **690**, 1726–1738.
- 27 K. M. Vyas, P. Mandal, R. Singh, S. M. Mobin and S. Mukhopadhyay, *Inorg. Chem. Commun.*, 2020, **112**, 107698.
- 28 M. Bispinghoff, Z. Benkó, H. Grützmacher, F. D. Calvo, M. Caporali and M. Peruzzini, *Dalton Trans.*, 2019, **48**, 3593–3600.
- 29 M. Hanif, S. M. Meier, W. Kandioller, A. Bytzeck, M. Hejl, C. G. Hartinger, A. A. Nazarov, V. B. Arion, M. A. Jakupec, P. J. Dyson and B. K. Keppler, *J. Inorg. Biochem.*, 2011, **105**, 224–231.
- 30 E. Klaimanee, T. Nhugeaw, S. Saithong, A. Ratanaphan, S. Phongpaichit, Y. Tantirungrotechai and N. Leesakul, *Polyhedron*, 2021, **204**, 115244.
- 31 G. H. Ribeiro, L. Colina-Vegas, J. C. T. Clavijo, J. Ellena, M. R. Cominetti and A. A. Batista, *J. Inorg. Biochem.*, 2019, **193**, 70–83.
- 32 S. Li, J. Zhao, Y. Guo, Y. Mei, B. Yuan, N. Gan, J. Zhang, J. Hu and H. Hou, *J. Inorg. Biochem.*, 2020, **210**, 111102.
- 33 T. Küster, N. Lense, F. Barna, A. Hemphill, M. K. Kindermann, J. W. Heinicke and C. A. Vock, *J. Med. Chem.*, 2012, **55**, 4178–4188.
- 34 M. Juszczak, M. Kluska, A. Kosińska, M. Palusiak, A. J. Rybarczyk-Pirek, K. Wzgarda-Raj, B. Rudolf and K. Woźniak, *Appl. Organomet. Chem.*, 2022, e6595.
- 35 B. Rudolf, J. Walendowska and J. Zakrzewski, *J. Organomet. Chem.*, 2002, **648**, 293–296.
- 36 R. S. Cahn, C. Ingold and V. Prelog, *Angew. Chem., Int. Ed. Engl.*, 1966, 385–415.
- 37 H. D. Flack, *Acta Crystallogr., Sect. A: Found. Crystallogr.*, 2009, **65**, 371–389.
- 38 I. Bernal, J. Cetrullo and W. G. Jackson, *J. Coord. Chem.*, 1993, **28**, 89–95.
- 39 J. W. Faller and P. P. Fontaine, *Organometallics*, 2005, **24**, 4132–4138.
- 40 J. W. Faller and N. Sarantopoulos, *Cryst. Growth Des.*, 2005, **5**, 2356–2361.
- 41 J. W. Faller and P. P. Fontaine, *J. Organomet. Chem.*, 2006, **691**, 4667–4675.
- 42 K. A. Lazarou, K. González-Nieves, I. Chakraborty and R. G. Raptis, *Angew. Chem., Int. Ed.*, 2019, **58**, 7324–7328.
- 43 C. L. Yadav, G. Rajput, K. K. Bisht, M. G. B. Drew and N. Singh, *Inorg. Chem.*, 2019, **58**, 14449–14456.
- 44 A. Lennartson, M. Vestergren and M. Håkansson, *Chem. – Eur. J.*, 2005, **11**, 1757–1762.
- 45 P. Bonakdarzadeh, F. Pan, E. Kalenius, O. Jurček and K. Rissanen, *Angew. Chem., Int. Ed.*, 2015, **54**, 14890–14893.
- 46 C. Xu, Q. Lin, C. Shan, X. Han, H. Wang, H. Wang, W. Zhang, Z. Chen, C. Guo, Y. Xie, X. Yu, B. Song, H. Song, L. Wojtas and X. Li, *Angew. Chem., Int. Ed.*, 2022, **61**, e202203099.
- 47 J. W. Faller, A. R. Lavoie and J. Parr, *Chem. Rev.*, 2003, **103**, 3345–3368.
- 48 P. H. Dixneuf, T. Guyot, M. D. Ness and S. M. Roberts, *Chem. Commun.*, 1997, 2083–2084.
- 49 Z. Zhang, T. Roisnel, P. H. Dixneuf and J.-F. Soulé, *Angew. Chem., Int. Ed.*, 2019, **58**, 14110–14114.
- 50 N. P. Singh, M. T. McCoy, R. R. Tice and E. L. Schneider, *Exp. Cell Res.*, 1988, **175**, 184–191.
- 51 M. Abid, F. Shamsi and A. Azam, *Mini-Rev. Med. Chem.*, 2016, **16**, 772–786.
- 52 I. Bratsos, S. Jedner, T. Gianferrara and E. Alessio, *Chimia*, 2007, **61**, 692.
- 53 J. Qian, R. Liu, N. Liu, C. Yuan, Q. Wu, Y. Chen, W. Tan and W. Mei, *Molecules*, 2022, **27**(10), 3046.
- 54 I. O. Travassos, F. Mello-Andrade, R. P. Caldeira, W. C. Pires, P. F. F. da Silva, R. S. Correa, T. Teixeira, A. Martins-Oliveira, A. A. Batista and E. P. de Silveira-Lacerda, *J. Biol. Inorg. Chem.*, 2021, **26**, 385–401.
- 55 R. A. De Grandis, K. M. Oliveira, A. P. M. Guedes, P. W. S. Dos Santos, A. F. Aissa, A. A. Batista and F. R. Pavan, *Front. Oncol.*, 2021, **11**, 682968.
- 56 J. Chen, Y. Zhang, G. Li, F. Peng, X. Jie, J. She, G. Dongye, Z. Zou, S. Rong and L. Chen, *J. Biol. Inorg. Chem.*, 2018, **23**, 261–275.
- 57 Y. Li, Q. Wu, G. Yu, L. Li, X. Zhao, X. Huang and W. Mei, *Eur. J. Med. Chem.*, 2019, **164**, 282–291.
- 58 J. Chen, F. Peng, Y. Zhang, B. Li, J. She, X. Jie, Z. Zou, M. Chen and L. Chen, *Eur. J. Med. Chem.*, 2017, **140**, 104–117.
- 59 J. Li, L. Zeng, Z. Wang, H. Chen, S. Fang, J. Wang, C.-Y. Cai, E. Xing, X. Liao, Z.-W. Li, C. R. Ashby Jr., Z.-S. Chen, H. Chao and Y. Pan, *Adv. Mater.*, 2022, **34**, 2100245.
- 60 H. R. Drew, R. M. Wing, T. Takano, C. Broka, S. Tanaka, K. Itakura and R. E. Dickerson, *Proc. Natl. Acad. Sci. U. S. A.*, 1981, **78**, 2179–2183.



- 61 H. Song, J. T. Kaiser and J. K. Barton, *Nat. Chem.*, 2012, **4**, 615–620.
- 62 D. Patel, M. Athar and P. C. Jha, *ChemistrySelect*, 2021, **6**, 8189–8199.
- 63 *CrysAlisPRO software system*, 2020.
- 64 G. M. Sheldrick, *Acta Crystallogr., Sect. C: Struct. Chem.*, 2015, **71**, 3–8.
- 65 A. L. Spek, *Acta Crystallogr., Sect. D: Biol. Crystallogr.*, 2009, **65**, 148–155.
- 66 L. J. Farrugia, *J. Appl. Crystallogr.*, 2012, **45**, 849–854.
- 67 A. J. Bodner, S. Tsai, R. C. Ting, S. J. Collins and R. C. Gallo, *Leuk. Res.*, 1980, **4**, 151–154.
- 68 K. Bhalla, A. Hindenburg, R. N. Taub and S. Grant, *Cancer Res.*, 1985, **45**, 3657–3662.
- 69 J. O'Brien, I. Wilson, T. Orton and F. Pognan, *Eur. J. Biochem.*, 2000, **267**, 5421–5426.
- 70 P. Tokarz, A. W. Piastowska-Ciesielska, K. Kaarniranta and J. Blasiak, *Int. J. Mol. Sci.*, 2016, **17**(6), 898.
- 71 A. A. Adeniyi and P. A. Ajibade, *Molecules*, 2013, **18**, 3760–3778.
- 72 G. M. Morris, R. Huey, W. Lindstrom, M. F. Sanner, R. K. Belew, D. S. Goodsell and A. J. Olson, *J. Comput. Chem.*, 2009, **30**, 2785–2791.
- 73 J. A. Lemkul, *Living J. Comp. Mol. Sci.*, 2018, **1**(1), 5068.



Supplementary material

Piano-stool ruthenium(II) complexes with maleimide and phosphine or phosphite ligands: Synthesis and activity against normal and cancer cells

Michał Juszcak ¹, Sujoy Das ², Aneta Kosińska ², Agnieszka J. Rybarczyk-Pirek ³, Kinga Wzgarda-Raj ³, Paulina Tokarz ¹, Saranya Vasudevan ⁴, Arkadiusz Chworos ⁴, Katarzyna Woźniak ^{1*}, Bogna Rudolf ^{2*}.

¹ University of Lodz, Faculty of Biology and Environmental Protection, Department of Molecular Genetics, Pomorska 141/143, 90-236, Lodz, Poland

² University of Lodz, Faculty of Chemistry, Department of Organic Chemistry, Tamka 12, 91-403 Lodz, Poland

³ University of Lodz, Faculty of Chemistry, Department of Physical Chemistry, Pomorska 163/165, 90-236 Lodz, Poland

⁴ Centre of Molecular and Macromolecular Studies, Polish Academy of Sciences, Sienkiewicza 112, 90-363 Lodz, Poland

Supplementary Materials

1.1. Crystallographic and experimental data

Table S1. Selected bond lengths [Å] and angles [°].

Table S2. Geometric parameters of selected hydrogen bonds—distances [Å] and angles [°].

Fig. S1. Molecular Hirshfeld surface analysis **2a** and **2b**.

1.2. Spectra and spectral data

Fig. S2-S6. Spectral data of compound **2a**.

Fig. S7-S11. Spectral data of compound **2b**.

Fig. S12-S16. Spectral data of compound **3a**.

Fig. S17-S21. Spectral data of compound **3b**.

Fig. S22-S26. Spectral data of compound **3c**.

1.3. Absorption and Emission studies

Fig. S27. Comparative absorbance (a) and emission (b) spectra of **1**, **2a**, **2b**, **3a**, **3b** and **3c** in Chloroform. Excitations were recorded at 300 nm.

1.4. Biological studies

Table S3. The viability of HL-60 cells, HL-60/DR cells and PBM cells after 2 h incubation with ruthenium complexes.

Table S4. The viability of HL-60 cells, HL-60/DR cells and PBM cells after 24 h incubation with ruthenium complexes.

Fig. S28. The process of derivation of doxorubicin resistant HL-60 cells line (HL-60/DR). First, HL-60 cells were treated with doxorubicin concentration from 1 to 10000 nM (0 nM). Then cells were treated for 6 days with 20 nM doxorubicin, as was described in the Materials and Methods section (20 nM – T0). Next cells were incubated with pure IMDM medium like HL-60 cells (20 nM – T7). Then cells were incubated for 6 days with 50 nM doxorubicin (50 nM – T0). After this time cells were harvested like normal HL-60 cells for one week (50 nM – T7). Then cells were used for experiments as HL-60/DR. The horizontal line represents viability at a level of 50%.

Fig. S29. The effect of ruthenium complexes **1**, **2a**, and **3a** on the apoptosis of HL-60 cells. Representative flow cytometric dot plots showing the percentage of cells in viable (Q3), early apoptotic (Q4), late apoptotic (Q2), and necrotic (Q1) stages. The positive control were cells incubated with 20 μ M camptothecin (CAM) for 24 h at 37 $^{\circ}$ C. Data represent means \pm SD of 3 experiments.

Fig. S30. The effect of ruthenium complexes **1**, **2a** and **3a** on the apoptosis of HL-60/DR cells. Data represent means \pm SD of three experiments. The CAM sample were cells incubated with 20 μ M camptothecin for 24 h at 37 $^{\circ}$ C.

1.5. Docking studies

Fig. S31. Ruthenium(II) complexes **1** (a, b) and **2b** (c, d) with fully complemented DNA (a, c) and with mismatched DNA (b, d).

1.1. X-ray structure determination

Hirshfeld surface analysis

Hirshfeld surfaces were generated with the use of *CrystalExplorer3.0* program [1] using the automatic procedures. They have been mapped with d_{norm} , a parameter which reflects intermolecular distances. Negative values of d_{norm} , indicating contacts shorter than the sum of van der Waals radii are visualized in red, while positive values of contacts longer than the sum of van der Waals radii, are colored in blue. The white color denotes intermolecular distances close to van der Waals contacts. The Hirshfeld surface fingerprint plots were generated using d_i (distance from the surface to the nearest atom in the molecule itself) and d_e (distance from the surface to the nearest atom in another molecule) as a pair of coordinates, at intervals of 0.01 \AA , in two-dimensional histograms. Under special investigations were contacts of the type H...O.

Table S1. Selected bond lengths [\AA] and angles [$^{\circ}$]

Ru1-N1	2.096(1)	2.104(1)
Ru1-P1	2.310(1)	2.285(2)
Ru1-C20	1.869(3)	1.865(2)
Ru1-Cg1	1.882(3)	1.875(2)
Ru1-C11	2.215(2)	2.213(1)
Ru1-C12	2.208(2)	2.251(2)
Ru1-C13	2.243(2)	2.258(2)
Ru1-C14	2.260(2)	2.239(2)
Ru1-C15	2.260(2)	2.201(2)
P1-C21	1.833(2)	1.808(2)
P1-C31	1.830(2)	1.801(1)
P1-C41	1.835(2)	1.808(1)
O20-C20	1.152(3)	1.151(2)
O2-C2	1.216(3)	1.216(2)
O5-C5	1.224(3)	1.222(2)
P1-Ru1-N1	91.4(1)	90.1(1)
P1-Ru1-C20	91.6(2)	87.9(2)
N1-Ru1-C20	93.3(1)	93.6(1)
P1-Ru1-Cg1	123.0(2)	126.7(2)
N1-Ru1-Cg1	122.2(2)	123.1(2)
O2-Ru1-Cg1	126.0(2)	124.9(2)

Ru1-P1-C21	116.9(1)	115.0(1)
Ru1-P1-C31	117.4(1)	113.3(1)
Ru1-P1-C41	112.8(2)	119.5(2)
C21-P1-C31	102.1(1)	103.4(1)
C31-P1-C41	101.1(1)	102.2(1)
C21-P1-C41	104.5(1)	101.2(1)
C5-N1-Ru1	124.2(2)	124.1(2)
C2-N1-Ru1	127.8(1)	127.8(1)
O2-C20-Ru1	172.4(2)	172.4(2)
C5-N1-C20	107.9(1)	107.9(1)
N1-Ru1-P1-C21	11.0(2)	30.4(2)
N1-Ru1-P1-C31	132.9(2)	149.1(2)
N1-Ru1-P1-C41	-110.3(2)	-90.3(2)
C2-N1-Ru1-C20	-9.2(2)	-12.9(2)
C5-N1-Ru1-C20	167.5(2)	161.3(2)

Table S2. Geometric parameters of selected hydrogen bonds—distances [\AA] and angles [$^\circ$]

hydrogen bond	D-H	H...A	D...A	\angle D-H...A	symmetry
2a					
C26-H26...O2	0.95	2.51	3.199(3)	129	1+x,y,z
C35-H35...O5	0.95	2.46	3.314(3)	149	3/2-x,1-y,-1/2+z
C33-H33...O20	0.95	2.54	3.344(3)	143	1/2-x,1-y,-1/2+z
2b					
C11-H11...O5	0.95	2.43	3.334(2)	159	-1+x,y,z
C12-H12...O2	0.95	2.59	3.469(2)	153	x,-1+y,z
C43-H43...O20	0.95	2.58	3.158(2)	120	1-x, 1-y, 1-z
C44-H44...O2	0.95	2.37	3.311(2)	168	1-x, 1-y, 1-z

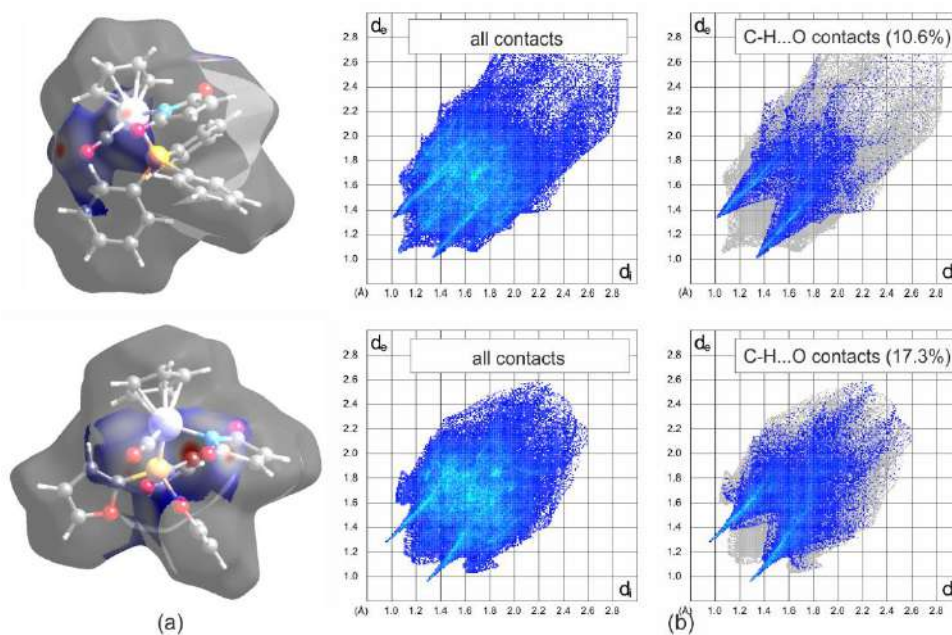


Figure S1. Molecular Hirshfeld surface analysis **2a** (at the top) and **2b** (at the bottom): surfaces mapped with color scale of d_{norm} parameter for C-H...O contacts (a) and corresponding fingerprint plots (b).

1.2. Spectra and spectral data

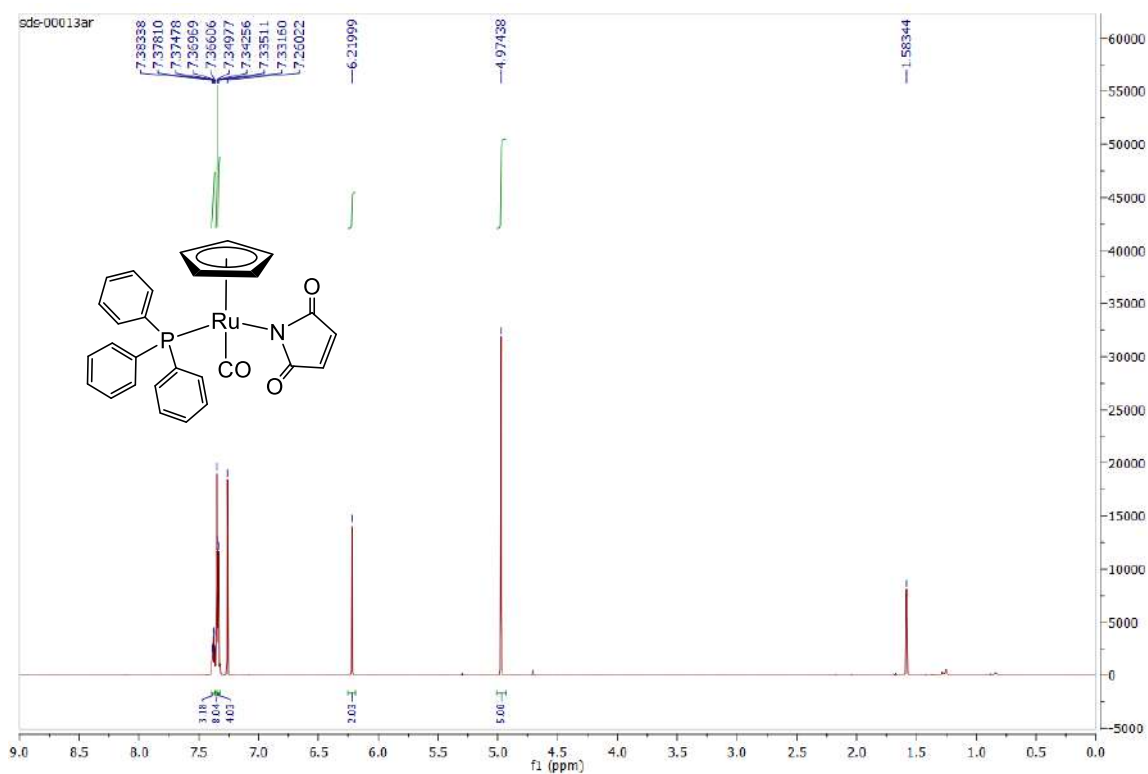


Figure S2. ^1H NMR spectra of **2a** in CDCl_3

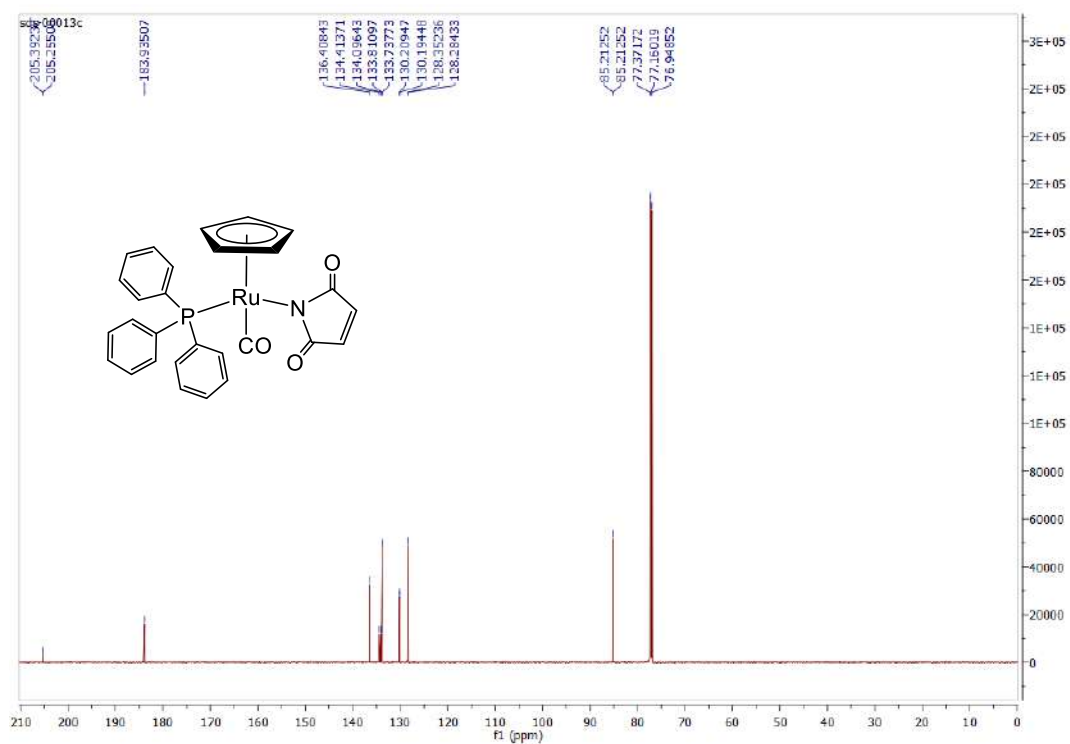


Figure S3. ^{13}C NMR spectra of **2a** in CDCl_3

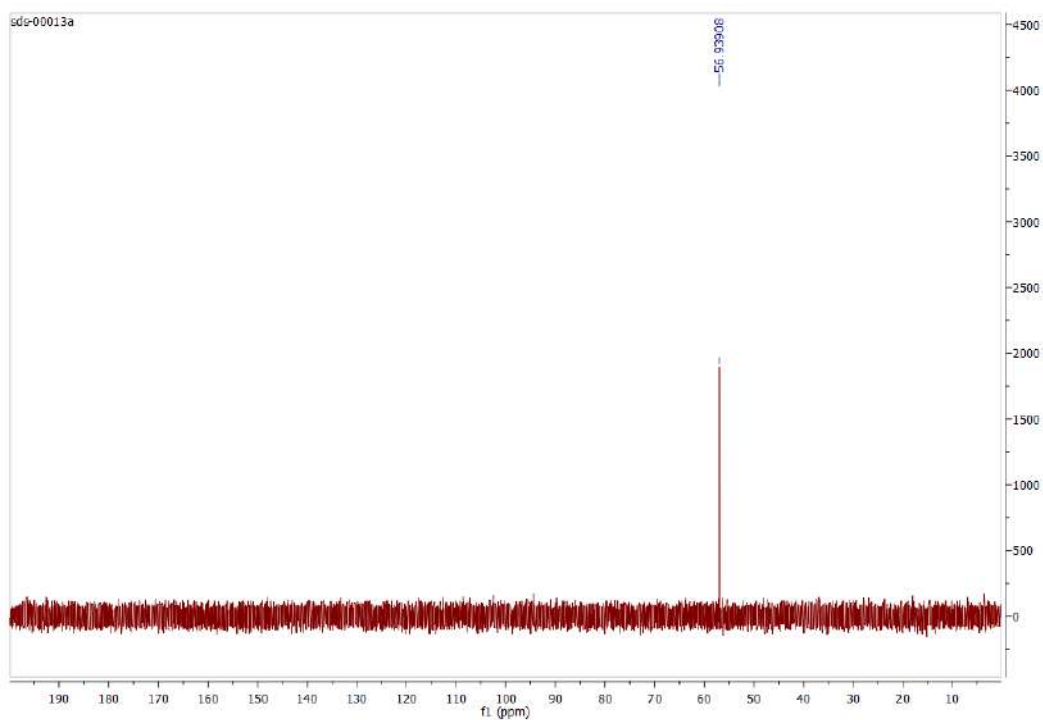


Figure S4. ^{31}P NMR spectra of **2a** in CDCl_3

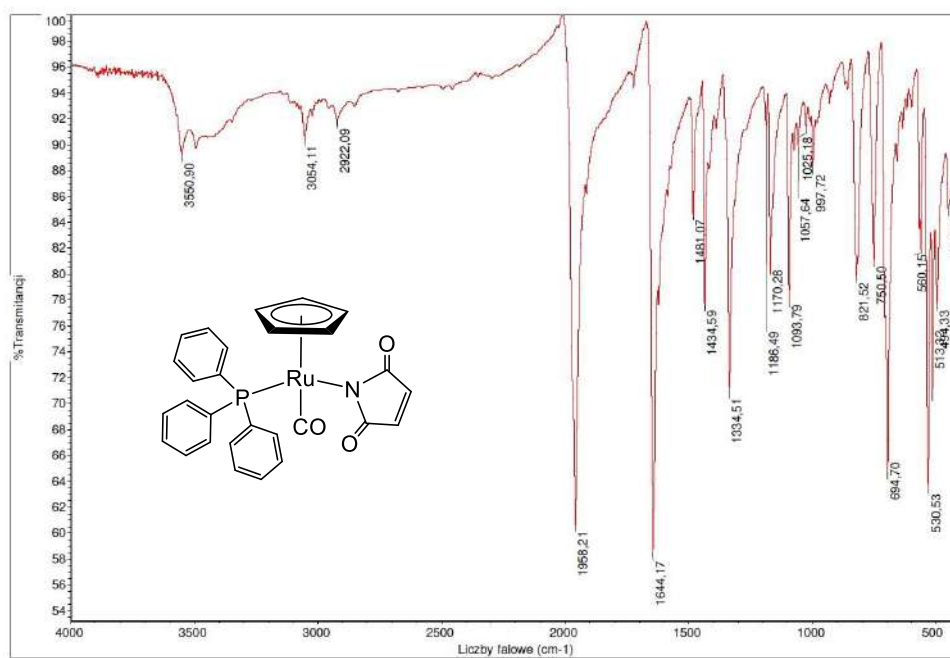


Figure S5. FTIR spectra of **2a**.

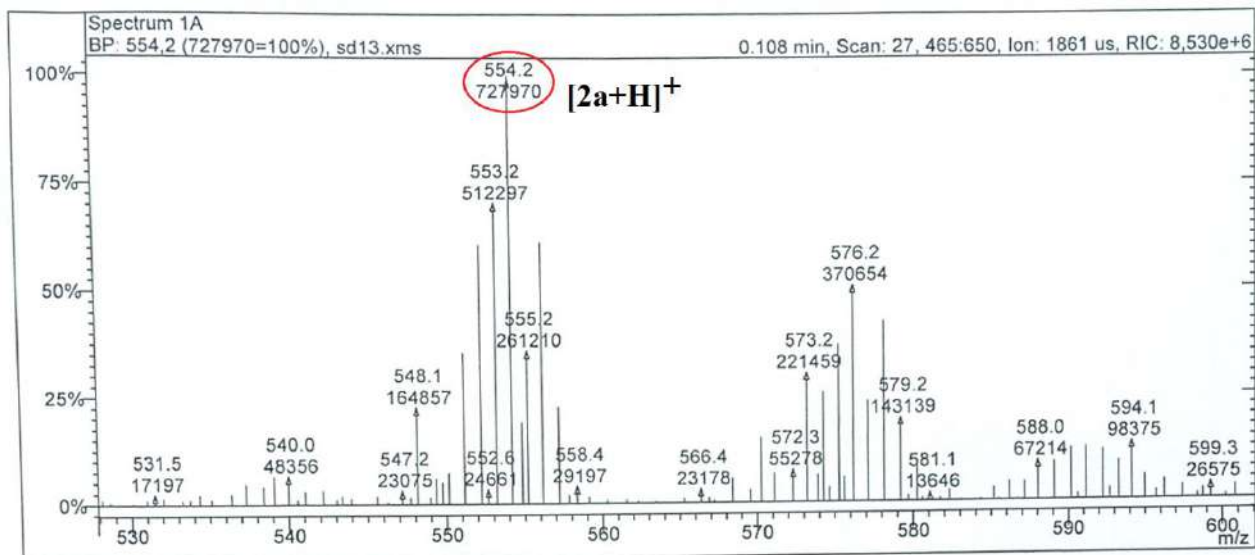


Figure S6. ESI-MS spectra of **2a**

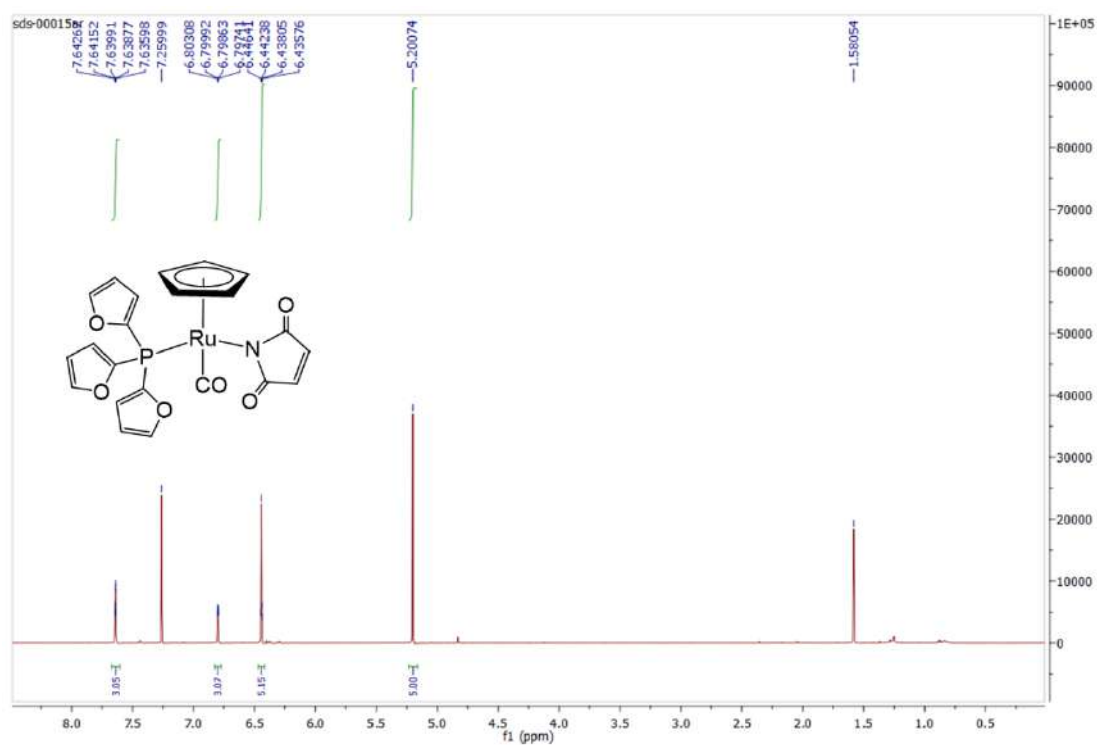


Figure S7. ¹H NMR spectra of **2b** in CDCl₃

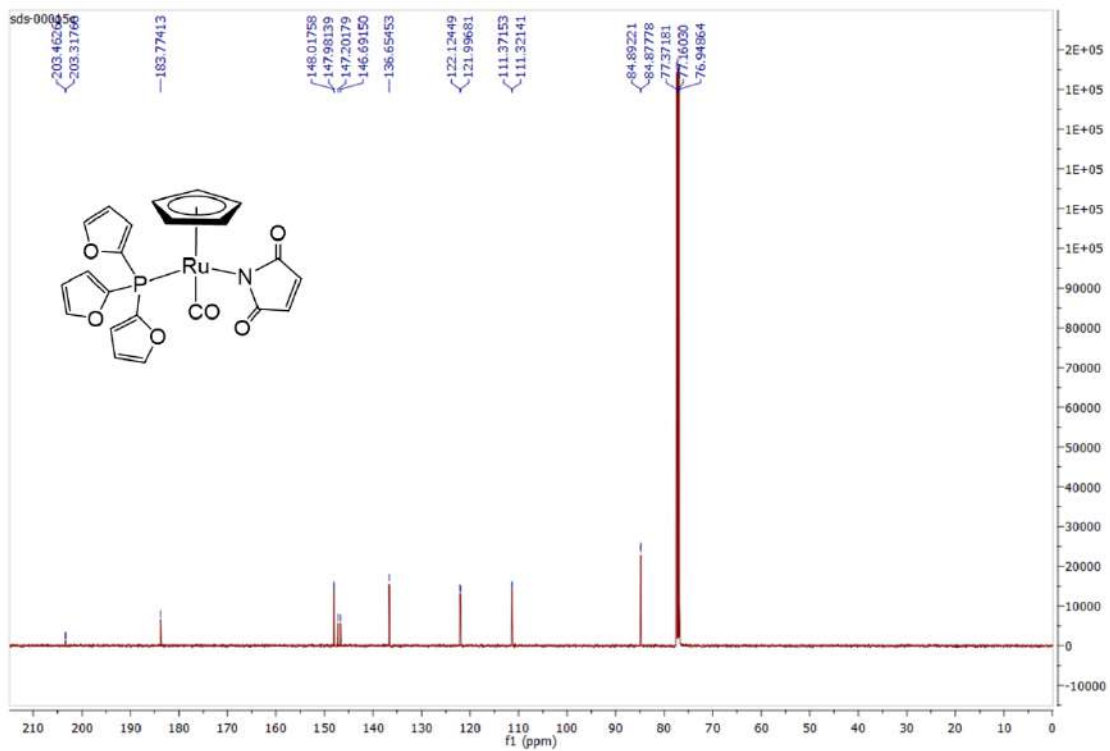


Figure S8. ^{13}C NMR spectra of **2b** in CDCl_3

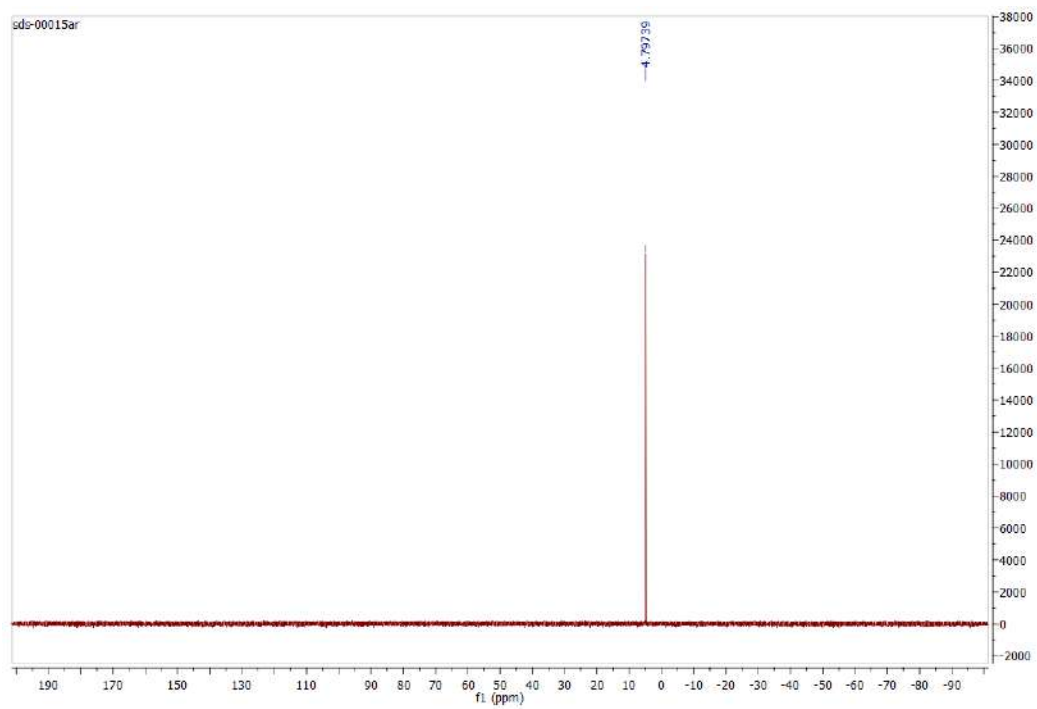


Figure S9. ^{31}P NMR spectra of **2b** in CDCl_3

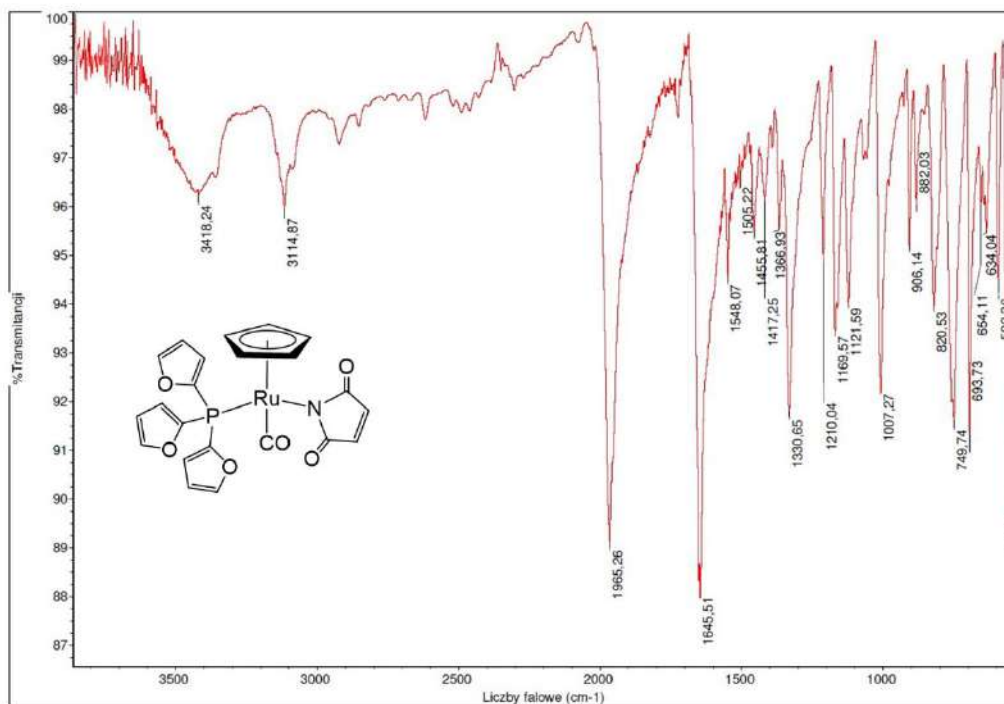


Figure S10. FTIR spectra of **2b**.

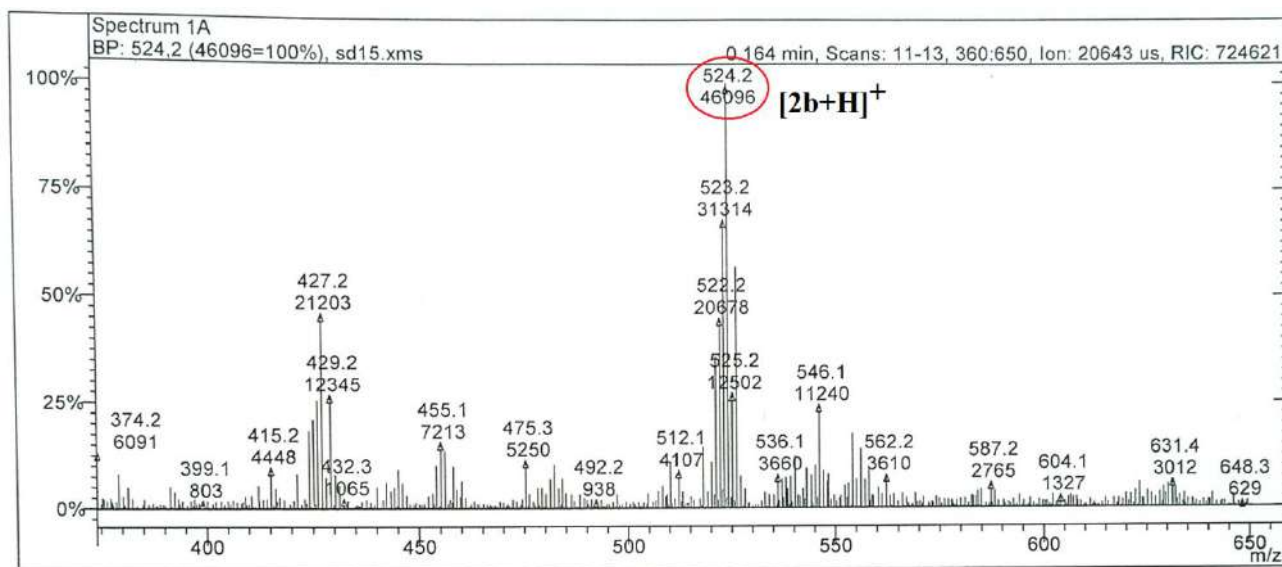


Figure S11. ESI-MS spectra of **2b**

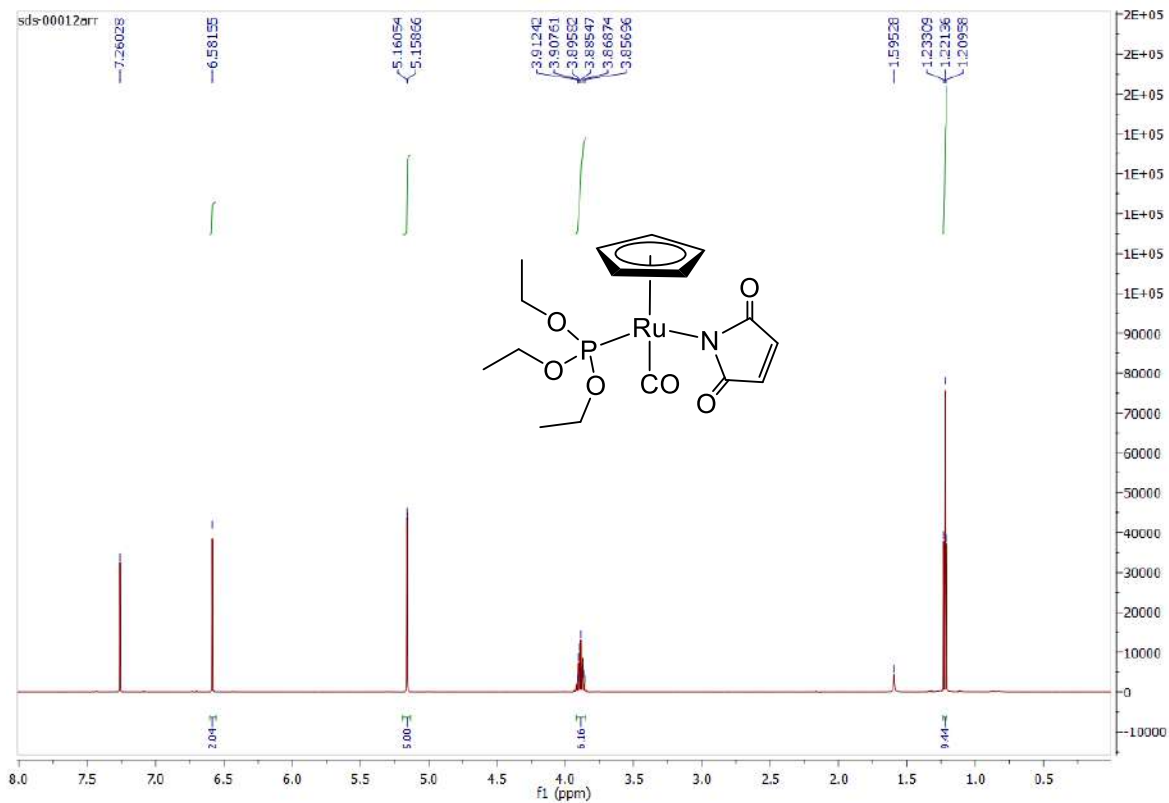


Figure S12. ¹H NMR spectra of **3a** in CDCl₃

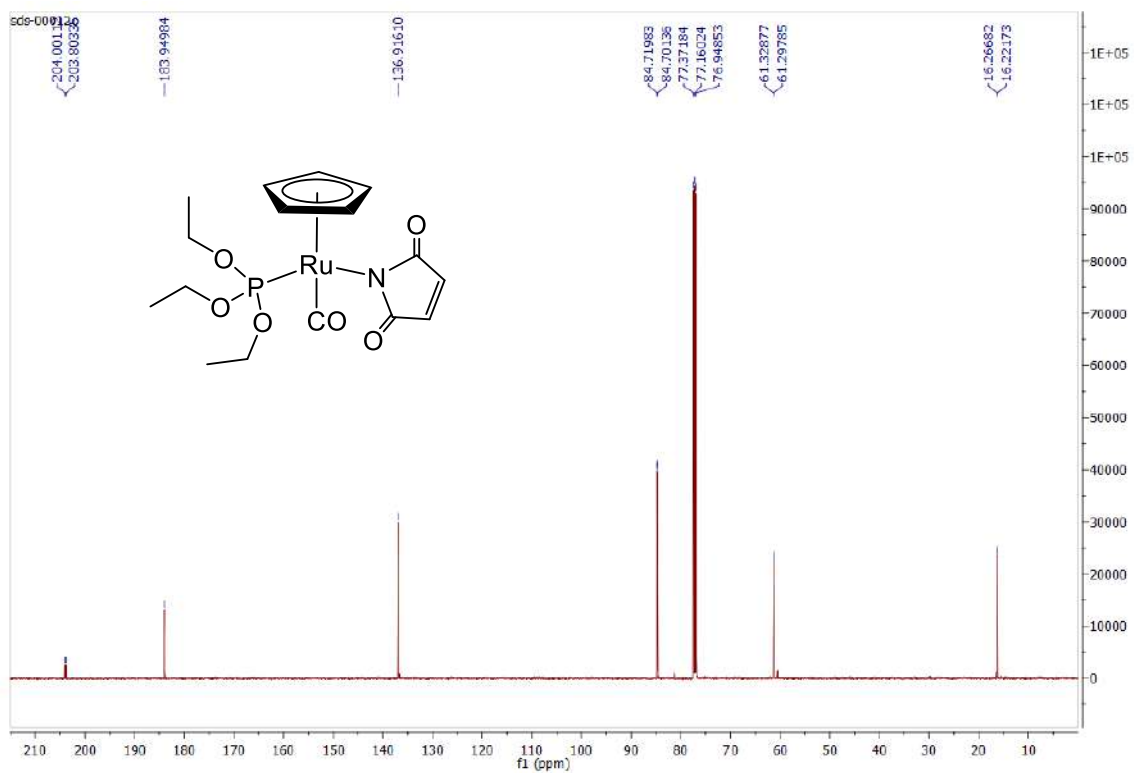


Figure S13. ¹³C NMR spectra of **3a** in CDCl₃

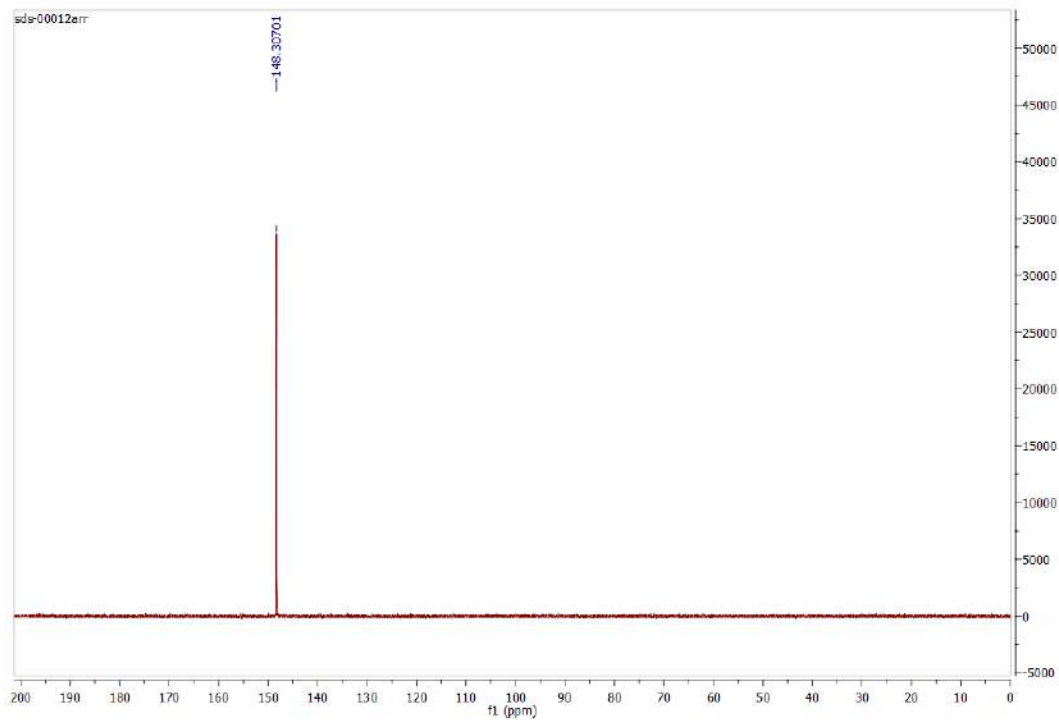


Figure S14. ³¹P NMR spectra of **3a** in CDCl₃

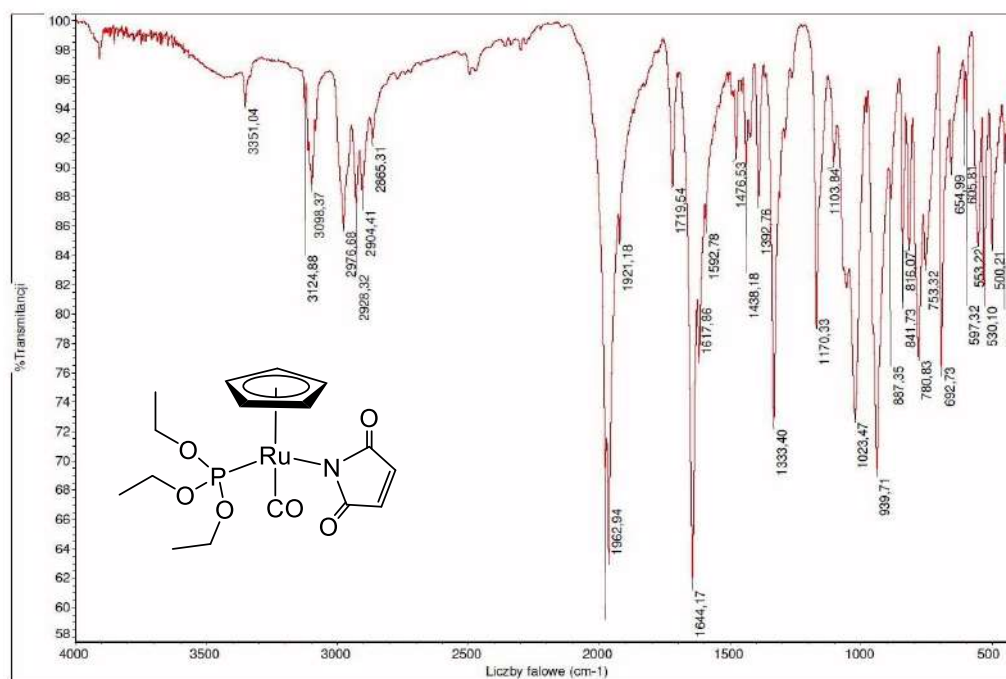


Figure S15. FTIR spectra of **3a**.

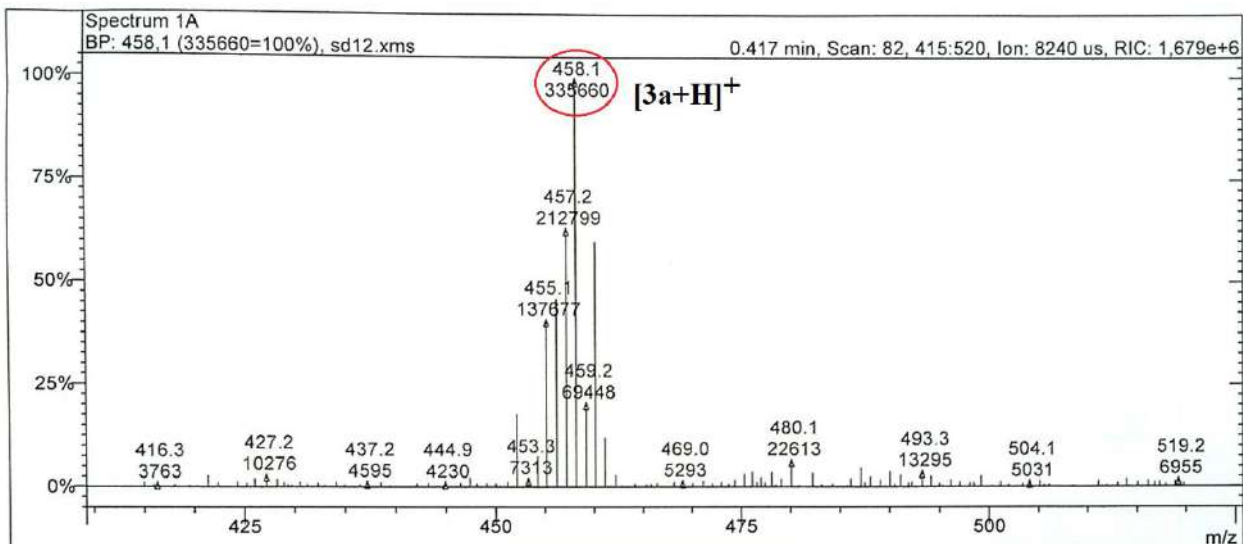


Figure S16. ESI-MS spectra of **3a**.

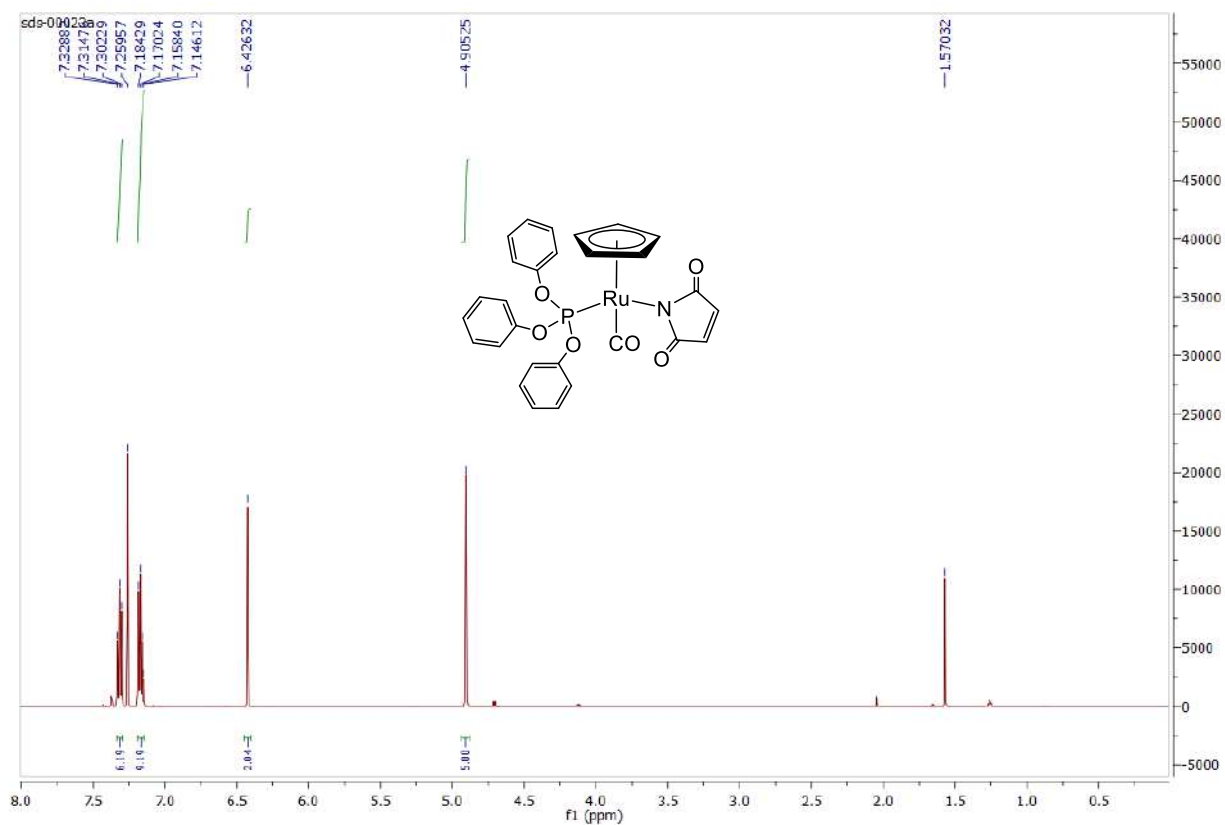


Figure S17. ^1H NMR spectra of **3b** in CDCl_3

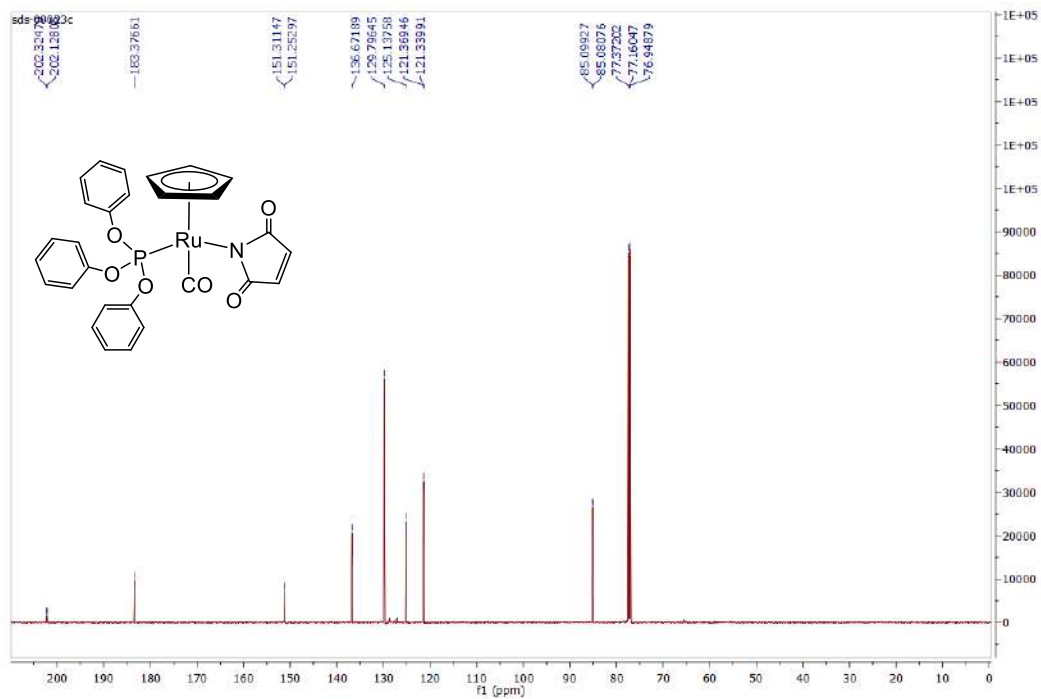


Figure S18. ^{13}C NMR spectra of **3b** in CDCl_3

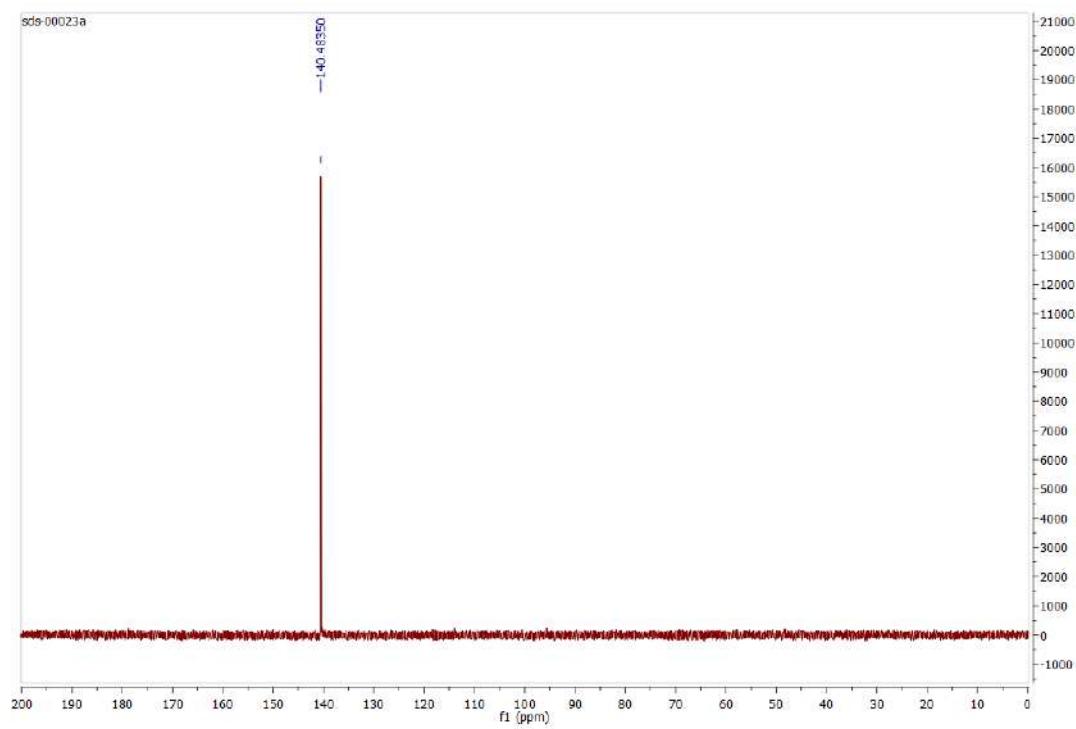


Figure S19. ^{31}P NMR spectra of **3b** in CDCl_3

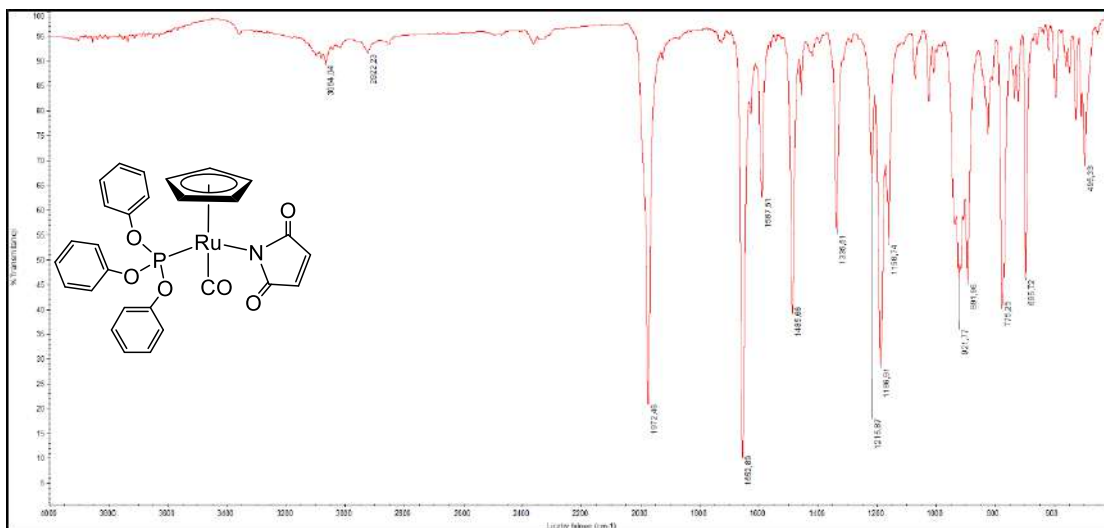


Figure S20. FTIR spectra of **3b**.

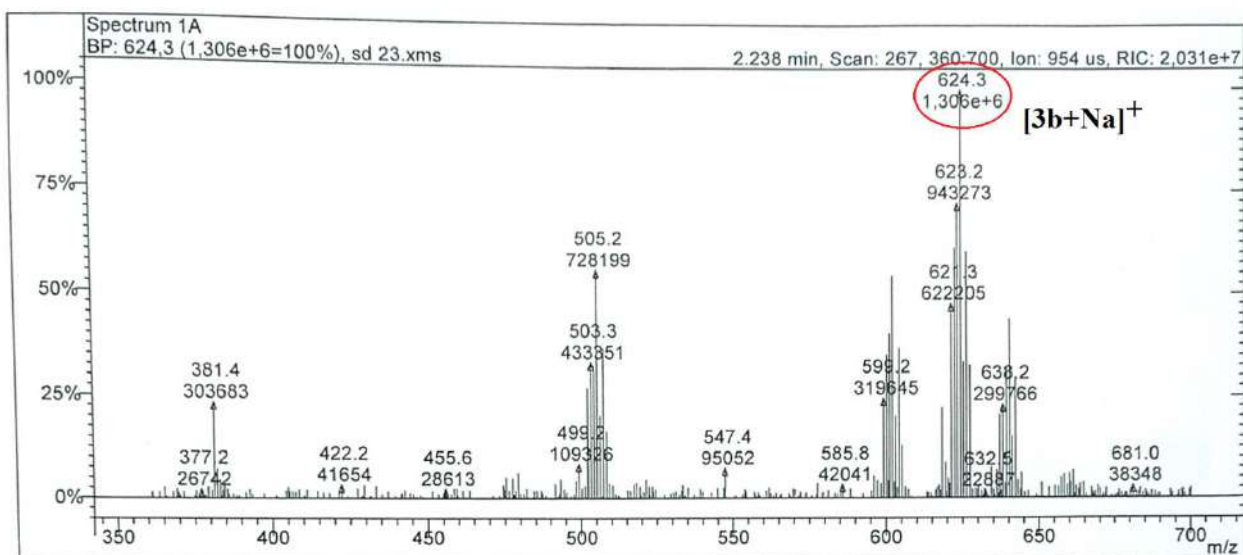


Figure S21. ESI-MS spectra of **3b**.

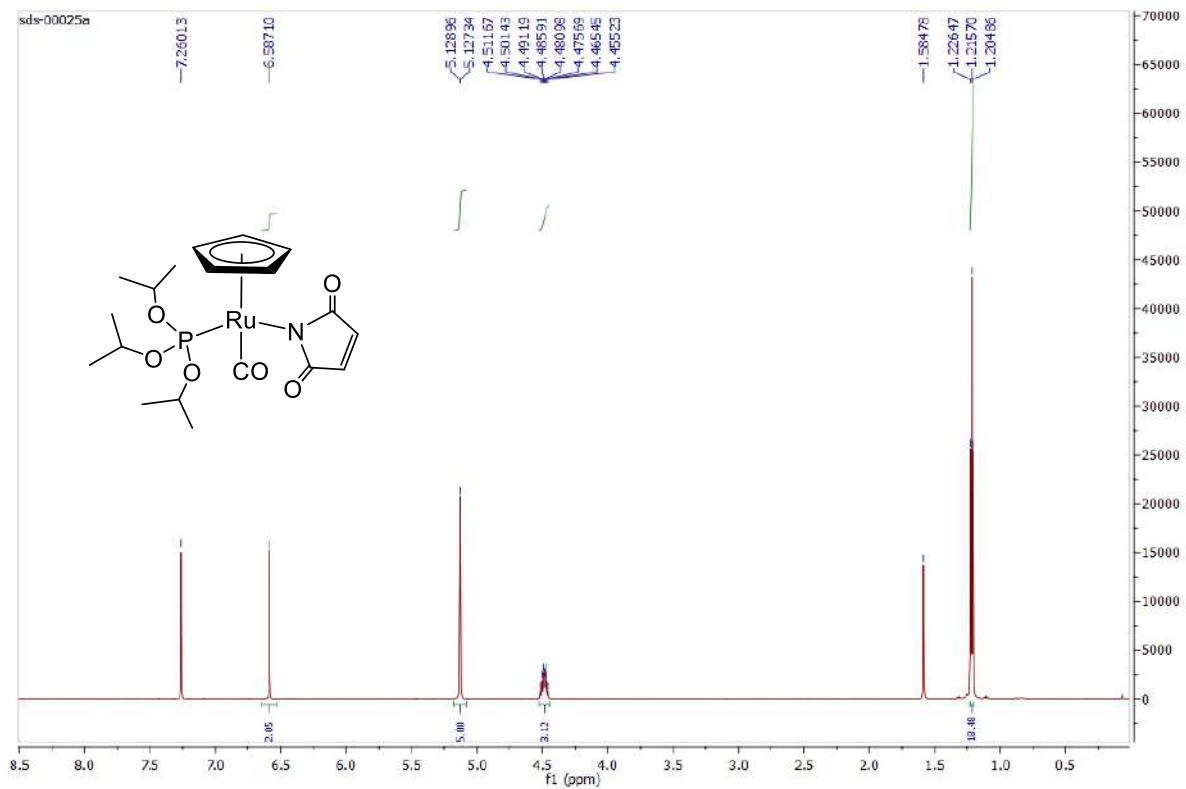


Figure S22. ^1H NMR spectra of **3c** in CDCl_3

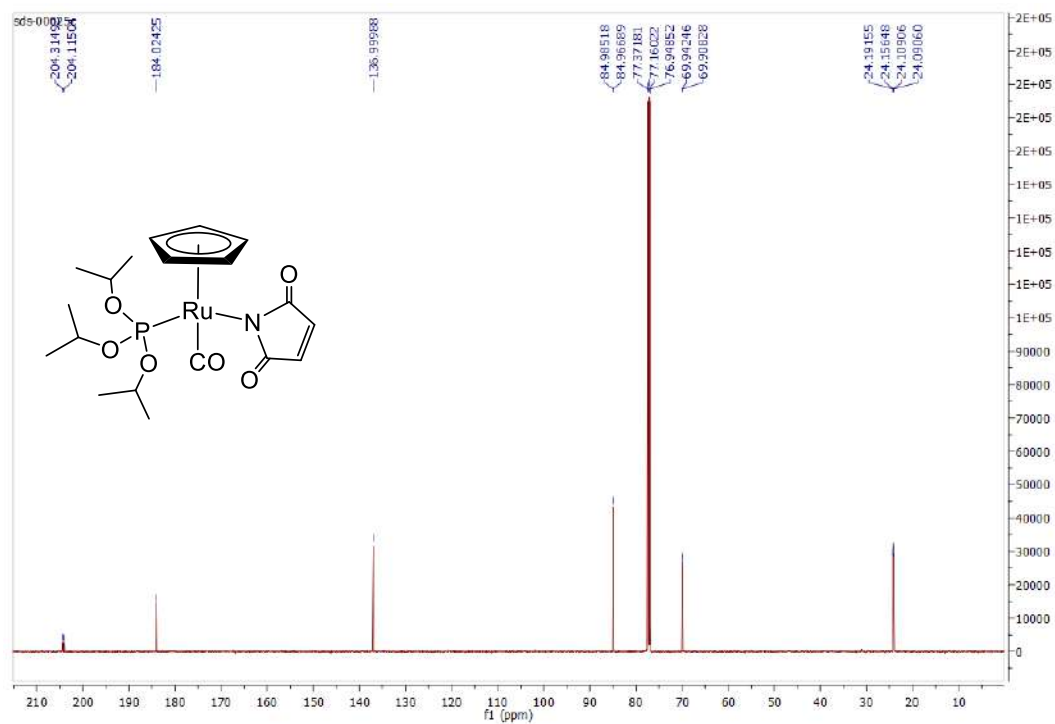


Figure S23. ^{13}C NMR spectra of **3c** in CDCl_3

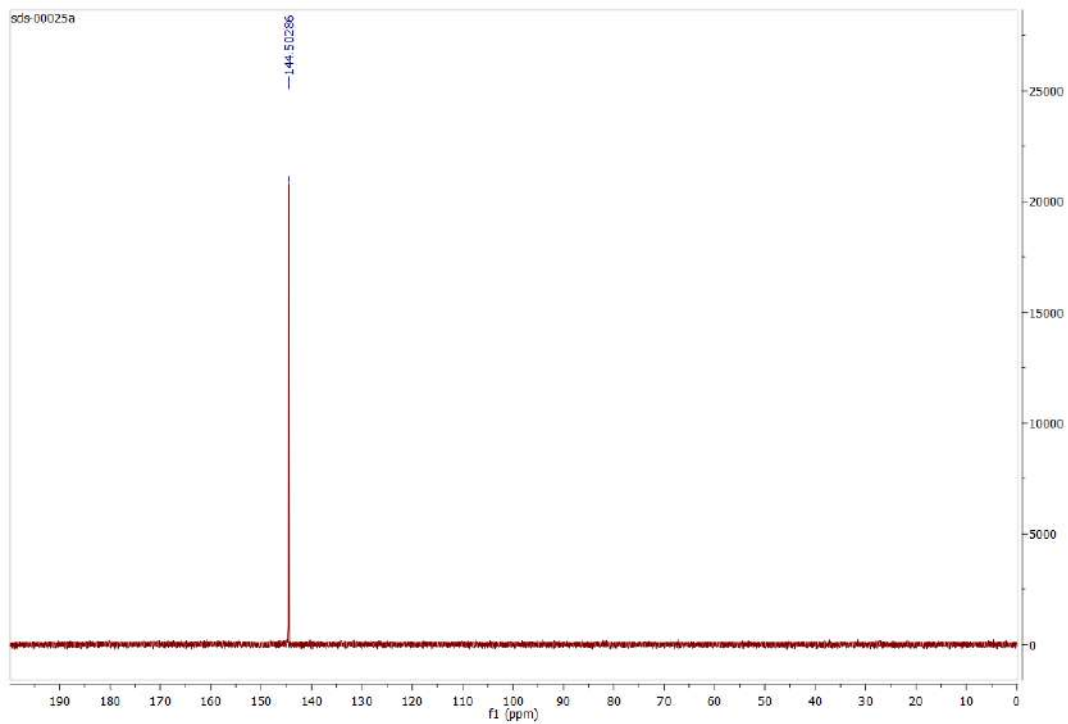


Figure S24. ^{31}P NMR spectra of **3c** in CDCl_3

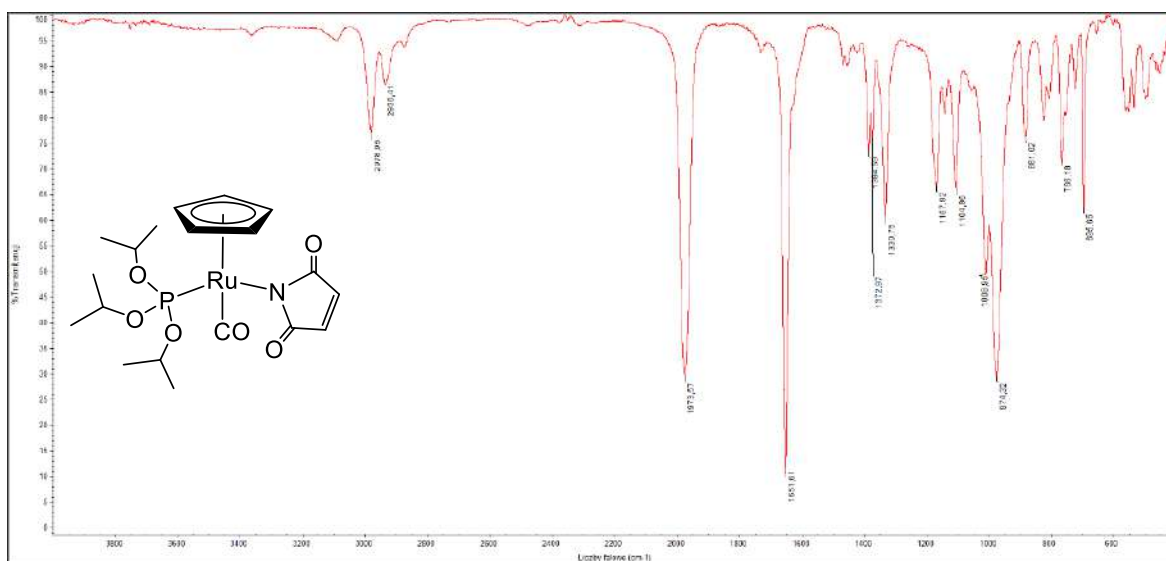


Figure S25. FTIR spectra of **3c**.

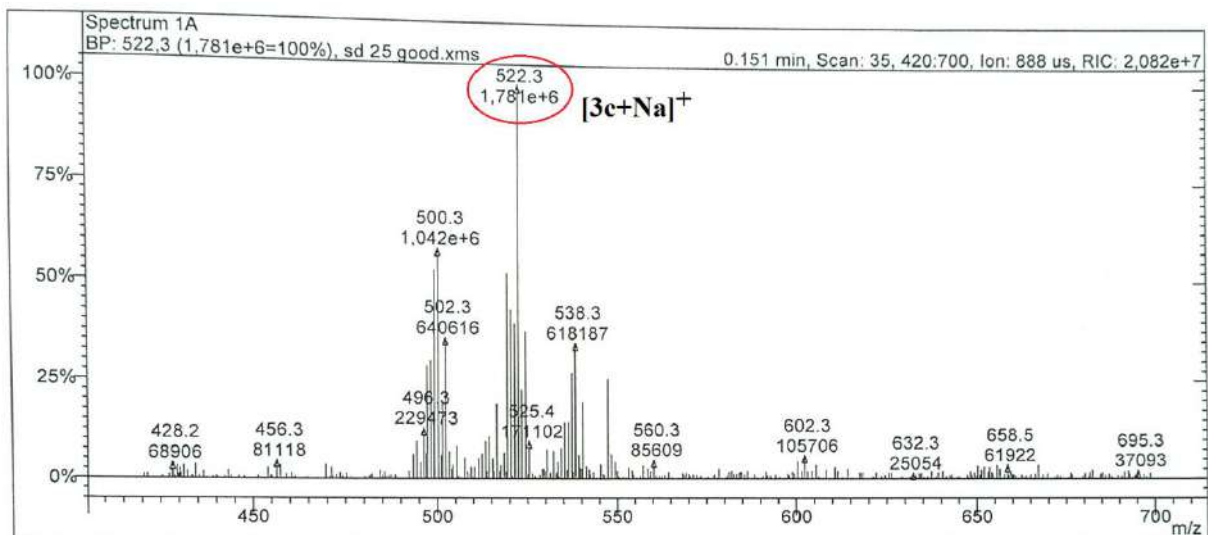


Figure S26. ESI-MS spectra of **3c**.

1.3. Absorption and Emission studies:

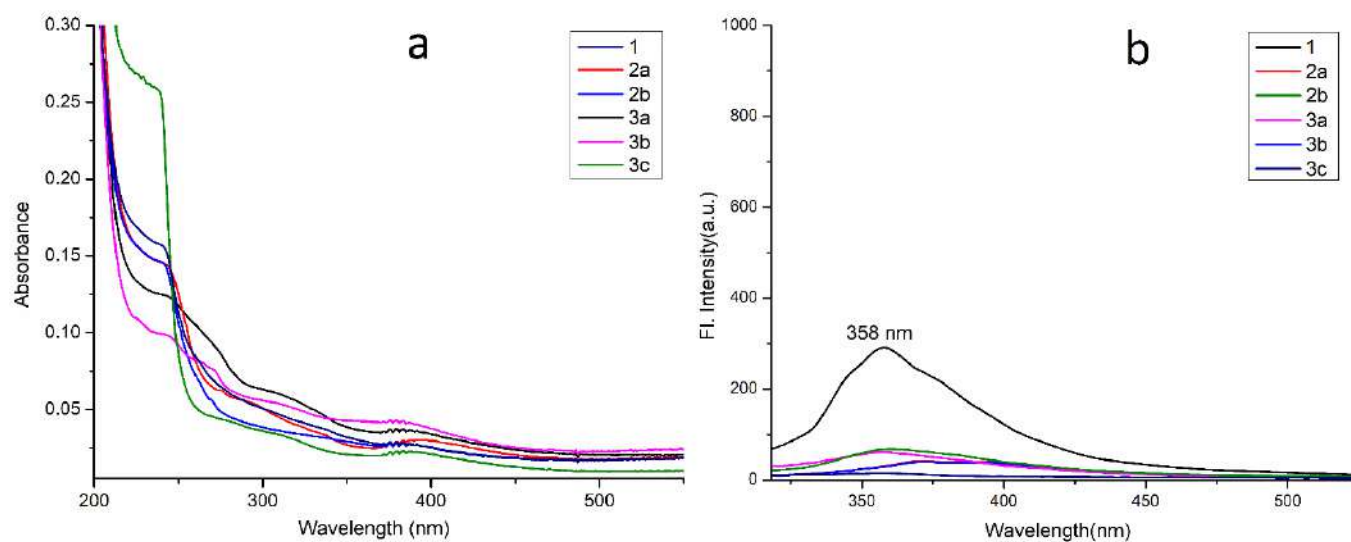


Figure S27. Comparative absorbance (a) and emission (b) spectra of **1**, **2a**, **2b**, **3a**, **3b** and **3c** in Chloroform. Excitations were recorded at 300 nm.

1.4. Biological studies

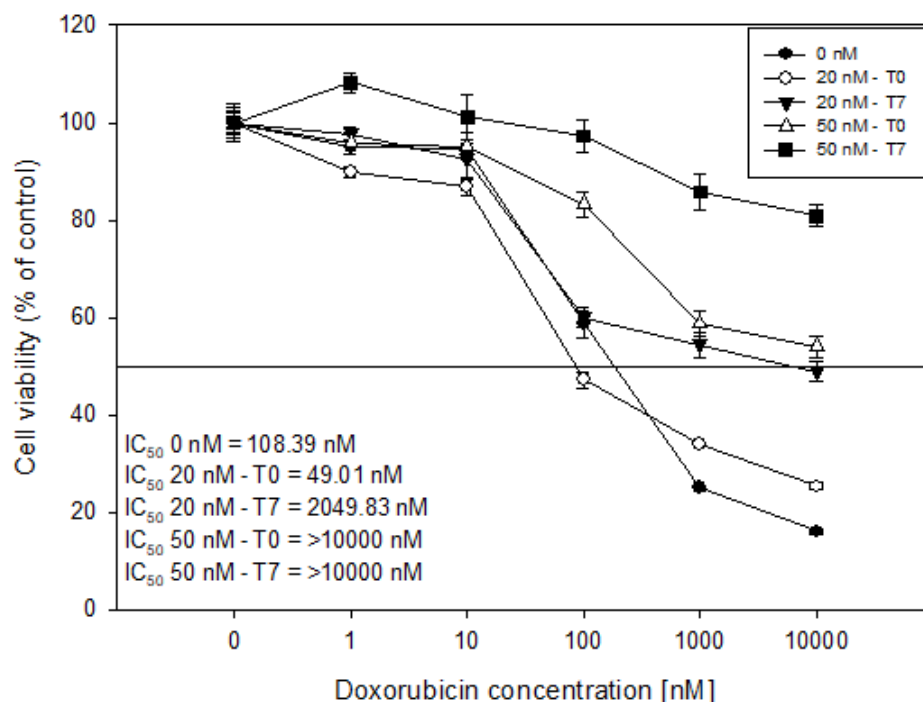


Figure S28. The process of derivation of doxorubicin resistant HL-60 cells line (HL-60/DR). First, HL-60 cells were treated with doxorubicin concentration from 1 to 10000 nM (0 nM). Then cells were treated for 6 days with 20 nM doxorubicin, as was described in the Materials and Methods section (20 nM – T0). Next cells were incubated with pure IMDM medium like HL-60 cells (20 nM – T7). Then cells were incubated for 6 days with 50 nM doxorubicin (50 nM – T0). After this time cells were harvested like normal HL-60 cells for one week (50 nM – T7). Then cells were used for experiments as HL-60/DR. The horizontal line represents viability at a level of 50%.

Table S3. The viability of HL-60 cells, HL-60/DR cells and PBM cells after 2 h incubation with ruthenium complexes. The viability for individual samples were calculated relative to control \pm SD

HL-60 cells						
Concentration (μ M)	1	2a	2b	3a	3b	3c
0.5	97.38 \pm 1.5 * \downarrow	101.56 \pm 0.29	101.67 \pm 2.77	101.8 \pm 0.53	99.94 \pm 1.63	101.42 \pm 1.73
1	96.29 \pm 1.35 ** \downarrow	98.96 \pm 2.71	100.93 \pm 1.56	99.92 \pm 2.88	98.64 \pm 2.04	98.55 \pm 1.78
2.5	91.46 \pm 2.13 *** \downarrow	99.75 \pm 1.02	99.97 \pm 2.7	99.05 \pm 1.64	99.03 \pm 1.38	101.01 \pm 0.9
5	91.62 \pm 1.52 *** \downarrow	99.36 \pm 2.36	99.89 \pm 0.56	101.79 \pm 2.37	101.16 \pm 1.74	102 \pm 1.18
10	87.03 \pm 0.28 *** \downarrow	99.94 \pm 2.31	99.59 \pm 0.35	101.83 \pm 1.95	109.95 \pm 0.43 *** \uparrow	101.11 \pm 2.28
25	73.25 \pm 2.01 *** \downarrow	99.96 \pm 0.67	99.4 \pm 3.31	98.62 \pm 3.29	123.89 \pm 1.87 *** \uparrow	122.72 \pm 4.07 *** \uparrow
50	69.16 \pm 1.74 *** \downarrow	98.85 \pm 0.48	93.77 \pm 1.6 *** \downarrow	92.26 \pm 0.96 *** \downarrow	106.79 \pm 3.9 *** \uparrow	108.46 \pm 3.83 *** \uparrow
100	59.99 \pm 0.31 *** \downarrow	91 \pm 0.71 *** \downarrow	84.6 \pm 1.89 *** \downarrow	81.85 \pm 2.67 *** \downarrow	100.13 \pm 1.35	106.61 \pm 1.6 *** \uparrow
250	16.23 \pm 0.45 *** \downarrow	94.34 \pm 0.57 *** \downarrow	47.82 \pm 4.51 *** \downarrow	87.8 \pm 0.25 *** \downarrow	88.71 \pm 0.58 *** \downarrow	102.1 \pm 0.99
HL-60/DR cells						
0.5	96.31 \pm 4.88	108.17 \pm 1.73 *** \uparrow	105.67 \pm 0.44 *** \uparrow	98.29 \pm 2.43	96.29 \pm 3.52 * \uparrow	99.43 \pm 1.25
1	94.18 \pm 1.61 *** \downarrow	105.04 \pm 4	103.85 \pm 2.49 * \uparrow	95.44 \pm 2.61	96.15 \pm 2.42 * \uparrow	97.69 \pm 1.84
2.5	94.72 \pm 2.8 *** \downarrow	101.96 \pm 5.35	103.11 \pm 1.1 ** \uparrow	96.38 \pm 2.1	97.52 \pm 2.65	97.39 \pm 3.57
5	95.14 \pm 1.19 *** \downarrow	104.61 \pm 2.75 *** \uparrow	102.92 \pm 3.24	93.24 \pm 1.96 *** \downarrow	100.65 \pm 3.12	96.52 \pm 3.69
10	92.67 \pm 0.98 *** \downarrow	110.07 \pm 4.59 *** \uparrow	102.33 \pm 2.8	94.8 \pm 4.91	103.56 \pm 1.6	101.91 \pm 2.75
25	92.87 \pm 2.68 *** \downarrow	114.54 \pm 3.8 *** \uparrow	101.95 \pm 1.71	95.92 \pm 5.31	110.73 \pm 1.87 *** \uparrow	115.31 \pm 3.89 *** \uparrow

50	91.62±1.12 *** ↓	122.85±3.33 *** ↑	103.22±0.98 ** ↑	95.57±3.32	117.61±1.1 *** ↑	120.96±2.73 *** ↑
100	93.61±2.73 *** ↓	123.91±3.86 *** ↑	105.56±1.78 *** ↑	100.71±2.7	121.13±1.64 *** ↑	135.41±2.97 *** ↑
250	91.02±2.79 *** ↓	133.47±5.23 *** ↑	115.28±2 *** ↑	112.35±4 *** ↑	125.55±1.91 *** ↑	147.02±3.43 *** ↑
PBM cells						
0.5	104.94±0.7 *** ↑	99.88±0.88	100.6±0.47	101.18±2.13	101.45±0.56	99.94±1.65
1	108.97±0.32 *** ↑	99.15±0.58	99.51±0.71	99.79±0.91	99.72±0.76	99.28±1.24
2.5	112.87±0.31 *** ↑	100.97±0.36	99.73±1.01	99.3±0.27	99.22±1.29	99.32±0.97
5	117.79±1.3 *** ↑	100.88±0.76	100.76±0.74	101.44±0.74	99.76±1.75	103.9±1.14
10	117.63±1.53 *** ↑	106.48±1.01 *** ↑	104.49±0.84 *** ↑	104.25±1.17 *** ↑	103.71±0.58 *** ↑	105.04±0.53 *** ↑
25	113.84±1.03 *** ↑	133.7±0.47 *** ↑	106.24±2.59 *** ↑	112.33±0.8 *** ↑	123.75±2.23 *** ↑	111.46±1.72 *** ↑
50	110±1.1 *** ↑	138.73±0.49 *** ↑	121.9±9.7 *** ↑	118.28±1.4 *** ↑	166.14±0.29 *** ↑	117.65±0.21 *** ↑
100	107.17±1.13 *** ↑	142.29±1.86 *** ↑	134.1±4.19 *** ↑	117.94±0.55 *** ↑	171.97±2.77 *** ↑	114.18±0.42 *** ↑
250	96.68±0.27 *** ↓	116.44±0.4 *** ↑	153.43±2.01 *** ↑	131.03±0.29 *** ↑	159.28±0.79 *** ↑	166.21±2.62 *** ↑

Cell viability in the control was taken as 100%. * p < 0.05. ** p < 0.01. *** p < 0.001. ↑ – increase. ↓ – decrease

Table S4. The viability of HL-60 cells, HL-60/DR cells and PBM cells after 24 h incubation with ruthenium complexes. The viability for individual samples were calculated relative to control ± SD.

Concentration (μM)	HL-60 cells					
	1	2a	2b	3a	3b	3c
0.5	108.6±0.49*** ↑	100.58±1.25	101.04±0.36	104.06±0.9*** ↑	99.54±2.15	100.44±1.9
1	109.83±3.3*** ↑	99.88±2.69	101.74±1.24	105.49±0.8*** ↑	104.42±2.8*** ↑	100.96±1.68
2.5	103.77±1.7*** ↑	98.95±2.14	103.88±2.16*** ↑	106.57±1.2*** ↑	102.39±3.48	102.81±1.38
5	56.77±1.77*** ↓	99.89±1.58	102.86±1	106.32±1.9*** ↑	102.19±2.39	104.3±1.02*** ↑
10	38.45±1.38*** ↓	101.36±1.63	99.74±0.83	72.02±7.4*** ↓	62.11±1.66*** ↓	98.55±3.27
25	36.46±0.32*** ↓	48.93±2.18*** ↓	55.44±4.36*** ↓	36.56±1.03*** ↓	63.73±3.53*** ↓	42.26±1.07*** ↓
50	8.14±0.44*** ↓	39.02±1.65*** ↓	34.01±0.3*** ↓	37.36±0.58*** ↓	46.62±1.01*** ↓	40±0.8*** ↓
100	4.1±0.28*** ↓	38.19±1.24*** ↓	35.27±1.17*** ↓	33.49±1.38*** ↓	42.31±1.02*** ↓	25.5±1.11*** ↓
250	2.14±0.12*** ↓	28.23±0.19*** ↓	4.96±0.17*** ↓	9.31±0.45*** ↓	44.05±0.52*** ↓	15.33±2.71*** ↓
HL-60/DR cells						
0.5	99.31±4.37	102.34±1.99	98.58±1.55	96.33±4.74	104.4±1.22*** ↑	97.79±9.71
1	95.75±4.99	96.98±3.8	97.63±2.02	97.36±4.66	101.9±3.23	104.08±1.27*** ↑
2.5	95.68±7.05	96.52±1.48	97.44±2.3	97.74±1.86	101.29±2.56	102.42±2.55
5	95.4±4.21	91.63±9.53	97.29±2.4	94.5±0.87*** ↓	102.02±1.75	102.08±1.86
10	92.72±3.09*** ↓	103.87±3.88	95.18±8.51	93.16±4.89*** ↓	107.78±6.08	105.42±4.15
25	91.18±2.04*** ↓	116.68±5.2*** ↑	101.41±5.79	93.18±3.98*** ↓	96.98±3.27	118.92±1.8*** ↑
50	89.09±2.71*** ↓	112.51±2.6*** ↑	101.85±4.07	92.17±2.88*** ↓	58.63±0.7*** ↓	128.04±1.0*** ↑
100	78.25±0.84*** ↓	102.81 ± 3.54	72.21±2.65	91.43±2.0*** ↓	52.8±1.19*** ↓	88.87±4.6*** ↓
250	46.9±1.36*** ↓	53.6±11.79*** ↓	26.75±0.68*** ↓	66.38±2.18*** ↓	36.42±2.03*** ↓	5.21±0.1*** ↓
PBM cells						
0.5	108.4±2.48*** ↑	100.44±0.73	103.79±2.53* ↑	103.32±0.75*** ↑	99.82±2.86	94.2±4.03*** ↓
1	119.9±3.65*** ↑	101.22±3.01	101.37±0.51	103.08±2.06* ↑	96.6±0.18** ↓	91.26±3.15*** ↓
2.5	112.9±0.56*** ↑	101.83±2.7	104.07±1.51*** ↑	104.83±2.1*** ↑	97.55±4.03	92.39±3.49*** ↓
5	103.41±1.68*** ↑	100.18±1.98	93.14±0.85*** ↓	108.4±1.81*** ↑	88.3±2.63*** ↓	80.62±0.84*** ↓
10	83.3±0.65*** ↓	44.63±0.13*** ↓	47.94±2*** ↓	106.8±2.71*** ↑	19.74±1.91*** ↓	55.19±2.08*** ↓

25	77±2.17***↓	10.31±1***↓	24.54±0.49***↓	85.14±1.42***↓	10.06±0.34***↓	28.77±2.03***↓
50	61.47±1.24***↓	9.87±0.25***↓	24.12±0.67***↓	83.76±0.55***↓	6.55±0.14***↓	15.11±0.25***↓
100	45.15±1.4***↓	10.97±0.39***↓	21.28±4.36***↓	64.48±0.7***↓	7.22±1.23***↓	13.77±0.2***↓
250	18.46±0.43***↓	9.36±0.72***↓	7.09±0.38***↓	56.73±0.35***↓	6.12±0.9***↓	8.34±0.25***↓

Cell viability in the control was taken as 100%. * $p < 0.05$. ** $p < 0.01$. *** $p < 0.001$. ↑ – increase, ↓ – decrease

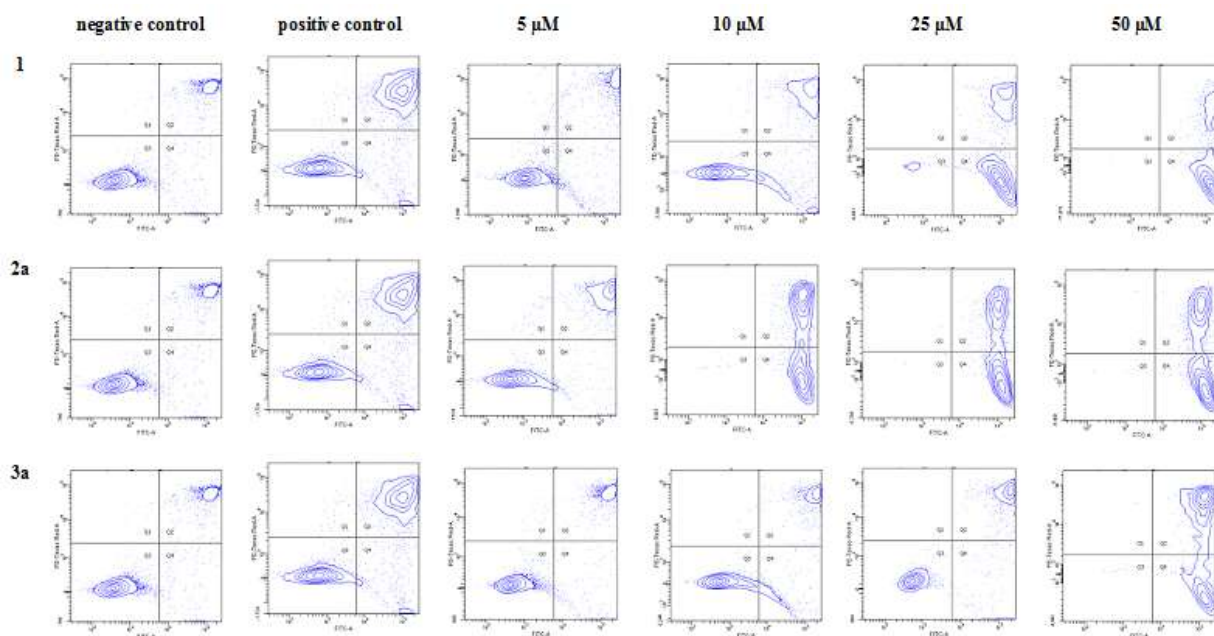


Figure S29. The effect of ruthenium complexes **1**, **2a** and **3a** on the apoptosis of HL-60 cells. Representative flow cytometric dot plots showing the percentage of cells in viable (Q3), early apoptotic (Q4), late apoptotic (Q2) and necrotic (Q1) stages. The positive control were cells incubated with 20 μM camptothecin (CAM) for 24 h at 37 °C. Data represent means \pm SD of 3 experiments.

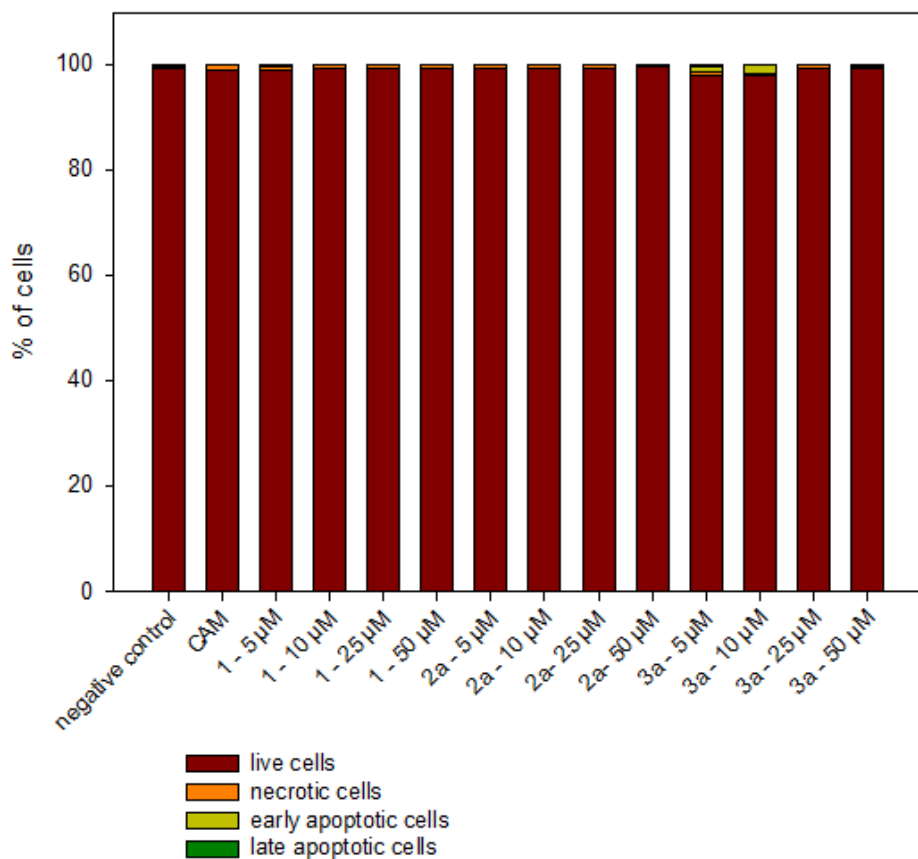
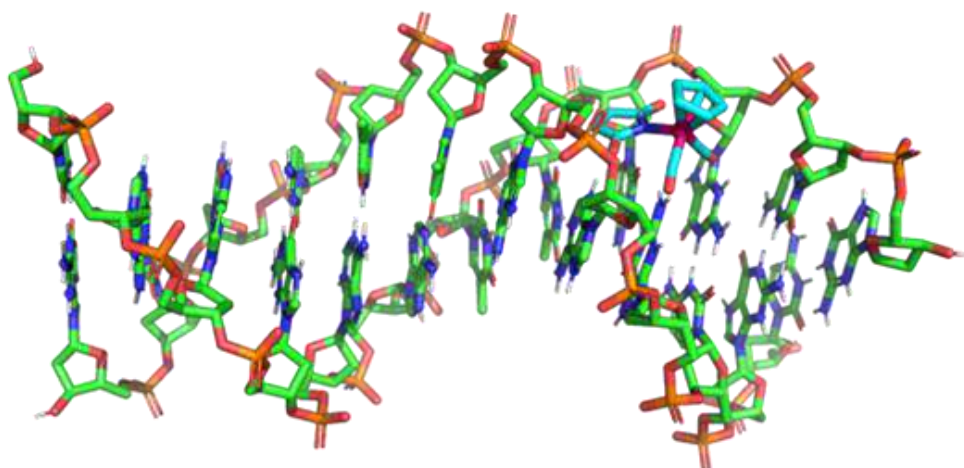


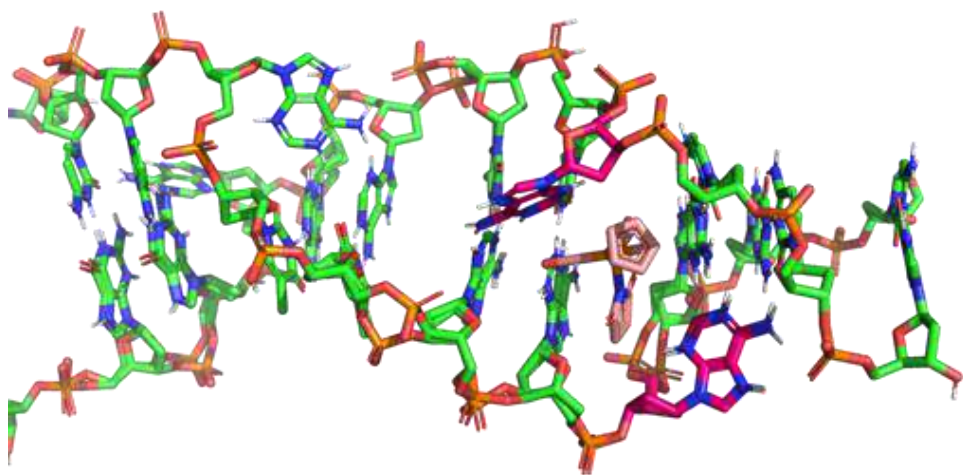
Figure S30. The effect of ruthenium complexes **1**, **2a** and **3a** on the apoptosis of HL-60/DR cells. Data represent means \pm SD of three experiments. The CAM sample were cells incubated with 20 μ M camptothecin for 24 h at 37 $^{\circ}$ C.

1.5. Docking studies

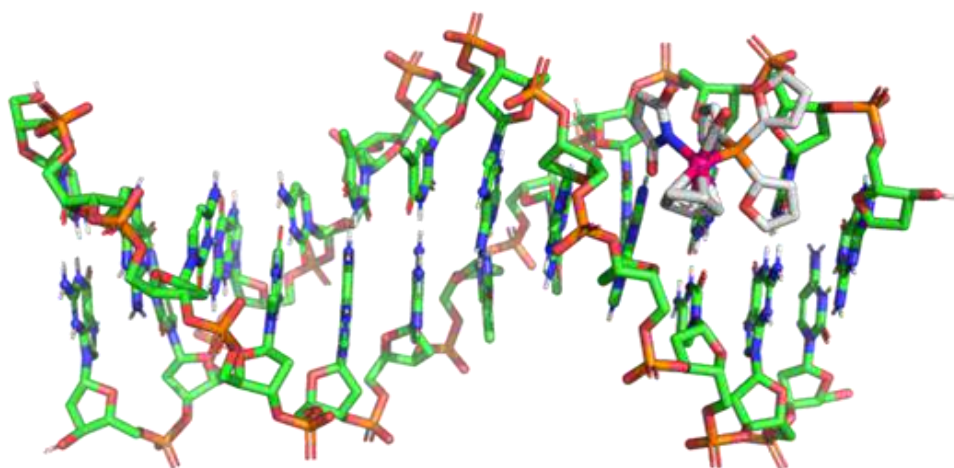
a



b



c



d

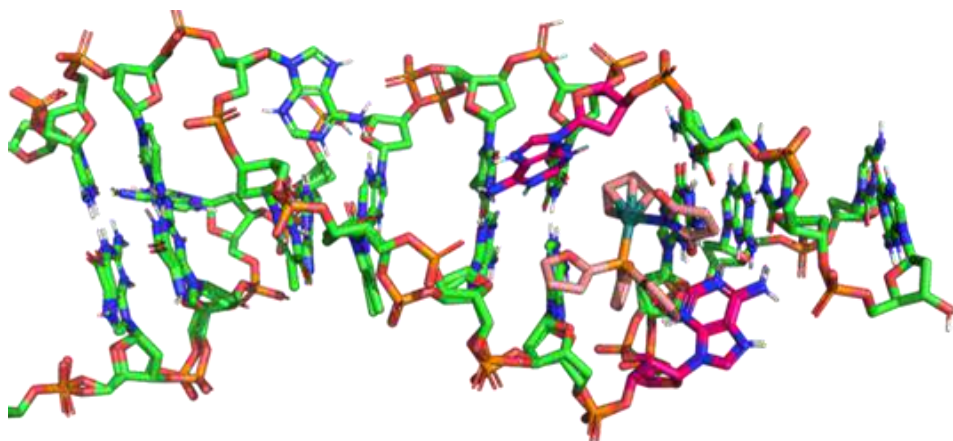


Figure S31. Ruthenium(II) complexes **1** (a, b) and **2b** (c, d) with fully complemented DNA (a, c) and with mismatched DNA (b, d).

Oświadczenia współautorów



WYDZIAŁ BIOLOGII
i OCHRONY
ŚRODOWISKA
Uniwersytet Łódzki



Łódź, dnia 29.03.2023 r.

mgr Michał Juszcak

Katedra Genetyki Molekularnej

Uniwersytetu Łódzkiego

Oświadczenie o udziale w publikacjach

Oświadczam, że w pracy: **Juszcak M**, Kluska M, Wysokiński D, Woźniak K. „Właściwości przeciwnowotworowe związków rutenu – NAMI-A i KP1019”. *Postępy Higieny i Medycyny Doświadczalnej*, 2020; 74:12-19 mój udział polegał na: wyszukaniu niezbędnej literatury, przygotowaniu rycin przedstawiających wzory strukturalne NAMI-A oraz KP1019, interakcje biologiczne odpowiadające za antymetastatyczne właściwości NAMI-A oraz poznane i potencjalne cele biologiczne KP1019, napisaniu części manuskryptu, a także odpowiednim sformatowaniu bibliografii.

Michał Juszcak
mgr Michał Juszcak

Oświadczam, że w pracy: **Juszcak M**, Kluska M, Wysokiński D, Woźniak K. „DNA damage and antioxidant properties of CORM-2 in normal and cancer cells”. *Scientific Reports*, 2020 Jul 22;10(1):12200 mój udział polegał na: współtworzeniu koncepcji pracy, zaplanowaniu i przeprowadzeniu części eksperymentalnej pracy obejmującej: hodowlę linii komórkowej HL-60, izolację jednojądrzastych komórek krwi obwodowej z kożuszków leukocyтарно-пłytkowych, ocenę żywotności testem redukcji resazuryny, analizę genotoksyczności z wykorzystaniem testu kometowego, określenie poziomu reaktywnych form tlenu z wykorzystaniem sondy H₂DCFDA oraz analizę poziomu ekspresji genu *HMOX1*, przeprowadzeniu analizy wyników, przygotowaniu wykresów, napisaniu części manuskryptu.

Michał Juszcak
mgr Michał Juszcak

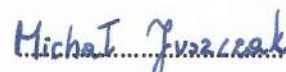
Oświadczam, że w pracy: **Juszczak M**, Kluska M, Kosińska A, Palusiak M. Rybarczyk-Pirek A J, Wzgarda-Raj K, Rudolf B, Woźniak K. „Cytotoxicity of piano-stool ruthenium cyclopentadienyl complexes bearing different imidato ligands”. *Applied Organometallic Chemistry*, 2022, 36(4), e6595 mój udział polegał na współtworzeniu koncepcji pracy, zaplanowaniu i przeprowadzeniu części eksperymentalnej pracy obejmującej: hodowlę linii komórkowej HL-60, izolację jednojądrzastych komórek krwi obwodowej z kożuszków leukocyтарно-пłytkowych, ocenę żywotności testem redukcji resazuryny, analizę genotoksyczności z wykorzystaniem testu kometowego, cytometryczną analizę apoptozy z wykorzystaniem podwójnego barwienia z jodkiem propidyny (PI) i izotiocyjanianem fluoresceiny (FITC), cytometryczną analizę zmian w przebiegu cyklu komórkowego oraz przeprowadzenie inkubacji badanych kompleksów rutenowych z genomowym DNA i wykonaniu elektroforezy DNA, przeprowadzeniu analizy wyników, przygotowaniu wykresów, napisaniu części manuskryptu.


mgr Michał Juszczak

Oświadczam, że w pracy: **Juszczak M**, Kluska M, Kosińska A, Rudolf B, Woźniak K. „Antioxidant Activity of Ruthenium Cyclopentadienyl Complexes Bearing Succinimidato and Phthalimidato Ligands”. *Molecules*, 2022; 27(9):2803 mój udział polegał na współtworzeniu koncepcji pracy, zaplanowaniu i przeprowadzeniu części eksperymentalnej pracy obejmującej: hodowlę linii komórkowej HL-60, izolację jednojądrzastych komórek krwi obwodowej z kożuszków leukocyтарно-пłytkowych, ocenę żywotności testem redukcji resazuryny, analizę genotoksyczności z wykorzystaniem testu kometowego, określenie poziomu reaktywnych form tlenu z wykorzystaniem sondy H₂DCFDA, cytometryczną analizę zmian w przebiegu cyklu komórkowego oraz oznaczenie aktywności dysmutazy ponadtlenkowej, przeprowadzeniu analizy wyników, przygotowaniu wykresów, napisaniu części manuskryptu.


mgr Michał Juszczak

Oświadczam, że w pracy: **Juszczak M**, Das S, Kosińska A, Rybarczyk-Pirek A J, Wzgarda-Raj K, Tokarz P, Vasudevan S, Chworos A, Woźniak K, Rudolf B. „Piano-stool ruthenium(II) complexes with maleimide and phosphine or phosphite ligands: synthesis and activity against normal and cancer cells”. *Dalton Transactions*, 2023; 10.1039/d2dt04083b mój udział polegał na współtworzeniu koncepcji pracy, zaplanowaniu i przeprowadzeniu części eksperymentalnej pracy obejmującej: hodowlę linii komórkowej HL-60, wyprowadzenie linii komórkowej HL-60/DR odpornej na doksorubicynę, izolację jednojądrzastych komórek krwi obwodowej z kożuszków leukocytno-płytkowych, ocenę żywotności testem redukcji resazuryny, analizę genotoksyczności z wykorzystaniem testu kometowego, cytometryczną analizę apoptozy z wykorzystaniem podwójnego barwienia z jodkiem propidyny (PI) i izotiocyjanianem fluoresceiny (FITC), określenie poziomu reaktywnych form tlenu z wykorzystaniem sondy H₂DCFDA, oznaczeniu aktywności kaspaz wykonawczych 3/7 oraz przeprowadzaniu testu konformacji plazmidu pUC19, wykonaniu analizy wyników, przygotowaniu wykresów oraz napisaniu części manuskryptu.


mgr Michał Juszczak

dr Magdalena Kluska

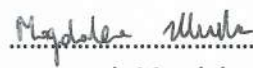
Łódź, dnia 29.03.2023 r.

Katedra Genetyki Molekularnej UŁ

Obecnie: Proteon Pharmaceuticals S.A.

Oświadczenie o udziale w publikacjach


Oświadczam, że w pracy: Juszcak M, Kluska M, Wysokiński D, Woźniak K. „Właściwości przeciwnowotworowe związków rutenu – NAMI-A i KP1019”. *Postępy Higieny i Medycyny Doświadczalnej*, 2020; 74: 12-19 mój udział polegał na analizie danych literaturowych oraz korekcie listy wykorzystanej literatury.


.....
dr Magdalena Kluska

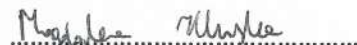
Oświadczam, że w pracy: Juszcak M, Kluska M, Wysokiński D, Woźniak K. „DNA damage and antioxidant properties of CORM-2 in normal and cancer cells”. *Scientific Reports*, 2020 Jul 22;10(1):12200 mój udział polegał na współprowadzeniu hodowli komórek HL-60 oraz wykonaniu części eksperymentów dotyczących uszkodzeń DNA oraz określenia poziomu reaktywnych form tlenu z wykorzystaniem sondy H₂DCFDA.


.....
dr Magdalena Kluska

Oświadczam, że w pracy: Juszcak M, Kluska M, Kosińska A, Palusiak M, Rybarczyk-Pirek A J, Wzgarda-Raj K, Rudolf B, Woźniak K. „Cytotoxicity of piano-stool ruthenium cyclopentadienyl complexes bearing different imidato ligands”. *Applied Organometallic Chemistry*, 2022, 36(4), e6595 mój udział polegał na współprowadzeniu hodowli komórek HL-60 oraz wykonaniu części eksperymentów z wykorzystaniem cytometrii przepływowej (oznaczenie apoptozy).


.....
dr Magdalena Kluska

Oświadczam, że w pracy: Juszczak M, **Kluska M**, Kosińska A, Rudolf B, Woźniak K. „Antioxidant Activity of Ruthenium Cyclopentadienyl Complexes Bearing Succinimidato and Phthalimidato Ligands”. *Molecules*, 2022; 27(9):2803 mój udział polegał na współprowadzeniu hodowli komórek HL-60 oraz wykonaniu części eksperymentów dotyczących oznaczeń aktywności enzymatycznej dysmutazy ponadtlenkowej.


.....
dr Magdalena Kluska

dr Daniel Wysokiński


Łódź, dnia 29.03.2023 r.

Katedra Genetyki Molekularnej

Uniwersytetu Łódzkiego

Oświadczenie o udziale w publikacjach

Oświadczam, że w pracy: Juszczak M, Kluska M, **Wysokiński D**, Woźniak K. „Właściwości przeciwnowotworowe związków rutenu – NAMI-A i KP1019”. *Postępy Higieny i Medycyny Doświadczalnej*, 2020; 74 : 12-19 mój udział polegał na napisaniu fragmentu manuskryptu oraz na korekcie językowej manuskryptu.


.....
dr Daniel Wysokiński

Oświadczam, że w pracy: Juszczak M, Kluska M, **Wysokiński D**, Woźniak K. „DNA damage and antioxidant properties of CORM-2 in normal and cancer cells”. *Scientific Reports*, 2020 Jul 22;10(1):12200 mój udział polegał na współudziale w eksperymentach dotyczących oznaczania żywotności komórek i ekspresji genu *HMOX1*.


.....
dr Daniel Wysokiński

dr Aneta Kosińska
Katedra Chemii Organicznej
Wydział Chemii UŁ

Oświadczenie o udziale w publikacjach

Oświadczam, że w pracy: Juszcak M, Kluska M, **Kosińska A**, Palusiak M. Rybarczyk-Pirek, A. J. Wzgarda-Raj, K, Rudolf B, Woźniak K. Cytotoxicity of piano-stool ruthenium cyclopentadienyl complexes bearing different imidato ligands. *Applied Organometallic Chemistry*, 2022, 36(4), e6595. Mój udział polegał na syntezie oraz dokonaniu fizyko-chemicznej charakterystyki kompleksów rutenu.



dr Aneta Kosińska

Oświadczam, że w pracy: Juszcak M, Kluska M, **Kosińska A**, Rudolf B, Woźniak K. Antioxidant Activity of Ruthenium Cyclopentadienyl Complexes Bearing Succinimidato and Phthalimidato Ligands. *Molecules*, 2022; 27(9):2803. Mój udział polegał na syntezie oraz dokonaniu fizyko-chemicznej charakterystyki kompleksów rutenu.



dr Aneta Kosińska

Oświadczam, że w pracy: Juszcak M, Das S, **Kosińska A**, Rybarczyk-Pirek A, Wzgarda-Raj K, Tokarz p, Vasudevan S, Chworoś A, Woźniak K, Rudolf B. Piano-stool Ruthenium(II) complexes with maleimide and phosphine or phosphite ligands: Synthesis and activity against normal and cancer cells. *Dalton Trans.* 2023, doi: 10.1039/D2DT04083B, mój udział polegał na syntezie oraz dokonaniu fizyko-chemicznej charakterystyki kompleksów rutenu.



dr Aneta Kosińska



**FACULTY OF
CHEMISTRY**

University of Lodz

prof. dr hab. Marcin Palusiak
Department of Physical Chemistry
Faculty of Chemistry, University of Lodz
Pomorska 163/165, 90-236 Lodz, Poland
mobile phone: +48 504984038
phone: +48 42 6355737
fax: +48 42 6355744
e-mail: marcin.palusiak@chemia.uni.lodz.pl

Oświadczenie o udziale w publikacji

Oświadczam, że w pracy: Juszczak M, Kluska M, Kosińska A, Palusiak M, Rybarczyk-Pirek, A. J. Wzgarda-Raj, K, Rudolf B, Woźniak K. „Cytotoxicity of piano-stool ruthenium cyclopentadienyl complexes bearing different imidato ligands”. Applied Organometallic Chemistry, 2022, 36(4), e6595 mój udział polegał na wykonaniu obliczeń kwantowo-chemicznych dla układów modelowych maleimidu i sukcyimidu.

Marcin Palusiak

Marcin Palusiak

dr hab. Agnieszka Rybarczyk-Pirek, prof. UŁ
Katedra Chemii Fizycznej
Wydział Chemii UŁ

Oświadczenie o udziale w publikacjach

Dotyczy publikacji:

1. Juszcak M., Kluska M., Kosińska A., Palusiak M., Rybarczyk-Pirek, A. J., Wzgarda-Raj, K., Rudolf B., Woźniak K. „Cytotoxicity of piano-stool ruthenium cyclopentadienyl complexes bearing different imidato ligands,,. *Applied Organometallic Chemistry*, 2022, 36(4), e6595
2. Juszcak M., Das S., Kosińska A., Rybarczyk-Pirek A. J., Wzgarda-Raj K., Tokarz P., Vasudevan S., Chworoś A., Woźniak K., Rudolf B. „Piano-stool Ruthenium(II) complexes with maleimide and phosphine or phosphite ligands: Synthesis and activity against normal and cancer cells,,. *Dalton Transactions*. DOI: <https://doi.org/10.1039/D2DT04083B>

Jako współautor powyższych publikacji oświadczam, że mój wkład w ich postanie polegał na ustaleniu struktury kryształów i określeniu budowy cząsteczkowej wybranych kompleksów metalokarbonylowych. Brałam udział w przygotowaniu kolejnych wersji manuskryptów, w szczególności w przygotowaniu części opisujących wyniki badań krystalograficznych w tym w przedstawieniu uzyskanych wyników w formie graficznej.

A. Rybarczyk - Pirek

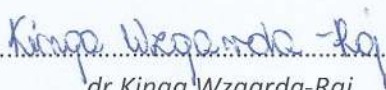
dr Kinga Wzgarda-Raj
Katedra Chemii Fizycznej
Wydział Chemii UŁ

Oświadczenie o udziale w publikacjach

Dotyczy publikacji:

1. Juszczak M., Kluska M., Kosińska A., Palusiak M., Rybarczyk-Pirek, A.J., **Wzgarda-Raj K.**, Rudolf B., Woźniak K. „Cytotoxicity of piano-stool ruthenium cyclopentadienyl complexes bearing different imidato ligands”. *Applied Organometallic Chemistry*, 2022, 36(4), e6595.
2. Juszczak M., Das S., Kosińska A., Rybarczyk-Pirek A.J., **Wzgarda-Raj K.**, Tokarz P., Vasudevan S., Chworoś A., Woźniak K., Rudolf B. “Piano-stool Ruthenium(II) complexes with maleimide and phosphine or phosphite ligands: Synthesis and activity against normal and cancer cells”. *Dalton Transactions*, 2023, DOI: 10.1039/D2DT04083B.

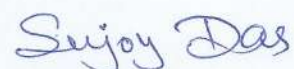
Jako współautor powyższych publikacji oświadczam, że mój wkład w ich powstanie polegał na samodzielnym wykonaniu pomiarów dyfraktometrycznych oraz redukcji danych otrzymanych próbek. Ponadto ustalałam strukturę kryształów i określałam budowę cząsteczkową wybranych kompleksów metalokarbonylowych.


.....
dr Kinga Wzgarda-Raj

Lodz, 21.03.2023 r.

dr Sujoy Das
Department of Organic Chemistry

Herein, I declare that in the paper published by: Juszcak M, **Das S**, Kosińska A, Rybarczyk-Pirek A, Wzgarda-Raj K, Tokarz p, Vasudevan S, Chworoś A, Woźniak K, Rudolf B. Piano-stool Ruthenium(II) complexes with maleimide and phosphine or phosphite ligands: Synthesis and activity against normal and cancer cells. Dalton Trans. 2023, doi: 10.1039/D2DT04083B, my part was the synthesis and characterization of the organometallic complexes.



.....
dr Sujoy Das



WYDZIAŁ BIOLOGII
i OCHRONY
ŚRODOWISKA
Uniwersytet Łódzki



Łódź, dnia 29.03.2023 r.

dr Paulina Tokarz

Katedra Genetyki Molekularnej

Uniwersytetu Łódzkiego

Oświadczenie o udziale w publikacjach

Oświadczam, że w pracy: Juszczak M, Das S, Kosińska A, Rybarczyk-Pirek A J, Wzgarda-Raj K, **Tokarz P**, Vasudevan S, Chworos A, Woźniak K, Rudolf B. „Piano-stool ruthenium(II) complexes with maleimide and phosphine or phosphite ligands: synthesis and activity against normal and cancer cells”. *Dalton Transactions*, 2023; 10.1039/d2dt04083b mój udział polegał na współprowadzeniu hodowli komórek HL-60/DR, współudziale w wykonaniu części eksperymentów dotyczących testu relaksacji plazmidu i oznaczaniu aktywności kaspaz wykonawczych 3/7.

Paulina Tokarz

dr Paulina Tokarz

Dr. Saranya Vasudevan

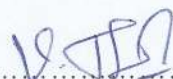
20.03.2023

Centrum Badań Molekularnych i Makromolekularnych

Polskiej Akademii Nauk w Łodzi

Declaration on the

Herein I declare that in the paper published by: Juszczak M, Das S, Kosińska A, Rybarczyk-
Pirek A, Wzgarda-Raj K, Tokarz P, **Vasudevan S**, Chworoś A, Woźniak K, Rudolf B., *Piano-
stool Ruthenium(II) complexes with maleimide and phosphine or phosphite ligands: Synthesis
and activity against normal and cancer cells. Dalton Trans. 2023, doi: [10.1039/D2DT04083B](https://doi.org/10.1039/D2DT04083B)*,
my part was to prepare a molecular docking of complex structure to DNA fragments.



.....
dr Saranya Vasudevan

prof. dr hab. Arkadiusz Chworos

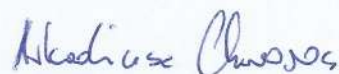
20.03.2023 r.

Centrum Badań Molekularnych i Makromolekularnych

Polskiej Akademii Nauk w Łodzi

Oświadczenie o udziale w publikacji

Oświadczam, że w pracy: Juszczak M, Das S, Kosińska A, Rybarczyk-Pirek A, Wzgarda-Raj K, Tokarz P, Vasudevan S, **Chworos A**, Woźniak K, Rudolf B. Piano-stool Ruthenium(II) complexes with maleimide and phosphine or phosphite ligands: Synthesis and activity against normal and cancer cells. *Dalton Trans.* 2023, doi: [10.1039/D2DT04083B](https://doi.org/10.1039/D2DT04083B), mój udział polegał na analizie i interpretacji wyników dokowania molekularnego badanych kompleksów do DNA oraz pomoc w redagowaniu tekstu manuskryptu.



.....
prof. dr hab. Arkadiusz Chworos

dr hab. Bogna Rudolf, prof. UŁ
Kierownik Katedry Chemii Organicznej

Oświadczenie o udziale w publikacjach

Oświadczam, że w pracy: Juszczak M, Kluska M, Kosińska A, Palusiak M. Rybarczyk-Pirek, A. J. Wzgarda-Raj, K, **Rudolf B**, Woźniak K. „Cytotoxicity of piano-stool ruthenium cyclopentadienyl complexes bearing different imidato ligands”. *Applied Organometallic Chemistry*, 2022, 36(4), e6595 mój udział polegał na koordynowaniu prac na syntezą oraz fizyko-chemiczną charakterystyką kompleksów rutenu, a także obejmował współtworzenie koncepcji pracy i jej przygotowanie do publikacji.



Oświadczam, że w pracy: Juszczak M, Kluska M, Kosińska A, **Rudolf B**, Woźniak K. Antioxidant Activity of Ruthenium Cyclopentadienyl Complexes Bearing Succinimidato and Phthalimidato Ligands. *Molecules*, 2022; 27(9):2803. mój udział polegał na koordynowaniu prac nad syntezą oraz fizyko-chemiczną charakterystyką kompleksów rutenu, a także obejmował współtworzenie koncepcji pracy i jej przygotowanie do publikacji.



Oświadczam, że w pracy: Juszczak M, Das S, Kosińska A, Rybarczyk-Pirek A, Wzgarda-Raj K, Tokarz P, Vasudevan S, Chworoś A, Woźniak K, **Rudolf B**,. Piano-stool Ruthenium(II) complexes with maleimide and phosphine or phosphite ligands: Synthesis and activity against normal and cancer cells. *Dalton Transactions* 2023 doi: 10.1039/d2dt04083b., mój udział polegał na koordynowaniu prac nad syntezą oraz fizyko-chemiczną charakterystyką kompleksów rutenu, a także obejmował współtworzenie koncepcji pracy i jej przygotowanie do publikacji.





WYDZIAŁ BIOLOGII
I OCHRONY
ŚRODOWISKA
Uniwersytet Łódzki



Łódź, dnia 29.03.2023 r.

prof. dr hab. Katarzyna Woźniak
Katedra Genetyki Molekularnej
Uniwersytetu Łódzkiego

Oświadczenie o udziale w publikacjach

Oświadczam, że w pracy: Juszczak M, Kluska M, Wysokiński D, **Woźniak K.** „Właściwości przeciwnowotworowe związków rutenu – NAMI-A i KP1019”. *Postępy Higieny i Medycyny Doświadczalnej*, 2020; 74: 12-19 mój udział polegał na współtworzeniu koncepcji pracy, sprawdzeniu poprawności rycin, napisaniu części manuskryptu oraz prowadzeniu korespondencji z edytorem.



prof. dr hab. Katarzyna Woźniak

Oświadczam, że w pracy: Juszczak M, Kluska M, Wysokiński D, **Woźniak K.** „DNA damage and antioxidant properties of CORM-2 in normal and cancer cells”. *Scientific Reports*, 2020 Jul 22;10(1):12200 mój udział polegał na współtworzeniu koncepcji pracy, koordynowaniu pracy doświadczalnej, sprawdzeniu poprawności rycin, napisaniu części manuskryptu oraz prowadzeniu korespondencji z edytorem.



prof. dr hab. Katarzyna Woźniak

Oświadczam, że w pracy: Juszczak M, Kluska M, Kosińska A, Palusiak M, Rybarczyk-Pirek A J, Wzgarda-Raj K, Rudolf B, **Woźniak K.** „Cytotoxicity of piano-stool ruthenium cyclopentadienyl complexes bearing different imidato ligands”. *Applied Organometallic Chemistry*, 2022, 36(4), e6595 mój udział polegał na współtworzeniu koncepcji pracy, koordynowaniu pracy doświadczalnej, sprawdzeniu poprawności rycin, napisaniu części manuskryptu oraz prowadzeniu korespondencji z edytorem.


.....
prof. dr hab. Katarzyna Woźniak

Oświadczam, że w pracy: Juszczak M, Kluska M, Kosińska A, Rudolf B, **Woźniak K.** „Antioxidant Activity of Ruthenium Cyclopentadienyl Complexes Bearing Succinimidato and Phthalimidato Ligands”. *Molecules*, 2022; 27(9):2803 mój udział polegał na współtworzeniu koncepcji pracy, koordynowaniu pracy doświadczalnej, sprawdzeniu poprawności rycin, napisaniu części manuskryptu oraz prowadzeniu korespondencji z edytorem.


.....
prof. dr hab. Katarzyna Woźniak

Oświadczam, że w pracy: Juszczak M, Das S, Kosińska A, Rybarczyk-Pirek A J, Wzgarda-Raj K, Tokarz P, Vasudevan S, Chworos A, **Woźniak K,** Rudolf B. „Piano-stool ruthenium(II) complexes with maleimide and phosphine or phosphite ligands: synthesis and activity against normal and cancer cells”. *Dalton Transactions*, 2023; 10.1039/d2dt04083b mój udział polegał na współtworzeniu koncepcji pracy, koordynowaniu pracy doświadczalnej, sprawdzeniu poprawności rycin, napisaniu części manuskryptu oraz prowadzeniu korespondencji z edytorem.


.....
prof. dr hab. Katarzyna Woźniak